X-552-72-244

PREPRINT

NASA TM X-65984

GODDARD TRAJECTORY DETERMINATION SUBSYSTEM MATHEMATICAL SPECIFICATIONS

MARCH 1972

GSFC

GODDARD SPACE FLIGHT CENTER

GREENBELT, MARYLAND

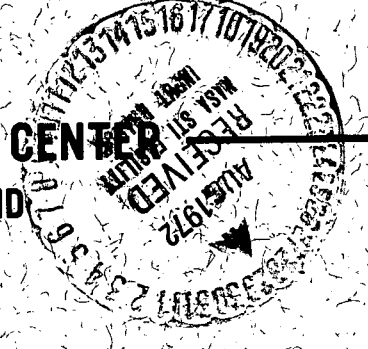

GODDARD TRAJECTORY DETERMINATION SUBSYSTEM

MATHEMATICAL SPECIFICATIONS

Edited by

W. E. Wagner
Computer Sciences Corporation

and

C. E. Velez
Goddard Space Flight Center

March 1972

GODDARD SPACE FLIGHT CENTER
Greenbelt, Maryland

ACKNOWLEDGEMENT

The editors wish to acknowledge the contribution made by many individuals at Goddard Space Flight Center and at Computer Sciences Corporation who participated in the technical preparation of manuscripts to these mathematical specifications. These individuals are:

P. D. Argentiero, GSFC
R. W. Barbieri, GSFC
N. R. Burton, CSC
L. H. Carpenter, GSFC
J. L. Cooley, GSFC
V. T. Laczo, GSFC
E. J. Lefferts, GSFC
D. H. Novak, CSC
C. E. Velez, GSFC
W. E. Wagner, CSC
D. S. Woolston, GSFC

A special acknowledgement is given to

J. W. Siry, GSFC
E. R. Watkins, Jr. GSFC
C. E. Doll, GSFC

for helpful technical discussions and consultation.

ABSTRACT

This document presents the mathematical specifications of the Goddard Trajectory Determination Subsystem (GTDS) of the Flight Dynamics System (FDS). These specifications include the mathematical description of the coordinate systems, dynamic and measurement model, numerical integration techniques, and statistical estimation concepts.

TABLE OF CONENTS

TABLE OF CONTENTS–(continued)

TABLE OF CONTENTS–(continued)

TABLE OF CONTENTS–(continued)

TABLE OF CONTENTS–(continued)

TABLE OF CONTENTS–(continued)

LIST OF ILLUSTRATIONS

LIST OF TABLES

CHAPTER 1

INTRODUCTION

This document presents the mathematical specifications for the earth/lunar interplanetary Goddard Trajectory Determination Subsystem (GTDS) of the Flight Dynamics System (FDS). The FDS is a multipurpose computer system designed

> "to provide operational support for individual earth, lunar, and planetary space missions and for the research and development requirements of the various projects of the Goddard Space Flight Center scientific community (Reference 1)."

The above objective establishes the required capabilities and scope of the system and thereby quantifies the operating modes, precision, speed, options, numerical procedures, and other characteristics which the GTDS must satisfy. These characteristics, in turn, influence the mathematical specifications of the system. Before proceeding to the detailed specifications described in the following chapters, the modes, options, and capabilities are highlighted in the following overview.

1.1 OPERATING MODES

To meet the varying demands imposed upon the system by operational support of the research and development requirements of various projects, the FDS includes the following operational modes

- Ephemeris Mode - Generates the trajectory of a spacecraft from specified initial conditions.
- Data Simulation Mode – Generates simulated observation data for subsequent analysis or processing.
- Compare Mode – Compares trajectories of two spacecraft and displays residuals.
- Data Management Mode - Manipulates prestored observational or physical parameter data in either working or permanent files.

These data vary from dynamic model parameters (e.g., atmosphere density tables, gravitational harmonic coefficients, or interplanetary constants) to simulated or real observational data.

- Matrix Mapping Mode - Propagates a specified covariance matrix from one epoch to another using a numerically integrated state transition matrix.

- File Report Mode - Generates reports on the content of various data files.

- Orbit Determination Mode - Estimates the position, velocity and model parameters from observed data recorded during the mission. The estimation is accomplished by means of weighted least squares criterion.

- Error Analysis Mode - Determines the uncertainty of an orbit determination estimate from a priori values of the uncertainty of the observation data, the position and velocity at an epoch, and model parameters.

The principle concern in this document is the Ephemeris, Data Simulation, Matrix Mapping, Orbit Determination and Error Analysis Modes, and, to a lesser extent, the Data Management Mode.

1.2 NEAR REAL-TIME AND POSTFLIGHT OPERATION

To provide operational support, FDS includes a near real-time capability with interactive graphics report and control facilities. The iteractive capabilities allow the user to edit individual data points based on graphical displays of their residuals; to modify iterative convergence criteria; to modify editing criteria such as data time spans, processing rates, data types etc.; or even to change modes during a run.

Near real-time operation usually necessitates a compromise in computational precision compared to that generally achieved during postflight processing. Several options are included for this purpose which permit more rapid computation without seriously jeopardizing precision. These options effect numerical integration (stepsize control), model approximations (omitting polar motion), and control over the number of variables being estimated or considered. Also, optional capability is being included to vary the amount of preprocessing performed on the data.

1.3 DATA PREPROCESSING

Preprocessing of observation (e.g., tracking) data is normally done by means of a computer program completely independent of the GTDS. Raw data are converted

from the form received from the tracking stations to forms for storage in the data base, suitable for use in the GTDS. Wild points are edited out; calibration corrections are applied to eliminate known instrumentation errors; ambiguities in the data measurement and/or recording are resolved; conversions are made from the measurement units to units which are more physically meaningful or convenient; and the data is smoothed and possibly compacted if large amounts of raw data are measured.

Data processing encompasses all operations performed in the GTDS to compare the preprocessed data with simulated observations computed at corresponding times from the estimated orbit. This involves modeling the observation phenomena so as to compute a data point corresponding in form to the preprocessed data stored in the data base.

Provision is made to GTDS to satisfy the conflicting requirements of high-speed real-time processing for operational support, and high precision processing for postflight analysis by providing two processing options. In processing option A (metric processing), the data are assumed to have had all calibrations and some systematic errors corrected to have ambiguities eliminated, to have been converted to physically meaningful units, and to have been smoothed and compacted in the preprocessor. This simplifies the observation model required in the GTDS and requires processing of fewer data points.

In processing option B (polynomial processing), the preprocessing is minimized so as not to introduce errors into the data by converting units, smoothing, and/or compacting. Furthermore, the statistical noise content of the data is not destroyed by smoothing. The preprocessor in option B makes only the calibration and systematic error corrections that are known with a high degree of confidence. The remaining are modeled into the GTDS. For example, a Doppler measurement is not converted to an instantaneous range rate, but instead is transformed into a count of the number of cycles of the two-way Doppler-shifted frequency over the measurement time interval or an equivalent range difference. The processing within the GTDS requires that the signal transmission geometry be accurately modeled and includes the finite signal propagation speed time delays and atmospheric effects. Since data compaction is not performed in option B, large amounts of data are generally "bunched" into the relatively short tracking time spans. To reduce the computational load, the GTDS calculates comparatively few observations over the data segment to which it fits polynomials. It then evaluates the polynomials to determine the modeled measurements at the time of the actual measurements for subsequent comparison.

1.4 TRACKING SYSTEMS

The GTDS is capable of simulating or processing, in the orbit determination mode, observation data from the following tracking systems.

- Goddard Range and Range-Rate (GRARR) VHF System - The GRARR system measures the two-way Doppler shift of a continuous wave VHF signal. The system determines the range and range-rate of the spacecraft relative to the station as well as two gimbal angles which define the direction of the signal path at the antenna.

- C-Band Pulse Radar - FPS-6 and FPS-16 pulse type radars measure the two-way light time to yield range and the azimuth and elevation of the pointing antenna.

- Minitrack Interferometer - Minitrack is a short baseline interferometer system. It measures two direction cosines of the station-vehicle vector relative to local tangent plane east and north pointing axes.

The capability to process other data types such as optical laser, range sum and range sum rate, altimeter, and S-band (GRARR or DSN) will be incorporated into GTDS as necessary.

1.5 SPACECRAFT DYNAMICS

To accommodate the varying requirements at Goddard Space Flight Center in near earth, lunar, and interplanetary mission analysis, the GTDS dynamic model includes the following acceleration sources.

- N-Body Point Mass Gravitational Accelerations - These include all planets in the solar system, the sun, and the earth's moon.

- Nonspherical Gravitational Accelerations - The nonspherical gravitational acceleration model allows the inclusion of up to a 15 $\times$ 15 potential field for the earth and moon.

- Atmospheric Drag Accelerations - The drag acceleration for earth includes a dynamic atmosphere model which accounts for variations in the solar flux on the earth's upper atmosphere. A modified Harris Priester model and a Jacchia (1971) model are available.

- Solar Radiation Accelerations - The solar radiation model includes shadowing and variations with distance from the sun.

- Attitude Control System Accelerations - A generalized model is included for estimating residual accelerations from an attitude control system.

- Thrusting Maneuver Accelerations - A generalized model is included for accommodating propulsive maneuvers.

The reference coordinate system for the equations of motion is optionally either the mean equinox and equator of 1950.0 or a true of data system at a specified epoch. Coordinate transformations account for precession, nutation, and polar motion of the earth's spin axis. True planetary positions are determined from a peripheral ephemeris file containing Chebychev polynomial coefficients derived from JPL ephemeris data.

The program is provided with "flight sectioning" capability wherein the complete trajectory arc can be partitioned into multiple subarcs. The dynamic model options, numerical integration characteristics, and output quantities and frequency can be suitably tailored for each subarc. The criteria for cross-over from one subarc to the next, are based on either time or spatial conditions which can be specified for each subarc.

The state transition matrix, required by the estimator algorithm is obtained by numerically integrating variational equations. A Cowell predictor-corrector numerical integration algorithm is used to integrate the second order equations of motion and associated variational equations. Automatic or semiautomatic error control is provided by adjusting the integration stepsize or by using a time regularization process.

Various options are provided in the dynamic models and numerical integration algorithms to give the versatility to accommodate both high-speed near real-time applications and precision postflight applications.

1.6 ESTIMATION PROCESS

The estimation algorithm included in GTDS is variously called "Weighted Least Squares With A Priori" or "Bayesian Weighted Least Squares." It minimizes the sum of the squares of the weighted residuals between actual and computed observations, while simultaneously constraining the state to satisfy an a priori state to within a specified uncertainty. The iterative estimation process differentially corrects the estimated variables and ultimately determines the weighted least squares solution. Both first and second order statistics (i.e., mean and covariance matrix) are determined for the estimated variables.

Two classes of variables can be accommodated in the statistical computations. The first, called "solve-for" variables, includes model parameters whose values are known with limited certainty and are being estimated. The second, called "consider" variables, includes model parameters which are not being estimated, but whose uncertainty will affect the statistics of the "solve-for" variables. Model parameters which can be included in either the solve-for or consider classes include the following:

- Spacecraft state
- Scale factor on the product of the drag coefficient times atmospheric density, $C_D \rho$
- Scale factor on the solar radiation acceleration
- All gravitational harmonic coefficients
- Parameters in the thrust model
- Parameters in the attitude control system model
- Tracking station locations
- Observation biases
- Systematic errors in planned observations.

Specified subsets of the spacecraft position and velocity components can optionally be estimated in mean of 1950.0 or true of epoch inertial Cartesian coordinates, classical orbital elements, spherical coordinates, or Definitive Orbit Determination System (DODS) type elements (Reference 2).

The following chapters describe the mathematical models and numerical procedures required to implement the differential correction process in the GTDS. Chapter 2 describes the tracking systems and preprocessing procedures. Chapter 3 presents the coordinates and time systems necessary to accurately model the spacecraft's dynamic motion, as well as tracker observations. Chapters 4 and 5 present the equations of motion and the associated variational equations. The integrated solution to these equations constitutes the spacecraft's trajectory and state transition matrix. The numerical integration procedure is described in Chapter 6. Chapter 7 describes the observation models and systematic error corrections performed in the GTDS. Finally, Chapter 8 describes the estimation algorithm and its associated statistics. Appendices A, B, C, and D complement Chapters 2, 7, and 8 by discussing the Doppler conversion to range-rate and the

more theoretical aspects of the estimation process, analyses performed on resulting observation residuals, and observation data weighting, respectively. References are presented at the end of each chapter.

1.7 REFERENCES

1. Goddard Space Flight Center internal report, Functional Requirements for the Lunar/Planetary Orbit Determination Subsystem of the Goddard Trajectory Determination System, 1970.

2. Goddard Space Flight Center, X-544-71-296, Definitive Orbit Determination Operating System Description, Edition II, July 1971.

CHAPTER 2

TRACKING SYSTEMS AND PREPROCESSING

The tracking systems measure the various propagation characteristics of electromagnetic signals transmitted between the tracking station and the spacecraft. These data are subsequently used to determine the spacecraft trajectory. The dependence of these measurements upon the relative states of the spacecraft and tracking stations provides the key to the orbit determination procedure.

The interface between the ODS and the independent tracking data preprocessor is optional. As described in Section 1.3, Option A (metric) requires more of the preprocessor but simplifies the ODS modeling; Option B (polynomial) requires less computation in the preprocessor but increases the complexity in the ODS processing models.

This chapter describes the three primary tracking systems currently included in GTDS and presents a discussion of the preprocessing computations. These computations are independent of the ODS and are for informational use only. They also provide an insight to the preprocessor/processor interface which is necessary to understand subsequent discussion of processor measurement models in Chapter 7. Since the interface is optional, some overlap exists between this chapter and Chapter 7.

2.1 TRACKING SYSTEM DESCRIPTION

2.1.1 Goddard Range and Range-Rate (GRARR) VHF System

The GRARR VHF System (References 1, 2, 3, 4) transmits a continuous wave signal from the tracking station antenna with carrier frequency, ν_T, and is modulated by a low-frequency tone, ν_L. This signal propagates to the spacecraft (omni-directional) antenna, where the carrier frequency appears to be $\nu_V \neq \nu_T$ because of the uplink Doppler shift (Reference 5). The received signal is modified by the spacecraft transponder electronics system and retransmitted back to the ground tracking station. Again, the signal experiences a downlink Doppler shift so that the received frequency, ν_R, at the ground differs from that transmitted by the spacecraft. The ground receiving antenna is automatically steered through two gimbal angles, X and Y, shown in Figure 2-1, to maximize the received signal. The ground receiver electronics system is designed so that,

as the signal is processed through it, the spacecraft transponder modification is undone and the transmitted carrier frequency is subtracted. At the output, the differenced Doppler signal (reflecting the uplink and downlink Doppler shifts) is modified by the addition of a bias signal of known frequence, ν_b.

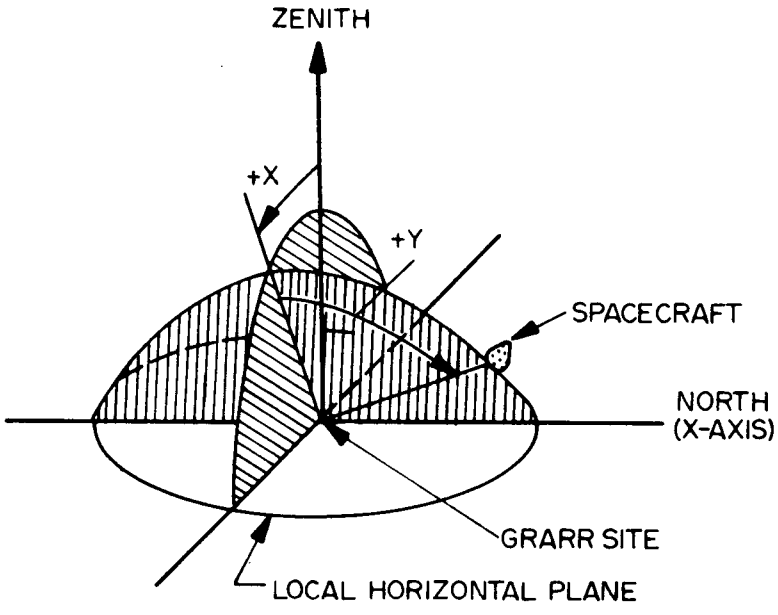

Figure 2-1. Schematic of GRARR Gimbal Angles

Three different types of measurement result from signals received during the "frame" time interval which commences at "frame" time, t_F:

1. The gimbal pickoff angles, X and Y, defining the direction of the received signal path at the antenna at time t_F, are recorded in degrees and decimal fractions.

2. The two-way range time delay is measured as a count C_1 of the number of cycles of a reference frequency, ν_{R_1}, which occurs between positive-going zero crossings of the low-frequency ranging tone (frequency = ν_L) associated with the transmitted and received signals. The counter is started and the frame time, t_F, is signaled simultaneously by a zero crossing of the transmitted signal. The counter is stopped by the next subsequent zero crossing of the received signal. Since the lowest sidetone frequency is 8 Hz, the maximum unambiguous one-way range measurement corresponds to a distance of approximately 18,737 kilometers. Distances greater than this produce phase shifts larger than one cycle of the ν_L

signal. When this occurs, the GRARR system utilizes a pseudo-random binary code to determine the range ambiguity number, ρ_a, the number of whole cycles to be added to the counter-measured fractional phase shift.

3. The two-way range-rate measurement is made as the count C_0 of the number of cycles of a reference frequency ν_{R_2} required to count simultaneously exactly N cycles of the Doppler-plus-bias signal $\nu_d + \nu_b$. The count is begun at time t_F and ended after accumulation of N cycles of the $\nu_d + \nu_b$ signal.

The gimbal angles, X and Y, are measured only at the frame time, t_F, but the range and range-rate measurements are made at the frame time and at three subsequent data sample times, t_S, within the frame-time interval. The spacing of these data samples (and hence the time span of a data frame) may be varied to give range and range-rate recording rates of 4, 2, or 1 sample per second or 6 samples per minute. The data, one angle sample and four range and range-rate samples for each frame, are punched on paper tape at the tracking station in standard Baudot 5-level teletype code and then transmitted to GSFC via teletype to be preprocessed.

2.1.2 C-Band Pulse Radar

The FPQ-6 and FPS-16 pulse type radars make two measurements: two-way light time and antenna pointing angle. The angle measurement is essentially the same as that described above for the GRARR system. The antenna gimbaling is different, however, and the C-band angles are recorded directly in terms of azimuth and elevation. The pickoffs record the angles in mils, where 6400 mils = 360 degrees (exactly).

The time-delay measurement is mechanized differently for pulse-type radars than for the continuous wave frequency shift measurement of the GRARR system. A pulse of very short duration is transmitted at the same instant that a reference frequency counter is triggered. The number of cycles C_1 of this reference ν_{R_1} is accumulated until the echo pulse is received. There is no ambiguity associated with this type of measurement.

Both the azimuth and elevation angles and the one-way range estimate are tagged at the ground reception time, t_S, in terms of UTC, corrected for the propagation delay from the National Bureau of Standards broadcasting station WWV to the tracking station. The data are then transmitted to GSFC in this form.

2.1.3 Minitrack Interferometer

The Minitrack short baseline interferometer system (Reference 6) consists of a series of six horizontal baselines at each station: three oriented east-west and three oriented north-south. A fixed-antenna system is located at each end of each baseline to receive a nominal 136-MHz signal (the spacecraft transmitter frequency can be preset to any of 2000 frequencies between 136.000 and 137.999 MHz in steps of 1 kHz) transmitted continuously from a spacecraft as it passes within view of the station. Each set of three (E-W or N-S) baselines consists of a fine, a medium, and a coarse baseline. The fine baselines are accurately surveyed to be 46 or 57 times the vacuum wavelength of the nominal 136-MHz signal. The medium baselines are 4.0 nominal wavelengths and the coarse ones are 3.5 wavelengths.

The geometry of the measurement on a baseline AB is illustrated in Figure 2-2 for the simple two-dimensional case. The spacecraft is presumed to be at an elevation angle, α, and displaced a very large distance from the grid compared with the length of the baseline. The baseline is expressed in multiples of N_B of the nominal wavelength. Therefore, the transmission arrives at the station in the form of essentially planar wavefronts BC and B'C'. At any given instant, the phase of the signal along the propagation paths AC' and BB' is shown as the two sinusoids. The separate signals received by the two antennas at A and B are fed to a phase counter which accumulates the number of cycles of a reference frequency from the time the counter is initiated until it is stopped. The fine counter reference frequency is 100 kHz. Although the actual mechanization is much more complicated, the effect is the same as though the counter were initiated by a positive-going zero crossing of the signal from A. The design of the circuitry is such that the phase difference count is normalized to the count for one complete cycle. Therefore, as illustrated in Figure 2-2, the measurement recorded is the fractional phase displacement, a_F. The fine baseline counters record fractional phase differences (fine phase counts) to three decimal digits: .000 to .999. The medium and coarse baseline counters record two decimal digits of the fractional phase differences: .00 to .99.

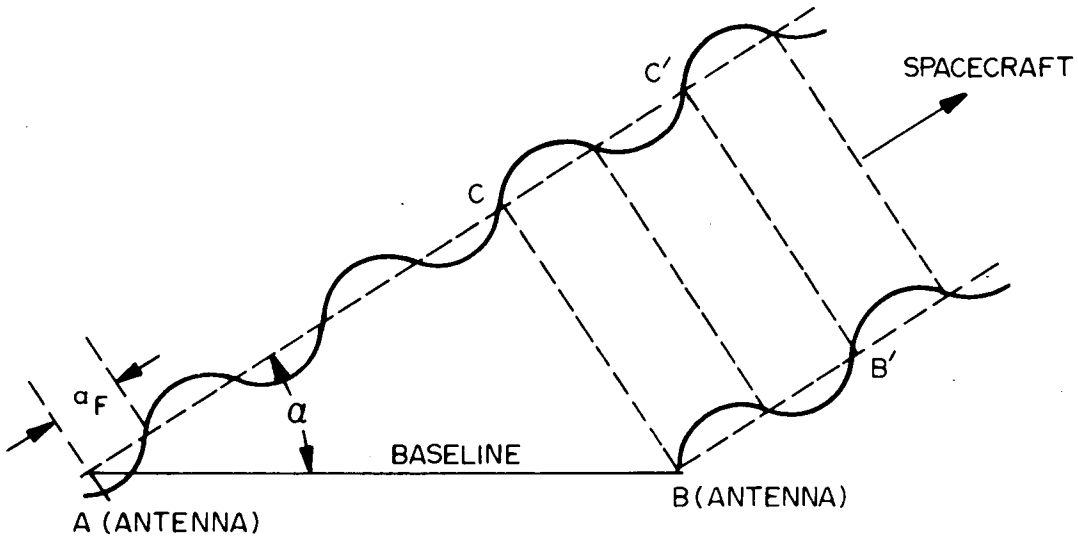

Figure 2-2. Minitrack Geometry (2-Dimensional)

A measurement on a single baseline gives no information concerning the extra number of whole wavelengths (two in the illustration of Figure 2-2) of the signal received along the path length to antenna A as compared with the parallel path to B. This ambiguous integral number, as well as the fractional phase displacement itself, is dependent upon the wavelength of the received signal and the length of the baseline, for a given spacecraft angular geometry α. Thus, the reason for the multiplicity of the parallel baselines is that the two smaller baseline measurements are necessary to resolve the integral cycle count ambiguity in the longer (fine) baseline. The difference between the medium (4.0 wavelength) and coarse (3.5 wavelength) baseline measurements corresponds to the reading for a fictitious 0.5 wavelength baseline. It would be impractical to build such a baseline and make the measurement directly because the antennas must be so large that they would physically interfere with each other. The 0.5 wavelength measurement is unambiguous since the extra path length, corresponding to AC in Figure 2-2, must be less than one wavelength. By similarity of the triangles, the absolute length of path AC to the fine baseline may be estimated from the 0.5 wavelength value by the ratio of the two baselines. The actual procedures used in the reduction during data preprocessing are more complicated than the simple explanation given here to ensure the highest possible accuracy in the ambiguity resolution. The principle, however, is essentially as described and serves to illustrate that the purpose of the measurement is to determine the direction of the signal path to the spacecraft. For the two-dimensional case of Figure 2-2, the ratio

$$\cos \alpha = \frac{AC}{AB} \qquad (2\text{-}1)$$

determines the cosine of the elevation angle α. For the actual three-dimensional case, the corresponding ratios for the orthogonal baselines (E-W and N-S) give the direction cosines, ℓ and m, of the signal path at the station.

Some of the hardware aspects of the data recording system are described next, since they influence the data preprocessing procedure to be discussed in the following section. Each fine baseline has its own phase difference counter, hence two measurements (E-W and N-S) are recorded simultaneously. The four ambiguity baselines (two for each fine baseline) share a single counter through a multiplexed digital recording system. Since all measurements cannot be made simultaneously, the sequence of recordings for each data frame occurs according to the schedule of Table 2.1. These data may be recorded at the rate of one frame every 1, 2, 10, 20, or 60 seconds.

Table 2-1
Minitrack Counter Sequence

Time Registered by Minitrack Data Clock	Initiation of Both Fine Baseline Counters	Initiation of Ambiguity Counter and Baseline Sampled
t_F*	X	E-W Medium
t_F + 0.2 sec	X	E-W Coarse
t_F + 0.4 sec	X	N-S Medium
t_F + 0.6 sec	X	N-S Coarse
t_F + 0.8 sec	X	

* t_F = GMT at the beginning of the frame

The fine baseline counter registers a decimal number between .000 and .999. This decimal number is referred to in the preprocessor as a number of counts which varies from 0 to 999. For example, 87 counts correspond to a decimal reading of .087. The medium and course baseline counter registers a decimal number from .00 to .99. This decimal number is referred to as a number of counts which varies from 0 to 99.

The frame rate generally is scheduled so that 30 frames give complete coverage of the usable data for a spacecraft pass over a station. A message,

consisting of up to 31 frames, is punched on paper tape at the tracking station in standard Baudot 5-level teletype code and transmitted via teletype to GSFC for preprocessing.

2.2 PREPROCESSING FOR OPTION A (METRIC) PROCESSING

In this section, methods are presented for preprocessing the tracking data for processing option A. This option requires the largest number of corrections to be made by the preprocessor. It, furthermore, corresponds to the preprocessor/processor interface most commonly used in post-orbit determination systems. Current GSFC preprocessing methods have been maintained intact to the maximum extent possible. Careful study has indicated the desirability of certain modifications, however, and these have been incorporated where appropriate. With one exception, output formats of the modified preprocessor are identical with programs already in use. Hence the GTDS is compatible with both the existing preprocessors as well as the one modified and described herein.

Present procedures for preprocessing GRARR and Minitrack observations consist of fitting low order polynomials to selected segments of the raw data. This provides a convenient method for editing the data by eliminating wild points which differ from the polynomials more than a preselected factor (usually three) times the standard deviation of the segment. The polynomial curve-fitting is also used as a method of smoothing and compressing data by replacing a series of actual measurements by a point interpolated from the polynomial.

The estimation procedure used in the ODS assumes that the data consist of true or perfect measurements plus random noise. The polynomial smoothing and/or compacting can introduce bias error and correlation into the data, thus violating the above-mentioned assumption. The violation is particularly serious if multiple data points are interpolated from the same polynomial or if the data segments for the polynomials overlap. Caution should be exercised to minimize such occurrences.

This presmoothing of the data may be beneficial in cases where the spacecraft is spinning at a rate which is slow compared with the data rate. The location of the antenna off the spin axis, coupled with the directional variations in the antenna pattern, combine to cause the data to oscillate at the spin frequency with small amplitude about the mean orbital variation. At best, this unmodeled oscillation would cause the noise level of the data to appear to be higher than it should. At worst, an erroneous bias in the data could appear if the data rate happened to be commensurate with the spin rate. Polynomial smoothing can effectively remove such oscillations. In the case of the Doppler data, these oscillations can

be prevented from affecting the raw data by counting over an interval at least as large as (and preferably some multiple of) the spin period.

In the three following sections, the metric preprocessing procedures are described for the GRARR, C-Band, and Minitrack systems. Simplifying assumptions made in the various reduction methods are pointed out.

After the conversion of each data type to metric form, the observation components are stored in the permanent data base with the appropriate time tag (in UTC). The data must be identified according to type, spacecraft, and tracking station. In addition, the transmission frequency must be given to facilitate the determination of the refraction effect in the GTDS processing later.

2.2.1 GRARR (VHF) System

2.2.1.1 Gimbal Angles

For the sake of compatibility with existing preprocessing procedures, the receive antenna gimbal pickoff angles, X and Y, are left unmodified. The time tag, however, is changed from the recorded measurement frame time t_F to correct for the downlink light time. The geometry of the downlink transmission path is shown in Figure 2-3, assuming no atmospheric refraction and straight line signal propagation.

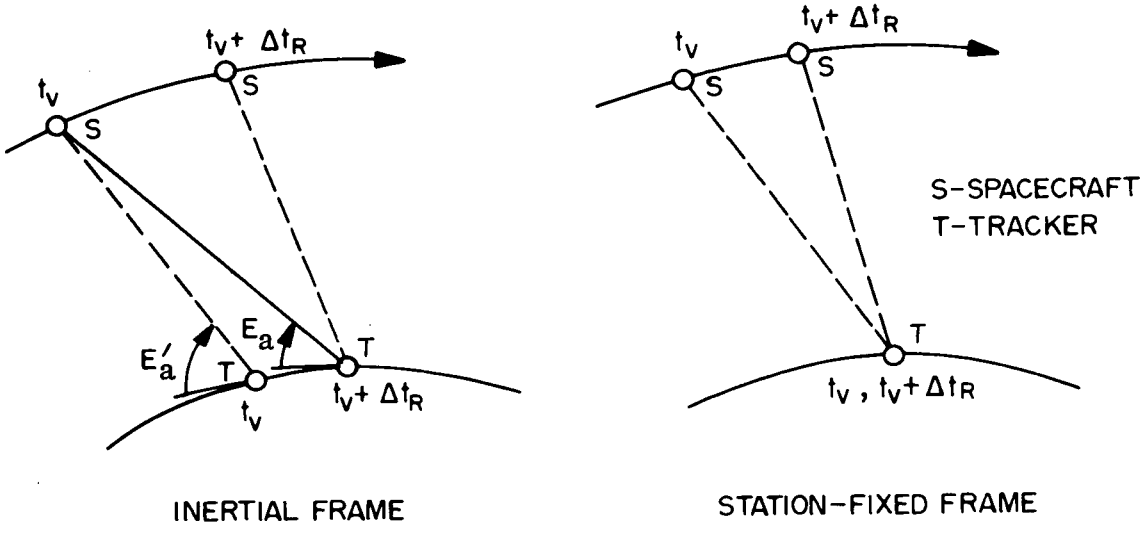

Figure 2-3. Downlink Transmission Path

The sketch on the left portrays signal paths in an inertial frame, whereas that on the right depicts them in a station-fixed system. The dashed lines represent instantaneous position vectors. The solid line (on the left) represents the true propagation path from the vehicle at time t_V to the tracking station at time $t_V + \Delta t_R$. This is the line which makes the observed angle E_a with the local horizontal and the X- and Y-gimbal angles on the antenna mount. One may conclude that since the station appears fixed in the figure on the right, the dashed line emanating from the vehicle at t_V is also the solid propagation path and also makes the angle E_a with the horizontal and the observed X- and Y-gimbal angles. But this is not true and it gives rise to an apparent discrepancy. This relative position vector makes the angle E_a' the same as the instantaneous relative position vector at time t_V in the left-hand sketch. The apparent discrepancy is explained when one realizes that the signal propagation path must appear to be curved in the rotating coordinate system on the right. Although the curvature is small, neglect of this effect is tantamount to neglecting the motion of the tracking station over the downlink propagation time interval, Δt_R.

Reference 7 reveals that the light-time correction for the DODS program neglects tracking station motion over the propagation time and assumes that E_a' is equal to E_a. This same assumption is made in GTDS, but the approximate light time correction is made in the preprocessor, rather than in the processor. Accordingly, the angle data (X, Y) is time-tagged as

$$t_A = t_F - \Delta t_R \tag{2-2}$$

where Δt_R is the one-way light time for the range sample corresponding to this angle measurement (at frame time $t_F = t_V + \Delta t_R$). The one-way light time correction is developed for the range measurement which follows (see Equation (2-8). These data are treated as instantaneous relative position vector components.

2.2.1.2 Range

The sample time for the range and range-rate data is determined for the appropriate sample in the frame to be

$$t_S = t_F + K t_{DR} \tag{2-3}$$

where

$K \sim 0, 1, 2, 3$ (the sample in the frame)

$t_{DR} \sim$ the time increment between consecutive samples, e.g., $t_{DR} = .5$ second for a data rate of two samples per second.

The Doppler count time increment is the ratio of the Doppler cycle count and the reference signal frequency

$$\Delta t_{RR} = \frac{C_0}{\nu_{R_2}} \tag{2-4}$$

From this, a time-averaged uplink Doppler frequency is computed as one-half the two-way average

$$\overline{\nu}_{du} = \frac{1}{2}\left(\frac{N}{\Delta t_{RR}} - \nu_b\right) \tag{2-5}$$

The spacecraft transponder delay depends upon the deviation of the received (uplink) signal from the nominal carrier frequency

$$\Delta\tau = f\ (\nu_{du}) \tag{2-6}$$

where f is assumed to be a known function. Reference 1 indicates that $\Delta\tau \approx 20$ microseconds for VHF transponders. The maximum one-way range error incurred if the transponder delay is neglected is 2.7 km. This warrants a reasonably accurate approximation for the value of $\Delta\tau$, or more precisely, the estimate of ν_{du}. The time-average of ν_{du}, given by Equation (2-5), is used to determine the transponder delay

$$\Delta\tau = f\ (\overline{\nu}_{du}) \tag{2-7}$$

The one-way light time is therefore

$$\Delta t_R = \frac{1}{2}\left[\frac{C_1}{\nu_{R_1}} + \frac{\rho_a}{\nu_L} - \Delta\tau - \Delta t_{RB}\right] \tag{2-8}$$

where

$C_1 \sim$ range cycle count

$\nu_{R_1} \sim$ range reference frequency (in Hz)

$\rho_a \sim$ range ambiguity number

$\nu_L \sim$ lowest sidetone frequency (8 Hz)

$\Delta t_{RB} \sim$ the two-way measurement bias which must be determined on-site by tower calibration

$\Delta\tau \sim$ transponder delay.

The one-way range is

$$\rho = c\,\Delta t_R \tag{2-9}$$

where

$c \sim$ the vacuum speed of light.

The data sample time, t_S, given by Equation (2-3), corresponds to the time that the range measurement of the received signal was begun. Therefore, the end of the measurement occurs at

$$t_{RM} = t_s + \frac{C_1}{\nu_{R_1}} - \Delta t_{RD}. \tag{2-10}$$

Note that the time of the return signal, t_{RM}, does not involve the range ambiguity number, ρ_a, since its effect would be to erroneously increase the return time rather than decrease the transmission time, t_S. The range ambiguity can be accounted for in the gross logic of the process since its omission accounts for a large range error of 18,737 kilometers. The range measurement delay term, Δt_{RD}, accounts for the combined effects of signal propagation delay between the antenna

and the counter and the delay in the counter itself. It must be determined by on-site equipment calibration.

Finally, under the assumption that the tracking station moves with uniform inertial velocity over the two-way time interval, the one-way range given by Equation (2-9) corresponds approximately to the instantaneous one-way relative range at the time

$$t_R = t_{RM} - \Delta t_R . \tag{2-11}$$

2.2.1.3 Range-Rate

The interpretation of the Doppler cycle count as a measure of the tracking station-to-spacecraft relative range-rate rests upon two very important assumptions:

- The Doppler effect can be adequately represented by the theory of special relativity.
- Some simplification must be made in the representation of the tracking station motion.

Assuming that the tracking station motion is uniform in inertial space, it is shown in Appendix A and Reference 5 that the average range-rate (in the sense of the Theorem of the Mean) over the time interval t_S to $t_S + \Delta t_{RR}$ is

$$\dot{\rho}_{avg} = \frac{c\left(\nu_b - \dfrac{N}{\Delta t_{RR}}\right)}{2\nu_T - \left(\nu_b - \dfrac{N}{\Delta t_{RR}}\right)} \tag{2-12}$$

where Δt_{RR} is the Doppler-plus-bias count time increment given by Equation (2-4). The metric observation is time tagged at t_{RR}, the midpoint of the vehicle turnaround time increment corresponding to the receiving station count interval Δt_{RR}. This is approximately given by (see Appendix A)

$$t_{RR} = t_S - \Delta t_R + \left[\frac{\nu_T - \nu_b + \dfrac{N}{\Delta t_{RR}}}{2\nu_T - \nu_b + \dfrac{N}{\Delta t_{RR}}}\right]\Delta t_{RR} \tag{2-13}$$

An alternative means of preprocessing the Doppler data is by means of the familiar range-difference formula

$$\Delta\rho = \frac{c}{\nu_T}(\nu_b \Delta t_{RR} - N) \tag{2-14}$$

where $\Delta\rho$ is the observed uplink plus downlink range difference at times $t_S + \Delta t_{RR}$ and t_S, i.e.,

$$\Delta\rho = (\rho_u + \rho_d)_{t_S+\Delta t_{RR}} - (\rho_u + \rho_d)_{t_S} \tag{2-15}$$

The observation components passed to the GTDS processor are $\Delta\rho$, Δt_{RR}, and t_S.

2.2.2 C-Band Radar

2.2.2.1 Gimbal Angles

The azimuth angle, A, and apparent elevation angle, E_a, are converted from the units in mils (designated with primes), as received from the tracking stations, to units of degrees (without primes)

$$A = A'\left(\frac{9}{160}\right)$$

and

$$E_a = E_a'\left(\frac{9}{160}\right) \tag{2-16}$$

The time tag, corresponding to the ground receive time t_S, is corrected for light time just as for the GRARR data.

2.2.2.2 Range

The one-way range estimate is determined from one-way light time as follows

$$\rho = \Delta t_R c \tag{2-17}$$

where ρ is in kilometers, c is the speed of light, and Δt_R is the one-way light time given by

$$\Delta t_R = \frac{1}{2}\left[\frac{C_1}{\nu_{R_1}} - \Delta\tau - \Delta t_{RB}\right] \tag{2-18}$$

where

$\Delta\tau \sim$ the spacecraft transponder delay

$\Delta t_{RB} \sim$ a bias which must be determined by on-site calibration.

The ground reception time, t_S, would be appropriate for this estimate of range if the tracking station were motionless. However, it is more accurate to treat this one-way range estimate as an instantaneous relative range at the midpoint of the measurement interval. Accordingly, the time tag, t_R, for the range data is computed as

$$t_R = t_S - \Delta t_R \tag{2-19}$$

2.2.3 Minitrack

The following description of the Minitrack preprocessing procedures are abstracted from References 6 and 8. The equations presented for correction of the phase count data and/or the time tags for unequal cable lengths, filter time delays, antenna pattern distortions, and other calibration biases are presented without any discussion. An understanding of their derivations can be given only in terms of a detailed description of the hardware and circuitry.

Recall from the Minitrack system description in Section 2.1.3 that five phase-difference measurements are recorded for each data frame on the two fine baselines. During this time interval, just one phase-difference measurement is recorded for each of the four ambiguity (medium and course) baselines. The first objective of the preprocessor, accordingly, is to compress the fine data to a single smoothed value at the midpoint $t_F + 0.4$ second of the frame time interval. The five consecutive fine phase differences (for either fine baseline) are denoted $a_1, a_2, \ldots, a_5$. For spacecraft orbiting earth at altitudes above 120 kilometers, the absolute phase difference between consecutive 0.2 second readouts is less than 500 counts. Since the counter registers only from 0 to 999 counts, it is possible that a difference $\delta_i = a_{i+1} - a_i$ may be negative and numerically larger than 500. This means that a new cycle crossing occurred during the count and that the measured data should be rectified to correct for the missing thousandth place readout. The first differences of the five data points are

$$\delta_1 = a_2 - a_1$$

$$\delta_2 = a_3 - a_2$$

$$\delta_3 = a_4 - a_3 \qquad (2\text{-}20)$$

$$\delta_4 = a_5 - a_4 \,.$$

The rectification process consists of sequentially testing each difference, δ_i, to determine if it lies in the range $-500 < \delta_i < 500$. If δ_i is within the range, no rectification occurs and the next difference is tested. If $\delta_i \geq 500$, then integer multiples of 1000 are subtracted from a_{i+1} until $-500 < \delta_i < 500$. If $\delta_i \leq -500$, then integer multiples of 1000 are added to a_{i+1} until $-500 < \delta_i < 500$.

A cubic polynomial is next least-square fitted to the five rectified points. The value interpolated at the midframe time $t_F + 0.4$ is

$$a_m = a_3 + \frac{9(\delta_3 - \delta_2) + 3(\delta_4 - \delta_1)}{35} \qquad (2\text{-}21)$$

and the average fine phase rate for the frame is estimated to be

$$\dot{a}_F = \frac{5}{4}(\delta_1 + \delta_2 + \delta_3 + \delta_4) \qquad (2\text{-}22)$$

The time corresponding to the smoothed midframe value in Equation (2-21) must be corrected to account for the fact that the counter requires a finite time to measure a changing signal. The fine counter frequency is 100 kHz; thus, each fine count takes 10^{-5} second. The time required for a_3 counts is

$$\Delta t_3 = a_3 (10^{-2}) \qquad (2\text{-}23)$$

and the corrected midframe time is

$$t_m = t_F + 0.4 + \Delta t_3. \qquad (2\text{-}24)$$

As noted earlier, the phase counters register only from 0 to 999 counts. Therefore, these readings must be rectified by converting them to a nonmodular number set in order to fit the data with polynomial curves over the 31-frame data arc. The ambiguity baseline readouts are considered first. It is assumed that the maximum difference between consecutive readings is less than 500. An indicated difference larger than this implies that a new cycle crossing has occurred. A numerical procedure is, again, used to rectify the readings, based on the first differences, δ_i, calculated as shown in Equation (2-20) for the 31 values. Each difference is sequentially tested. If it lies within the range $-500 < \delta_i < 500$, the data point a_{i+1} is unaltered and the next difference is tested. If $\delta_i \geq 500$ or $\delta_i \leq -500$ then integer multiples of 1000 are subtracted or added to a_{i+1} respectively, until the difference, δ_i, lies within the range $-500 < \delta_i < 500$. The resulting sequence of rectified values, $\bar{b}_{A_i}$, have the correct relative phase but differ from the correct absolute phase values, $\bar{\bar{a}}_i$, by an integral number.

A quadratic polynomial in time

$$\bar{C}_A(t) = A + B\,t + C\,t^2 \tag{2-25}$$

is next least-squares fitted to the rectified ambiguity data, $\bar{b}_{A_i}$. The times, t_i, corresponding to the data, b_{A_i}, must account for the multiplexing sequence within the frame shown in Table 2-1, as well as for the signal delay between the time of arrival at the baseline and the time at the counter due to a 2-Hz filter ($\Delta t = -0.15$ second). Combination of these effects gives the following transformations from the indicated frame times, t_{F_i},

$$t_i = t_{F_i} + \Delta t_A \tag{2-26}$$

where

$$\Delta t_A = \begin{cases} -0.15 & \text{E-W Medium} \\ 0.05 & \text{E-W Coarse} \\ 0.25 & \text{N-S Medium} \\ 0.45 & \text{N-S Coarse} \end{cases} \tag{2-27}$$

The polynomial smoothing procedure employs a sigma-rejection criterion for editing out wild points. A sigma multiplier of 2 gives the best results (Reference 8). Successive fits to the data are made until no further data rejection occurs.

The same rectification and polynomial fitting are now done to the 31 fine baseline data points calculated previously at the midframe times. The fine data rectification procedure is somewhat more complicated than that for the ambiguity data since the phase change between successive frames can be greater than 500 counts. An approximation to the phase change from one frame to the next is computed by estimating the fine phase rate, $\tilde{\dot{a}}_F$, and multiplying by the time increment, Δt_F, between frames. The rate estimate

$$\tilde{\dot{a}}_F = \frac{N_F}{2}\left(\frac{B_C}{3.5} + \frac{B_M}{4}\right) \tag{2-28}$$

is determined as the simple average of the ratioed midframe (relative to the 31 frame arc) slopes of medium and coarse smoothing polynomials. The value of N_F is 46 or 57, depending upon which fine baseline length was used. A numerical procedure, similar to that used previously, is used to rectify the a_i by means of the differences

$$\delta_i = a_{i+1} - a_i - \tilde{\dot{a}}_F \Delta t_F . \tag{2-29}$$

The relative phase adjusted data, $\bar{b}_{F_i}$, is then least-squares fitted with a polynomial. The procedure is identical with that for the ambiguity data except that a cubic polynomial

$$\bar{C}_F(t) = A + Bt + Ct^2 + Dt^3 \tag{2-30}$$

is used rather than the quadratic. The times in Equation (2-30) must account for the data formatting increment of 0.4 second and the 10-Hz filter delay Δt_{FF}

$$t_i = t_{F_i} + 0.4 - \Delta t_{FF} . \tag{2-31}$$

A single point is next interpolated from each of the six polynomials, corresponding to the (arbitrarily selected) E-W fine baseline midframe time

$$\bar{C}_{M_{E-W}},\ \bar{C}_{M_{N-S}},\ \bar{C}_{C_{E-W}},\ \bar{C}_{C_{N-S}},\ \bar{C}_{F_{E-W}},\ \bar{C}_{F_{N-S}}. \tag{2-32}$$

A calibration correction for each baseline is then applied to these interpolated values

$$\begin{aligned} \bar{C}'_F &= \bar{C}_F - Z_F \quad \text{(fine data)} \\ \bar{C}'_A &= \bar{C}_A - Z_A - \frac{\Delta L_A}{.846}(136.5 - \nu_V) \quad \text{(medium and course data).} \end{aligned} \tag{2-33}$$

The correction terms, Z, account for errors in baseline orientations, errors in locations of centers of antennas, inequalities in lengths of cables to counters, etc. These calibration corrections are determined partly by elaborate procedures at infrequent time intervals and partly by test procedures just prior to each pass. The additional correction term for the ambiguity baseline data accounts for the effect of differences in the signal frequency, ν_V (in MHz), from the calibration frequency of 136.5 MHz. The quantity, ΔL_A, represents the measured difference in cable lengths from the two antennas to the counter. There is no corresponding term for the fine baseline cables because they were carefully measured at installation to be equal in length.

Finally, the corrected relative phase adjusted values $\bar{C}'$ are truncated to their fractional parts

$$a = [\bar{C}'] \tag{2-34}$$

where the brackets indicate fractional part. The time (common for all six data) is corrected for the WWV propagation delay.

The ambiguity resolution is made next to the fine data. A fictitious half wavelength baseline is determined (unambiguously) from the 3.5 and 4.0 wavelength baseline data. This estimate is ratioed to resolve the ambiguities of those

(medium and coarse baseline) data. In turn, the resolved data are added to construct data for another fictitious baseline of wavelength 7.5. Finally, this value is ratioed to the fine baseline length to resolve the ambiguity there. Using the symbols

[ ] to denote fractional part

{ } to denote minimum phase difference (i.e., $-500 < \{\ \} \leq +500$.)

The procedure is as follows:

$$
\begin{aligned}
\bar{a}_{0.5} &= \{a_{4.0} - a_{3.5}\} \\
\bar{a}'_{3.5} &= 7\,\bar{a}_{0.5} \\
\bar{a}_{3.5} &= \bar{a}'_{3.5} - \{[\bar{a}'_{3.5} - a_{3.5}]\} \\
\bar{a}'_{4.0} &= 8\,\bar{a}_{0.5} \\
\bar{a}_{4.0} &= \bar{a}'_{4.0} - \{[\bar{a}'_{4.0} - a_{4.0}]\} \\
\bar{a}_{7.5} &= \bar{a}_{3.5} + \bar{a}_{4.0} \\
\bar{a}'_F &= \bar{a}_{7.5}\,(N_F/7.5) \\
\bar{a}_F &= \bar{a}'_F - \{[\bar{a}'_F - a_F]\}
\end{aligned}
\qquad (2\text{-}35)
$$

where N_F is the fine baseline length in terms of vacuum wavelengths of the nominal 136.0-MHz frequency (either 46 or 57).

The calibration correction given in Equation (2-33) was determined as an average over the usable antenna field. There are distortions in this field pattern, however, and these effects may be corrected now that the ambiguities have been resolved. The resolved fine data are corrected according to polynomials of the form

$$
\begin{aligned}
\bar{a}_x = {} & C_0 + C_1\,\bar{a}_{E\text{-}W} + C_2\,\bar{a}_{N\text{-}S} + C_3\,\bar{a}_{E\text{-}W}\bar{a}_{N\text{-}S} \\
& + C_4\,\bar{a}^2_{E\text{-}W} + C_5\,\bar{a}^2_{N\text{-}S} + C_6\,\bar{a}^3_Y \\
& + C_7 \sin(2\pi\,\bar{a}_X) + C_8 \cos(2\pi\,\bar{a}_X)
\end{aligned}
\qquad (2\text{-}36)
$$

where

subscript X ~ E-W or N-S, depending upon the baseline orientation

subscript Y ~ E-W or N-S, depending upon the antenna field orientation

C_i ~ polynomial coefficients depending upon baseline and antenna field orientations.

The absolute (fine) phase differences, a'_F, could be converted to direction cosines of the received signal path if the baseline length were known in terms of the wavelength of the received signal. The received signal wavelength is not known at this stage of data preprocessing. The stationary vacuum value is altered due to a Doppler-shift effect and also due to an atmospheric refraction effect. It is, therefore, convenient to write the preprocessor data output in the form of fictitious direction cosines

$$\ell' = \frac{\bar{a}'_{F_{E-W}}}{N_{F_{E-W}}} \left(\frac{136.0}{\nu_V} \right)$$

$$m' = \frac{\bar{a}'_{F_{N-S}}}{N_{F_{N-S}}} \left(\frac{136.0}{\nu_V} \right) \qquad (2\text{-}37)$$

These direction cosines would be correct if the tracking station and spacecraft were relatively motionless and if there were no atmpsphere. The terms N_F are the baseline lengths in terms of vacuum wavelengths of the nominal 136.0-MHz frequency signal. The ratio, $136/\nu_V$, corrects for the deviation of the spacecraft transmitter frequency, ν_V, (in MHz) from the nominal value.

The pseudo direction cosines, in Equation (2-37) are stored in the data base, together with the time tag, the tracking station and the spacecraft identification, and the transmitter frequency, ν_V. Note that it has not been possible to correct the Minitrack data for light time in the preprocessor. Therefore, unlike other data types described above in the metric mode, the Minitrack data do not represent estimates of components of instantaneous relative position vectors. This necessitates making a light-time correction to this data type in the data processing within the GTDS. This will be discussed in Chapter 7.

2.3 OPTION B (POLYNOMIAL PREPROCESSING)

The basic philosophy underlying the polynomial option processing is to minimize the assumptions made in converting the raw data to spacecraft state vector components so as to preserve the highest fidelity of representation. In the metric preprocessor, discussed in Section 2.2, many simplifying assumptions are made in deriving the relationships which convert the actual measurements of propagation characteristics of electromagnetic waves to estimates of spacecraft state relative to the tracking station. Since the ultimate comparison of computed and actual observations yields an accurate determination of the orbit, the polynomial preprocessor does not attempt to convert the actual data to state quantities. Instead, it makes calibration corrections to eliminate known instrumentation errors and converts to more convenient units. The "bridging of the gap" between the actual measurements and the spacecraft state is left entirely to the processor in the GTDS. In the GTDS, the relative state vector components, available from the estimated orbit, are used to compute the same observation quantity that is output by the preprocessor. This latter quantity may be characterized as "near-raw" data.

Polynomial and other curve fits are utilized in the preprocessors for the various types of measurements. Such curve fits are employed solely for rejection of wild data points, for obtaining estimates of statistical properties of data (prior to entry into the GTDS), and for resolution of ambiguities in the measured data. Data smoothing and/or compression is not accomplished by interpolation of points from fitted curves. As pointed out in Section 2.2, such interpolation can introduce bias and correlation into supposedly true data with random noise and seriously degrade the information content in the data. Data compression in the polynomial mode is accomplished, if desired, by selection of every n^{th} point, where the user specifies n.

Each time a tracking observation is made, the time is recorded in a convenient time system. The purpose of the time identification is to permit subsequent correlation of the observation geometry with the precise geometry of the planets' relative positions, and the earth's exact orientation in space. The measurement time system used for data tagging is atomic, A.1, time or a derivative of it, such as the UTC signal transmitted by radio station WWV. The planetary positions are given by an ephemeris defined by gravitational theory. The independent time argument of this theory is ephemeris time, ET. Spacecraft tracking data time tags are therefore converted to ET within the GTDS System. This conversion, of necessity, is based upon the current ephemeris.

The conversion of the raw tracking data to metric components of the relative state vector requires the use of the vacuum speed of light in absolute units in Equations (2-10) and (2-13). The subsequent determination of the computed

observations in the GTDS data processor implies that the state components (ρ and $\dot{\rho}$ in the examples) be expressed in the same units. Since the ephemeris is scaled only in terms of the speed of light, c, proper correlation with the preprocessed data can be ensured if the same value of c is used in the GTDS as was used in the preprocessor. Potential problems are avoided altogether in the proposed polynomial mode by not using c to convert the raw data to metric quantities. In the context of the data types described earlier, this requires that range data be left in the form of the measured time delays and that range-rate data be expressed in terms of counted cycles of the Doppler-shifted frequency over the measurement time interval.

2.3.1 GRARR

2.3.1.1 Gimbal Angles

The X- and Y-gimbal angle data are left unmodified. The time tag is not corrected for light time as was done in Section 2.2.1. Instead the tag is left as the frame time t_F, corresponding to the true time of measurement of the signal direction as received at the antenna. This necessitates a more sophisticated method of modeling the observation in the GTDS processor, described in Chapter 7.

2.3.1.2 Range and Range-Rate

The range and range-rate sample times, t_s, are determined by Equation (2-3). The Doppler count time increment, Δt_{RR}, is computed by Equation (2-4) and the transponder time delay is estimated by Equations (2-5) and (2-7). The round-trip light time is given by this obvious modification of Equation (2-8)

$$\Delta t_R = \frac{C_1}{\nu_{R_1}} + \frac{\rho_a}{\nu_L} - \Delta\tau - \Delta t_{RB}. \tag{2-38}$$

If the time-varying differenced Doppler signal frequency is ν_d and the (constant) bias signal frequency is ν_b, the count of N cycles over the interval t_S to $t_S + \Delta t_{RR}$ can be approximated mathematically by an integral. The representation is approximate in the sense that the counter accumulates whole numbers, whereas the integral gives a continuously variable whole number plus fraction. For large count ($N \approx 6 \times 10^6$ cycles at the slowest data rate), this error, of at most one cycle, becomes negligible. The integral is

$$N = \int_{t_S}^{t_S + \Delta t_{RR}} [\nu_d(\tau) + \nu_b]\, d\tau = N_d + \nu_b \Delta t_{RR} \tag{2-39}$$

where

$$N_d = \int_{t_S}^{t_S + \Delta t_{RR}} \nu_d (\tau)\, d\tau . \tag{2-40}$$

This latter quantity is modeled into the GTDS. The preprocessing computation is derived from Equation (2-39) as

$$N_d = N - \nu_b \Delta t_{RR} . \tag{2-41}$$

This quantity should not be truncated to a whole number. Observe that, whereas N is guaranteed to remain positive by the addition of the bias signal of sufficiently high frequency, the sign of the Doppler count, N_d, depends upon whether the relative range is increasing or decreasing. The time tag associated with this data point is the sample time t_S.

The data output by the preprocessor consists of:

Angles:	X, Y at time $t_A = t_F$
Round-trip light time:	Δt_R at time $t_R = t_S$
Doppler count:	N_d, Δt_{RR} at time $t_{RR} = t_S$

The transmitter frequency, ν_T, station ID, and satellite ID are also required.

2.3.2 C-Band Radar

2.3.2.1 Gimbal Angles

The preprocessing of the C-band azimuth and apparent elevation data consists only of converting the units from mils to degrees, exactly as given in Equation (2-16). The time tag is left as the ground receive time t_S (not corrected for light time).

2.3.2.2 Range

The one-way range is specified by the two-way light time derived from Equation (2-18).

$$\Delta t_{RT} = \frac{C_1}{\nu_{R_1}} - \Delta\tau - \Delta t_{RB} \tag{2-42}$$

The time tag is left as the ground receive time, t_S.

The data output consists of the time tag, t_S, the angles, A and E_a, the round-trip light time, Δt_{RT}, the station and satellite ID's, and the transmitter frequency, ν_T.

2.3.3 Minitrack

The procedure for preprocessing the Minitrack data follows that described in Section 2.2.3 with several significant variations. Similar to Section 2.2.3, the procedure consists of initially rectifying the fine baseline data by testing the first differences

$$\delta_i = a_{i+1} - a_i \qquad (i = 1, 2, 3, 4) \tag{2-43}$$

The average fine phase rate for the frame is then computed by Equation (2-22), as before. The data compression, however, does not involve interpolation from the fitted (cubic) polynomial. Rather, the deviation of the midpoint phase count from the polynomial is computed from Equation (2-21) as

$$\delta a_3 = a_m - a_3 = \frac{9(\delta_3 - \delta_2) + 3(\delta_4 - \delta_1)}{35} \tag{2-44}$$

If this deviation is smaller than a tolerance $\epsilon > 0$, i.e.

$$|\delta a_3| < \epsilon$$

then a_3 is assumed to be a valid point and is taken as the fine phase data point $a_F = a_3$ for the frame. The fine phase counter time correction is applied, as described in Section 2.2.3, using Equation (2-23). The original five data points $a_1, \ldots, a_5$ are then discarded.

The data times are corrected for filter delays and proper account is taken of the multiplexing sequence within each frame to adjust all the data, for the 31 frames, to the corrected UTC time base. Equation (2-26) is used for the ambiguity baseline data and Equation (2-31) for the fine baseline data.

Calibration corrections are applied to the data points in all 31 frames as follows (see Equation (2-33) for definitions of the calibration terms)

$$\begin{aligned} a'_F &= \left[a_F - Z_F\right] \\ a'_A &= \left[a_A - Z_A - \frac{\Delta L_A}{.846}(136.5 - \nu_V)\right] \end{aligned} \tag{2-45}$$

The brackets, [ ], denote that the quantities are truncated to the appropriate fractional part. If application of the correction terms causes the value to fall outside the range 0 to 999, the integer 1000 is added or subtracted as necessary to restore a′ to the desired fractional range. It is assumed that the correction terms are less than one cycle.

The data rectification (determination of absolute relative phase change between successive samples) and the ambiguity resolution in the polynomial preprocessor differ in absolute magnitude from that of the metric procedure. The average fine phase rate, given by Equation (2-22), for each frame is converted to phase rates for the medium and coarse baselines by the ratios of the baselines:

$$\dot{a}_M = \frac{4.0}{N_F}\dot{a}_F$$

$$\dot{a}_C = \frac{3.5}{N_F}\dot{a}_F \qquad (N_F = 46 \text{ or } 57). \tag{2-46}$$

Note that these rates apply at the same times, given by Equation (2-31), for the fine phase data points. If these rates were numerically integrated over the 31 frames the resulting time-histories, $\bar{b}$, would define relative absolute phase change on each baseline. The problem is to determine the initial conditions for these integrations so that the resulting curves best fit the actual data points. We can write these initial conditions as

$$\bar{b} = a_1' + \beta \tag{2-47}$$

where

$a_1' \sim$ the first frame phase count data point with calibration correction (see Equation (2-45))

$\beta \sim$ the additive correction to be determined for best fit.

Clearly the value of β does not influence the shape of the integrated curve. It only serves to displace it vertically. Thus, the integral may be written

$$\bar{b} = \bar{b}_0 + \beta \tag{2-48}$$

where

$\bar{b}_0 \sim$ the integral with $\beta = 0$ in Equation (2-47).

An algorithm may now be written for determining β and, in the process, for rectifying the data. The procedure for rectifying the data, a_i, is an adaptation of one of the formalisms of Equation (2-35). Define

$$\bar{c}_i = \bar{b}_i - \{[\bar{b}_i - a_i']\} \tag{2-49}$$

where, again, the symbol [ ] denotes fractional part, and $\{\}$ denotes minimum phase difference.

The values, $\bar{b}_i$, must be interpolated from the curve b at the times corresponding to the corrected data points a_i'. If the data are rectified according to Equation (2-49), the squares of the residuals from the curve are

$$B_i = \left(\bar{b}_i - \bar{c}_i\right)^2 = \left\{\left[\bar{b}_i - a_i'\right]\right\}^2 = \left\{\left[\bar{b}_{0_i} + \beta - a_i'\right]\right\}^2 \tag{2-50}$$

and the sum of the squares of the residuals are

$$B = \sum_i B_i \tag{2-51}$$

We seek a value of β which will minimize B. Because of the nature of the operations implied by the symbols [ ] and { }, it is not possible to write an analytic expression which minimizes B. Therefore, it is necessary to evaluate Equations (2-50) and (2-51) numerically for different values of β and to search for that value of β which minimizes B by an appropriate algorithm (e.g., Newton-Raphson).

Thus, the rectification of the data may be accomplished according to Equation (2-49). A check may be made upon the reasonableness of the answers by computing the differences between the maximum and minimum linearized data points on each baseline

$$\delta_m = \bar{c}_{max} - \bar{c}_{min} \tag{2-52}$$

and requiring that

$$|\delta_m| \leq N \tag{2-53}$$

where

$$N = \begin{cases} 7 \text{ for coarse baseline} \\ 8 \text{ for medium baseline} \\ 2N_F \text{ (92 or 114) for fine baseline.} \end{cases}$$

The ambiguity is resolved on the basis of points interpolated from the integrated curves which satisfy the data. Points may be computed for a fictitious half wavelength baseline from points interpolated from the medium and coarse baseline rectification curves (see Equation (2-49)) at corresponding times t_i

$$\bar{a}_{0.5} = \{\bar{b}_M - b_C\} . \tag{2-54}$$

A convenient choice for the t_i is the fine baseline data times since the integration scheme will have computed the value of b_0 at these times. This may necessitate the vertical displacement of the b_M or $\bar{b}_C$ curve by some whole number of cycles.

These unambiguous half wavelength baseline points may now be ratioed to the appropriate fine baseline length

$$\begin{aligned} \bar{a}_F^* &= \frac{N_F}{0.5} \bar{a}_{0.5} \\ &= (92 \text{ or } 114)\, a_{0.5} . \end{aligned} \tag{2-55}$$

Finally, an integral number is determined by which to displace the fine baseline linearizing curve $\bar{b}_F$ and the rectified corrected data points $\bar{c}_F$ for best

fit to the ratioed data points $\bar{a}_F^*$. Recall that $\bar{b}_F$ and $\bar{c}_F$ have already been adjusted relative to each other for best mutual fit in the linearizing process. Denoting α to be the true displacement (not necessarily an integer) required for best fit of $\bar{b}_F$ to $\bar{a}_F^*$, then the sum of the squares of the residuals between $\bar{a}_{F_i}$ and the curve $\bar{b}_F$ for K data points, is

$$M = \sum_{i=1}^{K} \left(\bar{b}_{F_i} + \alpha - \bar{a}_{F_i}^* \right)^2 \tag{2-56}$$

M is extremized when

$$\sum_{i=1}^{K} \left(\bar{b}_{F_i} + \alpha - \bar{a}_{F_i}^* \right) = 0 \tag{2-57}$$

or when

$$\alpha = \frac{\sum_{i=1}^{K} \left(\bar{b}_{F_i} - \bar{a}_{F_i}^* \right)}{K} \tag{2-58}$$

This gives the true minimum value for M; however, we can only shift the curve by a whole number of cycles. Therefore, α must be rounded to the nearest integer

$$\alpha' = \alpha - \{[\alpha]\} \tag{2-59}$$

in our adopted notation. Finally, the resolved fine baseline data are obtained from

$$\bar{a}_{F_i} = \bar{c}_{F_i} + \alpha' \tag{2-60}$$

The antenna field distortion corrections are applied using Equation (2-36). The use of corrected data points rather than interpolated points should pose no problem in this equation. The fine baselines have their own individual counters, hence the data points on the two baselines should correspond in time. The only possibility for a time discrepancy to occur is through the filter delay term Δt_{FF} in Equation (2-31). Current procedures use the same fixed value for both baselines for this delay. Should a different value be found more appropriate, the correction in Equation (2-36) would have to be made using interpolated values on the right side.

The final reduction to fictitious direction cosines is made using Equation (2-37). Again, the E-W and N-S data should correspond in time, as noted above. If they do not, the ℓ' and m' direction cosines should be individually computed and time-tagged. There is no necessity for these data to be paired.

In conclusion, it is noted that this preprocessing procedure does not smooth the data. Compression must be accomplished, if required, by selection of every n^{th} point. The rectification procedure should work for all data recording rates. The metric data preprocessor, described in Section 2.2.3 could experience some difficulty at a very slow data rate (e.g., one frame per minute). This case would violate the assumption that the ambiguity baseline count changes by less than half a cycle between frames. The simple rectification procedure would fail in that case.

2.4 REFERENCES

1. Goddard Space Flight Center, X-551-69-137, A Review of Goddard Range and Range Rate System Measurements and Data Processing Techniques, T. J. Grenchik and E. H. Putney, April 1969.

2. Goddard Space Flight Center, X-551-69-3, The Conversion of Fundamental Tracking Data to Metric Form, P. E. Schmid, January 1969.

3. Goddard Space Flight Center, X-541-69-322, Description of the Goddard Range-Range Rate Data Processing Program for the CDC-160A, E. R. Watkins and D. H. Rose, August 1969.

4. Goddard Space Flight Center, X-571-69-149, Data Formats of the Goddard Range and Range Rate System and the Application Technological Satellite Range and Range Rate System, D. J. Zillig, April 1969.

5. Computer Sciences Corporation, Mathematical Modeling of Radar Tracking Observations of Spacecraft, D. H. Novak, January 1971.

6. Control Systems Research, Incorporated, Minitrack Tracking Function Description, March 1970.

7. Computer Sciences Corporation, 5023-02710-01TR, Definitive Orbit Determination Operating System Description. Edition II, November 1970.

8. Goddard Space Flight Center, TND-5042, Preprocessing of Minitrack Data, E. R. Watkins, May 1969.

CHAPTER 3

COORDINATES AND TIME SYSTEMS

The orbit determination process involves measurements that are taken and forces that are modeled in several different space and time coordinate systems. This chapter defines these systems and gives the necessary transformations and partials between them.

3.1 GENERAL COMMENTS AND DEFINITIONS

The GTDS coordinate systems consist of the fundamental astronomical reference systems and other systems that were originally borrowed from aeronautics and originated from special requirements of space exploration. Requirements for different coordinate systems occur from the following three sources.

- input data
- internal computations
- output requirements.

For example, the input ephemerides of the planets are heliocentric and refer to the mean equator and equinox of 1950.0. The input observational data is in a topocentric coordinate system. The integration is done in either geocentric, selenocentric, planetocentric, or heliocentric rectangular coordinates referred to the mean equator and equinox of 1950.0 or of a specified epoch. The force model includes terms referred to a coordinate system that is fixed in the rotating earth and terms that are referred to the moon and planets. The output requirements may be osculating elements with respect to the earth, moon, or planets. These specific coordinate systems are defined and discussed later in this chapter.

Since several different coordinate systems are used in GTDS, these systems must be defined and provision must be made for transforming from one coordinate system to another. A coordinate system is defined by specifying the origin of the coordinates, a reference plane, and a principal direction in the reference plane. This specification of the reference plane includes an identification of the positive, or north, or outward sense along the normal to the plane. The reference plane is an equivalence class of mutually parallel planes. For example, the equator is defined to be the plane normal to the earth's axis of rotation. Usually, this plane contains the earth's center of mass however, in heliocentric equatorial coordinates,

the parallel plane contains the sun's center of mass. To avoid any such difficulty, the celestial sphere of infinite radius is introduced, and the celestial equator is the intersection of the equatorial plane with the celestial sphere. This is another way of identifying the equivalence classes of parallel planes and parallel lines. The reference plane often refers to that member of the equivalence class that contains the origin of coordinates. The corresponding statement holds for the equivalence of parallel lines in defining a principal direction.

For rectangular coordinates, the x-y plane is the reference plane. The x-axis is the principal direction, the z-axis is along the positive normal or northern direction, and the y-axis is orthogonal to the x and z axes, thus forming a right handed system. For spherical coordinates, the first angle (azimuth, hour angle, right ascension, or longitude) is measured from the principal direction to the projection of the point on the reference plane. The positive sense is specified for each system. The second angle is measured perpendicularly from the reference plane to the line from the origin to the point, positive on the plane's northern or outward side. The third coordinate is the distance from the origin. Other specialized systems are discussed later.

The designations of coordinate systems, according to the location of the origin, are given in the following table:

Origin of Coordinates	Designation of System
The observer	Topocentric
The center of the earth	Geocentric
The center of the moon	Selenocentric
The center of the sun	Heliocentric
The center of mass	Barycentric

The following reference planes are used:

- The Horizon. Without further designation, the horizon is the plane tangent to the oblate ellipsoid earth model at a specified point on the surface. The outward normal is directed away from the earth model. For topocentric coordinates, the reference plane is the geographic horizon corresponding to the point on the earth model whose normal passes through the observer.

- The Equator. The equator is the earth's equator, unless otherwise specified. This is the plane normal to the earth's axis of rotation, and north is in the direction of the angular velocity vector of the rotation, also called the celestial pole. The moon's equator is defined in the corresponding way.

- The Ecliptic. The ecliptic is the earth-sun orbital plane and is a special case of the plane of an orbit. North is the direction of the System's angular momentum, also called the ecliptic pole.

- The Plane of an Orbit. The plane of an orbit is defined by two-body motion and north is the direction of the angular momentum. In the problem of more than two bodies, the osculating plane corresponds to the state at a given epoch or the mean plane that has the periodic perturbations removed. The principal direction is usually specified by giving the sense along the intersection of the reference plane with some other plane. The other plane is either a meridian plane, an equatorial plane, or another orbital plane. A meridian plane is defined as any plane that contains the axis of rotation of one of the principal bodies, either the earth or moon. Three particular cases are of interest:

  The Greenwich of Prime Meridian. The Greenwich meridian is the earth's meridian plane that passes through the Royal Observatory at Greenwich, England.

  The Lunar Prime Meridian. The lunar prime meridian is the moon's meridian plane that passes through the moon's mean center point (that point on the moon's surface that lies on the earth-moon line when the moon is at its mean longitude and mean ascending node).

  The Local Meridian. The local meridian is the earth's or moon's meridian plane that passes through the observer's position. This concept is not meaningful when the observer is situated on the axis of rotation.

These same terms are used to denote the corresponding principal directions in the equatorial plane (the positive sense being from the origin to the projection of the position of the observer or Greenwich, etc. onto the equatorial plane).

- The Vernal Equinox or Equinox. The equinox is the fundamental principal direction used in astronomy. It is defined as the intersection of the ecliptic and the earth's equator with the positive sense being from the earth to the sun as the sun crosses the equator from south to north.

- The Ascending Node. The ascending node is the intersection of an orbital plane and the reference plane with the positive sense being from the origin toward the orbiting body as it crosses the reference plane from the south to the north. Thus the vernal equinox is an ascending node.

The continuous motion of the equator, the ecliptic, and the equinox (precession and nutation) is discussed in Section 3.3.1.

3.2 COORDINATE SYSTEM DESCRIPTIONS

3.2.1 Body-Centered Inertial (Geocentric, Selenocentric, or Planetocentric)

Origin:	Center of the body
Reference Plane:	Earth equatorial plane of epoch
Principal Direction:	Vernal equinox of epoch

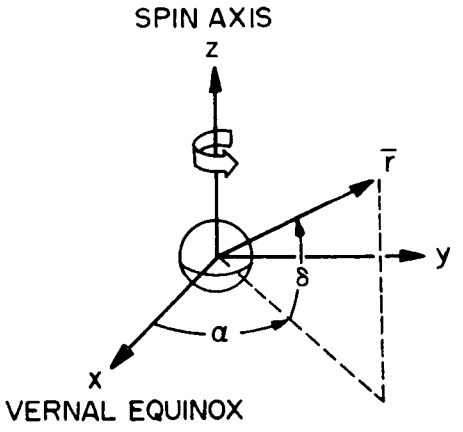

Figure 3-1. Body-Centered Inertial Coordinate System

Rectangular Cartesian Coordinates (see Figure 3-1):

x-axis ~ the principal direction
y-axis ~ the normal to the x-axis and z-axis to form a right-handed system
z-axis ~ the normal to the earth equator of epoch in the direction of the angular momentum vector

Within the following formulation, $\bar{R}$, X, Y, and Z designate the position vector and Cartesian coordinates referred to the mean equinox and equator of 1950.0. Similarly, $\bar{r}_E$, x_E, y_E, and z_E designate the position vector and Cartesian coordinates referred to the mean equinox and equator of epoch and $\bar{r}$, x, y, and z designate the position vector and Cartesian coordinates referred to the true equinox and equator of epoch.

Spherical Polar Coordinates:

$r \sim$ radial distance from the origin to the point being measured
$\alpha \sim$ right ascension, $\tan^{-1}$ (y/x)
$\delta \sim$ declination, $\sin^{-1}$ (z/r)

3.2.2 Body-Centered Rotating (Geographic or Selenographic)

Origin:	Center of the body
Reference Plane:	Body's equatorial plane (plane perpendicular to the axis of rotation at a given epoch)
Principal Direction:	Intersection of the prime meridian with the equator

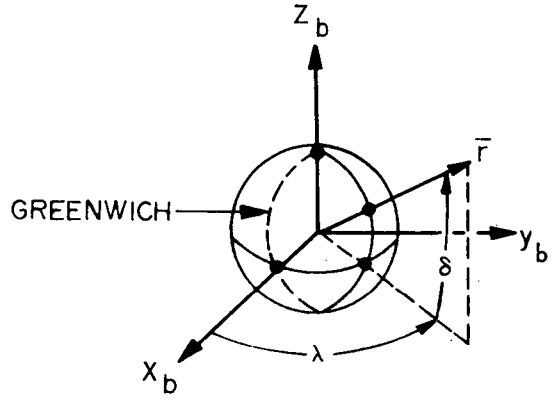

Figure 3-2. Body-Centered Rotating Coordinate System

Rectangular Cartesian Coordinates (see Figure 3-2):

x_b-axis $\sim$ the principal direction
y_b-axis $\sim$ the normal to the x_b and z_b axes to form a right-handed system
z_b-axis $\sim$ the direction of the axis of rotation toward the north celestial pole

Geocentric Spherical Coordinates:

$r_b \sim$ radial distance from the origin to the point being measured
$\lambda \sim$ longitude measured east from the prime meridian, $\tan^{-1}$ (y_b/x_b)
$\delta \sim$ latitude measured from the equator, $\sin^{-1}$ (z_b/r_b)

Geodetic Spherical Coordinates (see Figure 3-4):

$h \sim$ the perpendicular distance from the surface of the ellipsoid model to the point being measured
$\lambda \sim$ the same as longitude measured in the geocentric spherical coordinates
$\phi \sim$ the geodetic latitude angle between the vector normal to the ellipsoid model passing through the point of interest and the equatorial plane
$\phi' \sim$ the geocentric latitude of a point on the ellipsoid

Geodetic coordinates are used to reference a point from the surface of a body that is an ellipsoid of revolution rather than a sphere.

3.2.3 Local Plane System

Origin:	Center of the reference body
Reference Plane:	The axes are defined independently of a reference plane. The $x_{lp} - y_{lp}$ plane becomes the "reference plane"
Principal Direction:	The principal axis is along the radius vector from the origin to the satellite

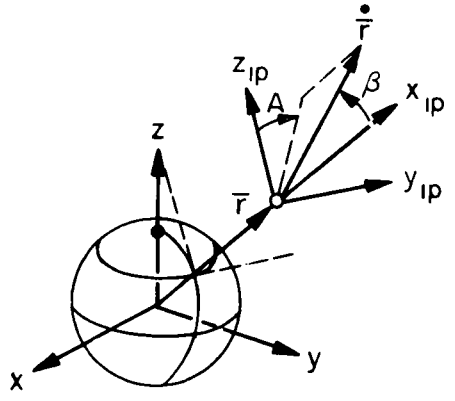

Figure 3-3. Local Plane System

Rectangular Cartesian Coordinates (see Figure 3-3)

x_{lp}-axis $\sim$ the principal direction
y_{lp}-axis $\sim$ the axis displaced from the inertial y-axis by the satellite's right ascension and lying in the original x-y plane
z_{lp}-axis $\sim$ the direction that forms a right-handed system with x_{lp} and y_{lp}. It is displaced from the inertial z-axis by the satellite's declination

Spherical Velocity Coordinates:

V ~ the velocity vector's magnitude ($|\dot{\bar{r}}|$)
β ~ the flight path angle measured from the principal direction to the velocity vector
A ~ the azimuth angle measured clockwise from the z_{1p} axis to the projection of the velocity vector on the y_{1p} - z_{1p} plane

3.2.4 Topocentric Local Tangent (East/North/Up)

Origin:	Observer (topocentric)
Reference Plane:	Plane tangent to the ellipsoidal earth model at the observer
Principal Direction:	Local east direction on the plane tangent to the earth model

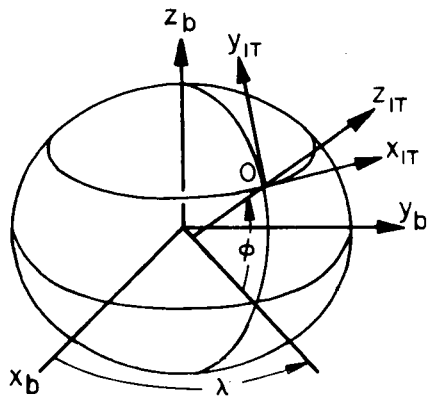

Figure 3-4. Topocentric Coordinates

Rectangular Cartesian Coordinates (see Figure 3-4):

x_{1t}-axis ~ the principal direction
y_{1t}-axis ~ the axis lying in the reference plane that points north
z_{1t}-axis ~ the upward direction along the geodetic vertical

3.2.5 Orbit Plane

Origin:	Center of the reference body
Reference Plane:	The plane of the orbit
Principal Direction:	The radius vector from the origin to the satellite

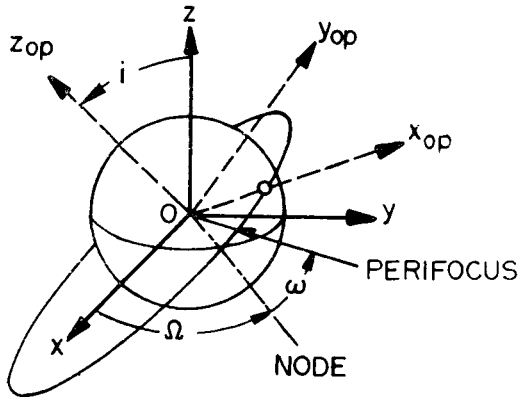

Figure 3-5. Orbit Plane Coordinates

Rectangular Cartesian Coordinates (see Figure 3-5)

x_{op}-axis ~ the direction along the satellite's position vector, $\bar{r}$
y_{op}-axis ~ the direction normal to x_{op} - z_{op} plane
z_{op}-axis ~ the direction along the vector $\bar{r} \times \dot{\bar{r}}$

The Cartesian components of the orbit plane system when the satellite is at perifocus are denoted x_p, y_p and z_p (see Figure 3-6).

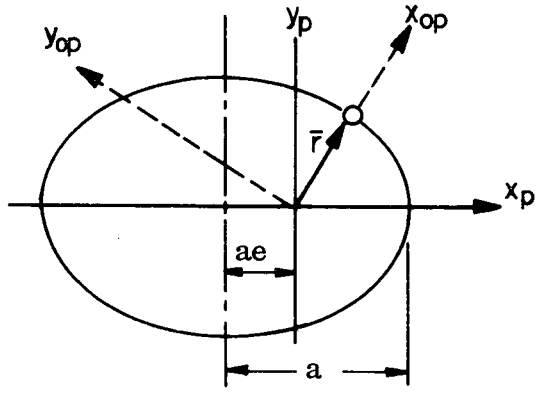

Figure 3-6. Orbital Parameters

3.2.6 Keplerian Elements

Origin:	Center of the reference body
Reference Plane:	Equatorial plane perpendicular to the central body's axis of rotation
Principal Direction:	Vernal equinox or prime meridian at a given epoch.

Keplerian Elements (see Figures 3-5 and 3-6):

- $a \sim$ the semimajor axis
- $e \sim$ the eccentricity specifying the elongation of the orbital conic section
- $i \sim$ the inclination specifying the orientation of the satellite's orbital plane to the equator of the central body
- $\Omega \sim$ the right ascension of the ascending node, i.e., the angle measured eastward along the equator between the principal direction and the point where the satellite crosses the equator traveling in a northerly direction
- $\omega \sim$ the argument of perigee, i.e., angle between the ascending node and the perifocal point measured positive with increasing mean anomaly
- $M \sim$ the mean anomaly, i.e., product of the satellite's mean angular motion and the time elapsed since perifocal passage

3.3 SPECIFIC TRANSFORMATIONS

3.3.1 1950.0 Inertial to Body-Fixed

The equinox, γ, is defined as the intersection of the planes of the earth's equator and the ecliptic. The equator is defined as being normal to the earth's pole. The primary motion of the equinox is called precession and is due mainly to the precession of the earth's pole. The precessional motion of the mean equinox is due to the combined motions of the two planes, the equator and the ecliptic, that define it.

The motion of the celestial pole or of the equator is due to the gravitational attraction of the sun and moon on the earth's equatorial bulge. It consists of two components: lunisolar precession and nutation (References 1, 2, 3). Lunisolar precession is the smooth long-period motion of the equator's pole around the ecliptic pole and has an amplitude of approximately 23.5 degrees and a period of approximately 26,000 years. Nutation is a relatively short-period motion that carries the actual, or the true, pole around the mean pole in a somewhat irregular

curve with an aplitude of approximately 9 seconds of arc and a period of approximately 18.6 years. The word "mean" indicates that nutation is being neglected. The motion of the ecliptic (i.e. the mean plane of the earth's orbit) is due to the planets' gravitational attraction on the earth and consists of a slow rotation of the ecliptic. This motion is known as planetary precession and gives a precession of the equinox of approximately 12 seconds of arc a century and a decrease of the obliquity of the ecliptic, the angle between the ecliptic and the earth's equator, of approximately 47 seconds of arc a century.

3.3.1.1 1950.0 Inertial to Mean Equator and Equinox of Epoch

The 1950.0 coordinates are transformed into the mean equator and equinox of epoch by correcting only for precession. This is done by the following three rotations (see Figure 3-7):

$R_z\ (\pi/2 - \zeta_o)$ ~ the rotation about the Z-axis that rotates the ascending node of the mean equator of epoch to the X-axis (1950.0 equinox)

$R_x\ (\theta_p)$ ~ the rotation of the 1950.0 equatorial plane into the mean equatorial plane of epoch about an axis that coincides with the ascending node of the mean equatorial plane of epoch on the 1950.0 equatorial plane

$R_z\ (\pi/2 + \xi_p)$ ~ the rotation around the new z_E-axis to align the x_E-axis with the mean equinox of epoch.

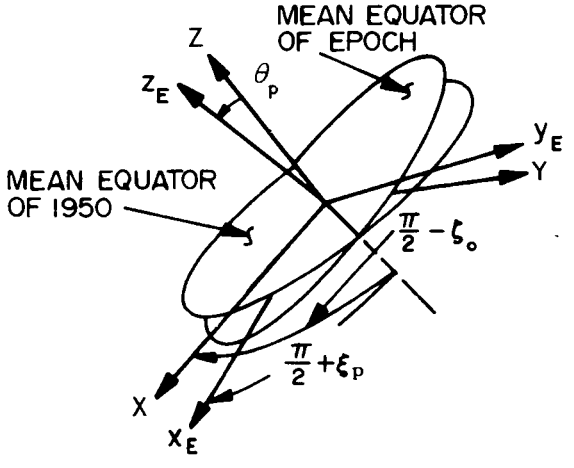

Figure 3-7. Precession Angles

The angles ζ_0, θ_p, and ξ_p are given by

$$\zeta_0 = + 2304.''948\ T + 0.''302\ T^2 + 0.''0179\ T^3 \tag{3-1}$$

$$\theta_p = 2004.''255\ T - 0.''426\ T^2 - 0.''416\ T^3 \tag{3-2}$$

$$\xi_p = + 2304.''948\ T + 1.''093\ T^2 - 0.''0192\ T^3 \tag{3-3}$$

where

T ~ the Ephemeris time in Julian centuries (36525 Julian days) elapsed from epoch to 1950.0 (JD 243 3282.5)

$$T = \frac{\text{JD of } t_o - 2433282.423357}{36525}.$$

The total rotation matrix may be expressed as

$$A = R_z\ (90° + \xi_p)\ R_x\ (\theta_p)\ R_z\ (90° - \zeta_o) = \{a_{ij}\} \tag{3-4}$$

Denoting the 1950.0 coordinates by $\bar{R}$ and the mean equator and equinox of epoch by $\bar{r}_E$, we have

$$\bar{r}_E = A\,\bar{R} \tag{3-5}$$

where the elements of A are

$$\begin{aligned}
a_{11} &= -\sin\zeta_o \sin\xi_p + \cos\zeta_o \cos\xi_p \cos\theta_p \\
a_{12} &= -\cos\zeta_o \sin\xi_p - \sin\zeta_o \cos\xi_p \cos\theta_p \\
a_{13} &= -\cos\xi_p \sin\theta_p \\
a_{21} &= \sin\zeta_o \cos\xi_p + \cos\zeta_o \sin\xi_p \cos\theta_p \\
a_{22} &= \cos\zeta_o \cos\xi_p - \sin\zeta_o \sin\xi_p \cos\theta_p \\
a_{23} &= -\sin\xi_p \sin\theta_p \\
a_{31} &= \cos\zeta_o \sin\theta_p \\
a_{32} &= -\sin\zeta_o \sin\theta_p \\
a_{33} &= \cos\theta_p.
\end{aligned} \tag{3-6}$$

The time derivative of A is assumed to be negligible. The velocity coordinates are transformed as follows

$$\dot{\bar{r}}_E = A\,\dot{\bar{R}} \tag{3-7}$$

3.3.1.2 Mean Equator and Equinox of Epoch to True of Epoch

The transformation from the mean equator and equinox of epoch to the true of epoch system involves correcting for the nutation effect. Nutation is measured as cyclic changes in the obliquity, the angle between the equatorial plane and the ecliptic, and the longitude of the equinox. These changes in obliquity, $\delta\epsilon$, and longitude, $\delta\psi$, are assumed known. They are input to GTDS by fitting polynomials through the JPL ephemeris data (Reference 4).

To compute the transformation, the mean obliquity is first determined

$$\bar{\epsilon} = 23.^{\circ}452294 - .^{\circ}130125 \times 10^{-1}\, T_E - .^{\circ}164 \times 10^{-5}\, T_E^2 + .^{\circ}503 \times 10^{-6}\, T_E^3 \tag{3-8}$$

where

$T_E \sim$ the time in Julian centuries (36525 Julian days) elapsed from epoch to 1900 Jan 0^d 12^h (ET = JD 2415020.0).

Then, defining

$\delta\epsilon \sim$ the difference between the true and the mean obliquity

$\tilde{\epsilon} = \bar{\epsilon} + \delta\epsilon \sim$ the true obliquity

$\delta\psi \sim$ the difference between the longitude of the true and mean equinox of epoch

the rotation from the mean equator and equinox of epoch to the true equator and equinox is given by the following three rotations: (see Figure 3-8)

$R_x(\bar{\epsilon}) \sim$ the rotation about the x_E axis into the ecliptic of epoch

$R_z(\delta\psi) \sim$ the negative rotation about the ecliptic pole, through the nutation in longitude to the true vernal equinox of epoch

C. 2

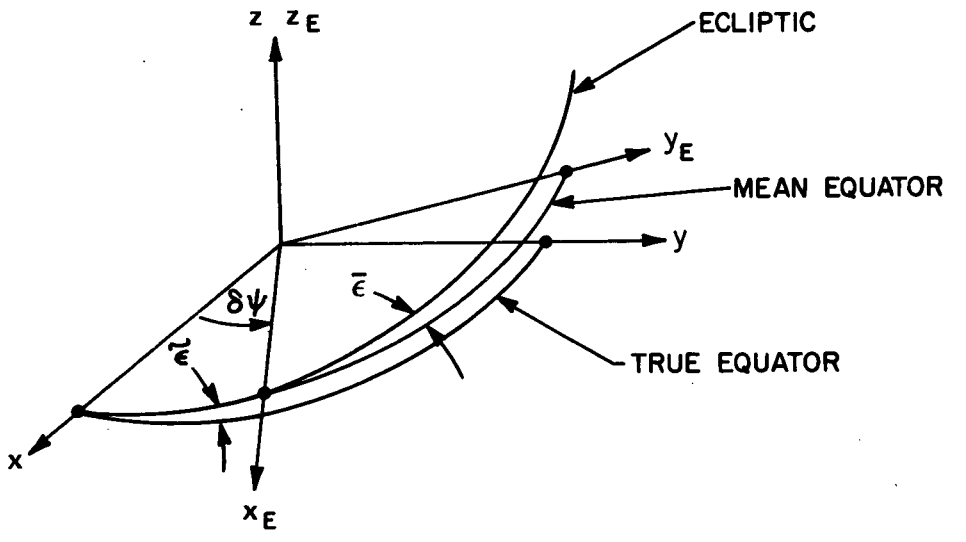

Figure 3-8. Nutation Angles

$R_x(\tilde{\epsilon})$ ~ the rotation about the new x-axis through the true obliquity to the true equator of epoch.

The total rotation matrix may be expressed as

$$N = R_x(\tilde{\epsilon})\, R_z(\delta\psi)\, R_x(\bar{\epsilon}) = \{n_{ij}\}. \tag{3-9}$$

Denoting the true of epoch coordinates by $\bar{r}$, we have

$$\bar{r} = N\, \bar{r}_E \tag{3-10}$$

where the elements of N are

$$\begin{aligned} n_{11} &= \cos\delta\psi \\ n_{12} &= -\sin\delta\psi\cos\bar{\epsilon} \\ n_{13} &= -\sin\delta\psi\sin\bar{\epsilon} \end{aligned} \tag{3-11}$$

$$
\begin{aligned}
n_{21} &= \sin\delta\psi\cos\tilde{\epsilon} \\
n_{22} &= \cos\delta\psi\cos\tilde{\epsilon}\cos\bar{\epsilon} + \sin\tilde{\epsilon}\sin\bar{\epsilon} \\
n_{23} &= \cos\delta\psi\cos\tilde{\epsilon}\sin\bar{\epsilon} - \sin\tilde{\epsilon}\cos\bar{\epsilon} \\
n_{31} &= \sin\delta\psi\sin\tilde{\epsilon} \\
n_{32} &= \cos\delta\psi\sin\tilde{\epsilon}\cos\bar{\epsilon} - \cos\tilde{\epsilon}\sin\bar{\epsilon} \\
n_{33} &= \cos\delta\psi\sin\tilde{\epsilon}\sin\bar{\epsilon} + \cos\tilde{\epsilon}\cos\bar{\epsilon}.
\end{aligned}
\tag{3-11}
$$

The time derivative of N is assumed to be negligible. Therefore the velocity coordinates are transformed as follows

$$
\dot{\bar{r}} = N\,\dot{\bar{r}}_E. \tag{3-12}
$$

The transformation matrix from inertial mean 1950.0 to inertial true of epoch is given by G = NA, and N and A are given by Equations (3-11) and (3-6), respectively.

3.3.1.3 Geocentric True of Epoch to Pseudo Body-Fixed

The transformation that relates the true of date coordinates to the body-fixed coordinates accounts for two separate effects. The first relates the true vernal equinox to the prime meridian of the rotating planet by means of the angle α_g, variously called the Greenwich sidereal time, the Greenwich hour angle of the true equinox of epoch, or the date right ascension of Greenwich (see Figure 3-9). The second effect, called polar motion, accounts for the fact that the pole of the body-fixed axis, z_b, does not coincide with the body's spin axis, the pole of the true of epoch geocentric axis. The first of these effects transforms the true of date coordinates to pseudo body-fixed coordinates. This pseudo coordinate system would be precisely the body-fixed axes if $z = z_b$, that is, if polar motion is omitted.

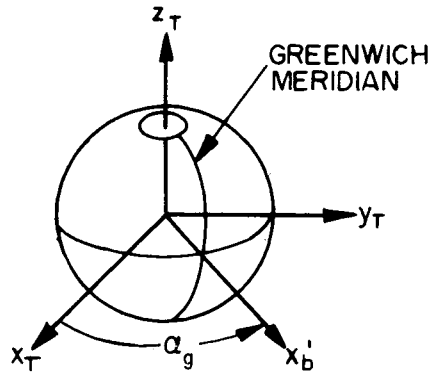

Figure 3-9. Greenwich Sideral Time

The transformation consists of a rotation about the z-axis through the true Greenwich sidereal time, α_g, yielding

$$B_1(\alpha_g) = \begin{bmatrix} \cos\alpha_g & \sin\alpha_g & 0 \\ -\sin\alpha_g & \cos\alpha_g & 0 \\ 0 & 0 & 1 \end{bmatrix} \tag{3-13}$$

where the true Greenwich sidereal time is obtained from the mean Greenwich sidereal time

$$\alpha_{GM} = UT1 + 6^h\ 38^m\ 45^s.836 + 8640184^s.542\ T_u + 0^s.0929\ T_u^2 \tag{3-14}$$

by applying the correction

$$\alpha_g = \alpha_{GM} + \Delta H \tag{3-15}$$

where

$$\Delta H = \delta\psi \cos(\bar{\epsilon} + \delta\epsilon). \tag{3-16}$$

The nutation in longitude, $\delta\psi$, and obliquity, $\delta\epsilon$, is discussed in Section 3.3.1.2. The times UT1 and T_u in Equation (3-14) are

UT1 ~ seconds of UT1 time (see Section 3.4.5) elapsed from January 1, 1950, 0^h UT1

T_u ~ the number of Julian centuries elapsed from 12 hours UT1 January 0, 1900 (JD = 2415020.0) to the UT1 time of epoch.

The true of date coordinates transform into the pseudo body-fixed coordinates as follows

$$\bar{r}_b' = B_1 \bar{r}. \tag{3-17}$$

Differentiation yields the velocity transformation

$$\dot{\bar{r}}_b' = B_1 \dot{\bar{r}} + \dot{B}_1 \bar{r} \tag{3-18}$$

where

$$\dot{B}_1 = \begin{bmatrix} -\sin\alpha_g & \cos\alpha_g & 0 \\ -\cos\alpha_g & -\sin\alpha_g & 0 \\ 0 & 0 & 0 \end{bmatrix} \dot{\alpha}_g \tag{3-19}$$

and where $\dot{\alpha}_g$ is considered constant.

3.3.1.4 Geocentric True of Epoch to Body-Fixed

The principal axis of the earth (angular momentum vector) is not coincident with the spin axis (angular velocity vector), and it moves with respect to the latter causing the polar motion effect. The path of the pole on the earth's surface is "semi-regular" but unpredictable due to random shifts in the earth's crust, etc. The motion of the pole is given with respect to the pole at some established epoch. The pole at the established epoch is referred to as the adopted pole (P_A), and the present position of the pole is referred to as the true pole (P_T). There are several adopted poles in the literature. Due to the small size of the polar motion correction (it takes place in a square less than 50 meters wide), the polar region of the earth may be considered a plane and the transformation from one adopted pole

to another reduces to a simple plane translation. Neglecting the earth's slight curvature at the pole, establish a left-handed rectangular coordinate system centered at P_A with the x_b axis directed along the Greenwich meridian and the y_b axis along the meridian of 90° west. (See Figure 3-10.) The coordinates of the instantaneous pole P_T are measured in terms of x_p and y_p components using units of seconds of arc. The measurements of x_p and y_p are performed by the International Polar Motion Service and published by the U.S. Naval Observatory.

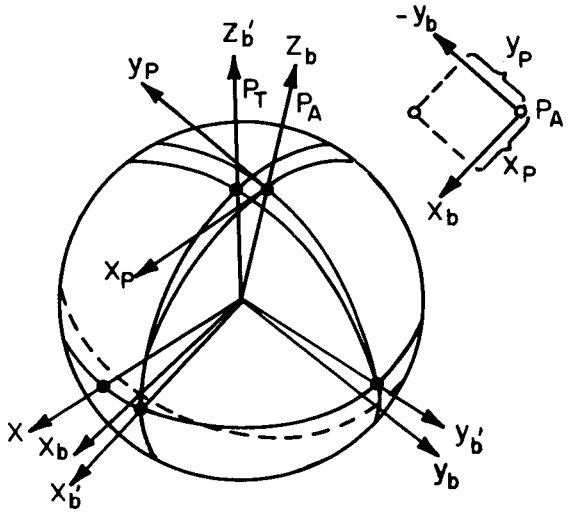

Figure 3-10 Polar Motion Schematic

In order to derive the expressions for the effects of x_p and y_p on a point's latitude and longitude, these two quantities are shown in relation to a regular right-handed orthogonal-rectangular coordinate system, whose z_b axis passes through P_A and whose x_b-z_b plane passes through Greenwich. In this system, a point's adopted longitude, λ_A, is measured positive in an eastward direction from x_b. The following notation is used:

λ_A ~ the adopted longitude

ϕ_A ~ the adopted latitude

λ_T ~ the instantaneous longitude with respect to (x_b', y_b', z_b')

ϕ_T ~ the instantaneous latitude with respect to (x_b', y_b', z_b')

$\Delta\phi$ ~ $\phi_T - \phi_A$, the difference between adopted and true latitude

$\Delta\lambda$ ~ $\lambda_T - \lambda_A$, the difference between adopted and true longitude

Let ϕ_T and λ_T be measured in a right-handed orthogonal-rectangular coordinate system (x_b', y_b', z_b') whose z_b' axis passes through P_T and whose x_b' axis lies in the z_b-x_b meridian plane, displaced from x_b by the angle x_p. The vector in the (x_b, y_b, z_b) and (x_b', y_b', z_b') systems may be written

$$\begin{bmatrix} x_b \\ y_b \\ z_b \end{bmatrix} = r_b \begin{bmatrix} \cos \phi_A \cos \lambda_A \\ \cos \phi_A \sin \lambda_A \\ \sin \phi_A \end{bmatrix} \tag{3-20}$$

and

$$\begin{bmatrix} x_b' \\ y_b' \\ z_b' \end{bmatrix} = r_b \begin{bmatrix} \cos \phi_T \cos \lambda_T \\ \cos \phi_T \sin \lambda_T \\ \sin \phi_T \end{bmatrix}. \tag{3-21}$$

The two systems are related by

$$\begin{bmatrix} x_b \\ y_b \\ z_b \end{bmatrix} = \begin{bmatrix} \cos x_p & 0 & \sin x_p \\ 0 & 1 & 0 \\ -\sin x_p & 0 & \cos x_p \end{bmatrix} \begin{bmatrix} 1 & 0 & 0 \\ 0 & \cos y_p & -\sin y_p \\ 0 & \sin y_p & \cos y_p \end{bmatrix} \begin{bmatrix} x_b' \\ y_b' \\ z_b' \end{bmatrix}. \tag{3-22}$$

This equation simplifies to

$$\bar{r}_b = B_2 \, \bar{r}_b' \tag{3-23}$$

Since x_p and y_p are small, all cosine terms are equated to unity, all sine terms equated to their angle, and all products neglected. Thus B_2 becomes

$$B_2 = \begin{bmatrix} 1 & 0 & x_p \\ 0 & 1 & -y_p \\ -x_p & y_p & 1 \end{bmatrix}. \tag{3-24}$$

To obtain the relationships between λ_T, λ_A, ϕ_A, and ϕ_T, the following formulas may be used

$$\phi_T - \phi_A = \Delta\phi = x_p \cos\lambda_A - y_p \sin\lambda_A \tag{3-25}$$

and

$$\lambda_T - \lambda_A = \Delta\lambda = \tan\phi_A \left[x_p \sin\lambda_A + y_p \cos\lambda_A\right]. \tag{3-26}$$

The complete transformation between the true of epoch coordinate system and the body-fixed system is given by

$$\bar{r}_b = B_2 (x_p, y_p) B_1 (\alpha_g) \bar{r} \tag{3-27}$$

where B_1 is presented in Equation (3-13) and B_2 in Equation (3-24).

The time derivative of B_2 is negligible, therefore the velocity is transformed as follows:

$$\dot{\bar{r}}_b = B_2 B_1 \dot{\bar{r}} + B_2 \dot{B}_1 \bar{r} \tag{3-28}$$

where $\dot{B}_1$ is given by Equation (3-19).

3.3.1.5 Summary of Transformations

The total transformation from mean equinox and equator of 1950.0 coordinates to body-fixed coordinates is the product of the transformations in Equations (3-5), (3-10), (3-17), and (3-23)

$$\bar{r}_b = B_2 (x_p, y_p) \cdot B_1 (\alpha_g) \cdot N(\delta\epsilon, \delta\psi) \cdot A(\zeta_o, \theta_p, \xi_p) \bar{R}. \tag{3-29}$$

Hereafter this transformation is written

$$\bar{r}_b = H \cdot G \bar{R} \tag{3-30}$$

where

$$H = B_2 (x_p, y_p) B_1 (\alpha_g) \tag{3-31}$$

$$G = N(\delta\epsilon, \delta\psi)\, A(\zeta_o, \theta_p, \xi_p). \tag{3-32}$$

The matrices G and H depend only on time (not on satellite position). The matrices N, A, and B_1 vary so slowly with time that their time rate of change can be neglected in velocity transformations. The matrix B_1 changes in proportion to the earth's spin rate; thus its time rate of change, given in Equation (3-19), must be accounted for. In GTDS the G matrix is synthesized during preprocessing computations using information from an ephemeris tape. Its elements are stored as polynomial functions of time for use during problem execution. The H matrix is optionally computed either precisely as shown in Equation (3-31), or approximately by neglecting polar motion (e.g., $B_2 = I$).

3.3.2 Selenocentric True of Epoch to Selenographic (References 5, 6, 7)

The rotation from the selenocentric true of epoch system (x, y, z) to a moon-fixed selenographic system (x_b, y_b, z_b) shown in Figure 3-11 accounts for the relative orientation of the fixed lunocentric axis relative to the inertial Cartesian true of epoch system. Several quantities must be evaluated to perform this rotation. The independent variables used in evaluating these quantities are labeled "T" and "d." The T-variable is the number of Julian centuries of 36525 Julian days past 0^h Jan 1, 1950 ET, and the d-variable is the number of days past the same time. The various quantities that are referred to the mean equinox and ecliptic of epoch are the following.

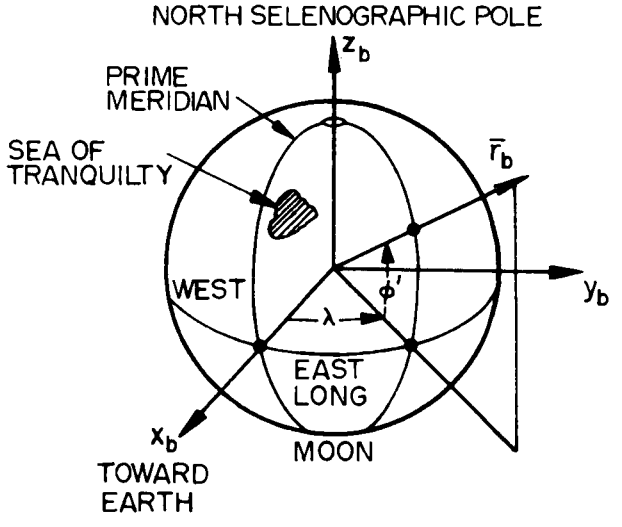

Figure 3-11. Selenographic Coordinate System

The longitude of the mean ascending node of the lunar orbit, Ω_M, is given by

$$\Omega_M = 12.1127902 - .0529539222\ d + .20795\ (10^{-2})\ T + .2081\ (10^{-2})\ T^2 + .2\ (10^{-5})\ T^3. \quad (3\text{-}33)$$

The geocentric mean longitude of the moon, λ_M, is given by

$$\lambda_M = 64.37545167 + 13.1763965268\ d - .1131575\ (10^{-2})\ T - .113015\ (10^{-2})\ T^2 + .19\ (10^{-5})\ T^3. \quad (3\text{-}34)$$

The mean longitude of the moon's perigee, Γ_M, is given by

$$\Gamma'_M = 208.8439877 + .1114040803\ d - .010334\ T - .010343\ T^2 - .12\ (10^{-4})\ T^3. \quad (3\text{-}35)$$

The mean longitude of the sun, L_S, is given by

$$L_S = 280.08121009 + .9856473354\ d + .302\ (10^{-3})\ T + .302\ (10^{-3})\ T^2. \quad (3\text{-}36)$$

The mean longitude of the sun's perigee, Γ_S, is given by

$$\Gamma_S = 282.08053028 + .470684\ (10^{-4})\ d + .45525\ (10^{-3})\ T + .4575\ (10^{-3})\ T^2 + .3\ (10^{-5})\ T^3. \quad (3\text{-}37)$$

The inclination of the mean lunar equator to the ecliptic, I_M, is given by

$$I_M = 1°32'.1. \quad (3\text{-}38)$$

From these quantities, the three angles g, g', and ω_M are obtained. The quantity g is the moon's mean anomaly and is given by

$$g = \lambda_M - \Gamma'_M = 215.^{\circ}54013 + 13.^{\circ}064992 \text{ d.} \tag{3-39}$$

The quantity g' is the sun's mean anomaly and is given by

$$g' = L_S - \Gamma_S = 358.^{\circ}009067 + .^{\circ}9856005 \text{ d.} \tag{3-40}$$

The quantity ω_M is the moon's argument of perigee and is given by

$$\omega_M = \Gamma'_M - \Omega_M = 196.745632 + .^{\circ}1643586 \text{ d.} \tag{3-41}$$

Hayn's physical librations, σ_M, τ_M, and ρ_M, may be computed from the preceding angles. The physical libration in node, Ω_M, is σ_M, where

$$\begin{aligned}\sigma_M = [&- 0.^{\circ}0302777 \sin (g) + 0.^{\circ}0102777 \sin (g + 2\omega_M) \\ &- .^{\circ}305555 (10^{-2}) \sin (2g + 2\omega_M)] / \sin I_M.\end{aligned} \tag{3-42}$$

The physical libration in longitude, λ_M, is τ_M, where

$$\tau_M = - .^{\circ}3333 (10^{-2}) \sin (g) + .^{\circ}0163888 \sin (g') + .^{\circ}5 (10^{-2}) \sin (2\omega_M). \tag{3-43}$$

The physical libration in inclination I_M, is ρ_M, where

$$\begin{aligned}\rho_M = &- .0297222 \cos (g) + .0102777 \cos (g + 2\omega_M) \\ &- .^{\circ}305555 (10^{-2}) \cos (2g + 2\omega_M).\end{aligned} \tag{3-44}$$

The next step is to define the rotation angles, i_s, Ω', and Δ. The quantity i_s is the inclination of the moon's equatorial plane to the earth's equatorial plane and is given by

$$\cos i_s = \cos (\Omega_M + \sigma_M \Delta\psi) \sin \tilde{\epsilon} \sin (I_M + \rho_M) + \cos \tilde{\epsilon} \cos (I_M + \rho_M) \tag{3-45}$$

and

$$\sin i_s = \sqrt{1 - \cos^2 i_s} \tag{3-46}$$

where $\tilde{\epsilon}$ and $\Delta\psi$ are the true obliquity and nutation in longitude described in Section 3.3.1.2.

The angle, Ω', is the right ascension to the ascending node of the lunar orbit and is given by

$$\sin \Omega' = - \sin (\Omega_M + \sigma_M + \Delta\psi) \sin (I_M + \rho_M)/\sin i_s \tag{3-47}$$

$$\cos \Omega' = [\cos (I_M + \rho_M) \sin \tilde{\epsilon} - \sin (I_M + P_M) \cos \tilde{\epsilon} \cos (\Omega_M + \sigma_M \Delta\psi]/\sin i_s. \tag{3-48}$$

The auxiliary angle, Δ, is computed as follows

$$\sin \Delta = - \sin (\Omega_M + \sigma_M \Delta\psi) \sin \tilde{\epsilon}/\sin i_s \tag{3-49}$$

$$\cos \Delta = - \sin (\Omega_M + \sigma_M + \Delta\psi) \sin \Omega' \cos \tilde{\epsilon} - \cos (\Omega_M + \sigma_M + \Delta\psi) \cos \Omega' \tag{3-50}$$

and

$$\Delta = \tan^{-1} (\sin \Delta/\cos \Delta). \tag{3-51}$$

The argument, Λ, to the x_b-axis is (see Figure 3-12)

$$\sin \Lambda = \sin [\Delta + (\lambda_M + \tau_M) - (\Omega_M + \sigma_M)] \tag{3-52}$$

and

$$\cos \Lambda = \cos [\Delta + (\lambda_M + \tau_M) - (\Omega_M + \sigma_M)]. \tag{3-53}$$

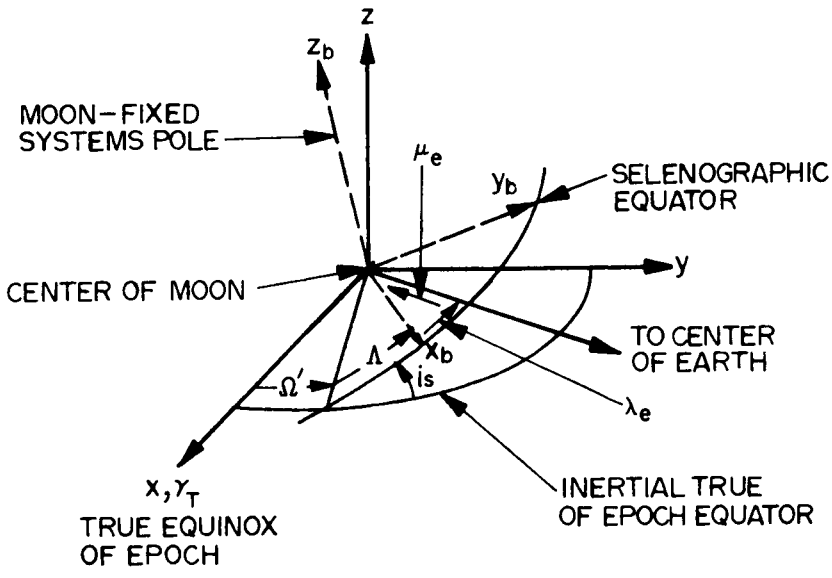

Figure 3-12. Lunar Geometry

The rotation may be expressed by the following formula

$$\overline{r}_b = M\,\overline{r} \tag{3-54}$$

where $\overline{r}_b$ is selenographic and $\overline{r}$ is selenocentric true of epoch coordinates (see Figure 3-12), and where

$$M = (m_{ij}) \tag{3-55}$$

with elements

$$\begin{aligned}
m_{11} &= \cos\Lambda\cos\Omega' - \sin\Lambda\sin\Omega'\cos i_s \\
m_{12} &= \cos\Lambda\cos\Omega' + \sin\Lambda\cos\Omega'\cos i_s \\
m_{13} &= \sin\Lambda\sin i_s \\
m_{21} &= -\sin\Lambda\cos\Omega' - \cos\Lambda\sin\Omega'\cos i_s \\
m_{22} &= -\sin\Lambda\sin\Omega' + \cos\Lambda\cos\Omega'\cos i_s \\
m_{23} &= \cos\Lambda\sin i_s
\end{aligned} \tag{3-56}$$

$$m_{31} = \sin \Omega' \sin i_s$$

$$m_{32} = -\cos \Omega' \sin i_s$$

$$m_{33} = \cos i_s. \tag{3-56}$$

The velocity transformations from selenocentric true of epoch to selenographic coordinates are obtained by the following time derivatives

$$\dot{\Delta} = [-\cos (\Omega_M + \sigma_M + \Delta\psi) \sin \tilde{\epsilon} (\dot{\Omega}_M + \dot{\sigma}_M)] / (\sin i_s \cos \Delta) \tag{3-57}$$

$$\dot{\lambda}_M = .266170762\,(10^{-5}) - .12499171\,(10^{-13})\,T \tag{3-58}$$

$$\dot{\Omega}_M = -.1069698435\,(10^{-7}) + .23015329\,(10^{-13})\,T \tag{3-59}$$

$$\dot{\tau}_M = -.1535272946\,(10^{-9}) \cos g + .569494067\,(10^{-10}) \cos g' + .579473484\,(10^{-11}) \cos 2\omega_M \tag{3-60}$$

and

$$\dot{\sigma}_M = -.520642191\,(10^{-7}) \cos g + .1811774451\,(10^{-7}) \cos (g + 2\omega_M) - .1064057858\,(10^{-7}) \cos (2\omega_M + 2g) \tag{3-61}$$

The derivative of Λ is then

$$\dot{\Lambda} = \dot{\Delta} + \dot{\lambda}_M + \dot{\tau}_M - \dot{\Omega}_M - \dot{\sigma}_M. \tag{3-62}$$

The time derivatives of Ω' and i_s are assumed to be negligible.

The rotation from selenocentric $(\dot{x}, \dot{y}, \dot{z})$ to selenographic $(\dot{x}_b, \dot{y}_b, \dot{z}_b)$ is given by

$$\dot{\bar{r}}_b = M\,\dot{\bar{r}} + \dot{M}\,\bar{r} \tag{3-63}$$

where the $\dot{M}$ transformation matrix is related to M and Λ by

$$\dot{M} = \dot{\Lambda} \begin{bmatrix} m_{21} & m_{22} & m_{23} \\ -m_{11} & -m_{12} & -m_{13} \\ 0 & 0 & 0 \end{bmatrix} \tag{3-64}$$

3.3.3 Spherical-Cartesian Transformations

3.3.3.1 Spherical Position and Velocity to Cartesian Coordinates

Using the spherical position coordinates, r, α, and δ, that are defined in Section 3.2.1, the transformation to Cartesian coordinates is seen from Figure 3-1 to be

$$\begin{bmatrix} x \\ y \\ z \end{bmatrix} = r \begin{bmatrix} \cos\delta\cos\alpha \\ \cos\delta\sin\alpha \\ \sin\delta \end{bmatrix}. \tag{3-65}$$

To transform the spherical velocity coordinates, V, β, and A, described in Section 3.2.3, it is convenient to transform to the local plane coordinate system (see Figure 3-3) and then to the body-centered inertial Cartesian coordinate system. If the local plane coordinates, x_{lp}, y_{lp}, and z_{lp}, are fixed inertially (nonrotating), $\dot{\bar{r}}_{lp}$ may be expressed as

$$\dot{\bar{r}}_{lp} = \begin{bmatrix} \dot{x}_{lp} \\ \dot{y}_{lp} \\ \dot{z}_{lp} \end{bmatrix} = V \begin{bmatrix} \cos\beta \\ \sin A\sin\beta \\ \cos A\sin\beta \end{bmatrix}. \tag{3-66}$$

The transformation between the local plane and the body-centered inertial Cartesian coordinate systems is

$$\bar{r}_{lp} = C\,\bar{r} \tag{3-67}$$

where

$$C = \begin{bmatrix} \cos\delta\cos\alpha & \cos\delta\sin\alpha & \sin\delta \\ -\sin\alpha & \cos\alpha & 0 \\ -\sin\delta\cos\alpha & -\sin\delta\sin\alpha & \cos\delta \end{bmatrix}. \tag{3-68}$$

Since the local plane system is fixed inertially, the velocity vector in Equation (3-66) may be transformed to the body-centered inertial Cartesian axes by means of the transformation C as follows

$$\dot{\bar{r}} = C^T\,\dot{\bar{r}}_{lp}. \tag{3-69}$$

The partial derivatives of x, y, z, $\dot{x}$, $\dot{y}$, and $\dot{z}$ with respect to r, α, δ, V, A, and β are

$$\frac{\partial \bar{r}}{\partial r} = \frac{\bar{r}}{r} \tag{3-70}$$

$$\frac{\partial \bar{r}}{\partial \alpha} = \begin{bmatrix} -y \\ x \\ 0 \end{bmatrix} \tag{3-71}$$

$$\frac{\partial \bar{r}}{\partial \delta} = -r \begin{bmatrix} \sin\delta\cos\alpha \\ \sin\delta\sin\alpha \\ -\cos\delta \end{bmatrix} = \begin{bmatrix} -z\cos\alpha \\ -z\sin\alpha \\ \sqrt{x^2+y^2} \end{bmatrix} \tag{3-72}$$

$$\frac{\partial \bar{r}}{\partial V} = \frac{\partial \bar{r}}{\partial A} = \frac{\partial \bar{r}}{\partial \beta} = \frac{\partial \dot{\bar{r}}}{\partial r} = 0 \tag{3-73}$$

$$\frac{\partial \dot{\bar{r}}}{\partial \alpha} = \begin{bmatrix} -\dot{y} \\ x \\ 0 \end{bmatrix} \tag{3-74}$$

$$\frac{\partial \dot{\bar{r}}}{\partial \alpha} = \begin{bmatrix} -\dot{z}\cos\alpha \\ -\dot{z}\sin\alpha \\ V(\cos\beta\cos\delta - \cos A\sin\beta\sin\delta) \end{bmatrix} \tag{3-75}$$

$$\frac{\partial \dot{\bar{r}}}{\partial V} = \frac{\dot{\bar{r}}}{V} \tag{3-76}$$

$$\frac{\partial \dot{\bar{r}}}{\partial A} = V \begin{bmatrix} \sin\beta(\sin A\sin\delta\cos\alpha - \cos A\sin\alpha) \\ \sin\beta(\sin A\sin\delta\sin\alpha + \cos A\cos\alpha) \\ -\sin A\cos\delta\sin\beta \end{bmatrix} \tag{3-77}$$

and

$$\frac{\partial \dot{\bar{r}}}{\partial \beta} = -V \begin{bmatrix} \cos\alpha(\cos\delta\sin\beta + \sin\delta\cos\beta\cos A) + \sin\alpha\cos\beta\sin A \\ \sin\alpha(\cos\delta\sin\beta + \sin\delta\cos\beta\cos A) - \cos\alpha\cos\beta\sin A \\ \sin\beta\sin\delta - \cos\beta\cos\delta\cos A \end{bmatrix} \tag{3-78}$$

3.3.3.2 Cartesian Position and Velocity to Spherical Coordinates

The inverse of the preceding transformations is described in the following text. The spherical radius, r, is given by

$$r = \sqrt{x^2 + y^2 + z^2.} \tag{3-79}$$

From Figure 3-1 the right ascension, α, and declination, δ, of $\bar{r}$ are

$$\sin \delta = \frac{z}{r} \qquad \cos \delta = \frac{\sqrt{x^2 + y^2}}{r} \qquad -\frac{\pi}{2} \leq \delta \leq \frac{\pi}{2} \tag{3-80}$$

and

$$\sin \alpha = \frac{y}{\sqrt{x^2 + y^2}} \qquad \cos \alpha = \frac{x}{\sqrt{x^2 + y^2}} \qquad 0 \leq \alpha \leq 2\pi. \tag{3-81}$$

The right ascension is measured positive east from the inertial x-axis. The declination is measured positive north from the x-y plane.

The velocity vector's magnitude is

$$V = \sqrt{\dot{x}^2 + \dot{y}^2 + \dot{z}^2} \tag{3-82}$$

and the azimuth, A, and flight path angle, β, are obtained from the local plane components of velocity

$$\sin \beta = \frac{\sqrt{\dot{y}_{lp}^2 + \dot{z}_{lp}^2}}{V} \qquad \cos \beta = \frac{\dot{x}_{lp}}{V} \qquad -\frac{\pi}{2} \leq \beta - \frac{\pi}{2} \tag{3-83}$$

and

$$\sin A = \frac{\dot{y}_{lp}}{\sqrt{\dot{y}_{lp}^2 + \dot{z}_{lp}^2}} \qquad \cos A = \frac{\dot{z}_{lp}}{\sqrt{\dot{y}_{lp}^2 + \dot{z}_{lp}^2}} \qquad 0 \leq A \leq 2\pi. \tag{3-84}$$

The azimuth and flight path angles may be obtained alternately from the vector products of r and $\bar{r}$ as follows

$$\sin \beta = \frac{|\bar{r} \times \dot{\bar{r}}|}{r\,V} \qquad \cos \beta = \frac{\bar{r} \cdot \dot{\bar{r}}}{r\,V} \tag{3-85}$$

and

$$\sin A = \bar{U}_{z_{lp}} \cdot \bar{U}_N \qquad \cos A = \frac{\bar{U}_{z_{lp}} \cdot \bar{U}_N \times \bar{r}}{r} \tag{3-86}$$

where $\bar{U}_{z_{lp}}$ is the unit vector in the $\bar{z}_{lp}$-axis direction and has components expressed in the body-centered Cartesian system

$$\bar{U}_{z_{lp}} = \begin{bmatrix} -\sin\delta\cos\alpha \\ -\sin\delta\sin\alpha \\ \cos\delta \end{bmatrix} \tag{3-87}$$

and $\bar{U}_N$ is the unit vector normal to $\bar{r}$ and $\dot{\bar{r}}$

$$\bar{U}_N = \frac{\dot{\bar{r}} \times \ddot{\bar{r}}}{r V}. \tag{3-88}$$

Substituting Equations (3-87) and (3-88) into Equation (3-86) yields

$$\sin A = \frac{(x\dot{y} - y\dot{x})}{r V}, \quad \cos A = \frac{y(y\dot{z} - z\dot{y}) - x(x\dot{z} - \dot{x}z)}{r^2 V}. \tag{3-89}$$

The partial derivatives of r, α, δ, V, A, and β with respect to x, y, z, $\dot{x}$, $\dot{y}$, and $\dot{z}$ are

$$\frac{\partial r}{\partial \bar{r}} = \frac{\bar{r}^T}{r} \tag{3-90}$$

$$\frac{\partial \alpha}{\partial \bar{r}} = \frac{1}{(x^2 + y^2)} \begin{bmatrix} -y \\ x \\ 0 \end{bmatrix}^T \tag{3-91}$$

$$\frac{\partial \delta}{\partial \bar{r}} = \frac{1}{r^2 \sqrt{x^2 + y^2}} \begin{bmatrix} -z\,x \\ -z\,y \\ (x^2 + y^2) \end{bmatrix}^T \tag{3-92}$$

$$\frac{\partial V}{\partial \bar{r}} = 0 \tag{3-93}$$

$$\frac{\partial A}{\partial \bar{r}} = \frac{1}{(V^2 - \dot{r}^2)(x^2 + y^2)} \begin{bmatrix} \dot{y}(r\dot{z} - z\dot{r}) - (x\dot{y} - y\dot{x})\left(x\dot{z} - z\dot{x} + \dfrac{x\,z\,\dot{r}}{r}\right)\Big/ r \\ -\dot{x}(r\dot{z} - z\dot{r}) + (x\dot{y} - y\dot{x})\left(y\dot{z} - z\dot{y} + \dfrac{y\,z\,\dot{r}}{r}\right)\Big/ r \\ (x\dot{y} - y\dot{x})(x^2 + y^2)\,\dot{r}/r^2 \end{bmatrix}^T \tag{3-94}$$

$$\frac{\partial \beta}{\partial \bar{r}} = \frac{1}{r^2 \sqrt{V^2 - \dot{r}^2}} \left(\frac{\bar{r}^T \dot{r}}{r} - \dot{\bar{r}}^T \right) \tag{3-95}$$

$$\frac{\partial r}{\partial \dot{\bar{r}}} = \frac{\partial \alpha}{\partial \dot{\bar{r}}} = \frac{\partial \delta}{\partial \dot{\bar{r}}} = 0 \tag{3-96}$$

$$\frac{\partial V}{\partial \dot{\bar{r}}} = \frac{\dot{\bar{r}}^T}{V} \tag{3-97}$$

$$\frac{\partial A}{\partial \dot{\bar{r}}} = \frac{1}{r(V^2 - \dot{r}^2)} \begin{bmatrix} (z\dot{y} - y\dot{z}) \\ (x\dot{z} - z\dot{x}) \\ (y\dot{x} - x\dot{y}) \end{bmatrix}^T \tag{3-98}$$

and

$$\frac{\partial \beta}{\partial \dot{\bar{r}}} = \frac{1}{r^2 \sqrt{V^2 - \dot{r}^2}} \left(\dot{\bar{r}} \frac{\dot{\bar{r}}^T \bar{r}}{V^2} - \bar{r} \right)^T . \tag{3-99}$$

3.3.4 Geocentric to Orbit Plane

The unit vectors in the x_{op}, y_{op}, and z_{op} directions (see Figure 3-5) that are measured in the body-centered inertial Cartesian system are

$$\bar{U} = \frac{\bar{r}_o}{|\bar{r}_o|}$$

$$\bar{V} = \bar{W} \times \bar{U} \tag{3-100}$$

$$\bar{W} = \frac{\bar{r}_o \times \dot{\bar{r}}_o}{|\bar{r}_o \times \dot{\bar{r}}_o|}$$

where $\bar{r}_o$ and $\dot{\bar{r}}_o$ are the earth-centered position and velicity vectors used to determine the orbit plane coordinate system. If Equations (3-100) are expanded, they yield the following transformation relations between the orbit plane coordinates and the body-centered inertial Cartesian coordinates

$$\bar{r}_{op} = E\,\bar{r} \tag{3-101}$$

where

$$E = \begin{bmatrix} U_x & U_y & U_z \\ V_x & V_y & V_z \\ W_x & W_y & W_z \end{bmatrix}. \tag{3-102}$$

Regarding the orbit plane system as fixed inertially, the velocity transforms as follows

$$\dot{\bar{r}}_{op} = E\,\dot{\bar{r}} \tag{3-103}$$

and the position and velocity partials are

$$\frac{\partial \bar{r}_{op}}{\partial \bar{r}} = \frac{\partial \dot{\bar{r}}_{op}}{\partial \dot{\bar{r}}} = E. \tag{3-104}$$

3.3.5 Earth-Fixed Geodetic Transformations

The transformations between the body-centered inertial Cartesian system and the geodetic axes system (described in Section 3.2.2) involves modeling the earth's

figure. In the following subsections, equations for an ellipsoidal earth model, the transformations, and the partial derivatives between the geodetic coordinates (h, λ, ϕ) and body-centered rotating coordinates (x_b, x_b, z_b) are presented.

3.3.5.1 Earth Figure

The shape of the earth's surface is very nearly an ellipsoid of revolution. A satisfactory means for modeling the earth is to characterize it as such and, where necessary, correct local anomalies to the reference ellipsoid (e.g., correct local geodetic zenith to ellipsoidal vertical). The polar axis of symmetry of the ellipsoid, z_b, is nearly colinear with the earth's spin axis. The ellipsoid's radius is greatest in the x_b - y_b equatorial plane. Letting R_p denote the equatorial radius, R_e the polar radius, and x_s, y_s, and z_s the coordinates of a point s on the ellipsoidal surface expressed in the body-centered rotating axis, then the coordinates of s must satisfy the following equation

$$\frac{x_s^2}{R_e^2} + \frac{y_s^2}{R_e^2} + \frac{z_s^2}{R_p^2} = 1. \tag{3-105}$$

Two convenient parameters which describe the elliptical cross-section are the flattening coefficient, f, defined by

$$f = \frac{R_e - R_p}{R_e} > 0 \tag{3-106}$$

and the eccentricity, e

$$e^2 = 1 - \left(\frac{R_e}{R_p}\right)^2 = f\,(2 - f). \tag{3-107}$$

Since the ellipsoid is symmetrical about the z_b-axis, there is no loss of generality in restricting the analysis to the x_b-z_b plane. The two-dimensional analysis utilizes the symbol $x_{b'}$, or $x_{s'}$, to denote that the y_b component is omitted.

The equation of the cross-section of the ellipsoid is

$$x_s'^2 + \frac{z_s^2}{(1 - e^2)} = R_e^2. \tag{3-108}$$

The equation for the normal to the ellipsoid is

$$\tan \phi = -\frac{d\, x_s'}{d\, z_s} \tag{3-109}$$

where ϕ is the geodetic latitude shown in Figure 3-13. Differentiating Equation (3-108) and equating to Equation (3-109) yields

$$\frac{z_s}{x_s'} = (1 - e^2) \tan \phi. \tag{3-110}$$

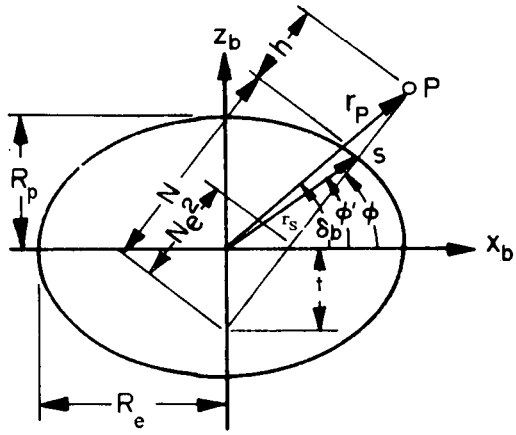

Figure 3-13. Ellipsoid Geometry

Solving Equations (3-108) and (3-110) simultaneously for x_s' yields

$$x_s' = \frac{R_e \cos \phi}{\sqrt{1 - e^2 \sin^2 \phi}}. \tag{3-111}$$

From Figure 3-13, it is apparent that

$$\cos \phi = \frac{x_s'}{N} \tag{3-112}$$

where N is the distance along the normal vector from the intersection of the normal and the ellipsoid to the z_b axis. Substituting Equation (3-111) into Equation (3-112) yields

$$N = \frac{R_e}{\sqrt{1 - e^2 \sin^2 \phi}}. \tag{3-113}$$

3.3.5.2 Geodetic to Earth-Fixed Transformation

Assume that point P in Figure 3-13 has the coordinates x_b, y_b and z_b in the body-axis system and is located a distance h from the reference ellipsoid. From Equation (3-110) and Figure 3-13, the x_b, and z_b coordinates are

$$x_b' = N \cos \phi + h \cos \phi \tag{3-114}$$

and

$$z_b = N (1 - e^2) \sin \phi + h \sin \phi. \tag{3-115}$$

Transforming Equations (3-114) and (3-115) to three dimensions yields

$$\begin{bmatrix} x_b \\ y_b \\ z_b \end{bmatrix} = \begin{bmatrix} (N + h) \cos \phi \cos \lambda \\ (N + h) \cos \phi \sin \lambda \\ (N + h - e^2 N) \sin \phi \end{bmatrix} \tag{3-116}$$

The partial derivatives of x_b, y_b, and z_b with respect to h, λ, and ϕ are

$$\begin{bmatrix} \partial x_b / \partial h \\ \partial y_b / \partial h \\ \partial z_b / \partial h \end{bmatrix} = \begin{bmatrix} \cos \phi \cos \lambda \\ \cos \phi \sin \lambda \\ \sin \phi \end{bmatrix} \tag{3-117}$$

$$\begin{bmatrix} \partial x_b/\partial \lambda \\ \partial y_b/\partial \lambda \\ \partial z_b/\partial \lambda \end{bmatrix} = \begin{bmatrix} -(N+h)\cos\phi\sin\lambda \\ (N+h)\cos\phi\cos\lambda \\ 0 \end{bmatrix} \tag{3-118}$$

$$\begin{bmatrix} \partial x_b/\partial \phi \\ \partial y_b/\partial \phi \end{bmatrix} = \left(N + h - \frac{N e^2 \cos^2\phi}{1 - e^2 \sin^2\phi}\right) \begin{bmatrix} -\sin\phi\cos\lambda \\ -\sin\phi\sin\lambda \end{bmatrix} \tag{3-119a}$$

and

$$[\partial z_b/\partial \phi] = \left(h + N(1 - e^2)\left(1 + \frac{e^2 \sin^2\phi}{1 - e^2 \sin^2\phi}\right)\right)[\cos\phi]. \tag{3-119b}$$

3.3.5.3 Earth-Fixed to Geodetic

In transforming geodetic coordinates to earth-fixed coordinates, the point of intersection of the height normal vector and the ellipsoid is given. In transforming from earth-fixed to geodetic, this point is not known a priori. This complicates the transformation. Since there is no set of equations in closed form giving this transformation.

Two solutions are presented. The first solution is iterative and can yield any required degree of accuracy. The second solution is a truncated binomial expansion that may be used when accuracy requirements are not so stringent.

The iterative technique is used primarily to determine geodetic tracking station positions where high accuracy is required. For this use (and for near earth satellites), the approximation $h \ll N$ is satisfied, and since the earth's figure is nearly spherical, $e^2 \ll 1$. Therefore the following approximation can be made: (see 3-116)

$$N \sin\phi \approx z_b. \tag{3-120}$$

Introducting t, the z_b intercept of the normal vector, it can be shown that

$$t = N e^2 \sin\phi. \tag{3-121}$$

Combining Equations (3-120) and (3-121), the following approximation for t is obtained

$$t \approx e^2 z_b. \tag{3-122}$$

Using Equation (3-122) as an initial estimate for t, the following sequence of equations may be solved iteratively to yield a solution for h and ϕ

$$z_t = z_b + t \tag{3-123}$$

$$N + h = \sqrt{x_b^2 + y_b^2 + z_t^2} \tag{3-124}$$

$$\sin \phi = \frac{z_t}{N + h} \tag{3-125}$$

$$N = \frac{R_e}{\sqrt{1 - e^2 \sin^2 \phi}} \tag{3-126}$$

$$t = N e^2 \sin \phi. \tag{3-127}$$

Upon convergence of t, ϕ and h are obtained from Equations (3-124) and (3-125). The longitude λ, is

$$\lambda = \tan^{-1}\left(\frac{y_b}{x_b}\right). \tag{3-128}$$

A second, computationally simpler, procedure for computing the values of ϕ and h to a specified point, P, is useful when accuracy requirements are less stringent. The latitude, ϕ, is solved from Equation (3-110) as follows

$$\tan \phi = \frac{z_b}{(1 - e^2)\, x_b,} = \frac{z_b}{(1 - e^2)\sqrt{x_b^2 + y_b^2}} \tag{3-129}$$

where x_b, y_b, and z_b of point P are used to approximate the subvehicle point on the ellipsoid, s, required in Equation (3-129).

This approximation yields the geodetic latitude to the normal vector of an expanded ellipse through point P. For $h << N$ and $e^2 << 1$, it is a good approximation for the geodetic latitude.

The ellipsoidal radius is

$$r_s = \sqrt{x_b^2 + z_b^2}. \tag{3-130}$$

Substituting Equation (3-107) into Equation (3-130) yields

$$r_s = \frac{R_e (1 - f)}{\sqrt{1 - (2f - f^2) \cos^2 \phi'}} \tag{3-131}$$

where ϕ' is the geocentric latitude. Applying the Binomial Theorem, we get

$$r_s = R_e \left[1 - \left(f + \frac{3}{2} f^2\right) \sin^2 \phi' + \frac{3}{2} f^2 \sin^4 \phi'\right] \tag{3-132}$$

where terms of f larger than third order are neglected. The (spheroid) height is

$$h = r_b - r_s. \tag{3-133}$$

Substituting Equation (3-132) into Equation (3-138) yields

$$h = \sqrt{x_b^2 + y_b^2 + z_b^2} - R_e + \left(R_e f + \frac{3}{2} R_e f^2\right) \sin \phi' - \frac{3}{2} R_e f^2 \sin^4 \phi'. \tag{3-134}$$

The height may be calculated optionally from Equation (3-133) by directly substituting Equation (3-131). In either case, the geocentric latitude is approximated by

$$\phi' = \sin^{-1}\left(\frac{z_b}{r_b}\right). \tag{3-135}$$

The partial derivatives of h, λ, and ϕ with respect to x_b, y_b, and z_b are obtained by differentiating Equations (3-124), (3-128), and (3-125) to yield

$$\begin{bmatrix} \partial h/\partial x_b \\ \partial h/\partial y_b \\ \partial h/\partial z_b \end{bmatrix} = -\left(\frac{e^2\, a\,(1-e^2)\sin\phi\cos\phi}{(1-e^2\sin^2\phi)^{3/2}} + \frac{z_b\cos\phi}{\sin^2\phi}\right)\begin{bmatrix} \partial\phi/\partial x_b \\ \partial\phi/\partial y_b \\ \partial\phi/\partial z_b \end{bmatrix} \tag{3-136}$$

$$\begin{bmatrix} \partial\lambda/\partial x_b \\ \partial\lambda/\partial y_b \\ \partial\lambda/\partial z_b \end{bmatrix} = \frac{1}{(x_b^2 + y_b^2)}\begin{bmatrix} -y_b \\ x_b \\ 0 \end{bmatrix} \tag{3-137}$$

and

$$\begin{bmatrix} \partial\phi/\partial x_b \\ \partial\phi/\partial y_b \\ \partial\phi/\partial z_b \end{bmatrix} = \frac{(1-e^2)}{\sqrt{x_b^2 + y_b^2}\left[(1-e^2)^2(x_b^2 + y_b^2) + z_b^2\right]}\begin{bmatrix} -x_b z_b \\ -y_b z_b \\ (x_b^2 + y_b^2) \end{bmatrix}. \tag{3-138}$$

3.3.6 Earth-Fixed to Topocentric Local Tangent (East, North, Up)

The topocentric local tangent system, described in Section 3.2.4, is used in processing ground based observation data. The transformation from geocentric earth-fixed coordinates (x_b, y_b, z_b) to local tangent coordinates (x_{lt}, y_{lt}, z_{lt}) requires a translation along the geocentric radius vector to the station and a rotation of the axis through the station's longitude and latitude angles. The earth's shape and station identification parameters are defined as follows

$\bar{r}_s$ ~ the body-fixed coordinates of the station
ϕ_s ~ the geodetic latitude of the station (positive north)
ϕ'_s ~ the geocentric latitude of the station
λ_s ~ the longitude of the station (positive east)
h_s ~ the height of the station above the reference ellispoid.

The magnitude of the normal vector to the reference spheroid's surface at the station is given by (see Equation (3-115))

$$N_s = \frac{R_e}{\sqrt{1 - (2f - f^2) \sin^2 \phi_s}} . \tag{3-139}$$

The components of the geocentric radius vector to the station along the x_b, y_b, and z_b axes are

$$\begin{bmatrix} x_s \\ y_s \\ z_s \end{bmatrix} = \begin{bmatrix} (N_s + h_s) \cos \phi_s \cos \lambda_s \\ (N_s + h_s) \cos \phi_s \sin \lambda_s \\ (N_s + h_s - e^2 N_s) \sin \phi_s \end{bmatrix} . \tag{3-140}$$

To bring the x_b, y_b, and z_b axes parallel to the x_{lt}, y_{lt}, and z_{lt} axes, a rotation is made about the z_b axis by the angle $(\pi/2 + \lambda)$ and about the new x_b axis by the angle $(\pi/2 - \phi)$. The resulting transformation matrix M_{lt}, may be written as

$$M_{lt} = \begin{bmatrix} -\sin \lambda & \cos \lambda & 0 \\ -\sin \phi \cos \lambda & -\sin \phi \sin \lambda & \cos \phi \\ \cos \phi \cos \lambda & \cos \phi \sin \lambda & \sin \phi \end{bmatrix} . \tag{3-141}$$

The local tangent coordinates of a point in space, x_b, y_b, and z_b, may be written as

$$\bar{r}_{lt} = M_{lt} (\bar{r}_b - \bar{r}_s). \tag{3-142}$$

This translates the system from the earth's center to the station and rotates it to the local tangent system.

The earth-fixed velocity in the local tangent system is given by

$$\dot{\bar{r}}_{lt} = M_{lt}\,\dot{\bar{r}}_b \tag{3-143}$$

since $\dot{M}_{lt} = 0$ and $\dot{r}_s = 0$.

Since the local tangent system, determined only by the station parameters, is not a function of the coordinates of a given earth-fixed point, the partials of its components with respect to the earth-fixed components are the respective elements of the M_{lt} matrix given by

$$\frac{\partial \bar{r}_{lt}}{\partial \bar{r}_b} = \frac{\partial \dot{\bar{r}}_{lt}}{\partial \dot{\bar{r}}_b} = M_{lt}. \tag{3-144}$$

3.3.7 Keplerian-Cartesian Transformations

3.3.7.1 Keplerian to Cartesian Coordinates

Consider the orbit geometry illustrated in Figure 3-5. The origin is the center of the reference body, the x-axis points to the vernal equinox, and the z-axis lies along the axis of the planet's rotation. The satellite orbital plane intersects the equator at the ascending node. The angle Ω is the right ascension of the ascending node. The axis z_{op} is normal to the orbital plane defining the orbit's inclination. The angle ω is the argument of perifocus. In Figure 3-6, the eccentricity, e, and semimajor axis, a, (q for a parabola) specify the orbit's shape and size, that is, they identify the orbit as being parabolic, elliptic, or hyperbolic. The final element necessary to predict a body's position and velocity is the mean anomaly M. The eccentric anomaly, or true anomaly, f, is often used instead of M. They define the satellite's motion around the central body.

First consider the transformation from the orbital elements (a, e, i, Ω, ω, M) to the orbital rectangular coordinate (x_p, y_p, z_p, $\dot{x}_p$, $\dot{y}_p$, $\dot{z}_p$). The x_p axis is directed toward perigee, the y_p axis is in the plane of motion advanced $\pi/2$ from the x_p-axis in the direction of motion, and the z_p axis completes a right-handed system. We then have for the various conics

- Ellipse: $0 < e < 1$

$$\begin{bmatrix} x_p \\ y_p \\ z_p \end{bmatrix} = a \begin{bmatrix} \cos E - e \\ \sqrt{1 - e^2} \sin E \\ 0 \end{bmatrix} \tag{3-145}$$

and

$$\begin{bmatrix} \dot{x}_p \\ \dot{y}_p \\ \dot{z}_p \end{bmatrix} = \frac{\sqrt{\mu/a}}{(1 - e \cos E)} \begin{bmatrix} \sin E \\ \sqrt{1 - e^2} \cos E \\ 0 \end{bmatrix} \tag{3-146}$$

where

$E \sim$ the eccentric anomaly
$\mu \sim$ the gravitational parameter of the reference body.

The eccentric anomaly, E, is computed by Kepler's equation

$$M = E - e \sin E \tag{3-147}$$

and is solved by the following iteration scheme.

$$F_{ct}(E_n) = E_n - e \sin E_n - M \tag{3-148}$$

$$D_n = 1 - e \cos [E_n - .5 F_{ct}(E_n)] \tag{3-149}$$

$$E_{n+1} = E_n - \frac{F_{ct}(E_n)}{D_n} \qquad n = 0, 1, 2, 3, \ldots \tag{3-150}$$

where

$$E_0 = M - e \sin M \tag{3-151}$$

- Hyperbola: $e > 1$

$$\begin{bmatrix} x_p \\ y_p \\ z_p \end{bmatrix} = a \begin{bmatrix} \cosh F - e \\ -\sqrt{e^2 - 1}\ \sinh F \\ 0 \end{bmatrix} \tag{3-152}$$

$$\begin{bmatrix} \dot{x}_p \\ \dot{y}_p \\ \dot{z}_p \end{bmatrix} = \frac{\sqrt{-\mu/a}}{e\,(\cosh F - 1)} \begin{bmatrix} \sinh F \\ -\sqrt{e^2 - 1}\ \cosh F \\ 0 \end{bmatrix} \tag{3-153}$$

where

$F \sim$ the hyperbolic anomaly computed using Kepler's equation for a hyperbola, $M = e \sin F - F$.

The hyperbolic Kepler equation may be solved by a Newton-Raphson iteration of the following form

$$F_{n+1} = F_n - \frac{(e \sinh F_n - F_n - M)}{e \cosh F_n - 1} \tag{3-149}$$

where $F_0 = M/2$. (Note: The preceeding equation is singular for orbits with $e \approx 1$.)

- Parabola: $e = 1$

$$\begin{bmatrix} x_p \\ y_p \\ z_p \end{bmatrix} = \begin{bmatrix} q - D^2/2 \\ \sqrt{2q}\, D \\ 0 \end{bmatrix} \tag{3-155}$$

$$\begin{bmatrix} \dot{x}_p \\ \dot{y}_p \\ \dot{z}_p \end{bmatrix} = \frac{1}{(q + D^2/2)} \begin{bmatrix} -D \\ \sqrt{2\,q} \\ 0 \end{bmatrix} \tag{3-156}$$

where

$$q = p/2. \tag{3-157}$$

D is computed from Barker's equation, that is

$$D^3 + 6\,q\,D = 6\,M. \tag{3-158}$$

The orbital rectangular coordinates are transformed to inertial Cartesian position and velocity coordinates as follows

$$\begin{bmatrix} x \\ y \\ z \end{bmatrix} = P \begin{bmatrix} x_p \\ y_p \end{bmatrix} \tag{3-159}$$

and

$$\begin{bmatrix} \dot{x} \\ \dot{y} \\ \dot{z} \end{bmatrix} = P \begin{bmatrix} \dot{x}_p \\ \dot{y}_p \end{bmatrix}. \tag{3-160}$$

The elements, p_{ij}, of the 3×2 rotation matrix, P, are

$$
\begin{aligned}
P_{11} &= \cos\Omega\cos\omega - \sin\Omega\cos i\sin\omega \\
P_{12} &= -\cos\Omega\sin\omega - \sin\Omega\cos i\cos\omega \\
P_{21} &= \sin\Omega\cos\omega + \cos\Omega\cos i\sin\omega \\
P_{22} &= -\sin\Omega\sin\omega + \cos\Omega\cos i\cos\omega \\
P_{31} &= \sin i\sin\omega \\
P_{32} &= \sin i\cos\omega .
\end{aligned}
\tag{3-161}
$$

3.3.7.2 Keplerian to Cartesian Partials

The functional relationships expressed in Equations (3-159) and (3-160) are

$$
\begin{aligned}
\bar{r} &= P(\Omega,\ \omega,\ i)\ \bar{r}_p\ (a,\ e,\ M) \\
\dot{\bar{r}} &= P(\Omega,\ \omega,\ i)\ \dot{\bar{r}}_p\ (a,\ e,\ M).
\end{aligned}
\tag{3-162}
$$

and

The partial derivatives of $\bar{r}$ with respect to the orbital elements may be written

$$
\frac{\partial \bar{r}}{\partial \zeta} = P\,\frac{\partial \bar{r}_p}{\partial \zeta}
\tag{3-163}
$$

and

$$
\frac{\partial \dot{\bar{r}}}{\partial \zeta} = P\,\frac{\partial \dot{\bar{r}}_p}{\partial \zeta}
$$

for ζ = a, e, and M, and

$$
\frac{\partial \bar{r}}{\partial \zeta} = \frac{\partial P}{\partial \zeta}\,\bar{r}_p
\tag{3-164}
$$

and

$$
\frac{\partial \dot{\bar{r}}}{\partial \zeta} = \frac{\partial P}{\partial \zeta}\,\dot{\bar{r}}_p
$$

for $\zeta = \Omega, \omega$, and i.

The partials of $\bar{r}_p$ and $\dot{\bar{r}}_p$ for elliptical orbits are

$$\frac{\partial \bar{r}_p}{\partial (a,\ e,\ i)} = \begin{bmatrix} \frac{x_p}{a} & \left(- a - \frac{y_p^2}{r\ (1 - e^2)} \right) & \left(- \frac{a\ y_p}{r\ \sqrt{1 - e^2}} \right) \\ \frac{y_p}{a} & \left(\frac{x_p\ y_p}{r\ (1 - e^2)} \right) & \left(\frac{a \sqrt{1 - e^2}\ (x_p + a\ e)}{r} \right) \\ 0 & 0 & 0 \end{bmatrix} \quad (3\text{-}165)$$

and

$$\frac{\partial \dot{\bar{r}}_p}{\partial (a,\ e,\ i)} = \begin{bmatrix} - \frac{\dot{x}_p}{2a} & \dot{x}_p \left(\frac{a}{r} \right)^2 \left(2 \left(\frac{x_p}{a} \right) + \frac{e}{1 - e^2} \left(\frac{y_p}{a} \right)^2 \right) & - n \left(\frac{a}{r} \right)^3 x_p \\ - \frac{\dot{y}_p}{2a} & \frac{n}{\sqrt{1 - e^2}} \left(\frac{a}{r} \right)^2 \left(\frac{x_p^2}{r} - \frac{y_p^2}{a\ (1 - e^2)} \right) & - n \left(\frac{a}{r} \right)^3 y_p \\ 0 & 0 & 0 \end{bmatrix} \quad (3\text{-}166)$$

where the mean motion, n, is

$$n = \frac{1}{a} \sqrt{\frac{\mu}{a}} . \quad (3\text{-}167)$$

The partials of P with respect to Ω, ω, and i are

$$\frac{\partial P}{\partial \Omega} = \begin{bmatrix} (- \sin\Omega \cos\omega - \cos\Omega \cos i \sin\omega) & (- \sin\Omega \sin\omega - \cos\Omega \cos i \cos\omega) \\ (\cos\Omega \cos\omega - \sin\Omega \cos i \sin\omega) & (- \cos\Omega \sin\omega - \sin\Omega \cos i \cos\omega) \\ 0 & 0 \end{bmatrix} \quad (3\text{-}168)$$

$$\frac{\partial P}{\partial \omega} = \begin{bmatrix} (-\cos\Omega\sin\omega - \sin\Omega\cos i\cos\omega) & (-\cos\Omega\cos\omega + \sin\Omega\cos i\sin\omega) \\ (-\sin\Omega\sin\omega + \cos\Omega\cos i\cos\omega) & (-\sin\Omega\cos\omega - \cos\Omega\cos i\sin\omega) \\ (\sin i\cos\omega) & (-\sin i\sin\omega) \end{bmatrix} \quad (3\text{-}169)$$

and

$$\frac{\partial P}{\partial i} = \begin{bmatrix} \sin\Omega\sin i\sin\omega & \sin\Omega\sin i\cos\omega \\ -\cos\Omega\sin i\sin\omega & -\cos\Omega\sin i\cos\omega \\ \cos i\sin\omega & \cos i\cos\omega \end{bmatrix} . \quad (3\text{-}170)$$

3.3.7.3 Cartesian Coordinates to Keplerian Elements

Given the position, $\bar{r}$, and velocity, $\dot{\bar{r}}$, are given at time t, the standard Keplerian elements (a, e, i, Ω, ω, M) are calculated as follows. Let the magnitude of the position, velocity, and angular momentum be denoted by

$$r = |\bar{r}| \quad (3\text{-}171)$$

$$V = |\dot{\bar{r}}| \quad (3\text{-}172)$$

$$h = |\bar{h}| = |\bar{r} \times \dot{\bar{r}}| . \quad (3\text{-}173)$$

The equations for the orbital elements and related parameters are then

Semimajor Axis

$$a = \frac{\mu r}{(2\mu - r V^2)} \quad (3\text{-}174)$$

Semilatus Rectum

$$p = \frac{1}{\mu}\left[(r\,V)^2 - (\bar{r}\cdot\dot{\bar{r}})^2\right] \tag{3-175}$$

Eccentricity

$$e = \sqrt{1 - \frac{p}{a}} \tag{3-176}$$

Inclination

$$\sin i = \frac{|\bar{r}\times\dot{\bar{r}}\times\bar{u}_z|}{r\,V} = \frac{\sqrt{h_x^2 + h_y^2}}{r\,V}$$

$$\cos i = \frac{(\bar{r}\times\dot{\bar{r}})\cdot\bar{u}_z}{r\,V} = \frac{h_z}{r\,V} \tag{3-177}$$

where $\bar{u}_x$, $\bar{u}_y$, and $\bar{u}_z$ are unit vectors associated with the coordinate axes that express $\bar{r}$ and $\dot{\bar{r}}$, and h_x, h_y, and h_z are components of h

Elliptic Motion	Hyperbolic Motion
$a > 0$	$a \le 0$

Eccentric Anomaly

$$\sin E = \frac{1}{e}\left(\frac{\bar{r}\cdot\dot{\bar{r}}}{\sqrt{\mu\,a}}\right) \qquad \sinh H = \frac{1}{e}\left(\frac{\bar{r}\cdot\dot{\bar{r}}}{\sqrt{-\mu\,a}}\right) \tag{3-178}$$

$$\cos E = \frac{1}{e}\left(1 - \frac{r}{a}\right) \qquad \cosh H = \frac{1}{e}\left(1 + \frac{r}{a}\right)$$

Elliptic Motion	Hyperbolic Motion	
$a > 0$	$a \leq 0$	
.ean Anomaly		
$M = E - \frac{\bar{r} \cdot \dot{\bar{r}}}{\sqrt{\mu a}}$	$M = \frac{\bar{r} \cdot \dot{\bar{r}}}{\sqrt{-\mu a}} - H$	(3-179)
Period		
$P = 2\pi \sqrt{\frac{a^3}{\mu}}$	$P = 0$	(3-180)
Energy (per unit mass)		
$\text{Energy} = -\frac{\mu}{2a}$	$\text{Energy} = \frac{\mu}{2a}$	(3-181)

Longitude of Ascending Node

$$\sin \Omega = \frac{h_y}{h}$$

$$\cos \Omega = \frac{h_x}{h} \qquad (3\text{-}182)$$

True Anomaly

$$\sin f = \frac{\sqrt{\mu p}\,(\bar{r} \cdot \dot{\bar{r}})}{\mu r e}$$

$$\cos f = \frac{\mu (p - r)}{\mu r e} \qquad (3\text{-}183)$$

Argument of Perifocus

$$\sin(\omega + f) = \frac{\sqrt{\mu p}\, r_z}{h\, r}$$

$$\cos(\omega + f) = \frac{r_y h_x - r_x h_y}{h\, r} \tag{3-184}$$

Perifocal and Apofocal Radius

$$r_p = a(1 - e) \tag{3-185}$$

$$r_a = a(1 + e) \tag{3-186}$$

Perifocal and Apofocal Height

$$h_p = r_p - a_p \tag{3-187}$$

$$h_a = r_a - a_p. \tag{3-188}$$

The partial derivatives of the Keplerian coordinates with respect to the Cartesian coordinates are given by the inverse of the Keplerian to Cartesian partials in Equations (3-163) and (3-164), i.e.

$$\begin{bmatrix} \partial a/\partial x & \partial a/\partial y \cdots & \partial a/\partial \dot{z} \\ \partial e/\partial x & \partial e/\partial y \cdots & \\ \partial i/\partial x & \partial i/\partial y \cdots & \\ \vdots & \vdots & \\ \partial M/\partial x & \partial M/\partial y \cdots & \partial M/\partial \dot{z} \end{bmatrix} = \begin{bmatrix} \partial x/\partial a & \partial x/\partial e & \partial x/\partial i \cdots & \partial x/\partial M \\ \partial y/\partial a & \partial y/\partial e & \partial y/\partial i \cdots & \\ \vdots & \vdots & \vdots & \\ \partial \dot{z}/\partial a & \partial \dot{z}/\partial e & \partial \dot{z}/\partial i \cdots & \partial \dot{z}/\partial M \end{bmatrix}^{-1} \tag{3-189}$$

3.4 TIME SYSTEMS

The GTDS orbit determination program uses the atomic time system, A.1, in the integration of the equations of motion. However, the program must interface with external input-output data sets which are referenced to other time systems, such as the ephemeris time system, ET, for the solar/lunar/planetary ephemerides, the universal time systems, UTC for input-output epochs and tracking data, and UT1 for computing Greenwich sidereal time. A brief description of the relevant time systems and their interelationships follows (Reference 8 and 9).

3.4.1 Ephemeris Time, ET

This is the uniform measure of time, which is the independent variables of the equations of motion, and the argument for the ephemerides of the planets, the moon, and the satellite. The unit of ET is the ephemeris second, which is defined as the fraction 1/31,556,925.9747 of the tropical year for 12^h ET of Jan 0^d, 1900. Ephemeris time is determined from the instant near the beginning of the calendar year 1900 when the geometric mean longitude of the sun, L_M, was 279^h 41'48!'04 at which instant the measure of ephemeris time was 1900 Jan 0^d 12^h.

3.4.2 Atomic Time, A.1

A.1 time is one of several types of atomic time. It is obtained from oscillations of the US Cesium Frequency Standard located at Boulder. Colrado. In 1958, the US Naval Observatory established the A.1 system based on an assumed frequency of 9,192,631,770 oscillations of the isotope 133 of cesium atom per A.1 second. The reference epoch of A.1 was established so that on Jan 1, 1958, $0^h0^m0^s$ UT2 the value of A.1 was $0^h0^m0^s$, Jan 1, 1958.

3.4.3 Universal Time, UT

This is the measure of time that is the theoretical basis for all civil time keeping. UT is related to the rotation of the earth on its axis. Compared to ephemeris time, which is uniform time, UT does not take into account the irregularities of the earth's rate of rotation.

The quantity UT is defined as 12 hours plus the Greenwich Hour Angle (GHA) of a point (representing a fictitious mean sun) on the mean equator of epoch whose right ascension measured from the mean equinox of epoch is

$$R_u = 18^h\ 38^m\ 45^s.836 + 8{,}640{,}184^s.542\ T_u + {}^s.0929\ T_u^2 \qquad (3\text{-}190)$$

where T_u is defined below Equation (3-16).

The Greenwich hour angle of this point, denoted by α_s in Figure 3-14 is

$$\alpha_s = \alpha_{GM} - R_u \qquad (3\text{-}191)$$

where α_{GM} is the Greenwich mean sidereal time; hence,

$$UT = 12^h + \alpha_{GM} - R_u. \qquad (3\text{-}192)$$

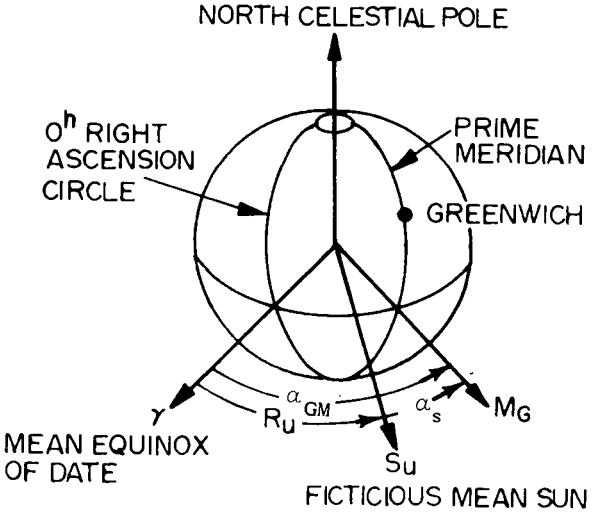

Figure 3-14. Greenwich Hour Angle

Adding 12 hours to both sides of the above equation yields

$$UT + 12^h = \alpha_{GM} - R_u \qquad (3\text{-}193)$$

and solving for α_{GM}

$$\alpha_{GM} = 12^h + UT + R_u. \qquad (3\text{-}194)$$

The practical determination of UT is obtained from meridian transits of stars by the US Naval Observatory. At the instant of observation, the right ascension of the observing station is equal to the observed star, relative to the true equator and equinox of date. Subtracting the east longitude of the observing station gives the true Greenwich sidereal time, α_g, at the instant of observation. α_g is also the Greenwich Hour Angle of the true equinox of date. Subtracting the nutation in right ascension gives the Greenwich Mean Sidereal Time, α_{GM} or GMST. UT is then determined from the above equation.

3.4.4 Uncorrected Universal Time, UTO

This measure of time is obtained from UT by assuming a nominal value of the longitude of each observing station. The resulting UT is labeled UTO. Actual determination of UTO is done by an instrument located at an observatory whose adopted conventional longitude is λ_A (see Section 3.3.1.4 for adopted longitude). When the longitude $-\lambda_A$ is added to the observed local hour angle of the point S_u, (see Figure 3-14), whose right ascension measured from the mean equator and equinox of date is R_u, then UTO is obtained (see Figure 3-15).

$$UTO = 12^h - \lambda_A + \text{LHA of } S_u. \tag{3-195}$$

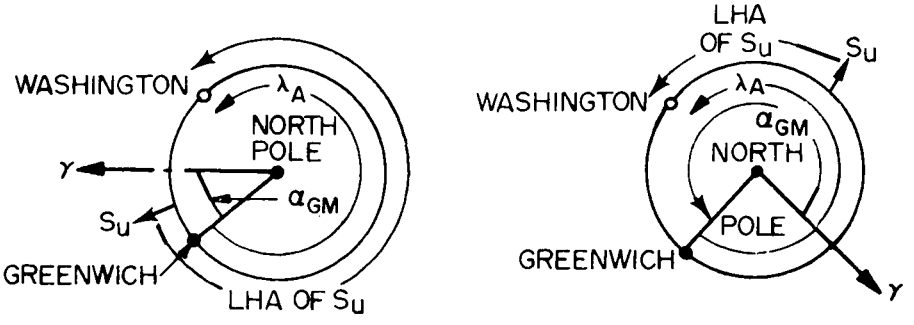

Figure 3-15. Universal Time References

3.4.5 Universal Time, UT1

This measure of time is defined in terms of UTO by applying an appropriate correction in longitude due to the motion of the pole and is the form of universal time used in GTDS. UT1 reflects the actual orientation of the earth with

respect to the vernal equinox at that instant. UT1 will be the same for all observatories. In contrast, UTO time, as determined by different observatories using their adopted longitude in calculations, results in a different value of UTO for each observatory.

Then

$$UT1 = UTO - \Delta\lambda \tag{3-196}$$

where $\Delta\lambda$ is given in Equation (3-26).

UT1 time is caused by GTDS to compute the α_{GM} as given in Equation (3-14).

3.4.6 Universal Time, UT2

If the extrapolated value of UT1 time is corrected for periodic seasonal variations, SV, in the earth's speed of rotation, the resulting time is UT2. UT2 does not represent the actual orientation of the earth with respect to the vernal equinox. UT1 should always be used when the actual orientation of the earth is required. UT2 is often referred to as GMT, Greenwich Mean Time, and ZULU time. The equations for UT2 are

$$UT2 = UT1 + SV \tag{3-197}$$

where

$$SV = {}^{s}.022 \sin 2\pi t - {}^{s}.017 \cos 2\pi t - {}^{s}.007 \sin 4\pi t + {}^{s}.006 \cos 4\pi t \tag{3-198}$$

or

$$SV = {}^{s}.022 \sin 2\pi t - {}^{s}.012 \cos 2\pi t - {}^{s}.006 \sin 4\pi t + {}^{s}.007 \cos 4\pi t. \tag{3-199}$$

Equation (3-198) was used prior to 1962 and Equation (3-199) has been in use since 1962. The quantity t equals the fraction of the tropical year elapsed from the beginning of the Besselian year for which the calculation is made. (One tropical year = 365.2422 days.) Since seasonal variations can be known precisely only after their occurrence, UT2 itself is rarely used. The Bureau International de l'Heure also issues corrections for $\Delta\lambda$ and SV.

3.4 Universal Time Coordinated, UTC

This is the standard time scale to which tracking stations are synchronized. UTC time is derived from atomic time, A.1, in a manner which makes it almost synchronous with Earth-rotation-derived time.

Up to January 1, 1972, the UTC time scale operated at a frequency offset from the atomic time scale. The value of the offset was periodically changed by international agreement so that the UTC scale would correspond more closely to time derived from the rotation of the Earth.

On January 1, 1972, a new improved UTC system, adopted by the International Radio Consultative Committee (CCIR), was internationally implemented by the time-keeping laboratories and time-broadcast stations (References 10 and 11).

The new UTC system eliminates the frequency offset from atomic time, thus making the UTC second constant and equal in duration to the A.1 second. The new UTC time scale is now kept in synchronism with the rotation of the earth to within ±0.7 second by step-time adjustments of exactly one second, when needed.

3.4.8 Station Time, ST

This measure of time is obtained at each station by counting cycles of a rubidium atomic frequency standard. The difference between ST and UTC is tabulated by each station. The observables are recorded in ST and then transformed to UTC.

3.5 TRANSFORMATIONS BETWEEN TIME SYSTEMS

Desired transformations between the time systems ET, A.1, UTC, and UT1 are carried out in the GTDS orbit determination program by evaluating either a standard formula or an appropriate time polynomial.

3.5.1 Transformations by Standard Formula

For most purposes, the difference between A.1 and ET may be considered a constant. The suspected discrepancy is roughly two parts in 10^9. The actual transformation between A.1 and ET time is given by

$$(ET - A.1) = \Delta T_{1958} - \frac{(JD - 2,436,204.5)\ (86,400)}{9,192,631,770} \times \Delta f_{cesium} + \frac{2\ e\ (\mu\ a)\ 1/2\ \sin E}{c^2} \qquad (3\text{-}200)$$

where

ΔT_{1958} ~ the ET - UT2 on 1 January 1958, $0^h0^m0^s$ UT2 minus the periodic term in Equation (3-200) evaluated at this same epoch

JD ~ the Julian date

2,436,204.5 ~ the Julian date on 1 January 1958, $0^h0^m0^s$

Δf_{cesium} ~ the correction to f_{cesium} = 9,192,631,770 cycles of cesium per ephemeris second

μ ~ the gravitational constant of the sun, $1.327,154,45 \times 10^{11}$ km^3/sec^2

a ~ the semimajor axis of the heliocentric orbit of the earth-moon barycenter, 149,599,000 km

e ~ the eccentricity of the heliocentric orbit of the earth-moon barycenter .01672

c ~ the speed of light at an infinite distance from the sun, 299,792.5 km/sec

E ~ the eccentric anomaly of the heliocentric orbit of the earth-moon barycenter.

The first term of Equation (3-200) arises since A.1 was set equal to UT2 at the beginning of 1958. The second term accounts for the difference between the lengths of ET and A.1 seconds (if Δf_{cesium} is nonzero). The periodic term arises from general relativity. It accounts for the fact that A.1, UTC, and ST time is a measure of proper time observed on earth, and that ET is a measure of coordinate time in the heliocentric (strictly barycentric) space-time frame of reference. The contribution of the last two terms in Equation (3-200) is negligible for the range of applications currently contemplated for the GTDS program. Hence, the transformation between ET and A.1 is accomplished using the approximate formula,

$$ET - A.1 = 32^s.15 \qquad (3\text{-}201)$$

3.5.2 Transformations by Time Polynomials

The remaining transformations between the time systems A.1, UTC, and UT1 are accomplished using the time difference data A.1-UTC, and A.1-UT1, supplied by the U. S. Naval Observatory. These data have been conveniently reduced by quadratic polynomial fits in order to improve the efficiency of the transformation procedure. The time difference polynomials derived for use by the GTDS program have the form

$$(A.1 - UTC)_i = a_{i1} + a_{i2}T + a_{i3}T^2 \tag{3-202}$$

$$(A.1 - UT1)_i = a_{i4} + a_{i5}T + a_{i6}T^2 \tag{3-203}$$

where

A.1-UTC - the difference between A.1 and UTC time, in seconds.
A.1-UT1 - the difference between A.1 and UT1 time, in seconds.
T - the number of days from the beginning of the time span covered by the polynomial, T = 1, 2, . . .
i - the index of the time span.

The coefficients a_{ij} are given in Table 3-1, next to Modified Julian dates (Mod 2,430,000) defining the time interval for which the coefficients are applicable. The table covers the time span from January 1, 1958, and is updated once every month as current data from the U.S. Naval Observatory becomes available. The last row of coefficients in the table is used to obtain extrapolated values of the time-differences for a short time in the future. The table is used by finding the value of i such that the given date, MJD_j, is in the range

$$MJD_i \leq MJD_j < MJD_{i+1}$$

The argument of interpolation, T, is then computed from,

$$T = MJD_j - MJD_i + 1. \tag{3-204}$$

Table 3-1. Time Difference Coefficients

GREGORIAN DATE	MODIFIED JULIAN DATE	A.1-UTC			A.1-UT1		
		a_{i1}	a_{i2}	a_{i3}	a_{i4}	a_{i5}	a_{i6}
01/01/1958	6204	-0.16180D-01	0.97458D-03	-0.39916D-05	0.18589D-01	0.20174D-02	-0.14093D-04
01/16/1958	6219	0.17585D-01	0.94021D-03	-0.22883D-05	0.45486D-01	0.16189D-02	0.17998D-05
02/06/1958	6240	0.56160D-01	0.83665D-03	-0.13736D-05	0.80117D-01	0.16625D-02	-0.26988D-05
02/20/1958	6254	0.87544D-01	0.83971D-03	0.45554D-06	0.10280D 00	0.16259D-02	0.26063D-05
04/10/1958	6303	0.14961D 00	0.94298D-03	-0.21318D-05	0.18746D 00	0.19940D-02	-0.60542D-05
05/31/1958	6354	0.19265D 00	0.86426D-03	0.20230D-05	0.27283D 00	0.12288D-02	-0.62937D-05
06/12/1958	6366	0.22331D 00	0.94086D-03	-0.14324D-05	0.28664D 00	0.10921D-02	-0.10284D-04
07/03/1958	6387	0.26262D 00	0.88819D-03	0.13736D-05	0.30501D 00	0.61568D-03	0.30381D-05
07/17/1958	6401	0.29520D 00	0.90079D-03	-0.18101D-06	0.31658D 00	0.29663D-03	0.66051D-05
10/23/1958	6499	0.40162D 00	0.84210D-03	-0.25981D-06	0.40965D 00	0.16710D-02	-0.13796D-06
11/27/1958	6534	0.45038D 00	0.76889D-03	0.22325D-05	0.46820D 00	0.16640D-02	-0.81837D-06
12/25/1958	6562	0.49405D 00	0.89040D-03	0.45974D-06	0.51425D 00	0.14852D-02	0.30961D-05
01/29/1959	6597	0.54583D 00	0.91691D-03	0.45577D-06	0.57006D 00	0.13938D-02	-0.13048D-05
02/26/1959	6625	0.59189D 00	0.94799D-03	-0.20746D-06	0.60282D 00	0.17050D-02	-0.32176D-05
08/02/1959	6782	0.73505D 00	0.11100D-02	-0.50000D-04	0.78856D 00	0.87143D-03	-0.28571D-04
08/06/1959	6786	0.75874D 00	0.87042D-03	-0.22586D-06	0.79189D 00	0.59155D-03	0.76440D-05
08/27/1959	6807	0.79697D 00	0.85872D-03	0.44598D-06	0.80767D 00	0.95180D-03	0.68977D-05
10/01/1959	6842	0.84726D 00	0.85073D-03	0.12137D-05	0.84928D 00	0.15959D-02	0.26686D-05
11/05/1959	6877	0.89834D 00	0.94242D-03	-0.32967D-05	0.90810D 00	0.17714D-02	0.26584D-05
11/19/1959	6891	0.93098D 00	0.86887D-03	0.46945D-06	0.93350D 00	0.17751D-02	-0.45688D-05
12/17/1959	6919	0.97625D 00	0.67294D-03	0.13598D-04	0.97980D 00	0.14695D-02	-0.30766D-05
01/14/1960	6947	0.10058D 01	0.12763D-02	-0.25468D-07	0.10155D 01	0.14312D-02	0.69049D-06
05/30/1960	7084	0.11800D 01	0.12766D-02	-0.70583D-07	0.12238D 01	0.69186D-03	-0.17062D-05
09/07/1960	7184	0.13070D 01	0.12517D-02	0.20064D-06	0.12779D 01	0.12722D-02	0.10631D-05
01/01/1961	7300	0.14599D 01	0.12906D-02	-0.12596D-07	0.14424D 01	0.70022D-03	0.52074D-05
04/20/1961	7409	0.16004D 01	0.12887D-02	-0.45082D-07	0.15729D 01	0.14314D-02	-0.48660D-05
08/01/1961	7512	0.16827D 01	0.12976D-02	-0.16113D-07	0.16664D 01	0.60244D-03	0.42234D-05
12/17/1961	7650	0.18616D 01	0.13000D-02	-0.12627D-15	0.18265D 01	0.59200D-03	0.64585D-04
01/01/1962	7665	0.18815D 01	0.11213D-02	0.94592D-08	0.18437D 01	0.12372D-02	0.13325D-05
06/02/1962	7817	0.20518D 01	0.11163D-02	0.27769D-07	0.20709D 01	0.47241D-03	0.19631D-05
09/12/1962	7919	0.21659D 01	0.11205D-02	0.58281D-09	0.21415D 01	0.14908D-02	0.17563D-05
01/05/1963	8034	0.22948D 01	0.11162D-02	0.66202D-07	0.23369D 01	0.56111D-03	0.71013D-05
04/13/1963	8132	0.24046D 01	0.11242D-02	-0.42667D-08	0.24604D 01	0.20227D-02	-0.83469D-05
08/14/1963	8255	0.25428D 01	0.11186D-02	0.10362D-07	0.26182D 01	0.11400D-02	0.68600D-05
11/01/1963	8334	0.27312D 01	0.11120D-02	0.15421D-06	0.27506D 01	0.22533D-02	-0.19756D-05
01/06/1964	8400	0.28058D 01	0.12980D-02	-0.10445D-07	0.28918D 01	0.19926D-02	0.74750D-06
04/01/1964	8486	0.30173D 01	0.12938D-02	0.13842D-08	0.30635D 01	0.26842D-02	-0.69351D-05
07/07/1964	8583	0.31429D 01	0.12948D-02	-0.40265D-07	0.32548D 01	0.96644D-03	0.42363D-05
09/01/1964	8639	0.33153D 01	0.12876D-02	0.31036D-06	0.33218D 01	0.15453D-02	0.10551D-04
10/01/1964	8669	0.33552D 01	0.12951D-02	-0.12980D-08	0.33793D 01	0.22855D-02	-0.42952D-06
01/01/1965	8761	0.35743D 01	0.12948D-02	0.45889D-08	0.35876D 01	0.20391D-02	0.52942D-06
03/01/1965	8820	0.37507D 01	0.12974D-02	-0.11539D-07	0.37053D 01	0.29024D-02	-0.46222D-05
07/01/1965	8942	0.40088D 01	0.12962D-02	-0.86563D-08	0.39920D 01	0.15425D-02	0.12374D-05
09/01/1965	9004	0.41892D 01	0.12961D-02	-0.15623D-08	0.40896D 01	0.24052D-02	0.25459D-05
12/09/1965	9103	0.43174D 01	0.12980D-02	-0.13370D-16	0.43475D 01	0.24460D-02	-0.14892D-04
01/02/1966	9127	0.43485D 01	0.25916D-02	0.16584D-08	0.43966D 01	0.23429D-02	0.12215D-05
06/14/1966	9290	0.47710D 01	0.25941D-02	-0.18556D-07	0.48113D 01	0.15947D-02	0.32520D-05
09/25/1966	9393	0.50380D 01	0.25909D-02	0.19487D-07	0.50122D 01	0.28620D-02	0.59360D-06
12/01/1966	9460	0.52110D 01	0.25922D-02	-0.42963D-08	0.52113D 01	0.20905D-02	0.27519D-05
04/23/1967	9603	0.55817D 01	0.25933D-02	-0.88063D-08	0.55701D 01	0.26816D-02	-0.63568D-05
08/11/1967	9713	0.58669D 01	0.26854D-02	0.34789D-07	0.57938D 01	0.16662D-02	0.72409D-05
11/30/1967	9824	0.61543D 01	0.25901D-02	0.33990D-07	0.60640D 01	0.24730D-02	0.90221D-06
02/01/1968	9887	0.62176D 01	0.25920D-02	-0.36377D-10	0.62273D 01	0.22595D-02	0.29557D-05
06/01/1968	10008	0.65313D 01	0.25920D-02	0.65706D-11	0.65394D 01	0.18464D-02	0.27527D-05
12/26/1968	10216	0.70704D 01	0.25920D-02	-0.61122D-10	0.70394D 01	0.23759D-02	0.34122D-05
05/18/1969	10359	0.74411D 01	0.25920D-02	0.12925D-09	0.74487D 01	0.23189D-02	-0.17309D-05
09/07/1969	10471	0.77314D 01	0.25920D-02	-0.54770D-11	0.76939D 01	0.29385D-02	-0.72185D-07
04/14/1970	10690	0.82990D 01	0.25920D-02	0.29500D-11	0.83395D 01	0.33310D-02	-0.75470D-05
08/17/1970	10815	0.86230D 01	0.25920D-02	-0.68960D-16	0.86399D 01	0.21509D-02	0.56553D-05
12/08/1970	10928	0.89159D 01	0.25920D-02	-0.25217D-11	0.89557D 01	0.23777D-02	0.28347D-05
04/17/1971	11058	0.92529D 01	0.25920D-02	0.22604D-16	0.98187D 01	0.31771D-02	-0.44673D-05
08/27/1971	11190	0.95950D 01	0.25920D-02	0.87452D-10	0.96634D 01	0.25250D-02	0.88343D-05
11/26/1971	11281	0.98309D 01	0.25922D-02	-0.48516D-08	0.99618D 01	0.33862D-02	-0.92477D-05
01/01/1972	11317	0.10034D 02	0.0	0.0	0.10066D 02	0.27600D-02	-0.44376D-14

3.6 TRAJECTORY RELATED EVENTS AND EQUATIONS

3.6.1 Geomagnetic Latitude and Longitude

A point that has the geographic latitude, φ, and longitude, λ, has a geomagnetic latitude, ϕ_g, and longitude, λ_g. If the geographic latitude and longitude of the north magnetic pole is ϕ_0 and λ_0, the equations for ϕ_g and λ_g are

$$\phi_g = \sin^{-1} [\sin\phi \sin\phi_0 + \cos\phi \cos\phi_0 \cos(\lambda - \lambda_0)] \tag{3-205}$$

and

$$\lambda_g = \tan^{-1} \left[\frac{\cos^2\phi \cos\phi_0 \sin(\lambda - \lambda_0)}{\cos\phi_g (\sin\phi_g \sin\phi_0 - \sin\phi)} \right]. \tag{3-206}$$

3.6.2 Apofocus and Perifocus Altitudes

If the instantaneous classical elements of the orbit, the semimajor radius of the central body, a_p, and the flattening coefficient of the body f are given, the apofocus and perifocus altitude are given by

$$h_a = a(1 + e) - b' \quad \text{apofocus} \tag{3-207}$$

$$h_p = a(1 - e) - b' \quad \text{perifocus.} \tag{3-208}$$

where

$$b' = a_p \left\{ 1 - f \sin^2 i \sin^2\omega \left[1 + \frac{3}{2} f (1 - \sin^2 i \sin^2\omega) \right] \right\}. \tag{3-209}$$

3.6.3 Rotation Rates of Node and Perifocus

The secular rate-of-change of the instantaneous right ascension of the ascending node, Ω, and the argument of perifocus, ω, with respect to time are

$$\dot{\Omega} = \frac{-\frac{3}{2} C_2^0 a_p^2 \sqrt{\mu} \cos i}{a^{3/2} p^2} \tag{3-210}$$

$$\dot{\omega} = \frac{-3 C_2^0 a_p^2 \sqrt{\mu} \left(1 - \frac{5}{4} \sin^2 i\right)}{a^{3/2} p^2} \tag{3-211}$$

where

$$p = \frac{(\bar{r} \times \dot{\bar{r}}) \cdot (\bar{r} \times \dot{\bar{r}})}{\mu} \tag{3-212}$$

and C_2^0 is the second zonal harmonic.

3.6.4 Keplerian, Anomalistic, and Nodal Periods

The Keplerian period is the classical two-body period associated with the orbital elements

$$P_K = 2\pi\sqrt{\frac{a^3}{\mu}}. \tag{3-213}$$

The anomalistic period is the time from one perifocus to the next. It is dependent on the rotation of perifocus

$$P_A = P_K \left[1 + \frac{3 C_2^0 a_p^2}{2 r^3} (1 - 3 \sin^2 i)\right] \tag{3-214}$$

The nodal period is the time from one ascending equatorial crossing to the next. It is dependent on the rotation of the node

$$P_N = P_A - P_K \left[\frac{-3 C_2^0 a_p^2 \left(2 - \frac{5}{2} \sin^2 i\right)}{a^2 (1 - e^2)^2}\right] \tag{3-215}$$

3.6.5 Apsis Points

The perifocus and apofocus are determined by a change in the sign of the function

$$g(t) \equiv \bar{r} \cdot \dot{\bar{r}} \tag{3-216}$$

with

$$\dot{g}(t) = \ddot{\bar{r}} \cdot \bar{r} + \dot{\bar{r}} \cdot \dot{\bar{r}} \tag{3-217}$$

when the function g(t) is zero, the flight path angle is 90°. The perifocus is distinguished from the apofocus by the smaller value of r.

3.6.6 Altitude Extremes

Minimum and maximum altitudes are obtained from

$$g(t) = \dot{h} \tag{3-218}$$

and

$$\dot{g}(t) = \ddot{h}. \tag{3-219}$$

The altitude, h, is given by

$$h = r - a_p \epsilon_1 g^{-1/2} \tag{3-220}$$

where

$$g = 1 - \epsilon_2 (x^2 + y^2)/r^2 \tag{3-221}$$

$$\epsilon_1 = 1 - f \tag{3-222}$$

$$\epsilon_2 = f(2 - f) \tag{3-223}$$

The first derivative of altitude, $\dot{h}$, is

$$\dot{h} = \frac{\dot{r} + (a_p \epsilon_1 \dot{g})}{2 g^{3/2}} \tag{3-224}$$

where

$$\dot{r} = \frac{\bar{r} \cdot \dot{\bar{r}}}{r} . \tag{3-225}$$

and

$$\dot{g} = -2 \epsilon_2 r^{-3} [r (x \dot{x} + y \dot{y}) - \dot{r} (x^2 + y^2)] \tag{3-226}$$

The second derivative of altitude, h, is

$$\ddot{h} = \ddot{r} + \left(\frac{a_p \epsilon_1}{2 g^{3/2}} \right) \left(\ddot{g} - \frac{3 \dot{g}^2}{2 g} \right) \tag{3-227}$$

where

$$\ddot{r} = \frac{\bar{r} \cdot \ddot{\bar{r}} + \dot{\bar{r}} \cdot \dot{\bar{r}}}{r - (\bar{r} \cdot \dot{\bar{r}})^2 / r^3} \tag{3-228}$$

$$\ddot{g} = -2 \epsilon_2 r^{-4} [r^2 (x \ddot{x} + y \ddot{y} + \dot{x}^2 \cdot + \dot{y}^2) - 4 r \dot{r} (x \dot{x} + y \dot{y}) \tag{3-229}$$

$$- r \ddot{r} (x^2 + y^2) + 3 \dot{r}^2 (x^2 + y^2)] .$$

3.6.7 Encounters

The closest approach to a specified point is determined by a change in the sign of the function

$$g (t) = \frac{(\bar{r} - \bar{r}') \cdot (\dot{\bar{r}} - \dot{\bar{r}}')}{(\bar{r} - \bar{r}')} \tag{3-230}$$

where $\bar{r}'$ and $\dot{\bar{r}}'$ are the position and velocity of the specified point relative to the central body in which $\bar{r}$ and $\dot{\bar{r}}$ are measured.

3.7 REFERENCES

1. Her Majesty's Stationery Office, Explanatory Supplement, Nautical Almanac Office, London, 1961.

2. U. S. Government Printing Office, The American Ephemeris and Nautical Almanac, Nautical Almanac Office, Washington, D. C., 1967.

3. Jet Propulsion Laboratory, JPL TR 32-1306, Constants and Related Information for Astrodynamic Calculations, 1968, W. G. Melbourne, J. D. Mulholland, W. L. Sjogren, and F. M. Sturnes, July 1968.

4. Jet Propulsion Laboratory, 32-580, User's Description of JPL Ephemeris Tapes, Peabody, Scott, and Orozeo, 1964.

5. Jet Propulsion Laboratory, 32-41, Selenographic Coordinates, B. E. Kalensher, 1961.

6. TRW Systems Group, TRW 70-FMT-792A, Houston Operations Predictor/ Estimator (HOPE) Engineering Manual, June 1970.

7. Jet Propulsion Laboratory, 32-223, Space Trajectories for the IBM 7090 Computer, D. B. Holdridge, 1962.

8. Jet Propulsion Laboratory, Double Precision Orbit Determination Program, Volume III, Warner, Brodie, Newell, and Ekelund.

9. Goddard Space Flight Center, Satellite Geodesy Theory and Applications, Wolf Research and Development Corporation, 1968.

10. Jet Propulsion Laboratory, 32-1526, DSN Frequency and Time Scale Change from UTC to IAT or New UTC, Vol. VIII, J. Curtright, 1972.

11. Goddard Space Flight Center, X-810-71-489, Changes in Standard Frequency and Time-Signal Broadcast – January 1, 1972, A. R. Chi and H. S. Fosque, November 1971.

CHAPTER 4

ACCELERATION MODEL

A spacecraft is influenced by many accelerations that tend to alter its motion or position vector. Some of these accelerations are generated by physical phenomena occurring in the solar system whereas other forces are generated by equipment placed on board the spacecraft. This chapter identifies these sources and constructs the appropriate acceleration model. The accelerations discussed include:

- the gravitational acceleration due to n-point masses, $\ddot{\bar{R}}_{PM}$
- the gravitational acceleration due to nonsphericity, $\ddot{\bar{R}}_{NS}$
- the acceleration due to atmospheric drag, $\ddot{\bar{R}}_{D}$
- the acceleration due to solar radiation pressure, $\ddot{\bar{R}}_{SR}$
- the acceleration due to attitude control system corrections, $\ddot{\bar{R}}_{TAC}$
- the acceleration due to thrust, $\ddot{\bar{R}}_{T}$.

The respective accelerations induced by each of these forces are computed in an inertial coordinate system (mean equator and equinox of 1950.0) and summed to yield the total acceleration vector of the spacecraft

$$\ddot{\bar{R}} = \ddot{\bar{R}}_{PM} + \ddot{\bar{R}}_{NS} + \ddot{\bar{R}}_{D} + \ddot{\bar{R}}_{SR} + \ddot{\bar{R}}_{TAC} + \ddot{\bar{R}}_{T}. \qquad (4\text{-}1)$$

4.1 CONTRIBUTION DUE TO N-POINT MASSES

In the development of the equations of motion of a satellite in the presence of n-massive bodies, the starting point is Newton's second law of motion and his law of gravitation (References 1, 2, 3).

The second law for a body of mass m_0 is given by

$$\bar{F} = \frac{d}{dt}\left(m_0 \frac{d\tilde{R}}{dt}\right) \qquad (4\text{-}2)$$

that becomes

$$\bar{F} = m_0 \frac{d^2\tilde{R}}{dt^2} \tag{4-3}$$

when m_0 is constant. Here $\tilde{R}$ is a vector from an unaccelerated, nonrotating coordinate system to the satellite.

In the presence of a massive body whose mass is m_k, the law of gravitation gives

$$\bar{F}_k = - \frac{Gm_0 m_k}{R_{kp}^3} \bar{R}_{kp} \tag{4-4}$$

where G is the universal gravitational constant and $\bar{R}_{kp}$ is the vector from the body k to the satellite.

Since the contribution from all bodies is required, a summation over k is used to obtain the total force on the satellite

$$\bar{F} = - \sum_{k=1}^{n} \frac{Gm_0 m_k}{R_{kp}^3} \bar{R}_{kp}. \tag{4-5}$$

When this expression is substituted into Equation (4-3), the equations of motion of the satellite are obtained in an unaccelerated, nonrotating coordinate system (see Figure 4-1).

$$\frac{d^2\tilde{R}}{dt^2} = - \sum_{k=1}^{n} \frac{Gm_k}{R_{kp}^3} \bar{R}_{kp}. \tag{4-6}$$

For convenience and ease in the interpretation of results, it is advantageous to refer the motion of the satellite to one of the massive bodies. The force on body j, understood to be the reference or central body, is given by

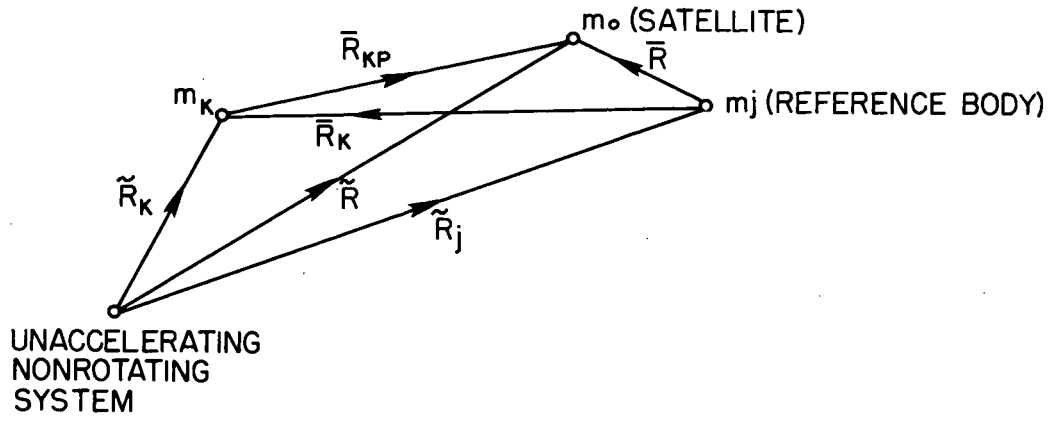

Figure 4-1. Schematic of Point Mass Gravitational Bodies

$$\bar{F}_j = \sum_{\substack{k=1 \\ k \neq j}}^{n} \frac{G m_j m_k}{R_k^3} \bar{R}_k \tag{4-7}$$

where $\bar{R}_k$ is a vector from the reference j^{th} body to the k^{th} body. The equations of motion of the reference body when referred to the unaccelerating, nonrotating coordinate system are given by

$$\frac{d^2 \tilde{R}_j}{dt^2} = \sum_{\substack{k=1 \\ k \neq j}}^{n} \frac{G m_k}{R_k^3} \bar{R}_k \tag{4-8}$$

If the planet motions are to be specified from semiempirically determined ephemerides, as is the case in GTDS, then Equations (4-7) and (4-8) must account for the non-point-mass accelerations. These effects mainly arise from gravitational harmonics which are present in the planetary ephemerides. Writing Equations (4-7) and (4-8) to account for such non-spherical effects yields

$$\bar{F}_j = \sum_{\substack{k=1 \\ k \neq j}}^{n} \frac{G m_j m_k}{R_k^3} \bar{R}_k + m_j \sum_{\substack{k=1 \\ k \neq j}}^{n} NS(j, k) \cdot \frac{\bar{R}_k}{R_k} \tag{4-7a}$$

$$\frac{d^2 \tilde{R}_j}{dt^2} = \sum_{\substack{k=1 \\ k \neq j}}^{n} \frac{G m_k}{R_k^3} \bar{R}_k + \sum_{\substack{k=1 \\ k \neq j}}^{n} NS(j, k) \cdot \frac{\bar{R}_k}{R_k} \tag{4-8a}$$

A subtraction of Equation (4-8) from Equation (4-6) yields

$$\frac{d^2\tilde{\bar{R}}}{dt^2} - \frac{d^2\tilde{\bar{R}}_j}{dt^2} = - \sum_{k=1}^{n} \frac{Gm_k}{R_{kp}^3} \bar{R}_{kp} - \sum_{\substack{k=1 \\ k\neq j}}^{n} \frac{Gm_k}{R_k^3} \bar{R}_k - \sum_{\substack{k=1 \\ k\neq j}}^{n} NS(j, k) \frac{\bar{R}_k}{R_k} \qquad (4\text{-}9)$$

Substituting $\tilde{\bar{R}} - \tilde{\bar{R}}_j = \bar{R} = \bar{R}_{jp}$ and $\bar{R}_{kp} = \bar{R} - \bar{R}_k$ into Equation (4-9), yields the acceleration due to n-point masses to be

$$\ddot{\bar{R}}_{PM} = \frac{d^2\bar{R}}{dt^2} = -\frac{\mu}{R^3} \bar{R} + \sum_{\substack{k=1 \\ k\neq j}}^{n} \mu_k \left(\frac{(\bar{R}_k - \bar{R})}{|\bar{R}_k - \bar{R}|^3} - \frac{\bar{R}_k}{|\bar{R}_k|^3} \right) - \sum_{\substack{k=1 \\ k\neq j}}^{n} NS(k) \cdot \frac{\bar{R}_k}{R_k} \qquad (4\text{-}10)$$

where $\bar{R}_{PM}$, $\bar{R}$, and $\bar{R}_k$ are expressed in mean of 1950.0 coordinates or true of epoch coordinates, whichever is the basic coordinate frame. The gravitational parameter, μ, is the product of the mass of a body and the universal gravitational constant. In particular $\mu_k = Gm_k$ for the k^{th} body and $\mu = GM$ (unsubscripted) for the central body.

The last term on the right in Equation (4-10) is usually only significant when the orbit of a celestial body is perturbed by the gravitational harmonics of a nearby body as is the case with the earth's moon. Sufficient accuracy has been achieved by accounting for the indirect effect of the earth's oblateness on the lunar orbit.

4.2 NONSPHERICITY

The next acceleration considered is that due to the nonsphericity of a massive body. The method described is classical and may be found in numerous reports and texts (References 3, 4, 9). The gravitational field of a planet is derived from a scalar potential that satisfies Poisson's equation

$$\nabla^2 \psi(r, \phi, \lambda) = - \rho(r, \phi, \lambda) \qquad (4\text{-}11)$$

where $r \sim$ the magnitude of the vectors from the central body's center of mass to the satellite

$\phi \sim$ the latitude

$\lambda \sim$ the longitude (measured east from the prime meridian)

Since attention is focused upon regions above the planet's surface, the mass density, ρ, is zero; consequently, the equation of Laplace, $\nabla^2\psi = 0$, must be solved. A standard separation of variables technique yields the solution

$$\psi(r,\phi,\lambda) = \frac{\mu}{r} + \frac{\mu}{r}\sum_{n=1}^{\infty} C_n^0 \left(\frac{a_p}{r}\right)^n P_N^0(\sin\phi) + \frac{\mu}{r}\sum_{n=1}^{\infty}\sum_{m=1}^{n}\left(\frac{a_p}{r}\right)^n P_n^m(\sin\phi)\left[S_n^m \sin m\lambda + C_n^m \cos m\lambda\right] \tag{4-12}$$

where

μ ~ the gravitational parameter of the central body

a_p ~ the radius of the body (usually taken as the equatorial radius)

P_n^m ~ the associated Legendre function

S_n^m, C_n^m ~ harmonic coefficients.

The term n = 1 is usually not present when the origin of the coordinate system is placed at the center of mass.

The accelerations due to the nonspherical portion of this potential are obtained in the body-fixed, true of date coordinate system shown in Figure 4-2, where the coordinate directions are defined as follows:

x_b axis lies along the intersection of the central body's equatorial plane and the plane of the prime merdian

z_b axis lies along the axis to the adopted North Pole

y_b axis completes a right-handed coordinate system.

The acceleration due to nonsphericity in this coordinate system may be obtained as a vector $\ddot{\bar{r}}_b$ with components $\ddot{x}_b$, $\ddot{y}_b$, and $\ddot{z}_b$ where

$$\ddot{\bar{r}}_b = \begin{bmatrix} \ddot{x}_b \\ \ddot{y}_b \\ \ddot{z}_b \end{bmatrix} = \frac{\partial\psi}{\partial r}\frac{\partial r}{\partial \bar{r}_b} + \frac{\partial\psi}{\partial\phi}\frac{\partial\phi}{\partial \bar{r}_b} + \frac{\partial\psi}{\partial\lambda}\frac{\partial\lambda}{\partial \bar{r}_b} \tag{4-13}$$

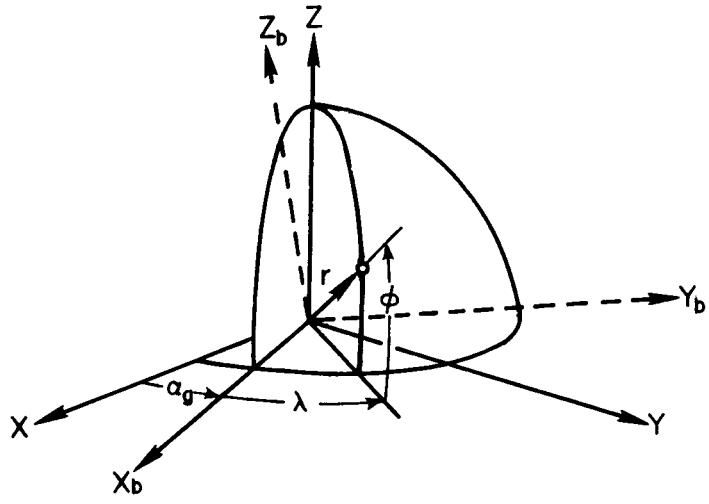

Figure 4–2. Body-Fixed System

The partial derivatives of the nonspherical portion of the potential with respect to r, ϕ, and λ are given by

$$\frac{\partial \psi}{\partial r} = -\frac{1}{r}\left(\frac{\mu}{r}\right)\sum_{n=2}^{N}\left(\frac{a_p}{r}\right)^n (n+1)\sum_{m=0}^{n}(C_n^m \cos m\lambda + S_n^m \sin m\lambda)P_n^m(\sin\phi) \quad \text{(a)} \tag{4-14}$$

$$\frac{\partial \psi}{\partial \phi} = \left(\frac{\mu}{r}\right)\sum_{n=2}^{N}\left(\frac{a_p}{r}\right)^n \sum_{m=0}^{n}(C_n^m \cos m\lambda + S_n^m \sin m\lambda)\,[P_n^{m+1}(\sin\phi) - m\tan\phi\, P_n^m(\sin\phi)] \quad \text{(b)}$$

$$\frac{\partial \psi}{\partial \lambda} = \left(\frac{\mu}{r}\right)\sum_{n=2}^{N}\left(\frac{a_p}{r}\right)^n \sum_{m=0}^{n} m(S_n^m \cos m\lambda - C_n^m \sin m\lambda)\, P_n^m(\sin\phi). \quad \text{(c)}$$

The Legendre functions and the terms cos $m\lambda$, sin $m\lambda$, and m tan ϕ are computed via recursion formulae:

$$P_n^0(\sin\phi) = [(2n-1)\sin\phi\, P_{n-1}^0(\sin\phi) - (n-1)\, P_{n-2}^0(\sin\phi)]/n \tag{4-15}$$

$$P_n^m(\sin\phi) = P_{n-2}^m(\sin\phi) + (2n-1)\cos\phi P_{n-1}^{m-1}(\sin\phi) \quad m \neq 0,\ m < n \tag{4-16}$$

$$P_n^n(\sin\phi) = (2n-1)\cos\phi\, P_{n-1}^{n-1}(\sin\phi) \quad m \neq 0,\ m = n \tag{4-17}$$

where

$$P_0^0(\sin\phi) = 1, \qquad P_1^0(\sin\phi) = \sin\phi, \qquad P_1^1(\sin\phi) = \cos\phi \tag{4-18}$$

$$\sin m\lambda = 2 \cos \lambda \sin (m-1)\lambda - \sin (m-2)\lambda \quad \text{(a)}$$

$$\cos m\lambda = 2 \cos \lambda \cos (m-1)\lambda - \cos (m-2)\lambda \quad \text{(b)} \qquad (4\text{-}19)$$

$$m \tan \phi = [(m-1) \tan \phi)] + \tan \phi. \qquad (4\text{-}20)$$

The partial derivatives of r, ϕ, and λ with respect to x_b, y_b, and z_b are computed from the expressions

$$\frac{\partial r}{\partial \bar{r}_b} = \frac{\bar{r}_b^T}{r} \qquad (4\text{-}21)$$

$$\frac{\partial \phi}{\partial \bar{r}_b} = \frac{1}{\sqrt{x_b^2 + y_b^2}} \left[- \frac{z_b \bar{r}_b^T}{r^2} + \frac{\partial z_b}{\partial \bar{r}_b} \right] \qquad (4\text{-}22)$$

$$\frac{\partial \lambda}{\partial \bar{r}_b} = \frac{1}{(x_b^2 + y_b^2)} \left[x_b \frac{\partial y_b}{\partial \bar{r}_b} - y_b \frac{\partial x_b}{\partial \bar{r}_b} \right] \qquad (4\text{-}23)$$

where

$$\frac{\partial x_b}{\partial \bar{r}_b}, \frac{\partial y_b}{\partial \bar{r}_b}, \text{ and } \frac{\partial z_b}{\partial \bar{r}_b}$$

are the row vectors (1, 0, 0), (0, 1, 0), and (0, 0, 1), respectively.

Substituting Equations (4-21) through (4-23) into (4-13) yields

$$\ddot{x}_b = \left(\frac{1}{r} \frac{\partial \psi}{\partial r} - \frac{z_b}{r^2 \sqrt{x_b^2 + y_b^2}} \frac{\partial \psi}{\partial \phi} \right) x_b - \left(\frac{1}{(x_b^2 + y_b^2)} \frac{\partial \psi}{\partial \lambda} \right) y_b \quad \text{(a)}$$

$$\ddot{y}_b = \left(\frac{1}{r} \frac{\partial \psi}{\partial r} - \frac{z_b}{r^2 \sqrt{x_b^2 + y_b^2}} \frac{\partial \psi}{\partial \phi} \right) y_b + \left(\frac{1}{x_b^2 + y_b^2} \frac{\partial \psi}{\partial \lambda} \right) x_b \quad \text{(b)} \qquad (4\text{-}24)$$

$$\ddot{z}_b = \left(\frac{1}{r} \frac{\partial \psi}{\partial r} \right) z_b + \frac{\sqrt{x_b^2 + y_b^2}}{r^2} \frac{\partial \psi}{\partial \phi} . \quad \text{(c)}$$

Since the numerical computations of the program are calculated in the inertial mean equator and equinox of 1950.0 coordinate system, a series of transformations are made to represent the acceleration vector in this system. For the case of the earth, there are two options available to accomplish this: the first is the more accurate whereas the second is computationally faster.

For the more accurate option the acceleration, $\ddot{\bar{r}}_b$, expressed in body (geographic) coordinates is transformed to the inertial mean of 1950.0 axes by means of the transformation

$$\ddot{\bar{R}}_{NS} = G^T H^T \ddot{\bar{r}}_b \tag{4-25}$$

where H^T transforms from body-fixed to true of epoch coordinates and G^T from true of epoch to inertial mean of 1950 coordinates as discussed in Section 3.3.1.5. The matrix H^T accounts for polar motion and Greenwich sidereal time.

The simpler option neglects polar motion by assuming the geographic pole, z_b, to be aligned with the spin axes z in the true of epoch system. This allows the nonspherical gravity components to be expressed directly in true of epoch coordinates. Thus by replacing (r_b, x_b, y_b, z_b) in Equations (4-13) and (4-21) through (4-24) by (r, x, y, z) the true of epoch components are calculated directly. The longitude and latitude are calculated as follows

$$\lambda = \alpha - \alpha_g \tag{4-26}$$

$$\phi = \sin^{-1}\left(\frac{z}{r}\right) \tag{4-27}$$

where

$\alpha \sim$ the right ascension of the spacecraft, $\alpha = \tan^{-1}\left(\frac{y}{x}\right)$

$\alpha_g \sim$ the right ascension of Greenwich.

Computation of the acceleration due to the nonspherical moon in 1950.0 coordinates requires some different operations than those used for the earth. The right ascension of the Greenwich meridian has no meaning so that the step of going from body-fixed coordinates to the true of date system cannot be implemented.

The lunar body-fixed coordinates (also known as selenographic coordinates) are coincident with the principal axes of inertia and are defined in the following way: the x' axis lies along a direction nearly colinear with the moon to earth vector; the z' axis lies along the axis of rotation, or polar axis, of the moon; and the y' axis lies in the equatorial plane of the moon and completes a right-handed coordinate system. In the absence of librations of the moon, the x' axis would point towards the center of the earth at all times.

C. 3

Three rotations are necessary to transform the selenographic acceleration vector to a vector referred to the mean earth equator and equinox of 1950.0 system.

The first rotation takes the acceleration vector to the true earth equator and equinox of date coordinate system centered at the moon (selenocentric). The other two rotations involve the precession and nutation effects that are included to express the acceleration in the 1950.0 system. Each of these rotations are discussed in Chapter 3, Section 3.3.

Under certain circumstances, it is desirable to compute the acceleration of a spacecraft in the vicinity of the moon with a triaxial model rather than a sophisticated model involving many calculations with spherical harmonics. The computation yields components of acceleration in the selenocentric true of date coordinate system

$$\ddot{x} = \frac{\partial \psi}{\partial x} = -\frac{3}{2}\frac{k}{r^5}\left\{(A_2 + B_2 + C_2 - 5I)x + 2\left[A_2 m_{11} x_b + B_2 m_{21} y_b + C_2 m_{31} z_b\right]\right\} \quad \text{(a)}$$

$$\ddot{y} = \frac{\partial \psi}{\partial y} = -\frac{3}{2}\frac{k}{r^5}\left\{(A_2 + B_2 + C_2 - 5I)y + 2\left[A_2 m_{12} x_b + B_2 m_{22} y_b + C_2 m_{32} z_b\right]\right\} \quad \text{(b)} \quad (4\text{-}28)$$

$$\ddot{z} = \frac{\partial \psi}{\partial z} = -\frac{3}{2}\frac{k}{r^5}\left\{(A_2 + B_2 + C_2 - 5I)z + 2\left[A_2 m_{13} x_b + B_2 m_{23} y_b + C_2 m_{33} z_b\right]\right\} \quad \text{(c)}$$

where A_2, B_2, C_2 ~ the principal moments of inertia of the moon

x, y, z ~ the selenocentric coordinates of the spacecraft

x_b, y_b, z_b ~ the selenographic coordinates of the spacecraft

k ~ the universal gravitational constant

I ~ the moment of inertia about the moon-spacecraft line, i.e.

$$I = A_2\left(\frac{x_b}{r}\right)^2 + B_2\left(\frac{y_b}{r}\right)^2 + C_2\left(\frac{z_b}{r}\right)^2 \qquad (4\text{-}29)$$

m_{ij} ~ the elements of the matrix that rotate from selenographic to selenocentric coordinates (see Chapter 3, Equation (3-54).

Then

$$\ddot{\bar{R}}_{NS} = G^T \ddot{\bar{r}}. \tag{4-30}$$

Another method for computing the acceleration due to nonsphericity has received considerable attention since 1966. The potential from which the force is derived is no longer characterized in terms of spherical harmonics but rather in terms of large mass concentrations. The existence of such mass concentrations (Mascons) has been predicted by Urey (Reference 5). Further work in this area, in particular with the lunar potential, has been carried out by Sjogren and Muller at JPL (References 6, 7, 8).

The model for point Mascons is similar to the model for n-point masses described earlier. Let the coordinates of the satellite in a body-fixed coordinate system be $\bar{r}_b$, and let $(\bar{r}_b)_i$ be the body-fixed coordinates of the i^{th} Mascon whose mass is denoted by m_i. From earlier considerations, the acceleration of the satellite is given by

$$\ddot{\bar{r}}_b = \sum_{i=1}^{N} \tilde{\mu}_i \frac{(\bar{r}_b)_i - \bar{r}_b}{|(\bar{r}_b)_i - \bar{r}_b|^3} \tag{4-31}$$

where

$\tilde{\mu}_i \sim$ the gravitational parameter of the i^{th} Mascon.

4.3 DRAG AND ATMOSPHERIC MODELS

One of the more complicated forces acting on the satellite is aerodynamic drag. The complications arise because of the presence in the mathematical model of the atmospheric density, a parameter whose properties and characteristics are not well known. The model for this force is only as good as the model for the atmospheric density and if consideration is given to the hourly, daily, monthly, and even yearly variations of atmospheric constituents, then the complexity begins to become more evident.

The braking effect of this force is characterized by a deceleration of the satellite which, in turn, tends to secularly decrease the energy and lower the altitude.

The direction of the force is opposite to the direction of motion and is dependent upon the shape, size, orientation and velocity of the satellite as well as the density

of the atmosphere. The atmosphere is rotating; consequently, the velocity referred to above is not the inertial velocity of the satellite but rather the velocity relative to the rotating atmosphere. The consequence of using a rotating atmosphere is that the force is no longer in the plane of undisturbed motion.

The force is defined in terms of these factors to be

$$\bar{F} = - \frac{AC_D}{2} \rho V_{REL} \bar{V}_{REL} \tag{4-32}$$

where

$A \sim$ the effective cross-sectional area

$C_D \sim$ the aerodynamic drag coefficient

$\rho \sim$ the density of the atmosphere

$\bar{V}_{REL} \sim$ the velocity vector of the satellite relative to the atmosphere.

In the 1950.0 coordinate system, the relative velocity vector is given by

$$\bar{V}_{REL} = \dot{\bar{R}} - (\bar{\omega} \times \bar{R}) \tag{4-33}$$

where

$\bar{\omega} \sim$ the angular rotation vector of the earth expressed in 1950.0 coordinates

$\bar{R}, \dot{\bar{R}} \sim$ the earth-centered 1950.0 position and velocity vectors of the satellite.

The required acceleration is given by

$$\ddot{\bar{R}}_D = \frac{-C_D A}{2m_0} \rho V_{REL} \bar{V}_{REL} \tag{4-34}$$

where m_0 is the mass of the spacecraft.

Atmospheric density models are categorized into two types: static and dynamic. The static models are noted by their sole dependence upon altitude and their independence of any other parameters such as latitude, longitude, season of the year, and time of day. The dynamic models are noted by their dependence not only on altitude but also upon the relative position of the sun relative to the earth and the amount of energy emitted from the sun.

Dynamic models have been constructed over the last ten years to take into account various earth and solar activity. There are three main types of solar activity known to affect the atmosphere density. The first type results from solar ultraviolet radiation impinging on the atmosphere and its effect on density is maximum at the subsolar point, commonly known as local noon. This radiation heats the atmosphere by conduction and thereby increases the density at higher altitudes. The process is known as the diurnal (or day-night) effect and causes a redistribution of the density resulting in a diurnal bulge in the atmosphere. The second type of solar activity affecting the atmosphere results from extreme ultraviolet radiation. The atmospheric oscillations that are in phase with this solar flux are often referred to as the erratic or 27-day variations. The latter designation comes from the fact that the oscillations sometimes exhibit a semiregular character for intervals of several months, during which a period of 27 days is easily recognizable. It has been found that the decimetric flux from the sun apparently varies in the same manner as the extreme ultraviolet emission, and that it therefore can be used as a fairly reliable index of short-term solar activity. The decimetric flux, specifically the 10.7 cm radiation, is expressed in units of 10^{-22} watt/m^2/cps bandwidth and is denoted by the symbol $F_{10.7}$. The third type of activity is corpuscular in nature and referred to as solar wind. It is responsible for the changes in intensity and energy spectrum observed in the cosmic radiation and is by far the largest single factor affecting atmospheric density. Experiments on board Pioneer V were the first to establish that the 11-year solar cycle (the period of the solar wind) is a phenomenon that is not localized near the earth or its immediate environment but rather affects large volumes of the inner solar system. The solar wind is modeled as an interplanetary plasma streaming radially and irregularly outward from the sun, compressing the earth's magnetic field on the sunward side and extending it on the night side.

Atmospheric oscillations connected with geomagnetic storms are of significant amplitude but of very short duration (one or two days), thereby making their detection difficult. Present-day studies indicate a correlation with the solar wind.

The following dynamic models have been included in the following survey:

- Jacchia 1960 – Accounts for diurnal and 27-day effects.
- Paetzold 1962 – Accounts for each effect mentioned above.
- Jacchia-Nicolet 1963-1964 – Presents values for density versus temperature. Accounts for all four types of activity.
- Harris-Priester 1962 – Presents mean atmospheric conditions.
- Modified Harris-Priester – This atmosphere is a derivative of the Harris-Priester concept but attempts to account for diurnal effects.

4.3.1 Jacchia 1960

L. G. Jacchia was among the first to propose a dynamic model based upon reduction of satellite data and attempted to account for the diurnal and 27-day solar effects (Reference 10). This model assumes the diurnal bulge to be axially symmetric and to have the same latitude as the subsolar point but to lag the sun in longitude by a constant angle, $\bar{\lambda}$ (see Figure 4-3). The model was constructed to be a function of the angle, ψ, between the maximum of the diurnal bulge and the point in the atmosphere in question. The best fit to the data was obtained with the function

$$\rho_0 = \rho_0'(h)\,\frac{F_{10.7}}{100}\,\{1 + 0.19\,[e^{.0055h} - 1.9]\,\cos^n(1/2\psi)\} \qquad (4\text{-}35)$$

where

$$\log \rho_0'(h) = -16.021 - 1.985 \times 10^{-3}\,h + 6.383e^{-.0026h} \qquad (4\text{-}36)$$

and

$\rho_0 \sim$ density (grams/cm^3)

$h \sim$ altitude (km)

$F_{10.7} \sim$ 10.7 cm. solar flux (10^{-22} watt/m^2/cps)

$n = 6.$

The angle, ψ, is related to the astronomical equatorial coordinates of the point in question, α and δ, and of the subsolar point, α_s and δ_s, and the constant angle, $\bar{\lambda}$, by the relation

$$\cos \psi = \sin \delta \sin \delta_s + \cos \delta \cos \delta_s \cos (\alpha - \alpha_s - \bar{\lambda}). \quad (4\text{-}37)$$

Jacchia determined $\bar{\lambda}$ to be 25° - 30°.

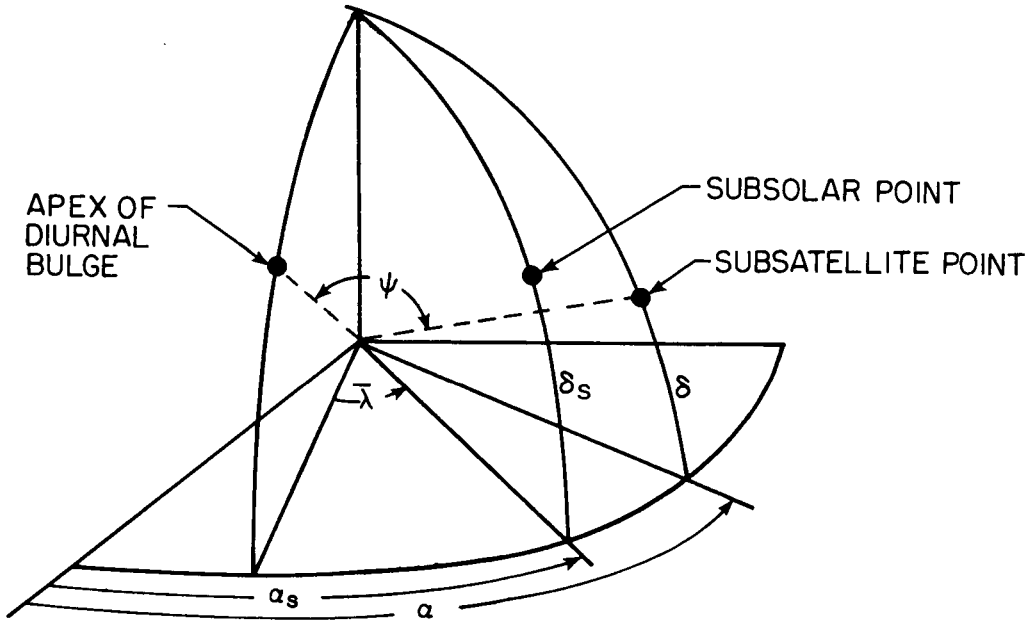

Figure 4–3. Schematic of Diurnal Bulge Lag Angle (Jacchia)

4.3.2 Paetzoid 1962

In 1962, at the Third International Space Science Symposium, H. K. Paetzold presented a complex model of the atmospheric density (Reference 11). This model was derived from the analysis of data obtained from seven satellites in 1958 and 1959 and accounts for the diurnal effect, the extreme ultraviolet effect, the solar wind effect, and the magnetic storm effect. He also includes the annual and semiannual effect of the interaction of the solar wind with the ionospheric plasma.

The total model is represented by

$$\log \rho_0 = \log \rho_s + \log \rho_1 + \log \rho_2 + \log \rho_3 + \log \rho_4 \tag{4-38}$$

where the empirical equations representing these separate effects are as follows:

The solar activity (27-day and 11-year) is modeled as

$$\log \rho_1 = -i(220,\ h)\ \frac{220 - F_{10.7}}{F_{10.7}}\ [1 + i(\theta)\ \theta_i(h)] \tag{4-39}$$

The diurnal effect is

$$\log \rho_2 = \theta(h)\ f(\theta) \tag{4-40}$$

where

$$\theta(h) = \theta_s(h) - \Delta_1\theta(h) \left[\frac{i(220,\ h)\ \frac{220 - F_{10.7}}{F_{10.7}} + a(F_{10.7},\ h)\ g(a)}{i(220,\ h) + a(220,\ h)} \right] - \Delta_2\ \theta(h)\ \frac{220 - F_{10.7}}{F_{10.7}} \tag{4-41}$$

The magnetic storm effect is

$$\log \rho_3 = K(200,\ h)\ \frac{Ap}{200}\ . \tag{4-42}$$

The semiannual - annual effect is

$$\log \rho_4 = a(F_{10.7},\ h)\ g(a) \tag{4-43}$$

where

$$a(F_{10.7},\ h) = a(220,\ h)\ \{g(a) + (220 - F_{10.7})\ [0.0060 - 0.0020\ g(a)]\} \tag{4-44}$$

Quantities in Equations (4-39) through (4-43) are

ρ_0 ~ density (grams/cm^3)

h ~ altitude (km)

θ ~ local hour angle (0 corresponds to midnight)

$F_{10.7}$ ~ 10.7 cm solar flux (10^{-22} watt/m^2/cps)

a ~ month (1 corresponds to January)

Ap ~ magnetic index, 2γ

ρ_s ~ average maximum value of density; tabulated as function of altitude in Reference 11.

θ_s(h) ~ average composition of the upper atmosphere; tabulated as a function of altitude in Reference 11.

i(220, h)
a(220, h)
k(200, h)
i(θ)
θ_i(h)
f(θ)
g(a)
$\Delta_1\theta$(h)
$\Delta_2\theta$(h)

} functions representing the best numerical solutions to observed satellite data; tabulated in Reference 11.

4.3.3 Jacchia-Nicolet 1963-1964

The atmospheric parameter most directly affected by solar activity is the temperature. However, before 1960, attempts to construct dynamic atmospheric models were based on the assumption that the density was linearly related to the 20 cm. solar flux; no correlation with temperature was introduced. In 1960, Nicolet (Reference 12) presented his discovery that atmospheric densities from satellite drag observations could be satisfactorily represented on the basis of diffusion equilibrium assuming the temperature reaches a constant value at altitudes greater than 200 km. Then in 1963, Jacchia (Reference 13) presented an expression for temperature, which, when used with Nicolet's tables, yields the atmospheric density at any given altitude. The temperature is given by Equation (4-45).

$$T = \left[635^\circ + 0.^\circ 3\,\bar{F}_{10.7} + 0.^\circ 012\,\bar{F}^2_{10.7}\right]\left[1 + 0.^\circ 4\cos^4\left(\frac{\psi}{2}\right)\right]$$

$$+ 0.^\circ 5\,\bar{F}_{10.7}\cos 4\pi\left(\frac{t - \text{Apr. } 7}{365}\right) + 2.^\circ 5\,(F_{10.7} - \bar{F}_{10.7}) + 1.^\circ 2a_p \qquad (4\text{-}45)$$

where

$F_{10.7}$ ~ the daily value of the 10.7 cm. solar flux in units of 10^{-22} watts/m^2/cps

$\bar{F}_{10.7}$ ~ monthly average of $F_{10.7}$

t ~ the time in days from January 1

ψ ~ the geocentric angular distance from the center of the diurnal bulge

a_p ~ the 3-hour geomagnetic index.

The first term gives the 11-year cycle contribution and the diurnal variation, the second term gives the semiannual variation due to the plasma effect, the third term gives the 27-day variation, and the last term is the geomagnetic effect (Reference 14). Values for $F_{10.7}$ and $\bar{F}_{10.7}$ may be obtained from Jacchia's SAO Special Report, No. 150. Values for a_p range between 10 and 20 during periods of average geomagnetic activity. Magnetic storms raise the value of a_p above 40 and can raise it as high as 200 to 300.

A model that discards the assumption of axial symmetry of the diurnal variation and introduces an asymmetry to account for the observation that the diurnal maxima and minima were not separated by 2π was introduced by Jacchia in 1964 (Reference 15). It again uses Nicolet's tables but has a different model for the temperature.

$$T = T_0\,(1 + 0.30\sin^{2.5}\theta)\left[1 + 0.30\,\frac{\cos^{2.5}\eta - \sin^{2.5}\theta}{1 + 0.30\sin^{2.5}\theta}\cos^{2.5}\left(\frac{\psi}{2}\right)\right] + 1.0\,a_p \qquad (4\text{-}46)$$

In this equation, T_0, is given by

$$T_0 = 974^\circ + 4.^\circ 203\,(\bar{F}_{10.7} - 150) + 0.^\circ 0042\,(\bar{F}_{10.7} - 150)^2 + 1.^\circ 9\,(F_{10.7} - \bar{F}_{10.7}) \tag{4-47}$$

$$+ \left(0.^\circ 39 + 0.^\circ 15 \sin 2\pi \frac{\tilde{t} - 151}{365}\right) \bar{F}_{10.7} \sin 4\pi \left(\frac{\tilde{t} - 59}{365}\right)$$

and

$$\eta = 1/2\,(\phi - \delta_s) \tag{4-48a}$$

$$\theta = 1/2\,(\phi + \delta_s) \tag{4-48b}$$

$$\tau = H - 45^\circ + 12^\circ \sin (H + 45^\circ) \qquad -\pi < \tau < \pi \tag{4-49}$$

with

$\tilde{t}$ ~ the number of days from January 1

ϕ ~ the geographic latitude

δ_s ~ the declination of the sun

H ~ the hour angle of the sun.

4.3.4 Harris-Priester 1962

In 1962 Harris and Priester determined the physical properties of the upper atmosphere theoretically by solving the heat conduction equation under quasi-hydrostatic conditions (References 16-18). Flux from the extreme ultraviolet and corpuscular heat sources are included. The model, however, averages the semiannual variations and does not attempt to account for the extreme ultraviolet 27-day effect. It does represent mean atmospheric conditions over several weeks in low-latitude regions. The model is in tabular form for each hourly interval and for five representative values of a heating parameter, S, which is quite similar to the smoothed decimetric flux $\bar{F}_{10.7}$. Essentially the model represents the atmospheric density as a function of time in the equatorial plane (the sun is assumed to be located in the same plane). It is assumed that the heating due to both sources is proportional to the monthly averages of S such that

$$T = 4.^{\circ}47\ S + 275^{\circ}, \text{ diurnal minimum} \qquad \text{(a)}$$

$$T = 7.^{\circ}05\ S + 372^{\circ}, \text{ diurnal maximum.} \qquad \text{(b)} \qquad (4\text{-}50)$$

4.3.5 Modified Harris-Priester

The atmosphere presebtly included in GTDS is a modification of the Harris-Priester concept (Reference 18). The modification attempts to account for the diurnal bulge at the subsolar point by including a cosine variation between a maximum density profile at the subsolar point and a minimum density profile at the antisolar point. Discrete values of the maximum and minimum density-altitude profiles, shown in Table 4-1, correspond to mean solar activity and are stored in tabular form as $\rho_M\ (h_i)$ and $\rho_m\ (h_i)$ respectively. Different maximum and minimum profiles can be retrieved from disk storage for different levels of solar activity. Exponential interpolation is used between entries, i.e.

$$\rho_M(h) = \rho_M(h_i)\ \exp\left[\frac{h_i - h}{H_M}\right] \qquad \text{(a)}$$

$$\rho_m(h) = \rho_m(h_i)\ \exp\left[\frac{h_i - h}{H_m}\right] \qquad \text{(b)} \qquad (4\text{-}51)$$

where

$$H_M = \frac{h_i - h_{i+1}}{\ln\left[\rho_M(h_i + 1)/\rho_M(h_i)\right]} \qquad \text{(a)}$$

$$H_m = \frac{h_i - h_{i+1}}{\ln\left[\rho_m(h_i + 1)/\rho_m(h_i)\right]} \qquad \text{(b)} \qquad (4\text{-}52)$$

and

$$h_i \le h \le h_{i+1} \qquad (4\text{-}53)$$

Table 4-1

Density Altitude Tables

Height (km)	Min. Density (kg/km^3)	Max. Density (kg/km^3)	Height (km)	Min. Density (kg/km^3)	Max. Density (kg/km^3)
100	497400.	497400.	420	1.558	5.684
120	24900.	24900.	440	1.091	4.355
130	8377.	8710.	460	.7701	3.362
140	3899.	4059.	480	.5474	2.612
150	2122.	2215.	500	.3916	2.042
160	1263.	1344.	520	.2819	1.605
170	800.8	875.8	540	.2042	1.267
180	528.3	601.0	560	.1488	1.005
190	361.7	429.7	580	.1092	.7997
200	255.7	316.2	600	.08070	.6390
210	183.9	239.6	620	.06012	.5123
220	134.1	185.3	640	.04519	.4121
230	99.49	145.5	660	.03430	.3325
240	74.88	115.7	680	.02632	.2691
250	57.09	93.08	700	.02043	.2185
260	44.03	75.55	720	.01607	.1779
270	34.30	61.82	740	.01281	.1452
280	26.97	50.95	760	.01036	.1190
290	21.39	42.26	780	.008496	.09776
300	17.08	35.26	800	.007069	.08059
320	10.99	25.11	840	.004680	.05741
340	7.214	18.19	880	.003200	.04210
360	4.824	13.37	920	.002210	.03130
380	3.274	9.955	960	.001560	.02360
400	2.249	7.492	1000	.001150	.01810

Assuming the density to be maximum at the apex of the bulge then the cosine variation between maximum and minimum density profiles is

$$\rho_0(h) = \rho_m(h) + [\rho_M(h) - \rho_m(h)] \cos^n\left(\frac{\psi}{2}\right) \qquad (4\text{-}54)$$

where ψ is the angle between the satellite position vector and the apex of the diurnal bulge. The angle, ψ, is given in Equation (4-37). It can be calculated in vector notation as follows

$$\psi = \cos^{-1}\left(\frac{\bar{r} \cdot \bar{U}_B}{r}\right) \tag{4-55}$$

where

$\bar{r}$ ~ the satellite position vector expressed in inertial geocentric coordinates

$\bar{U}_B$ ~ the vector directed toward the apex of the diurnal bulge expressed in inertial geocentric coordinates.

The vector $\bar{U}_B$ has components which are calculated as follows

$$\begin{aligned} U_{B_x} &= \cos\delta_s \cos(\alpha_s + \bar{\lambda}) \\ U_{B_y} &= \cos\delta_s \sin(\alpha_s + \bar{\lambda}) \\ U_{B_z} &= \sin\delta_s \end{aligned} \tag{4-56}$$

with

δ_s ~ the declination of the sun

α_s ~ the right ascension of the sun

$\bar{\lambda}$ ~ the lag angle between the sun line and the apex of the diurnal bulge.

In the modeling of accelerations in GTDS, the drag coefficient, C_D, and atmospheric density, ρ (h), always occur together as a product. To account for a systematic error in either C_D or ρ, the following error model is included

$$C_D \cdot \rho = C_{D_0}(1 + \rho_1)\ [1 + \rho_2 (t - t_0)]\left[1 + \rho_3 \cos^n\left(\frac{\psi}{2}\right)\right]\rho_0(h) \tag{4-57}$$

where

C_{D_0} ~ a priori specified drag coefficient

ρ_1 ~ scale factor error coefficient on $C_D \rho$

ρ_2 ~ error coefficient of time variation of $C_D \rho$

ρ_3 ~ error coefficient accounting for deviations in the diurnal variation of ρ (h)

t ~ the time of the instantaneous satellite position

t_0 ~ the epoch time

The altitude density function, $\rho_0(h)$, is determined from Equation (4-54). The quantities ρ_1, ρ_2, ρ_3, and n are adjustable parameters for the error model.

The height, h, of the satellite above the earth's surface is required by Equation (4-51). A good approximation for the height (neglecting pole wander) is given by

$$h = r - r_s \tag{4-58}$$

where r_s is the earth radius given by Equation (3-131) to be

$$r_s = \frac{R_e (1 - f)}{\sqrt{1 - (2f - f^2) \cos^2 \delta}} \tag{4-59}$$

with

r ~ the magnitude of the satellite position vector

R_e ~ the equatorial radius of earth

f ~ the earth's flattening coefficient

δ ~ the satellite declination. It is assumed that $\delta = \phi'$, the geocentric latitude of the subsatellite point.

4.4 SOLAR RADIATION PRESSURE

The force due to solar radiation pressure on a vehicle's surface is proportional to the effective area A of the surface normal to the incident radiation, to the surface reflectivity, η, to the luminosity, L_s, of the sun, and inversely proportional to the square of the distance R_{vs} from the sun, and to the speed of light, c.

The magnitude of the force due to direct solar radiation pressure on an area A is therefore given by

$$F = \frac{L_s \gamma A}{4\pi R_{vs}^2 c} . \tag{4-60}$$

where

$$\gamma = 1 + \eta \quad (\text{e.g. } \gamma = 1.95 \text{ for aluminum}) \tag{4-61}$$

The magnitude of the acceleration on a spacecraft of mass, m_0, and area, A, due to direct solar radiation pressure at one astronomical unit from the sun is

$$\frac{F}{m_0} = \frac{S}{c} \frac{\gamma A}{m_0} \tag{4-62}$$

where S denotes the mean solar flux at one astronomical unit. The quantities γ, A and m_0 are grouped together since they are spacecraft properties and can be determined prior to flight. The magnitude of the acceleration on a spacecraft due to direct solar radiation at the actual distance R_{vs} from the sun is given by

$$\frac{F}{m_0} = \frac{S}{c} \frac{R_{sun}^2}{R_{vs}^2} \frac{\gamma A}{m_0} \tag{4-63}$$

where R_{sun} designates one astronomical unit, i.e. the semimajor axis of the earth's orbit.

All of the above factors except R_{vs} are constant for a given spacecraft and mission. For computational convenience, P_s replaces S/c. P_s is defined as the force on a perfectly absorbing surface ($\eta = 0$) due to solar radiation pressure at one astronomical unit.

The acceleration due to direct solar radiation is away from the sun; that is, in the direction of

$$\bar{R}_{vs} = \bar{R} - \bar{R}_s \tag{4-64}$$

where

$\bar{R}$ ~ the position vector of the vehicle in the inertial mean of 1950.0 coordinate system

$\bar{R}_s$ ~ the position vector of the sun in the inertial mean of 1950.0 coordinate system.

The model for the acceleration $\ddot{\bar{R}}_{SR}$ due to direct solar radiation is

$$\ddot{\bar{R}}_{SR} = \nu P_s R_{sun}^2 \frac{\gamma A}{m_0} \frac{\bar{R}_{vs}}{R_{vs}^3} \tag{4-65}$$

where

ν - eclipse factor such that = $\begin{cases} 0 \text{ if the satellite is in shadow (umbra)} \\ 1 \text{ if the satellite is in sunlight and} \\ 0 < \nu < 1 \text{ if the satellite is in penumbra.} \end{cases}$

To determine the eclipsing factor, ν, a simple cylindrical shadow model is used. More sophisticated models accounting for penumbral regions and reflected radiation effects may be considered in later versions of the program, as required. From Figure 4-4 it is apparent that the satellite is in sunlight ($\nu = 1$) if

$$D = \bar{R}' \cdot \bar{U}_s > 0 \tag{4-66}$$

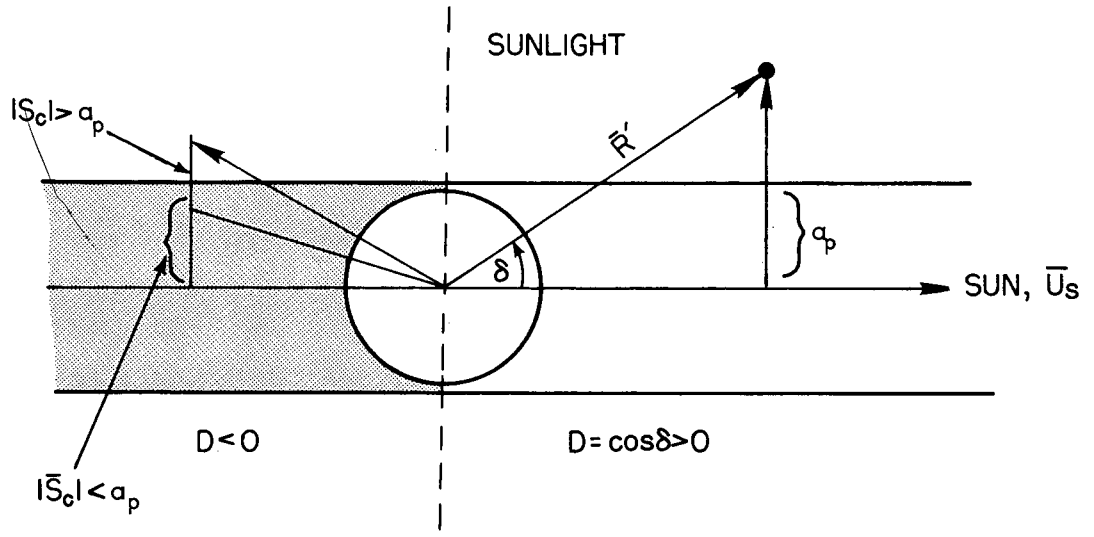

Figure 4–4. Cylindrical Shadow Model

where

$\bar{R}'$ ~ the satellite position vector relative to the shadowing body

$\bar{U}_s$ ~ the solar position unit vector relative to the shadowing body.

If D < 0 and the vector

$$S_c = \bar{R}' - DU_s \tag{4-67}$$

has a magnitude less than the body radius, a_p, then the spacecraft is shadowed (i.e. $\nu = 0$); otherwise, assume the satellite is in sunlight and $\nu = 1$.

4.5 ATTITUDE CONTROL

The function of the attitude control system is related to two modes of operation. During the first mode, commonly known as the acquisition and cruise mode, the attitude control system is used to establish and maintain three-axis stable orientation of the satellite. Such an orientation is obtained during an interplanetary flight, for example, by fixing two directions in space. One

direction is always such that the sensitive surface of the solar panels face the sun and the other direction is determined by pointing an on-board sensor toward a predetermined star. Usually another requirement that must be satisfied during the latter portion of the flight is that the high-gain antenna used for communications should point toward the earth.

In the second mode of operation, applicable during midcourse maneuvers, the attitude control system orients the satellite so that the thrust vector of the body-fixed rocket motor is aligned along a predetermined direction in space. This orientation is maintained by controlling the thrust vector to pass through the center of gravity of the satellite. After the maneuver, the attitude control system re establishes the cruise orientation.

The low-thrust forces, generated by the normal functions of the attitude control system, can produce accelerations of 1×10^{-7} cm/sec^2 to 3×10^{-7} cm/sec^2. This can result in a target miss of 100 to 300 km at Mars, for example. The translational forces producing the acceleration are the result of thrusters not acting in couples, thruster misalignment and unbalance, or the result of gas leaks through the values during times that the thrusters are not firing.

The model used to account for such accelerations has been constructed from the application of curve-fitting techniques to telemetered data and is defined as follows:

$$\ddot{\bar{r}}_{TAC} = \begin{Bmatrix} a_x + b_x(t - T_{ac1}) + c_x(t - T_{ac1})^2 \\ a_y + b_y(t - T_{ac1}) + c_y(t - T_{ac1})^2 \\ a_z + b_z(t - T_{ac1}) + c_z(t - T_{ac1})^2 \end{Bmatrix} [u(t - T_{ac1}) - u(t - T_{ac2})] . \quad (4\text{-}68)$$

The coefficients (a_x, a_y, a_z . . . c_x, c_y, c_z) are low-thrust polynomial coefficients to be solved for. The terms T_{ac1} and T_{ac2} are input epochs at which the attitude control acceleration polynomials are turned on and off, respectively. The function u is defined by

$$u(t - T_{ac1}) = \begin{cases} 1, & t \geq T_{ac1} \\ 0, & t < T_{ac1} \end{cases} \quad (4\text{-}69)$$

$$u(t - T_{ac2}) = \begin{cases} 1, & t \geq T_{ac2} \\ 0, & t < T_{ac2} \end{cases} \tag{4-70}$$

The subscript x denotes the acceleration component along the spacecraft's x_b axis that is assumed to be the roll axis; the subscript y denotes the acceleration component along the spacecraft's y_b axis that is assumed to be the pitch axis; and the subscript z denotes the force component along the spacecraft's z_b axis that is assumed to be the yaw axis.

In order to represent this acceleration in the 1950.0 coordinate system, the following transformations are necessary:

Transformation 1: Transforms the body axes (x_b, y_b, z_b) to the true of epoch Cartesian axes system (x, y, z).

Transformation 2: Transforms the true of epoch Cartesian system to the mean of 1950.0 system (X, Y, Z).

Transformation 1 is the product of three orthogonal transformations, shown in Figure 4-5, which involve the Euler angles α, δ, and ϕ. The angles α and δ are

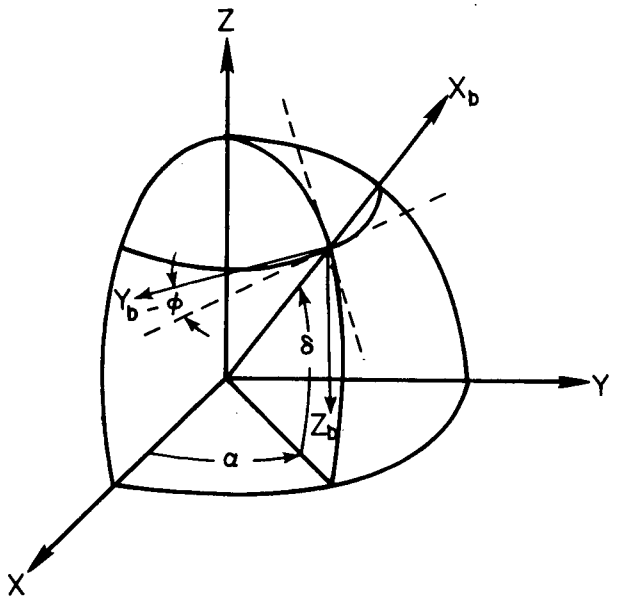

Figure 4-5. Spacecraft Body Axes Orientation

the right ascension and declination of the spacecraft's x_b-axis (roll axis), and ϕ rotates the y_b-axis out of the equatorial plane.

The transformation from body axes to the true of epoch system is therefore

$$\bar{r} = Q\,\bar{r}_b \tag{4-71}$$

where

$$\begin{aligned}
q_{11} &= \cos\alpha\cos\delta \\
q_{12} &= \sin\alpha\cos\phi - \cos\alpha\sin\delta\sin\phi \\
q_{13} &= \sin\alpha\sin\phi + \cos\alpha\sin\delta\cos\phi \\
q_{21} &= \sin\alpha\cos\delta \\
q_{22} &= -\cos\alpha\cos\phi - \sin\alpha\sin\delta\sin\phi \\
q_{23} &= -\cos\alpha\sin\phi + \sin\alpha\sin\delta\cos\phi \\
q_{31} &= \sin\delta \\
q_{32} &= \cos\delta\sin\phi \\
q_{33} &= \cos\delta\cos\phi
\end{aligned} \tag{4-72}$$

The matrix, G^T, which transforms from the true of epoch system to the mean of 1950.0 system is presented in Section 3.3.1. Thus the total transformation is

$$\ddot{\bar{R}}_{TAC} = G^T Q\,\ddot{\bar{r}}_{TAC} \tag{4-73}$$

4.6 THRUST

There are many forces acting on a spacecraft during the transfer phase and during the orbiting phase of its trajectory. Even though such forces have been modeled, the state of the vehicle is still uncertain primarily because of the imprecision associated with the injection conditions and the physical parameters

appearing in the mathematical models. Very small errors in the thrust magnitude and/or thrust direction at injection magnify into very large errors in position and velocity near the target body. In order to avoid such errors and attain pre-assigned terminal conditions, spacecraft are designed with the capability to perform multiple propulsive maneuvers during the interplanetary phase of a mission. Furthermore, if the spacecraft is to orbit a distant planet, maneuvering capability must be available to inject into orbit.

The model describing the acceleration during such corrective maneuvers is based on the reduction of data taken during the motor burn testing procedures and is represented in an inertial true of date system by

$$\ddot{\bar{r}}_T = a\{u(t - T_0) - u(t - T_f)\}\,\bar{U}_T \qquad (4\text{-}74)$$

where

$a \sim$ the magnitude of the thrust acceleration

$\bar{U}_T \sim$ the direction of the thrust acceleration

$T_0 \sim$ the effective initiation time of the motor burn (ET)

$T_f \sim$ the effective termination time of the motor burn (ET)

and u is defined as in Equations (4-69) and (4-70).

The motor's effective burn time is

$$T_b = T_f - T_0. \qquad (4\text{-}75)$$

The propulsive acceleration is modeled as follows

$$a = a_0 + a_1 \tau + a_2 \tau^2 + a_3 \tau^3 + a_4 \tau^4 \qquad (4\text{-}76)$$

where

$$\tau = t - T_0. \tag{4-77}$$

Equation (4-76) characterizes the thrust acceleration as a fourth degree polynomial in τ, the time from effective thrust initiation. The polynomial coefficients a_0, a_1, a_2, a_3, and a_4 are dynamic model parameters which can optionally be specified or estimated and represent the effective thrust-mass ratio as a function of time.

The unit vector $\bar{U}_T$ is assumed to be directed along the spacecraft's thrust axis direction. The true of epoch components of the thrust axis (assumed to be x_b-axis) are obtained from Equation (4-72) to be

$$U_T = \begin{bmatrix} \cos \alpha_T \cos \delta_T \\ \sin \alpha_T \cos \delta_T \\ \sin \delta_T \end{bmatrix} \tag{4-78}$$

where

$\alpha_T \sim$ the right ascension of the spacecraft's thrust axis relative to the true equinox and equator of epoch

$\delta_T \sim$ the declination of the spacecraft's thrust axis relative to the true equinox and equator of epoch.

The thrust axis orientation is represented by the fourth-degree polynomials in τ

$$\alpha_T = \alpha_0 + \alpha_1 \tau + \alpha_2 \tau^2 + \alpha_3 \tau^3 + \alpha_4 \tau^4 \tag{4-79}$$

$$\delta_T = \delta_0 + \delta_1 \tau + \delta_2 \tau^2 + \delta_3 \tau^3 + \delta_4 \tau^4 \tag{4-80}$$

where $\alpha_0, \alpha_1, \ldots, \alpha_4$, $\delta_0, \ldots, \delta_4$ are dynamic parameters which can optionally be estimated.

The thrust acceleration is expressed in the true earth equator and equinox of epoch coordinate system (via the unit vector $\bar{U}_T$). The transformation to the inertial mean equinox and equator of 1950.0 system is accomplished as follows:

$$\ddot{\bar{R}}_T = G^T \ddot{\bar{r}}_T. \tag{4-81}$$

4.7 REFERENCES

1. Brouwer, D., and G. M. Clemence, Methods of Celestial Mechanics, Academic Press, New York, 1961.

2. Danby, J. M. A., Fundamentals of Celestial Mechanics, Macmillan, New York, 1962.

3. Escobal, P. R., Methods of Orbit Determination, John Wiley & Sons, New York, 1965.

4. Kaula, W. M., Theory of Satellite Geodesy, Blaisdell Press, Los Angeles, California, 1966.

5. Urey, H. C., Vistas in Astronomy, Volume II, Pergamon Press, New York, 1956.

6. Jet Propulsion Laboratory, Report SPS 37-53, Mascons: Lunar Mass Concentrations, Volume II, W. L. Sjogren and P. M. Muller, September 1968.

7. Jet Propulsion Laboratory, Report 32-1307, Consistency of Lunar Orbiter Residuals with Trajectory and Local Gravity Effects, W. L. Sjogren and P. M. Muller, September 1968.

8. Jet Propulsion Laboratory, Report SPS 37-55, Lunar Orbiter Gravity Analysis, Volume II, W. L. Sjogren and P. M. Muller, January 1969.

9. Jet Propulsion Laboratory, Report SPS 37-29, Equations of Motion for a Double Precision Trajectory Program, Volume IV, F. M. Sturms.

10. Jacchia, L. G., "A Variable Atmospheric-Density Model From Satellite Accelerations," Journal & Geophysical Research, 65(9), 1960, pp. 2775-82.

11. Paetzold, H. K., "Model for the Variability of the Terrestrial Atmosphere Above 150 km After Satellite Observations," submitted for publications to the COSPAR Working Group IV, January 1962. Also Third International Space Science Symposium, Space Research III, 1962.

12. Smithsonian Astrophysical Observatory, Special Report No. 75, Density of the Heterosphere Related to Temperature, M. Nicolet, Cambridge, Massachusetts, 1961.

13. Jacchia, L. G., "Variations in the Earth's Upper Atmosphere as Revealed by Satellite Drag," Rev. Mod. Phys., 35(4), October 1963, pp. 973-91.

14. Bartels, J., "The Geomagnetic Measures for the Time-Variation of Solar Corpuscular Radiation, Described for Use in Correlation Studies in Other Geophysical Fields," Annals of the International Geophysical Year, Volume IV, Parts I, II, and III, Pergammon Press, New York, 1957, pp. 227-36.

15. Smithsonian Astrophysical Observatory, Special Report No. 150, The Temperature Above the Thermopause, L. G. Jacchia, Cambridge, Massachusetts, April 1964.

16. Harris, I., and W. Priester, "Time Dependent Structure of the Upper Atmosphere," Jour. Atmos. Sciences, 19(4), July 1952; also NASA TN D-1443, 1962.

17. Goddard Space Flight Center, NASA TN D-144, Theoretical Models for the Solar Cycle Variation of the Upper Atmosphere, I. Harris and W. Priester, August 1962.

18. Harris, I., and W. Priester, "Atmospheric Structure and Its Variations in the Region from 120 to 80 KM," COSPAR International Reference Atmosphere (CIRA) 1965, Space Research IV, North Holland Publishing Co., Amsterdam, 1965.

CHAPTER 5

VARIATIONAL EQUATIONS

The equations of motion of the satellite may be written in the form

$$\ddot{\bar{R}} = f\,(\bar{R},\ \dot{\bar{R}},\ t,\ \bar{p}) \tag{5-1}$$

where

$\bar{R} \sim$ column vector of vehicle position coordinates.

$\bar{p} \sim$ vector of dynamic parameters of dimension ℓ

and

$$\bar{p} = (\bar{R}\,(t_0),\ \dot{\bar{R}}\,(t_0), \bar{p}^*)^T \tag{5-2}$$

where

$\bar{p}^* \sim$ constant model parameters pertaining to drag, gravitational harmonics. etc.

These parameters are to be determined in such a way as to reduce the differences between a computed and an observed orbit. This orbit determination process requires the computation of variations in the state variables, $\bar{R}(t)$ and $\dot{\bar{R}}(t)$, as functions of variations in this parameter set.

If Equation (5-1) is differentiated with respect to $\bar{p}$, the matrix equation

$$\frac{\partial \ddot{\bar{R}}}{\partial \bar{p}} = \frac{\partial \ddot{\bar{R}}}{\partial \bar{R}}\ \frac{\partial \bar{R}}{\partial \bar{p}} + \frac{\partial \ddot{\bar{R}}}{\partial \dot{\bar{R}}}\ \frac{\partial \dot{\bar{R}}}{\partial \bar{p}} + \left(\frac{\partial \ddot{\bar{R}}}{\partial \bar{p}}\right)_{\text{explicit}} \tag{5-3}$$

is obtained. If time t and the parameter set $\bar{p}$ are independent, the differentiation with respect to t and $\bar{p}$ may be interchanged to give

$$\frac{d^2}{dt^2}\left(\frac{\partial \bar{R}}{\partial \bar{p}}\right) = \frac{\partial \ddot{\bar{R}}}{\partial \bar{R}}\frac{\partial \bar{R}}{\partial \bar{p}} + \frac{\partial \ddot{\bar{R}}}{\partial \dot{\bar{R}}}\frac{d}{dt}\left(\frac{\partial \bar{R}}{\partial \bar{p}}\right) + \left(\frac{\partial \ddot{\bar{R}}}{\partial \bar{p}}\right)_{explicit} \tag{5-4}$$

Defining the matrices

$$A(t) = \left[\frac{\partial \ddot{\bar{R}}(t)}{\partial \bar{R}}\right]_{3\times 3} \quad C(t) = \left[\left(\frac{\partial \ddot{\bar{R}}(t)}{\partial \bar{p}}\right)_{explicit}\right]_{3\times \ell}$$

$$B(t) = \left[\frac{\partial \ddot{\bar{R}}(t)}{\partial \dot{\bar{R}}}\right]_{3\times 3} \quad Y(t) = \left[\frac{\partial \bar{R}(t)}{\partial \bar{p}}\right]_{3\times \ell} \tag{5-5}$$

Equation (5-4) takes the form of a system of linear differential equations

$$\ddot{Y} = A(t)\,Y + B(t)\,\dot{Y} = C(t) \tag{5-6}$$

called the variational equations.

As the basic Equation (5-1) is numerically integrated to obtain the position $\bar{R}(t)$ and velocity $\dot{\bar{R}}(t)$ of the satellite, the variational equations are also integrated to obtain the matrices $Y(t)$ and $\dot{Y}(t)$, which yield the required partials. These partials are used to form the observation partials required by the orbit determination process. This is discussed in Chapter 7. The technique applied for numerical integration is discussed in Chapter 6.

The model parameters $\bar{p}$, which may be included in the variational equations, are as follows:

- Position and velocity of the spacecraft in mean of 1950.0 coordinates, true of epoch coordinates, classical orbital elements at epoch, spherical coordinates, or DODS variables
- Gravitational parameter of the central body
- Harmonics of the central body
- Gravitational parameters of perturbing bodies
- Aerodynamic drag parameter
- Solar radiation pressure parameter
- Powered flight parameters
- Attitude control parameters.

The matrices A, B, and C are formulated for the case when $\ddot{\bar{R}}$ of Equation (5-1) is of the form

$$\ddot{\bar{R}} = \ddot{\bar{R}}_{PM} + \ddot{\bar{R}}_{NS} + \ddot{\bar{R}}_{D} + \ddot{\bar{R}}_{SR} + \ddot{\bar{R}}_{TAC} + \ddot{\bar{R}}_{T} \tag{5-7}$$

where

$\ddot{\bar{R}}_{PM}$ ~ acceleration due to n-point masses

$\ddot{\bar{R}}_{NS}$ ~ acceleration due to nonsphericity of the central body

$\ddot{\bar{R}}_{D}$ ~ acceleration due to drag

$\ddot{\bar{R}}_{SR}$ ~ acceleration due to solar radiation pressure

$\ddot{\bar{R}}_{TAC}$ ~ acceleration due to attitude control

$\ddot{\bar{R}}_{T}$ ~ acceleration due to thrust.

The matrices A, B, and C are then given by

$$A = \frac{\partial \ddot{\bar{R}}_{PM}}{\partial \bar{R}} + \frac{\partial \ddot{\bar{R}}_{NS}}{\partial \bar{R}} + \frac{\partial \ddot{\bar{R}}_{D}}{\partial \bar{R}} + \frac{\partial \ddot{\bar{R}}_{SR}}{\partial \bar{R}} + \frac{\partial \ddot{\bar{R}}_{TAC}}{\partial \bar{R}} + \frac{\partial \ddot{\bar{R}}_{T}}{\partial \bar{R}} \qquad \text{(a)}$$

$$B = \frac{\partial \ddot{\bar{R}}_{D}}{\partial \dot{\bar{R}}} \qquad \text{(b)} \qquad (5\text{-}8)$$

$$C = \left(\frac{\partial \ddot{\bar{R}}}{\partial \bar{p}}\right)_{\text{explicit}} = \left[\frac{\partial \ddot{\bar{R}}}{\partial \bar{R}_0}, \frac{\partial \ddot{\bar{R}}}{\partial \dot{\bar{R}}_0}, \frac{\partial \ddot{\bar{R}}}{\partial \bar{p}^*}\right]_{\text{explicit}} = \left[0_3, 0_3, \frac{\partial \ddot{\bar{R}}}{\partial \bar{p}^*}\right] \qquad \text{(c)}$$

where

$$0_3 \sim 3 \times 3 \text{ null matrix}$$

$\frac{\partial \ddot{\bar{R}}}{\partial \bar{p}^*}$ ~ columns of explicit partial derivatives of acceleration with respect to model parameters:

$$\frac{\partial \ddot{\bar{R}}_{PM}}{\partial \mu}, \frac{\partial \ddot{\bar{R}}_{PM}}{\partial \mu_k}, \frac{\partial \ddot{\bar{R}}_{NS}}{\partial C_n^m}, \ldots \text{etc.}$$

5.1 CONTRIBUTION DUE TO N-POINT MASSES

The acceleration of the satellite due to n-poiny masses (neglecting the non-spherical term) is given by (see Equation (4-10))

$$\ddot{\bar{R}}_{PM} = \frac{-\mu \bar{R}}{R^3} + \sum_{k=1}^{n} \mu_k \left[\frac{(\bar{R}_k - \bar{R})}{|\bar{R}_k - \bar{R}|^3} - \frac{\bar{R}_k}{R_k^3} \right] \tag{5-9}$$

where

$\bar{R}$ ~ vector from the central body to the satellite

$\bar{R}_k$ ~ vector from the central body to the k^{th} mass.

The associated partials are given by

$$\frac{\partial \ddot{\bar{R}}_{PM}}{\partial \bar{R}} = -\left(\frac{\mu}{R^3} + \sum_{k=1}^{n} \frac{\mu_k}{|\bar{R}_k - \bar{R}|^3} \right) I + 3 \left(\frac{\mu \bar{R} \bar{R}^T}{R^5} + \sum_{k=1}^{n} \left[\mu_k \frac{(\bar{R}_k - \bar{R})(\bar{R}_k - \bar{R}^T)}{|\bar{R}_k - \bar{R}|^5} \right] \right) \tag{5-10}$$

$$\frac{\partial \ddot{\bar{R}}_{PM}}{\partial \dot{\bar{R}}} = 0_3. \tag{5-11}$$

The associated C-matrix columns for the model parameters μ and μ_k are given by

$$\frac{\partial \ddot{\bar{R}}_{PM}}{\partial \mu} = -\frac{\bar{R}}{R^3} \tag{5-12}$$

$$\frac{\partial \ddot{\bar{R}}_{PM}}{\partial \mu_k} = \frac{(\bar{R}_k - \bar{R})}{|\bar{R}_k - \bar{R}|^3} - \frac{\bar{R}_k}{R_k^3}. \tag{5-13}$$

5.2 NONSPHERICITY

The acceleration due to nonsphericity is dependent upon the geometry of the satellite relative to the central body and is of the form (see Equations (4-24) and 4-25))

$$\ddot{\bar{R}}_{NS} = G(t)^T H(t)^T \ddot{\bar{r}}_b \tag{5-14}$$

where

$G^T \sim$ the transformation from true of epoch to mean of 1950.0 coordinate system

$H^T \sim$ the transformation from body-fixed to true of epoch coordinate system

$\ddot{\bar{r}}_b \sim$ the acceleration due to nonsphericity in the body-fixed coordinates.

The partials of $\ddot{\bar{r}}_b$ with respect to $\bar{r}_b$ are obtained by differentiating Equation (4-13) yielding

$$\frac{\partial \ddot{\bar{r}}_b}{\partial \bar{r}_b} = \frac{\partial}{\partial \bar{r}_b}\left(\frac{\partial \psi}{\partial r}\right)\frac{\partial r}{\partial \bar{r}_b} + \frac{\partial}{\partial \bar{r}_b}\left(\frac{\partial \psi}{\partial \phi}\right)\frac{\partial \phi}{\partial \bar{r}_b} + \frac{\partial}{\partial \bar{r}_b}\left(\frac{\partial \psi}{\partial \lambda}\right)\frac{\partial \lambda}{\partial \bar{r}_b}$$

$$+\frac{\partial \psi}{\partial r}\frac{\partial^2 r}{\partial \bar{r}_b^2} + \frac{\partial \psi}{\partial \phi}\frac{\partial^2 \phi}{\partial \bar{r}_b^2} + \frac{\partial \psi}{\partial \lambda}\frac{\partial^2 \lambda}{\partial \bar{r}_b^2}. \tag{5-15}$$

The required partials of $\partial\psi/\partial r$, $\partial\psi/\partial\phi$, and $\partial\psi/\partial\lambda$ with respect to $\bar{r}_b$ are obtained by differentiating Equation (4-14) as follows

$$\frac{\partial}{\partial \bar{r}_b}\begin{bmatrix} \partial\psi/\partial r \\ \partial\psi/\partial\phi \\ \partial\psi/\partial\lambda \end{bmatrix} = \begin{bmatrix} \frac{\partial^2\psi}{\partial r^2} & \frac{\partial^2\psi}{\partial r\,\partial\phi} & \frac{\partial^2\psi}{\partial r\,\partial\lambda} \\ \frac{\partial^2\psi}{\partial\phi\,\partial r} & \frac{\partial^2\psi}{\partial\phi^2} & \frac{\partial^2\psi}{\partial\phi\,\partial\lambda} \\ \frac{\partial^2\psi}{\partial\lambda\,\partial r} & \frac{\partial^2\psi}{\partial\lambda\,\partial\phi} & \frac{\partial^2\psi}{\partial\lambda^2} \end{bmatrix}\begin{bmatrix} \partial r/\partial \bar{r}_b \\ \partial\phi/\partial \bar{r}_b \\ \partial\lambda/\partial \bar{r}_b \end{bmatrix}. \tag{5-16}$$

To minimize computations, the symmetry property of the second partials of ψ is utilized as indicated below

$$\frac{\partial^2 \psi}{\partial r^2} = \frac{\mu}{r^3} \sum_{n=2}^{N} \left(\frac{a_p}{r}\right)^n (n+2)(n+1) \sum_{m=0}^{n} (C_n^m \cos m\lambda + S_n^m \sin m\lambda) P_n^m (\sin\phi)$$

$$\frac{\partial^2 \psi}{\partial r \partial \phi} = \frac{\partial^2 \psi}{\partial \phi \partial r} = -\frac{\mu}{r^3} \sum_{n=2}^{N} \left(\frac{a_p}{r}\right)^n (n+1) \sum_{m=0}^{n} (C_n^m \cos m\lambda + S_n^m \sin m\lambda) \times$$

$$[P_n^{m+1} (\sin\phi) - m \tan\phi P_n^m (\sin\phi)]$$

$$\frac{\partial^2 \psi}{\partial r \partial \lambda} = \frac{\partial^2 \psi}{\partial \lambda \partial r} = -\frac{\mu}{r^3} \sum_{n=2}^{N} \left(\frac{a_p}{r}\right)^n (n+1) \sum_{m=0}^{n} m (S_n^m \cos m\lambda - C_n^m \sin m\lambda) P_n^m (\sin\phi)$$

$$\frac{\partial^2 \psi}{\partial \phi^2} = \frac{\mu}{r} \sum_{n=2}^{N} \left(\frac{a_p}{r}\right)^n \sum_{m=0}^{n} (C_n^m \cos m\lambda + S_n^m \sin m\lambda) \{\tan\phi P_n^{m+1} (\sin\phi) \quad (5\text{-}17)$$

$$+ [m^2 \sec^2\phi - m \tan^2\phi - n(n+1)] P_n^m (\sin\phi)\}$$

$$\frac{\partial^2 \psi}{\partial \phi \partial \lambda} = \frac{\partial^2 \psi}{\partial \lambda \partial \phi} = \frac{\mu}{r} \sum_{n=2}^{N} \left(\frac{a_p}{r}\right)^n \sum_{m=0}^{n} m (S_n^m \cos m\lambda - C_n^m \sin m\lambda) (P_n^{m+1} (\sin\phi)$$

$$- m \tan\phi P_n^m (\sin\phi))$$

$$\frac{\partial^2 \psi}{\partial \lambda^2} = -\frac{\mu}{r} \sum_{n=2}^{N} \left(\frac{a_p}{r}\right)^n \sum_{m=0}^{n} m^2 (C_n^m \cos m\lambda + S_n^m \sin m\lambda) P_n^m (\sin\phi).$$

The partials of r, ϕ, and λ with respect to $\bar{r}_b$ are given in Equations (4-21) through (4-23). The required second partials of r, ϕ, and λ with respect to $\bar{r}_b$ are obtained by differentiating Equations (4-21) through (4-23) with respect to $\bar{r}_b$ yielding

$$\frac{\partial^2 r}{\partial \bar{r}_b^2} = \frac{1}{r}\left[I - \frac{\bar{r}_b \bar{r}_b^T}{r^2}\right] \tag{5-18}$$

$$\frac{\partial^2 \phi}{\partial \bar{r}_b^2} = -\frac{1}{(x_b^2 + y_b^2)^{3/2}}\left[\left(\frac{\partial z_b}{\partial \bar{r}_b}\right)^T - \frac{z_b \bar{r}_b}{r^2}\right]\left[x_b\left(\frac{\partial x_b}{\partial \bar{r}_b}\right) + y_b\left(\frac{\partial y_b}{\partial \bar{r}_b}\right)\right]$$

$$-\frac{1}{r^2\sqrt{x_b^2 + y_b^2}}\left[\bar{r}_b\left(\frac{\partial z_b}{\partial \bar{r}_b}\right) + z_b I - \frac{2 z_b}{r^2}\bar{r}_b \bar{r}_b^T\right] \tag{5-19}$$

$$\frac{\partial^2 \lambda}{\partial \bar{r}_b^2} = -\frac{2}{(x_b^2 + y_b^2)}\begin{bmatrix} -y_b \\ x_b \\ 0 \end{bmatrix}\left[x_b\left(\frac{\partial x_b}{\partial \bar{r}_b}\right) + y_b\left(\frac{\partial y_b}{\partial \bar{r}_b}\right)\right] + \frac{1}{(x_b^2 + y_b^2)}\begin{bmatrix} 0 & -1 & 0 \\ 1 & 0 & 0 \\ 0 & 0 & 0 \end{bmatrix} \tag{5-20}$$

where $\partial x_b/\partial \bar{r}_b$, $\partial y_b/\partial \bar{r}_b$, and $\partial z_b/\partial \bar{r}_b$ are (1, 0, 0), (0, 1, 0), and (0, 0, 1), respectively.

The symmetry properties of the second partials of r, ϕ, and λ yield

$$\frac{\partial^2}{\partial x_b \partial y_b} = \frac{\partial^2}{\partial y_b \partial x_b}, \quad \frac{\partial^2}{\partial x_b \partial z_b} = \frac{\partial^2}{\partial z_b \partial x_b}, \quad \frac{\partial^2}{\partial y_b \partial z_b} = \frac{\partial^2}{\partial z_b \partial y_b}. \tag{5-21}$$

As noted in Chapter 4, the potential function, ψ, in a solution to Laplace's equation gives $\Delta^2\psi = 0$. Therefore

$$\frac{\partial^2 \psi}{\partial x_b^2} = -\left(\frac{\partial^2 \psi}{\partial y_b^2} + \frac{\partial^2 \psi}{\partial z_b^2}\right) \tag{5-22}$$

In view of this, and since the matrix in Equation (5-16) is symmetric, it is necessary to compute only the three elements above the principal diagonal and two elements on the principal diagonal.

The equations for computing the C-matrix columns for the model parameters C_n^m and S_n^m are obtained by explicit differentiation of Equations (4-13) with respect to the C_n^m and S_n^m parameters

$$\frac{\partial \ddot{\bar{r}}_b}{\partial C_n^m} = \frac{\partial}{\partial C_n^m}\left(\frac{\partial \psi}{\partial r}\right)\frac{\partial r}{\partial \bar{r}_b} + \frac{\partial}{\partial C_n^m}\left(\frac{\partial \psi}{\partial \phi}\right)\frac{\partial \phi}{\partial \bar{r}_b} + \frac{\partial}{\partial C_n^m}\left(\frac{\partial \psi}{\partial \lambda}\right)\frac{\partial \lambda}{\partial \bar{r}_b} \tag{5-23}$$

$$\frac{\partial \ddot{\bar{r}}_b}{\partial S_n^m} = \frac{\partial}{\partial S_n^m}\left(\frac{\partial \psi}{\partial r}\right)\frac{\partial r}{\partial \bar{r}_b} + \frac{\partial}{\partial S_n^m}\left(\frac{\partial \psi}{\partial \phi}\right)\frac{\partial \phi}{\partial \bar{r}_b} + \frac{\partial}{\partial S_n^m}\left(\frac{\partial \psi}{\partial \lambda}\right)\frac{\partial \lambda}{\partial \bar{r}_b} \tag{5-24}$$

where the second partials of ψ are obtained by differentiating Equation (4-14) with respect to C_n^m and S_n^m

$$\frac{\partial}{\partial C_n^m}\begin{bmatrix} \partial\psi/\partial r \\ \partial\psi/\partial\phi \\ \partial\psi/\partial\lambda \end{bmatrix} = \left(\frac{\mu}{r}\right)\left(\frac{a_p}{r}\right)^n \begin{bmatrix} -\frac{1}{r}(n+1)\cos m\lambda\ P_n^m(\sin\phi) \\ \cos m\lambda\ [P_n^{m+1}(\sin\phi) - m\tan\phi\ P_n^m(\sin\phi)] \\ -m\sin m\lambda\ P_n^m(\sin\phi) \end{bmatrix} \tag{5-25}$$

$$\frac{\partial}{\partial S_n^m}\begin{bmatrix} \partial\psi/\partial r \\ \partial\psi/\partial\phi \\ \partial\psi/\partial\lambda \end{bmatrix} = \left(\frac{\mu}{r}\right)\left(\frac{a_p}{r}\right)^n \begin{bmatrix} -\frac{1}{r}(n+1)\sin m\lambda\ P_n^m(\sin\phi) \\ \sin m\lambda\ [P_n^{m+1}(\sin\phi) - m\tan\phi\ P_n^m(\sin\phi)] \\ m\cos m\lambda\ P_n^m(\sin\phi) \end{bmatrix} \tag{5-26}$$

As in the case of the accelerations due to nonsphericity that were developed in Chapter 4, Section 4.2, the partial derivatives for use in the variational equations must be transformed from the body-fixed axes to the inertial mean of 1950.0 coordinates. In a manner completely analogous to Chapter 4, these partials can optionally be calculated precisely, or by a simpler and faster method, which neglects polar motion.

In the more accurate option where polar motion is accounted for, the transformation of the partials of $\ddot{\bar{R}}_{NS}$ with respect to $\bar{R}$ are determined by taking partial derivatives of Equation (5-14) as follows:

$$\frac{\partial \ddot{\bar{R}}_{NS}}{\partial \bar{R}} = (HG)^T \frac{\partial \ddot{\bar{r}}_b}{\partial \bar{r}_b} \frac{\partial \bar{r}_b}{\partial \bar{R}} = (HG)^T \frac{\partial \ddot{\bar{r}}_b}{\partial \bar{r}_b} HG. \tag{5-27}$$

The matrices H and G are presented in Chapter 3, Section 3.3.1.5.

In the simpler option, polar motion is neglected and $\ddot{\bar{r}}_b$, as well as its partials, are calculated with respect to the true of epoch coordinates. This is accomplished by replacing (r_b, x_b, y_b, z_b) in Equations (5-14) through (5-16) and (5-18) through (5-22) by (r, x, y, z), the true of epoch coordinates, and by replacing the matrix H by the identity, I, in Equations (5-14) and (5-27).

The partials of $\ddot{\bar{R}}_{NS}$ with respect to model parameters C_n^m and S_n^m are obtained as follows for the more accurate option

$$\frac{\partial \ddot{\bar{R}}_{NS}}{\partial C_n^m} = (HG)^T \frac{\partial \ddot{\bar{r}}_b}{\partial C_n^m} \tag{5-28}$$

$$\frac{\partial \ddot{\bar{R}}_{NS}}{\partial S_n^m} = (HG)^T \frac{\partial \ddot{\bar{r}}_b}{\partial S_n^m} \tag{5-29}$$

For the simplier option, (r_b, x_b, y_b, z_b) is replaced by (r, x, y, z) in Equations (5-23) and (5-24) and the matrix H is replaced by the identity matrix in Equations (5-28) and (5-29).

5.3 DRAG

The contribution of drag to the acceleration of the satellite is given by Equation (4-34) to be

$$\ddot{\bar{R}}_D = -\frac{C_D A}{2 m_0} \rho V_{REL} \bar{V}_{REL} \tag{5-30}$$

where

$$\bar{V}_{REL} = \dot{\bar{R}} - \bar{\omega} \times \bar{R} \tag{5-31}$$

with

$\bar{\omega}$ ~ the angular velocity vector of the earth in the 1950.0 coordinate system

$\bar{R}$, $\dot{\bar{R}}$ ~ the satellite position and velocity vectors in the 1950.0 coordinate system

A ~ the effective cross-sectional area of the satellite

C_D ~ the aerodynamic drag coefficient of the satellite

ρ ~ the density of the atmosphere at the satellite position

m_0 ~ the mass of the satellite.

The quantity $\bar{\omega} \times \bar{R}$ may be represented in the form $\bar{\omega} \times \bar{R} = \Omega_\omega \bar{R}$ where

Ω_ω ~ the skew symmetric matrix whose elements are given in terms of the components of the vector $\bar{\omega}$, i.e.

$$\Omega_\omega = \begin{bmatrix} 0 & -\omega_z & \omega_y \\ \omega_z & 0 & -\omega_x \\ -\omega_y & \omega_x & 0 \end{bmatrix} \tag{5-32}$$

The relative velocity can therefore be written

$$\bar{V}_{REL} = \dot{\bar{R}} - \Omega_\omega \bar{R}. \tag{5-33}$$

The partial derivatives of $\ddot{\bar{R}}_D$ with respect to $\dot{\bar{R}}$ and $\bar{R}$ are obtained by differentiating Equations (5-30) and (5-33) giving

$$\frac{\partial \ddot{\bar{R}}_D}{\partial \dot{\bar{R}}} = -\frac{C_D A}{2 m_0} \rho \left\{ \frac{\bar{V}_{REL} \bar{V}_{REL}^T}{V_{REL}} + V_{REL} I \right\} \tag{5-34}$$

$$\frac{\partial \ddot{\bar{R}}_D}{\partial \bar{R}} = \frac{\ddot{\bar{R}}_D}{\rho}\left(\frac{\partial \rho}{\partial \bar{R}}\right) + \frac{C_D A}{2 m_0}\rho\left\{\frac{\bar{V}_{REL}\,\bar{V}_{REL}^T}{V_{REL}} + V_{REL}\, I\right\}\Omega_\omega$$

$$= \frac{\ddot{\bar{R}}_D}{\rho}\left(\frac{\partial \rho}{\partial \bar{R}}\right) - \frac{\partial \ddot{\bar{R}}_D}{\partial \dot{\bar{R}}}\Omega_\omega . \qquad (5\text{-}35)$$

The drag coefficient and density can be partitioned as follows

$$C_D = C_{D_0}\,(1 + \rho_1)\,[1 + \rho_2\,(t - t_0)] \qquad (5\text{-}36)$$

$$\rho\,(h) = \left(1 + \rho_3 \cos^n \frac{\psi}{2}\right)\left[\rho_m + (\rho_n - \rho_m)\cos^n \frac{\psi}{2}\right] \qquad (5\text{-}37)$$

where

$$\psi = \cos^{-1}\left(\frac{\bar{R}\cdot\bar{U}_B}{R}\right) \qquad (5\text{-}38)$$

with

$\bar{U}_B \sim$ the unit vector directed towards the apex of the diurnal bulge and is given in terms of the right ascension and declination of the sun (see Equation (4-56)).

$\rho\,(h) \sim$ the height-dependent density.

The minimum and maximum densities, ρ_m and ρ_M, are given by

$$\rho_m = \rho_m\,(h_i)\,\exp\left(\frac{h_i - h}{H_m}\right) \qquad \text{(a)}$$

$$h_i \le h \le h_{i+1} \qquad (5\text{-}39)$$

$$\rho_M = \rho_M\,(h_i)\,\exp\left(\frac{h_i - h}{H_M}\right) \qquad \text{(b)}$$

and respective scale heights, H_m and H_M, by

$$H_m = \frac{h_i - h_{i+1}}{\ell n\,[\rho_m(h_i + 1)/\rho_m(h_i)]} \qquad \text{(a)}$$

$$H_M = \frac{h_i - h_{i+1}}{\ell n\,[\rho_M(h_i + 1)/\rho_M(h_i)]}\,. \qquad \text{(b)} \qquad (5\text{-}40)$$

The height is computed by (see Chapter 3, Section 3.3.5)

$$h = r - \frac{R_e\,(1 - f)}{[1 - (2f - f^2)\cos^2\delta]^{1/2}} \qquad (5\text{-}41)$$

where

R_e = the equatorial radius of the earth

f = the earth's flattening coefficient

$\cos\delta$ = $(x^2 + y^2)^{1/2}/r$; this assumes that $\delta = \phi'$, the latitude of the subsatellite point.

The partial of density with respect to position is then given by

$$\frac{\partial\rho}{\partial\bar{R}} = \left(\frac{\partial\rho}{\partial\rho_m}\,\frac{\partial\rho_m}{\partial h} + \frac{\partial\rho}{\partial\rho_M}\,\frac{\partial\rho_M}{\partial h}\right)\frac{\partial h}{\partial\bar{R}} + \frac{\partial\rho}{\partial\psi}\,\frac{\partial\psi}{\partial R} \qquad (5\text{-}42)$$

where

$$\frac{\partial\rho}{\partial\rho_m} = \left(1 - \cos^n\frac{\psi}{2}\right)\left(1 + \rho_3\cos^n\frac{\psi}{2}\right) \qquad (5\text{-}43)$$

$$\frac{\partial\rho}{\partial\rho_M} = \cos^n\frac{\psi}{2}\left(1 + \rho_3\cos^n\frac{\psi}{2}\right) \qquad (5\text{-}44)$$

$$\frac{\partial\rho_m}{\partial h} = -\frac{\rho_m}{H_m} \qquad (5\text{-}45)$$

$$\frac{\partial\rho_M}{\partial h} = -\frac{\rho_M}{H_M} \qquad (5\text{-}46)$$

The partial derivative of density with respect to ψ and the partial of ψ with respect to $\bar{R}$ are

$$\frac{\partial \rho}{\partial \psi} = -\frac{n}{2} \cos^{n-1}\frac{\psi}{2} \sin\frac{\psi}{2}\left\{(\rho_M - \rho_m)\left(1 + \rho_3 \cos^n\frac{\psi}{2}\right)\right. \tag{5-47}$$

$$\left. + \rho_3\left[\rho_m + (\rho_M - \rho_m)\cos^n\frac{\psi}{2}\right]\right\}$$

$$\frac{\partial \psi}{\partial \bar{R}} = \frac{1}{\sin\psi}\left[\left(\frac{\bar{R}\cdot\bar{U}_B}{R^3}\right)\bar{R} - \frac{\bar{U}_B}{R}\right]. \tag{5-48}$$

The partial of the height is obtained by differentiating Equation (5-41) with respect to $\bar{R}$ yielding

$$\frac{\partial h}{\partial \bar{R}} = \frac{\bar{R}}{R} - R_e\left\{\frac{(1-f)(2f-f^2)\cos\delta}{[1-(2f-f^2)\cos^2\delta]^{3/2}}\right\}\frac{\partial(\cos\delta)}{\partial \bar{R}} \tag{5-49}$$

where

$$\frac{\partial(\cos\delta)}{\partial \bar{R}} = \frac{1}{R^4\cos\delta}\begin{bmatrix} XZ^2 \\ YZ^2 \\ -Z(X^2+Y^2)\end{bmatrix}. \tag{5-50}$$

Substituting Equations (5-43) through (5-50) into (5-42) determines the partial of ρ with respect to $\bar{R}$ required by Equation (5-35).

The drag model parameter, ρ_1, contributes the following partial to the C matrix

$$\frac{\partial \ddot{\bar{R}}_D}{\partial \rho_1} = \frac{\ddot{\bar{R}}_D}{C_D} C_{D_0}\left[1 + \rho_2 (t - t_0)\right] = \frac{\ddot{\bar{R}}_D}{(1+\rho_1)}. \tag{5-51}$$

5.4 SOLAR RADIATION PRESSURE

The contribution of solar radiation pressure to the acceleration of the satellite is given by Equation (4-65)

$$\ddot{\bar{R}}_{SR} = \nu P_s R_{sun}^2 \frac{\gamma A}{m_0} \left[\frac{\bar{R} - \bar{R}_s}{|\bar{R} - \bar{R}_s|^3} \right] \tag{5-52}$$

where

$\nu \sim$ eclipse factor: $\nu = 1$ in sunlight, $\nu = 0$ in shadow

$P_s \sim$ the force due to solar pressure at one astronomical unit

$R_{sun} \sim$ one astronomical unit

$\gamma \sim$ constant (reflectively) coefficient

$\bar{R} \sim$ the satellite position in the 1950.0 coordinate system

$\bar{R}_s \sim$ the solar position vector in the 1950.0 coordinate system

$m_0 \sim$ the mass of the satellite

$A \sim$ the reference area.

The partial derivative at $\ddot{\bar{R}}_{SP}$ with respect to position is

$$\frac{\partial \ddot{\bar{R}}_{SR}}{\partial \bar{R}} = \nu \frac{P_s R_{sun}^2 \gamma A}{m_0 |\bar{R} - \bar{R}_s|^3} \left[I - \frac{3 [\bar{R} - \bar{R}_s] \cdot [\bar{R} - \bar{R}_s]^T}{|\bar{R} - \bar{R}_s|^2} \right] \tag{5-53}$$

$$\frac{\partial \ddot{\bar{R}}_{SR}}{\partial \dot{\bar{R}}} = 0_3 \tag{5-54}$$

and for the solar pressure model parameter

$$k = \frac{P_s A}{m_0} \tag{5-55}$$

$$\frac{\partial \ddot{\bar{R}}_{SR}}{\partial k} = \nu R_{sun}^2 \gamma \frac{[\bar{R} - \bar{R}_s]}{|\bar{R} - \bar{R}_s|^3} . \tag{5-56}$$

5.5 ATTITUDE CONTROL

The acceleration due to the attitude control system is assumed due to leaks and misalignments. These small effects are modeled as (see Section 4.5)

$$\ddot{\bar{R}}_{TAC} = G^T Q \ddot{\bar{r}}_{TAC} \tag{5-57}$$

where

$$\ddot{\bar{r}}_{TAC} = \begin{Bmatrix} a_x + b_x (t - T_{ac1}) + c_x (t - T_{ac1})^2 \\ a_y + b_y (t - T_{ac1}) + c_y (t - T_{ac1})^2 \\ a_z + b_z (t - T_{ac1}) + c_z (t - T_{ac1})^2 \end{Bmatrix} [u (t - T_{ac1}) - u (t - T_{ac2})]. \tag{5-58}$$

The matrix Q is the transformation from vehicle axes to the true of epoch system and has the following elements

$$\begin{aligned}
q_{11} &= \cos \alpha \cos \delta \\
q_{12} &= \sin \alpha \cos \phi - \cos \alpha \sin \delta \sin \phi \\
q_{13} &= \sin \alpha \sin \phi + \cos \alpha \sin \delta \cos \phi \\
q_{21} &= \sin \alpha \cos \delta \\
q_{22} &= - \cos \alpha \cos \phi - \sin \alpha \sin \delta \sin \phi \\
q_{23} &= - \cos \alpha \sin \phi + \sin \alpha \sin \delta \cos \phi \\
q_{31} &= \sin \delta \\
q_{32} &= \cos \delta \sin \phi \\
q_{33} &= \cos \delta \cos \phi
\end{aligned} \tag{5-59}$$

where

$\alpha \sim$ the right ascension of the spacecraft roll axis relative to the true equinox and equator of epoch

$\delta \sim$ the declination of the spacecraft roll axis relative to the true equinox and equator of epoch

$\phi \sim$ the roll angle from the westerly direction to the y_b - axis measured clockwise about the x_b-axis (see Figure 4-5).

Neither G, Q, nor $\ddot{\bar{r}}_{TAC}$ are functions of the satellite position nor velocity but instead are functions of time only. Therefore

$$\frac{\partial \ddot{\bar{R}}_{TAC}}{\partial \bar{R}} = \frac{\partial \ddot{\bar{R}}_{TAC}}{\partial \dot{\bar{R}}} = 0_3 . \tag{5-60}$$

The contribution to the C matrix of the control system acceleration parameters $a_x, a_y, a_z, \ldots, c_z$ are

$$\frac{\partial \ddot{\bar{R}}_{TAC}}{\partial \bar{a}} = G^T Q \left[u (t - T_{ac1}) - u (t - T_{ac2})\right] \tag{5-61}$$

$$\frac{\partial \ddot{\bar{R}}_{TAC}}{\partial \bar{b}} = (t - T_{ac1}) \frac{\partial \ddot{\bar{R}}_{TAC}}{\partial \bar{a}} \tag{5-62}$$

$$\frac{\partial \ddot{\bar{R}}_{TAC}}{\partial \bar{c}} = (t - T_{ac1})^2 \frac{\partial \ddot{\bar{R}}_{TAC}}{\partial \bar{a}} \tag{5-63}$$

where $\bar{a}$, $\bar{b}$, and $\bar{c}$ denote the vectors

$$\bar{a} = \begin{bmatrix} a_x \\ a_y \\ a_z \end{bmatrix} \quad \bar{b} = \begin{bmatrix} b_x \\ b_y \\ b_z \end{bmatrix} \quad \bar{c} = \begin{bmatrix} c_x \\ c_y \\ c_z \end{bmatrix} \tag{5-64}$$

5.6 THRUST

The thrust model in Equations (4-74) and (4-81) is

$$\ddot{\bar{R}}_T = a \{u (t - T_o) - u (t - T_f)\} G^T \bar{U}_T \tag{5-65}$$

where

$\bar{U}_T \sim$ the direction of thrust acceleration

$a \sim$ the magnitude of the acceleration given by

$$a = a_0 + a_1 \tau + a_2 \tau^2 + a_3 \tau^3 + a_4 \tau^4 \tag{5-66}$$

where

$$\tau = t - T_o. \tag{5-67}$$

The quantities $a_0, a_1, a_2, \ldots, a_4$ are parameters to be estimated. The vector $\bar{U}_T$ is given by Equation (4-78) to be

$$\bar{U}_T = \begin{bmatrix} \cos \alpha_T \cos \delta_T \\ \sin \alpha_T \cos \delta_T \\ \sin \delta_T \end{bmatrix} \tag{5-68}$$

where α_T and δ_T are given by

$$\alpha_T = \alpha_0 + \alpha_1 \tau + \alpha_2 \tau^2 + \alpha_3 \tau^3 \tag{5-69}$$

$$\delta_T = \delta_0 + \delta_1 \tau + \delta_2 \tau^2 + \delta_3 \tau^3 \tag{5-70}$$

and α_i and δ_i are parameters to be estimated.

The acceleration $\ddot{\bar{R}}_T$ is independent of both $\bar{R}$ and $\dot{\bar{R}}$, therefore

$$\frac{\partial \ddot{\bar{R}}_T}{\partial \bar{R}} = \frac{\partial \ddot{\bar{R}}_T}{\partial \dot{\bar{R}}} = 0_3. \tag{5-71}$$

The C matrix components resulting from the acceleration model parameters $a_0, \ldots, a_4$ are

$$\frac{\partial \ddot{\bar{R}}_T}{\partial \bar{a}} = \frac{\ddot{\bar{R}}_T}{a} \bar{\Gamma}_4^T \tag{5-72}$$

$$\frac{\partial \ddot{\bar{R}}_T}{\partial \bar{\alpha}} = a \{u(t - T_o) - u(t - T_f)\} G^T \bar{U}_\alpha \bar{\Gamma}_3^T \tag{5-73}$$

$$\frac{\partial \ddot{\bar{R}}_T}{\partial \bar{\delta}} = a \{u(t - T_o) - u(t - T_f)\} G^T \bar{U}_\delta \bar{\Gamma}_3^T \tag{5-74}$$

where

$$\bar{a} = \begin{bmatrix} a_0 \\ a_1 \\ \cdot \\ \cdot\cdot \\ \cdot\cdot \\ a_4 \end{bmatrix}, \quad \bar{\alpha} = \begin{bmatrix} \alpha_0 \\ \alpha_1 \\ \cdot\cdot \\ \cdot\cdot \\ \cdot\cdot \\ \alpha_3 \end{bmatrix}, \quad \bar{\delta} = \begin{bmatrix} \delta_0 \\ \delta_1 \\ \cdot\cdot \\ \cdot\cdot \\ \cdot\cdot \\ \delta_3 \end{bmatrix} \tag{5-75}$$

$$\overline{\Gamma}_n^T = [1,\ \tau,\ \tau^2,\ \ldots\ldots,\ \tau^n] \tag{5-76}$$

$$\overline{U}_\alpha = \frac{\partial \overline{U}_T}{\partial \alpha_T} = \begin{bmatrix} -\sin\alpha_T \cos\delta_T \\ \cos\alpha_T \cos\delta_T \\ 0 \end{bmatrix} \tag{5-77}$$

$$\overline{U}_\delta = \frac{\partial \overline{U}_T}{\partial \delta_T} = \begin{bmatrix} -\cos\alpha_T \sin\delta_T \\ -\sin\alpha_T \sin\delta_T \\ \cos\delta_T \end{bmatrix}. \tag{5-78}$$

CHAPTER 6

NUMERICAL INTEGRATION OF THE EQUATIONS OF MOTION AND VARIATIONAL EQUATIONS

6.1 ADAMS-COWELL ORDINATE SECOND SUM FORMULAS

The formulas for the integration and interpolation of the equations of motion and the variational equations are basically of the Newtonian type derivable from standard difference operator techniques. For the integration, these formulas define the well-known predictor-corrector Adams method for first-order equations and Cowell method for second-order systems. Formulas of the same class may be used to perform the required interpolations to determine values not given in the integration process and also to form the starting set of solution values required by the predictor-corrector process.

In the following discussion, an outline of the derivations of the required formulas is given. In addition, a detailed description of the computational algorithms necessary to perform the integrations is presented.

Let s and h denote real numbers and consider the linear operators, ∇, E^s, D, and I, which are defined as

$$\nabla f(t) = f(t) - f(t-h) \quad \left\{\begin{matrix}\text{Backward}\\ \text{Difference}\\ \text{Operator}\end{matrix}\right\} \tag{6-1}$$

$$E^s f(t) = f(t + s\,h) \quad \left\{\begin{matrix}\text{Shifting}\\ \text{Operator}\end{matrix}\right\} \tag{6-2}$$

$$D f(t) = \frac{d}{d t} f(t) = \dot{f}(t) \quad \left\{\begin{matrix}\text{Differentiation}\\ \text{Operator}\end{matrix}\right\} \tag{6-3}$$

$$I f(t) = f(t). \quad \left\{\begin{matrix}\text{Identity}\\ \text{Operator}\end{matrix}\right\} \tag{6-4}$$

Two well-known relations among these operators are

$$E^s = (I - \nabla)^{-s} \tag{6-5}$$

and

$$h\,D = -\ln(I - \nabla). \tag{6-6}$$

Utilizing Equations (6-5) and (6-6), the following operator identities can be derived

$$E^s = h\left[\frac{(I - \nabla)^{-s}}{-\ln(I - \nabla)}\right] D$$

$$E^s = h^2\left[\frac{(I - \nabla)^{-s}}{[\ln(I - \nabla)]^2}\right] D^2.$$

Expanding the bracketted terms in a ∇ series yields

$$E^s = h\left[\nabla^{-1} + \sum_{i=0}^{\infty} \gamma'_{i+1}(s)\,\nabla^i\right] D \tag{6-7}$$

$$E^s = h^2\left[\nabla^{-2} + (s-1)\,\nabla^{-1} + \sum_{i=0}^{\infty} \gamma''_{i+2}(s)\,\nabla^i\right] D^2 \tag{6-8}$$

where the $y'_i(s)$ and $y''_i(s)$ are given by the following recursive formulas in s, (see Reference 1)

$$\gamma_0(s) = \gamma'_0(s) = \gamma''_0(s) = 1 \tag{6-9}$$

$$\gamma'_i(s) = \sum_{j=0}^{i} \gamma'_j(0)\,\gamma_{i-j}(s) \tag{6-10}$$

$$\gamma''_i(s) = \sum_{j=0}^{i} \gamma''_j(0)\,\gamma_{i-j}(s) \qquad i = 0,\ 1,\ 2,\ \ldots\ldots \tag{6-11}$$

where

$$\gamma_i(s) = \frac{s + i - 1}{i}\,\gamma_{i-1}(s) \tag{6-12}$$

and

$$\gamma_i'(0) = -\sum_{j=0}^{i-1} \frac{1}{i - j + 1}\,\gamma_j'(0) \tag{6-13}$$

$$\gamma_i''(0) = \sum_{j=0}^{i} \gamma_j'(0)\,\gamma_{i-j}'(0). \tag{6-14}$$

Applying the operators (6-7) and (6-8) to the functions $\dot{x}(t)$ and $x(t)$, respectively, and truncating after k terms, gives

$$\dot{x}(t + s\,h) = h\left[\nabla^{-1}\ddot{x}(t) + \sum_{i=0}^{k} \gamma_{i+1}'(s)\,\nabla^i \ddot{x}(t)\right] \tag{6-15}$$

$$x(t + s\,h) = h^2\left[\nabla^{-2}\ddot{x}(t) + (s - 1)\,\nabla^{-1}\ddot{x}(t) + \sum_{i=0}^{k} \gamma_{i+2}''(s)\,\nabla^i \ddot{x}(t)\right]. \tag{6-16}$$

The quantities $\nabla^{-1}\ddot{x}(t)$ and $\nabla^{-1}\ddot{x}(t)$ are called the first and second sums of $\ddot{x}(t)$ and satisfy the relationships

$$\nabla^{-1}\ddot{x}(t) - \nabla^{-1}\ddot{x}(t - h) = \ddot{x}(t) \tag{6-17}$$

and

$$\nabla^{-2}\ddot{x}(t) - \nabla^{-2}\ddot{x}(t - h) = \nabla^{-1}\ddot{x}(t). \tag{6-18}$$

By varying the value for s, Equations (6-15) and (6-16) define the Adams-Cowell predictor-corrector formulas, as well as the Newtonian interpolation and starting formulas (Reference 2). For example, the Adams-Cowell predictor formulas are obtained by setting $s = 1$ and $x = x(t_n) = x(t_0 + nh)$ to give

$$\dot{x}_{n+1} = h \left[\nabla^{-1} \ddot{x}_n + \sum_{i=0}^{k} \gamma'_{i+1} (1) \nabla^i \ddot{x}_n \right] \tag{6-19}$$

and

$$x_{n+1} = h^2 \left[\nabla^{-2} \ddot{x}_n + \sum_{i=0}^{k} \gamma''_{i+2} (1) \nabla^i \ddot{x}_n \right] . \tag{6-20}$$

The preceding equations may be expressed in ordinate form as

$$\dot{x}_{n+1} = h \left[{}^{I}S_n + \sum_{i=0}^{k} \beta_i \ddot{x}_{n-i} \right] \tag{6-21}$$

$$x_{n+1} = h^2 \left[{}^{II}S_n + \sum_{i=0}^{k} \alpha_i \ddot{x}_{n-i} \right] \tag{6-22}$$

where

$${}^{I}S_n = \nabla^{-1} \ddot{x}_n \tag{6-23}$$

$${}^{II}S_n = \nabla^{-2} \ddot{x}_n . \tag{6-24}$$

The coefficients α_i and β_i can be expressed as functions of γ'_i and γ''_i from the recursive relations given by Equations (6-9) through (6-14), e. g.

$$\alpha_i = (-1)^i \sum_{m=i}^{k} \binom{m}{i} \gamma''_{m+2} (1) \tag{6-25}$$

$$i = 0, 1, 2, \ldots . k$$

The Adams-Cowell corrector formulas are obtained from Equations (6-15) and (6-16) by setting $s = 0$ and $t = t_{n+1}$ yielding

$$\dot{x}_{n+1} = h \left[{}^{I}S_n + \sum_{i=0}^{k} \beta_i^* \ddot{x}_{n+1-i} \right] \tag{6-26}$$

and

$$x_{n+1} = h^2 \left[{}^{II}S_n + \sum_{i=0}^{k} \alpha_i^* \ddot{x}_{n+1-i} \right] \tag{6-27}$$

where α_i^* and β_i^* are computed similar to α_i and β_i but using $\gamma_i''(0)$ and $\gamma_i'(0)$. The β_i and β_i^* are called the summed ordinate Adams-Moulton predictor-corrector coefficients and α_i and α_i^* the corresponding Störmer-Cowell coefficients.

These coefficients are tabulated in rational form in Reference 1 for formulas of order 4 through 15.

6.2 PREDICT-PSEUDO CORRECT ALGORITHM FOR EQUATION OF MOTION

The following describes the procedure for the integration of the equations of motion (Reference 3). Assume that the equations to be integrated have the form

$$\ddot{\bar{R}} = \frac{-\mu \bar{R}}{R^3} + P(t, \bar{R}, \dot{\bar{R}}) \tag{6-28}$$

where the first term represents the primary attracting body acting on the satellite. Assuming the accelerations and sums

$$\ddot{\bar{R}}(t_{n-i}), \quad {}^{I}S_n = \nabla^{-1} \ddot{\bar{R}}_n, \quad {}^{II}S_n = \nabla^{-2} \ddot{\bar{R}}_n, \quad i = 0, 1, 2, \ldots k \tag{6-29}$$

are known; then the iterative algorithm to advance to time t_{n+1} is

(A) Predict: Using Equations (6-21) and (6-22), predict values (denoted by superscript p)

$$\bar{R}^{(p)}(t_{n+1}) = [X_{n+1}^{(p)}, Y_{n+1}^{(p)}, Z_{n+1}^{(p)}] \tag{6-30}$$

$$\dot{\bar{R}}^{(p)}(t_{n+1}) = [\dot{X}_{n+1}^{(p)}, \dot{Y}_{n+1}^{(p)}, \dot{Z}_{n+1}^{(p)}]. \tag{6-31}$$

(B) Evaluate: Using Equation (6-28), evaluate

$$\ddot{\bar{R}}(t_{n+1}) = \frac{-\mu \bar{R}_{n+1}^{(p)}}{R_{n+1}^{(p)3}} + P(t_{n+1}, \bar{R}_{n+1}^{(p)}, \dot{\bar{R}}_{n+1}^{(p)}). \tag{6-32}$$

(C) Correct: Using Equations (6-26) and (6-27), obtain improved values, (denoted by the superscript c) $\bar{R}_{n+1}^{(c)}$ and $\dot{\bar{R}}_{n+1}^{(c)}$.

(D) Test: Compare the magnitude of the vector $[\bar{R}^{(p)}(t_{n+1}) - \bar{R}^{(c)}(t_{n+1})]$ against a prescribed tolerance. If this quantity is sufficiently small, proceed to Step (E); otherwise, replace the values $\bar{R}^{(p)}$ and $\dot{\bar{R}}^{(p)}$ with $\bar{R}^{(c)}$ and $\dot{\bar{R}}^{(c)}$ and repeat Steps (B), (C), and (D).

(E) Pseudo Correct: Compute the acceleration

$$\ddot{\bar{R}}(t_{n+1}) = \frac{-\mu \bar{R}_{n+1}^{(c)}}{R_{n+1}^{(c)3}} + P(t_{n+1}, \bar{R}_{n+1}^{(p)}, \dot{\bar{R}}_{n+1}^{(p)}) \tag{6-33}$$

where the P term is obtained from Step B.

(F) Update Sums: Compute the updated sums

$${}^{I}S_{n+1} = {}^{I}S_n + \ddot{\bar{R}}(t_{n+1}) \tag{6-34}$$

$${}^{II}S_{n+1} = {}^{II}S_n + {}^{I}S_{n+1}. \tag{6-35}$$

The computational cycle (A) → (F) may then be repeated with n = n + 1.

In n-body or earth-moon trajectory computations, the equations of motion will frequently be independent of the velocity term $\dot{\bar{R}}$, i. e., the acceleration is of the form

$$\ddot{\bar{R}} = \frac{-\mu \bar{R}}{R^3} + P(t, \bar{R}). \tag{6-36}$$

For trajectory segments possessing this characteristic, the preceding computational cycle may be simplified. Particularly in Step (A), the predicted $\dot{\bar{R}}^{(p)}$ need not be computed and in Step (C), the provisional corrected values $\dot{\bar{R}}^{(c)}$ are not required. After the test in Step (D) is satisfied, $\bar{R}^{(c)}$ may be obtained by one application of the corrector formula in Equation (6-27).

6.3 CORRECTOR-ONLY COWELL INTEGRATION FOR LINEAR SYSTEMS

From the Adams-Cowell corrector equations

$$y_{n+1} = h^2 \left[{}^{II}S_n + \sum_{i=0}^{k} \alpha_i^* \ddot{y}_{n+1-i} \right] \tag{6-37}$$

and

$$\dot{y}_{n+1} = h \left[{}^{I}S_n + \sum_{i=0}^{k} \beta_i^* \ddot{y}_{n+1-i} \right], \tag{6-38}$$

closed form equations can be derived when the equation being integrated is linear. Such a linear equation is

$$\ddot{y} = a(t)\, y + b(t)\, \dot{y} + f(t) \tag{6-39}$$

where a(t) and b(t) and f(t) are known time varying functions.

Equations (6-37) and (6-38) can be written as

$$y_{n+1} = h^2 \left[{}^{II}S_n + \alpha_0^* \ddot{y}_{n+1} + \sum_{i=1}^{k} \alpha_i^* \ddot{y}_{n+1-i} \right] \tag{6-40}$$

$$\dot{y}_{n+1} = h \left[{}^{I}S_n + \beta_0^* \ddot{y}_{n+1} + \sum_{i=1}^{k} \beta_i^* \ddot{y}_{n+1-i} \right]. \tag{6-41}$$

By expanding the derivative $\ddot{y}_{n+1}$, we obtain

$$y_{n+1} = h^2 \left[{}^{II}S_n + \alpha_0^* a_{n+1} y_{n+1} + \alpha_0^* b_{n+1} \dot{y}_{n+1} + \alpha_0^* f_{n+1} + \sum_{i=1}^{k} \alpha_i^* \ddot{y}_{n+1-1} \right] \tag{6-42}$$

$$\dot{y}_{n+1} = h \left[{}^{I}S_n + \beta_0^* a_{n+1} y_{n+1} + \beta_0^* b_{n+1} \dot{y}_{n+1} + \beta_0^* f_{n+1} + \sum_{i=1}^{k} \beta_i^* \ddot{y}_{n+1-i} \right]. \tag{6-43}$$

Defining the known quantities

$$x_n = h^2 \left[{}^{II}S_n + \alpha_0^* f_{n+1} + \sum_{i=1}^{k} \alpha_i^* \ddot{y}_{n+1-i} \right] \tag{6-44}$$

$$v_n = h \left[{}^{I}S_n + \beta_0^* f_{n+1} + \sum_{i=1}^{k} \beta_i^* \ddot{y}_{n+1-i} \right], \tag{6-45}$$

and the matrix

$$H = \begin{bmatrix} h^2 \alpha_0^* a_{n+1} & h^2 \alpha_0^* b_{n+1} \\ h \beta_0^* a_{n+1} & h \beta_0^* b_{n+1} \end{bmatrix} \tag{6-46}$$

then Equations (6-42) and (6-43) may be written as a single-vector equation

$$\begin{bmatrix} y_{n+1} \\ \\ \dot{y}_{n+1} \end{bmatrix} = H \begin{bmatrix} y_{n+1} \\ \\ \dot{y}_{n+1} \end{bmatrix} + \begin{bmatrix} x_n \\ \\ v_n \end{bmatrix} . \tag{6-47}$$

The solution to Equation (6-47) is

$$\begin{bmatrix} y_{n+1} \\ \\ \dot{y}_{n+1} \end{bmatrix} = [I - H]^{-1} \begin{bmatrix} x_n \\ \\ v_n \end{bmatrix} . \tag{6-48}$$

It should be noted that the inverse in the preceding equation will always exist if h is sufficiently small. The inverse depends only on the coefficients a and b, and need be computed only once when solving equations of the form of Equation (6-39) with different nonhomogeneous terms f(t).

6.4 CORRECTOR-ONLY ALGORITHM FOR VARIATIONAL EQUATIONS

The position and velocity partials of the satellite motion with respect to any parameter appearing in the acceleration model in Equation (6-28) or state (dynamic parameters) may be obtained by the numerical integration of a system of equations of the form

$$\ddot{Y} = A(t)\, Y + B(t)\, \dot{Y} + C(t) \tag{6-49}$$

from initial conditions at t_0 given by

$$Y(t_0) = \frac{\partial \bar{R}(t_0)}{\partial \bar{p}} \qquad \dot{Y}(t_0) = \frac{\partial \dot{\bar{R}}(t_0)}{\partial \bar{p}} \tag{6-50}$$

where

$$A(t) = \left[\frac{\partial \ddot{\bar{R}}(t)}{\partial \bar{R}}\right]_{3 \times 3} \tag{6-51}$$

$$B(t) = \left[\frac{\partial \ddot{\bar{R}}(t)}{\partial \dot{\bar{R}}}\right]_{3 \times 3} \tag{6-52}$$

$$C(t) = \left[\frac{\partial \ddot{\bar{R}}(t)}{\partial \bar{p}}\right] \quad \left\{\begin{array}{l} 3 \times \ell \text{ matrix of} \\ \text{acceleration partials} \end{array}\right\} \tag{6-53}$$

$$Y(t) = \left[\frac{\partial \bar{R}(t)}{\partial \bar{p}}\right] \quad \left\{\begin{array}{l} 3 \times \ell \text{ matrix of} \\ \text{position partials} \end{array}\right\} \tag{6-54}$$

and

$$\dot{Y}(t) = \left[\frac{\partial \dot{\bar{R}}(t)}{\partial \bar{p}}\right] \quad \left\{\begin{array}{l} 3 \times \ell \text{ matrix of} \\ \text{velocity partials} \end{array}\right\} \tag{6-55}$$

The vector $\bar{p}$ contains the parameters in the acceleration model to be estimated.

The components of the matrices A, B, and C were developed in Chapter 5.

Note that the components of $\bar{p}$ correspond to the spacecraft's position and velocity at epoch and can be expressed, optionally, in mean of 1950.0 Cartesian coordinates, true of epoch Cartesian coordinates, classical Keplerian orbital elements, spherical coordinates, or DODS variables. The initial conditions for the variational equations, Equation (6-50), are dependent upon the coordinate systems selected to be estimated. The partials of $\bar{R}$ and $\dot{\bar{R}}$ with respect to Keplerian elements and spherical coordinates can be obtained from Sections 3.3.7 and 3.3.3, respectively. Note that since the first six elements of $\bar{p}$ are the state, then the first six columns of C are zero. Most model parameters such as thrust, drag, harmonic coefficients, etc. enter into $P(t, \bar{R}, \dot{\bar{R}})$ of Equation (6-28) linearly; so that the computation of $C(t)$ may be simplified by retaining many of the quantities used in the computation of $\ddot{\bar{R}}(t)$.

The integration of system Equation (6-49) may be performed by the utilization of the corrector-only formula Equation (6-48) as follows. Assuming that the satellite position and velocity, $\bar{R}(t_{n+1})$ and $\dot{\bar{R}}(t_{n+1})$, the matrices $\ddot{Y}_{n+1}$ i = 0, 1, 2, . . . k and summation matrices ${}^{I}P_n$ and ${}^{II}P_n$ $(3 \times \ell)$ are known then the algorithm to advance Y to time t_{n+1} is:

(A) Compute the matrices $A(t_{n+1})$, $B(t_{n+1})$, and $C(t_{n+1})$, which depend only on t_{n+1}, $\bar{R}_{n+1}$, and $\dot{\bar{R}}_{n+1}$.

(B) Compute the 6×6 matrix $[I - H]^{-1}$ where

$$H = \begin{bmatrix} h^2\ \alpha_0^*\ A_{n+1} & h^2\ \alpha_0^*\ B_{n+1} \\ h\beta_0^*\ A_{n+1} & h\beta_0^*\ B_{n+1} \end{bmatrix} \tag{6-56}$$

α_0^* and β_0^* are the corrector coefficients of Equations (6-26) and (6-27), and h is the stepsize.

(C) Form the $3 \times \ell$ matrices, X_n and V_n

$$X_n = h^2 \left[{}^{II}P_n + \sum_{i=1}^{k} \alpha_i^*\ \ddot{Y}_{n+1-i} + \alpha_0^*\ C_{n+1} \right] \tag{6-57}$$

$$V_n = h \left[{}^{I}P_n + \sum_{i=1}^{k} \beta_i^*\ \ddot{Y}_{n+1-i} + \beta_0^*\ C_{n+1} \right] \tag{6-58}$$

(D) Compute the required position and velocity partials, Y_{n+1} and $\dot{Y}_{n+1}$, by the matrix equation

$$\begin{bmatrix} Y_{n+1} \\ \dot{Y}_{n+1} \end{bmatrix}_{6 \times \ell} = [I - H]^{-1} \begin{bmatrix} X_n \\ V_n \end{bmatrix}_{6 \times \ell} \tag{6-59}$$

(E) Update acceleration and sums by

$$\ddot{Y}_{n+1} = A_{n+1}\, Y_{n+1} + B_{n+1}\, \dot{Y}_{n+1} + C_{n+1} \tag{6-60}$$

$$^{I}P_{n+1} = {}^{I}P_{n} + \ddot{Y}_{n+1} \tag{6-61}$$

$$^{II}P_{n+1} = {}^{II}P_{n} + {}^{I}P_{n+1} \tag{6-62}$$

completing the cycle. After computing $\bar{R}_{n+2}$ and $\dot{\bar{R}}_{n+2}$, Steps (A) - (E) may be repeated with n = n + 1.

At points along the trajectory where the equations of motion are velocity-free, i. e., of the form of Equation (6-36), the matrix B in Equation (6-49) is zero, so that we are required to solve a system of the form

$$\ddot{Y} = A(t)\, Y + C(t). \tag{6-63}$$

As in the case of the equations of motion, the computational algorithm can then be simplified. In particular, in Step (A), only the matrices A and C are required, and in Step B, H becomes the 3×3 matrix

$$H = h^2\, \alpha_0^*\, A_{n+1}. \tag{6-64}$$

The required partials are then given by

$$Y_{n+1} = [I - H]^{-1}\, X_n \tag{6-65}$$

$$\dot{Y}_{n+1} = h\, \beta_0^*\, A_{n+1}\, Y_{n+1} + V_n. \tag{6-66}$$

The order and stepsize used in the integration of the variational equations may differ from that used in the integration of the equations of motion without any significant difficulty.

6.5 MAPPING OF POSITION PARTIALS

It is well known from the theory of linear differential equations that the solution of the n-dimensional linear system

$$\dot{\bar{x}} = D(t)\,\bar{x} \tag{6-67}$$

satisfying the initial condition

$$\bar{x}(t_0) = \bar{x}_0 \tag{6-68}$$

is given by

$$\bar{x}(t) = \Phi(t,\ t_0)\,\bar{x}_0 \tag{6-69}$$

where Φ is a fundamental matrix solution of Equation (6-67), i. e., an $n \times n$ matrix satisfying

$$\dot{\Phi} = D(t)\,\Phi \tag{6-70}$$

with initial condition

$$\Phi(t_0,\ t_0) = I. \tag{6-71}$$

In our context, $\Phi(t, t_0)$ is called the state transition matrix. The properties of Φ can be used to enhance the computational algorithm for position and velocity partials as follows: during the integration of a trajectory, a column of C(t) corresponding to a dynamic parameter may become zero. For example, when leaving the sphere of influence of the earth, the acceleration partial with respect to a geopotential coefficient of the earth will become effectively zero. If we denote this time by T, then the position partial with respect to this parameter, which we denote by $x_j(t)$, will satisfy an equation of the form of Equation (6-67) for $t > T$ where

$$D(t) = \begin{bmatrix} 0 & I \\ A(t) & B(t) \end{bmatrix}_{6\times 6} \tag{6-72}$$

with an initial condition $\bar{x}(T)$. Let $\Phi(t, T)$ be the state transition matrix satisfying $\Phi(T,T) = I$. Then, the required position partial may be obtained for any $t > T$ by

$$x(t) = \Phi(t, T)\, x(T). \tag{6-73}$$

The overall state transition matrix $\Phi(t, t_0)$ for $t > T$ may be computed by

$$\Phi(t, t_0) = \Phi(t, T)\, \Phi(T, t_0) \tag{6-74}$$

where the elements of the matrix $\Phi(T, t_0)$ are

$$\Phi(T, t_0) = \begin{bmatrix} \dfrac{\partial \bar{R}(T)}{\partial \bar{R}_0} & \dfrac{\partial \bar{R}(T)}{\partial \dot{\bar{R}}_0} \\ \dfrac{\partial \dot{\bar{R}}(T)}{\partial \bar{R}_0} & \dfrac{\partial \dot{\bar{R}}(T)}{\partial \dot{\bar{R}}_0} \end{bmatrix} \tag{6-75}$$

which are contained in the Y and $\dot{Y}$ matrices when $t = T$ (assuming $\bar{p}$ contains the state). The computational strategy for the computation of the partial of $\bar{x}(t)$ is then, to use the method of Section 6.3 up to $t = T$. At that time the matrix $\Phi(T, t_0)$ is stored, $\Phi(T, T)$ is initialized, and for any $t > T$, $\bar{x}(t)$ is computed using Equation (6-73) and $\Phi(t, t_0)$ is computed using Equation (6-74). A similar process may be used for multiple event times $T_1, T_2, \ldots T_r$ at which various columns of C(t) become zero. Assuming $T_1 \leq T_2 \leq \ldots \leq T_r \leq t$, Equation (6-74) becomes

$$\Phi(t, t_0) = \Phi(t, T_r)\, \Phi(T_r, T_{r-1}) \cdots \Phi(T_1, t_0). \tag{6-76}$$

6.6 THE STARTING PROCEDURE

The starting arrays

$$\ddot{\bar{R}}_{n-i},\ \ddot{Y}_{n-i},\ i = 0, 1, 2, \ldots k \tag{6-77}$$

and the associated first and second sums required by the integration process may be computed by an iterative process based on Equations (6-15) and (6-16) using varying values for s. Let $m = [(k + 1)/2]$, where the brackets indicate the greatest integer function, and $\bar{R}_0$, $\dot{\bar{R}}_0$, and $\ddot{\bar{R}}_0$ be the given initial values at $t = t_0$ of Equations (6-28) (the process is analogous for Equation (6-49)). We will compute the values

$$\bar{R}_i, \dot{\bar{R}}_i, \ddot{\bar{R}}_i, \quad i = \pm 1, \pm 2, \cdots \pm m$$

by successive approximations, yielding the required starting values.

Let $\delta_i'(s)$ and $\delta_i''(s)$ be the coefficients of the ordinate forms of Equations (6-15) and (6-16) with $k = 2m$

$$\dot{x}(t_n + s\,h) = h\left[{}^{I}S_n + \sum_{i=0}^{2m} \delta_i'(s)\,\ddot{x}_{n-i}\right] \tag{6-78}$$

$$x(t_n + s\,h) = h^2\left[{}^{II}S_n + (s-1)\,{}^{I}S_n + \sum_{i=0}^{2m} \delta_i''(s)\,\ddot{x}_{n-i}\right]. \tag{6-79}$$

Then letting $\bar{R}^{(j)}$ denote the j^{th} approximation, the $(j+1)^{st}$ approximation is given by the following procedure

(A) Compute the sums ${}^{I}S_m$ and ${}^{II}S_m$ using

$${}^{I}S_m = \frac{\dot{\bar{R}}_0}{h} - \sum_{i=0}^{2m} \delta_i'(-m)\,\ddot{\bar{R}}_{m-i}^{(j)} \tag{6-80}$$

$${}^{II}S_m = \frac{\bar{R}_0}{h^2} + (m+1)\,{}^{I}S_m - \sum_{i=0}^{2m} \delta_i''(-m)\,\ddot{\bar{R}}_{m-i}^{(j)}. \tag{6-81}$$

C.4

(B) Compute the corrected position and velocity vectors using Equations (6-79) and (6-78) with n = m and s = (i-m)

$$\bar{R}_i^{(j+1)} = h^2 \left[{}^{II}S_m + (i - m - 1)\, {}^{I}S_m + \sum_{\ell=0}^{2m} \delta''_\ell\, (i - m)\, \ddot{\bar{R}}_{m-\ell}^{(j)} \right] \tag{6-80}$$

$$\dot{\bar{R}}_i^{(j+1)} = h \left[{}^{I}S_m + \sum_{\ell=0}^{2m} \delta'_\ell\, (i - m)\, \ddot{\bar{R}}_{m-\ell}^{(j)} \right], \qquad i = \pm 1, \pm 2, \ldots \pm m. \tag{6-81}$$

(C) Compute the acceleration $\ddot{\bar{R}}_i^{(j+1)}$ using the force model. This completes the iteration. Steps (A) → (C) are repeated until the successive values of $\bar{R}_i$ and $\dot{\bar{R}}_i$ converge.

As in the process described in Section 6.2, if the accelerations are velocity-free, simplifications in the computational algorithm may be made. In particular, in Step (B), the computation of $\dot{\bar{R}}_i^{(j+1)}$ may be omitted until convergence on the positions $\bar{R}_i$.

The first approximation (j = 1) may be obtained by a variety of methods: near a primary, two-body analysis, either in the form of orbital elements or f and g series may be used effectively; between two primaries, either a single step low-order method or the use of a prestored ephemeris should be used.

6.7 INTERPOLATION

Interpolation for values of $\bar{R}(t)$ and $\dot{\bar{R}}(t)$ for $t_{n-1} < t < t_n$ may be obtained from Equations (6-79) and (6-78) using $s = (t - t_n)/h$. The accuracy of this interpolation is consistent with that of the integration.

6.8 LOCAL ERROR CONTROL

Local error control is performed by a variable stepsize process automatically and semiautomatically (see Reference 4). In the automatic mode, stepsizes are selected based on the magnitude of the local error, ϵ_n, computed on a step-by-step basis by the Milne formula

$$\epsilon_n = \frac{C\,|\bar{R}_n^{(p)} - \bar{R}_n^{(c)}|}{|R_n^{(c)}|} \tag{6-84}$$

where C is a constant depending on the order of the formulas (6-22) and (6-27). $\bar{R}_n^{(p)}$ and $\bar{R}_n^{(c)}$ are the predicted and finally accepted position vectors, respectively, computed at time $t = t_n$. The stepsizes are selected so that ϵ_n at each step satisfies the constraint equation

$$T_2 \leq \epsilon_n \leq T_1 \tag{6-85}$$

where T_1 and T_2 are specified upper and lower bounds on the local error.

The variable step integration algorithm is as follows: at each step n, the test in Equation (6-85) is performed. There are three cases:

(A) $\epsilon_n > T_1$; the stepsize is decreased, the n^{th} computed point is rejected and recomputed with the new stepsize where the required back values are obtained by interpolation.

(B) $\epsilon_n < T_2$; the stepsize is increased, the n^{th} computed point is accepted and the integration proceeds with the new stepsize where the required back values are obtained by using every other point from a saved array of points if $h_{new} = 2h$ or by interpolation if $h < h_{new} < 2h$. A maximum increase of 2h is allowed.

(C) ϵ_n satisfies Equation (6-85); the integration proceeds uninterrupted.

In either case (A) or (B), h_{new} is computed by the formula

$$h_{new} = h\left[\frac{T_3}{\epsilon_n}\right]^{1/k} \tag{6-86}$$

where T_3 is a specified "allowable" local error satisfying $T_2 \leq T_3 \leq T_1$.

The stepsizes used for the integration of the variational equations are determined by the equations of motion integrator.

In the semiautomatic mode, the method of shells is used wherein stepsizes are specified as a function of radial distances from the primary (Reference 4). The

required stepsizes and radial distances may be determined by an integration calibration process using the automatic variable stepsize integrator. Since the stepsize distribution over the orbit generally depends on the orbital elements, particularly the semimajor axis and eccentricity, such a calibration would be repeated only if these elements changed considerably. This model of integration is generally less sensitive to the numerical difficulties generally associated with variable stepsize integration. The use of a regularized time variable also proves useful for this problem. This technique is described in the next section.

6.9 TIME REGULARIZATION

Accurate direct integration of Equation (6-28) or (6-49), with time as the independent variable for orbits that are highly eccentric or that connect regions with significantly different gravitational force magnitudes, generally requires either a very small fixed stepsize, or, in a variable stepsize scheme, many step changes. Frequent step changes are costly and result in propagating errors due to the interpolation procedure used to restart.

To improve this situation, the classical approach is to transform the independent variable to a new variable, denoted by τ, defined by the relation (Reference 5)

$$\frac{dt}{d\tau} = \frac{R^n}{\sqrt{\mu}}, \quad 1 \leq n \leq 2. \tag{6-87}$$

For n = 1 or 2, this variable corresponds to the use of true anomaly as the independent variable in the integration of elliptic motion. The use of regularization on the computation of free-flight earth-moon trajectories is investigated in Reference 6. The results of this study indicate increased computational accuracy and significant reduction in computation time due to regularization.

To transform systems (6-28) or (6-49) to systems with respect to the new independent variable τ, we use the notation

$$D\,g = \frac{dg}{d\tau} = \frac{R^n}{\sqrt{\mu}}\,\dot{g} \tag{6-88}$$

$$D^2 g = \frac{d^2 g}{d\tau^2} = \frac{R^n}{\mu} \left[n R^{n-1} \dot{R} \dot{g} + R^n \ddot{g} \right] \tag{6-89}$$

where

$$\dot{R} = \frac{\bar{R} \cdot \dot{\bar{R}}}{R} \tag{6-90}$$

and g(t) is any arbitrary vector-valued function in the t system. Similarly, we denote

$$D^{-1} g = \dot{g} = \frac{\sqrt{\mu}}{R^n} g' \tag{6-91}$$

$$D^{-2} g = \ddot{g} = \frac{\mu}{R^n} \left[R^{-n} g'' - \frac{n R'}{R^{n+1}} g' \right] \tag{6-92}$$

where $()' = d()/d\tau$, i.e., prime indicates differentiation with respect to τ, and

$$R' = \frac{R^{n-1}}{\sqrt{\mu}} (\bar{R} \cdot \dot{\bar{R}}). \tag{6-93}$$

The transformed system (6-28) may then be expressed as

$$\bar{R}'' = D^2 \bar{R}(t) \tag{6-94}$$

$$t'' = \frac{n R^{2n-1} \dot{R}}{\mu}. \tag{6-95}$$

The integration of Equation (6-95) is required to compute the time t as a function of the new independent variable τ.

The integration of Equations (6-94) and (6-95) may be carried out with essentially the same procedures outlined in the previous sections. The additional remarks required are:

(A) Given $t(\tau)$, $\bar{R}(\tau)$, and $\bar{R}'(\tau)$, a corresponding $\bar{R}''(\tau)$ is computed by first computing the time derivatives

$$\dot{\bar{R}}(\tau) = D^{-1}\,\bar{R}' = \frac{\sqrt{\mu}}{R^n(\tau)}\,\bar{R}'(\tau) \tag{6-96}$$

and

$$\ddot{\bar{R}}(\tau) = \frac{-\mu\,\bar{R}(\tau)}{R^3(\tau)} + P\left[t(\tau),\ \bar{R}(\tau),\ \dot{\bar{R}}(\tau)\right] \tag{6-97}$$

yielding

$$\bar{R}''(\tau) = D^2\,\bar{R}(\tau) = \frac{R^n}{\mu}\left(n\,R^{n-1}\,\dot{R}\,\dot{\bar{R}} + R^n\,\ddot{\bar{R}}\right). \tag{6-98}$$

(B) The value of the independent variable τ corresponding to an output request time or observation time t_r may be obtained by inverse interpolation on the t_i array obtained by the integration of Equation (6-95). The value of τ, so obtained, may then be used to compute the required $\bar{R}$ and $\dot{\bar{R}}$ by the usual interpolation procedure indicated in Section 6.8.

It should be noted that analogous regularization procedures may be used for Equation (6-49). The regularized variational equations are of the form

$$Y'' = \left[\frac{R^{2n}}{\mu}\,A(t)\right] Y + \frac{R^n}{\sqrt{\mu}}\left[B(t) + \frac{n\dot{R}I}{R}\right] Y' + \frac{R^{2n}}{\mu}\,C(t) \tag{6-99}$$

An additional advantage of using regularized time is that the initial (fixed) step-size may be conveniently selected as a fraction of the regularized period S, where if T is the satellite period

$$S = \int_0^T \frac{\sqrt{\mu}}{R^n}\,dt. \tag{6-100}$$

The integral may be evaluated by quadrature for the two-body problem by a change of variable from t to true anomaly, f, resulting in the formula

$$S = \frac{1}{p^{(n-2+1/2)}} \int_0^{2\pi} (1 + e\cos f)^{n-2}\,df \tag{6-101}$$

where p is the semilatus rectum of the ellipse. A fraction of this period (of the order 1/100) will frequently serve as an adequate stepsize for the integration of Equations (6-92) and (6-93).

A drawback of the method is that the equations of motion in the tau system in Equation (6-94) always contain explicit first derivatives, regardless of the situation in the t system, (see Equation (6-92)) so that the computational simplifications possible for velocity-free accelerations will not apply. Hence, the tradeoff between the advantages and disadvantages of the regularized time integration depend upon the stepsize, length of arc, efficiency requirements, and eccentricity magnitude.

6.10 REFERENCES

1. Goddard Space Flight Center, 553-69-46, Cowell Type Numerical Integration as Applied to Satellite Orbit Computation, J. L. Maury, and G. P. Brodsky, December 1969.

2. Computer Sciences Corporation, ND-9758-104-2-1, DODS Mod-N Design, P. R. Peabody, August 1967.

3. Goddard Space Flight Center, 553-69-544, GEOSTAR-I, A Geopotential and Station Position Recovery System, C. E. Velez, and G. P. Brodsky, November 1969.

4. Jet Propulsion Laboratory, DPODP System Documentation, Volume I, November 1966.

5. Tapley, Szebehely, and Lewallen, "Trajectory Optimization Using Regularized Variables," (paper presented at AAS/AIAA Astrodynamics Conference, 1968).

6. Szebehely, Pierce, and Standish, A Group of Earth to Moon Trajectories with Consecutive Collisions, 1964.

CHAPTER 7

OBSERVATION MODELS

This chapter presents the models and associated equations for computing the observations within the GTDS. The models consist of kinematic equations which yield the "ideal" value of the observations in trajectory related units (e.g., range, range-rate, azimuth, and elevation) as functions of the spacecraft's best estimated position and velocity, as well as specified model parameters (e.g., tracking station location and timing errors). The calculated ideal observations do not include some sources of systematic error inherent in the "actual" data resulting from the preprocessor. As a result, these systematic errors must be included in the calculated observations in the GTDS. For processing Option A (metric), the preprocessor has calibrated, time-corrected, smoothed, compacted, and converted the data to units compatible with the calculated observation; but it has not corrected for the effects of refraction and time delay caused by the atmosphere. Furthermore, the actual data may still contain systematic errors as a result of the smoothing and compaction performed in the preprocessor. For processing Option B (polynomial), the "actual" data has only been calibrated and, for some observations, does not even correspond to the same units as the calculated ideal observation. For example, the station-to-spacecraft relative range-rate in kilometers/second may have been the ideal observation calculated in the processor whereas the preprocessed data is the two-way Doppler shift in cycles/second obtained from the GRARR. Therefore, the GTDS measurement model must include all necessary conversion to make the calculated observation compatible with the actual data provided by the preprocessor. Furthermore, the time tag on the actual data corresponds to the time the signal was received at the tracking station and must be corrected for signal propagation time delay.

In the following sections the procedures and formulations apply principally to Option A (metric) processing. Section 7.1 presents a general description of the computed observations and their partials. Section 7.2 presents equations and transformations for determining the ideal observations and their partials. Section 7.3 is devoted to a discussion of atmospheric effects on the observations. Procedures are described for correcting these effects. Section 7.4 merges the perfect observations with the systematic error models and describes the GTDS (metric) processing procedures. A general discussion of Option B (polynomial) processing concepts is presented in Section 7.5. Finally Section 7.6 summarizes the role of the metric observation models in the estimation process.

7.1 GENERAL DESCRIPTION

The basic orbit determination process consists of differentially correcting estimates for a set of parameters from an observational model to minimize the sum of squares of the weighted differences between the measured observations and the corresponding quantities computed from the model. In GTDS, this model is assumed to be of the form

$$O_c = f_0 \left[\bar{r}_{1t} (t + \delta t, \bar{p}, \bar{r}_s), \dot{\bar{r}}_{1t} (t + \delta t, \bar{p}, \bar{r}_s)\right] + b + R F_C \qquad (7\text{-}1)$$

where

$t \sim$ the time tag of observation

$\delta t \sim$ the timing bias

$O_c \sim$ the computed observation at corrected time $t + \delta t$

$\bar{r}_{1t}, \dot{\bar{r}}_{1t} \sim$ the vehicle position and velocity at time $t + \delta t$ in local tangent coordinates with respect to a station position, $\bar{r}_s$, and dependent upon the dynamic parameter vector $\bar{p}$

$b \sim$ the measurement bias or offset

$f_0 \sim$ the geometric relationship defined by the observation type at time $t + \delta t$

$R F_C \sim$ correction to the observation due to atmospheric refraction, light time, etc.

The observational model parameters which may be estimated are:

$\bar{p} \sim$ the dynamic parameters in the equations of motion which can be estimated. These include satellite position and velocity variables, gravitational harmonic coefficients, drag parameters, etc.

$\bar{r}_s \sim$ the station location in earth-fixed coordinates.

$b \sim$ the measurement bias, both measurement type and station dependent.

$\delta t \sim$ the timing bias, both station and pass dependent.

The observation models simulate the following tracking system data types:

- C-Band

  (1) Range
  (2) Azimuth
  (3) Elevation

- Goddard VHF

  (1) Range
  (2) Range-Rate
  (3) X
  (4) Y

- Minitrack

  (1) Direction cosine ℓ
  (2) Direction cosine m.

The observations are assumed to be in metric form. It is also assumed that the time tag on each observation has been converted to universal time (UTC).

The differential correction process requires the computation of the "computed" measurements, including all systematic errors which exist in the actual observation data. The process also requires computation of partial derivatives of the measurements with respect to the model parameters $\bar{p}$, $\bar{r}_s$, b, and δt. These partial derivatives can be expressed as follows:

$$\frac{\partial O_c}{\partial \bar{p}} = \frac{\partial f_0}{\partial \bar{p}}$$

$$\frac{\partial O_c}{\partial \bar{r}_s} = \frac{\partial f_0}{\partial \bar{r}_s} \qquad (7\text{-}2)$$

$$\frac{\partial O_c}{\partial b} = 1$$

$$\frac{\partial O_c}{\partial (\delta t)} = \frac{\partial f_0}{\partial (\delta t)} = \dot{f}_0.$$

It is assumed that the partial of RF_C with respect to $\bar{p}$, $\bar{r}_s$, b or δt is either zero or negligible. In the following sections, the "perfect" observations, f_0, are presented along with their partial derivatives.

7.2 IDEAL OBSERVATIONS

The computed measurements, in metric form, are defined in terms of observer-centered topocentric local tangent coordinates. However, the trajectory is updated through the geocentric Cartesian mean equator and equinox of 1950.0 or true of epoch coordinates using ephemeris time.

This section presents the transformations and equations for computing the ideal measurements (i.e., no systematic errors b, RF_C, or δt present).

7.2.1 Transformation of Coordinates-Geocentric Inertial to Topocentric Local Tangent

After a data type is preprocessed into metric form, its time tag is corrected for propagation delay and transformed to universal time, t. At this time the geocentric Cartesian coordinates of the spacecraft are assumed available in the mean of 1950.0 system or the true of epoch system, whichever is being used as the basis in integrating the equations of motion. These coordinates are transformed to the true of date earth-fixed system as described in Section 3.3.1.5. Assuming the base coordinate system for the integration is the mean of 1950.0, the transformations are

$$\bar{r}_b(t) = H(t)\, G(t)\, \bar{R}(t) \tag{7-3}$$

and

$$\dot{\bar{r}}_b(t) = \dot{H}(t)\, G(t)\, \bar{R}(t) + H(t)\, G(t)\, \dot{\bar{R}}(t) \tag{7-4}$$

where

$\bar{R}$, $\dot{\bar{R}}$ ~ the spacecraft position and velocity in mean of 1950.0 geocentric inertial coordinates.

$\bar{r}_b$, $\dot{\bar{r}}_b$ ~ the spacecraft position and velocity in earth-fixed coordinates

$G(t) \sim$ the precession-nutation matrix described in Sections 3.3.1

$H(t) \sim$ the transformation matrix from true of epoch geocentric coordinates to body-fixed coordinates. This matrix is described in Section 3.3.1.5 to be

$$H = B_2 (x_p, y_p) \cdot B_1 (\alpha_g). \tag{7-5}$$

When the basic coordinate system for the integration is true of epoch, then the G matrix in Equations (7-3) and (7-4) is set equal to the identity matrix and $\bar{R}$ and $\dot{\bar{R}}$ are replaced by $\bar{r}$ and $\dot{\bar{r}}$. If polar motion is neglected then B_2 in Equation (7-5) is set equal to the identity matrix.

The body-fixed coordinates are next transformed to local tangent coordinates at the tracking station, $\bar{r}_s$, as described in Section 3.3.6, that is,

$$\bar{r}_{1t} = M_{1t} (\bar{r}_b - \bar{r}_s) \tag{7-6}$$

$$\dot{\bar{r}}_{1t} = M_{1t} \dot{\bar{r}}_b. \tag{7-7}$$

7.2.2 Observation Equations

The observations are next determined from the local tangent coordinates as follows.

7.2.2.1 Goddard Range and Range-Rate (GRARR) VHF

- Range

  The distance from the tracking station to the spacecraft

$$\rho = \sqrt{x_{1t}^2 + y_{1t}^2 + z_{1t}^2} = |\bar{r}_{1t}|. \tag{7-8}$$

- Range-Rate

The time derivative of the magnitude of the station-to-vehicle vector is

$$\dot{\rho} = \frac{\bar{r}_{1t} \cdot \dot{\bar{r}}_{1t}}{\rho} . \tag{7-9}$$

Using the range difference form of the Doppler measurement (see Equation (2-15)), the range, Equation (7-8), is used to iteratively solve the uplink and downlink light paths which terminate at the tracking station at the two times, t_S and $t_S + \Delta t_{RR}$.

- Gimbal Angles

X is the angle between the projection of the station-vehicle vector into the east-vertical plane and the vertical axis (see Figure 2-1). The angle is measured positive when the vehicle is east of the station.

$$X = \tan^{-1}\left(\frac{x_{1t}}{z_{1t}}\right) \qquad -\frac{\pi}{2} \le X \le \frac{\pi}{2} \tag{7-10}$$

Y is the angle between the station-vehicle vector and the projection of this vector into the east-vertical plane. The angle is measured positive when the vehicle is north of the station.

$$Y = \tan^{-1}\left(\frac{y_{1t}}{\sqrt{x_{1t}^2 + z_{1t}^2}}\right) \qquad -\frac{\pi}{2} \le Y \le \frac{\pi}{2} \tag{7-11}$$

7.2.2.2 C-Band Radar

- Range

The distance from the tracking station to the spacecraft is

$$\rho = |\bar{r}_{1t}| . \tag{7-12}$$

- Gimbal Angles

The azimuth is the angle in the local tangent (horizon) plane measured clockwise from north to the projection of the station-vehicle vector in the local tangent plane. The angle is measured positive east from north.

$$A = \sin^{-1}\left(\frac{x_{1t}}{\sqrt{x_{1t}^2 + y_{1t}^2}}\right) \tag{7-13a}$$

$$A = \cos^{-1}\left(\frac{y_{1t}}{\sqrt{x_{1t}^2 + y_{1t}^2}}\right) \qquad 0 \leq A \leq 2\pi \tag{7-13b}$$

The elevation is the angle between the station-vehicle vector and its projection in the local tangent plane. The angle is positive for positive z_{1t} (up-direction).

$$E = \tan^{-1}\left(\frac{z_{1t}}{\sqrt{x_{1t}^2 + y_{1t}^2}}\right) \qquad 0 \leq E \leq \frac{\pi}{2} \tag{7-14}$$

7.2.2.3 Minitrack

Direction cosine ℓ is the cosine of the angle between the station-vehicle vector and the local tangent east-pointing axis. The angle is positive when the vehicle is east of the station.

$$\ell = \frac{x_{1t}}{\rho} \qquad -1 \leq \ell \leq 1. \tag{7-15}$$

Direction cosine m is the cosine of the angle between the station-vehicle vector and the local tangent north-pointing axis. The angle is positive when the vehicle is north of the station

$$m = \frac{y_{1t}}{\rho} \qquad -1 \leq m \leq 1 \tag{7-16}$$

7.2.3 Measurement Partials

The partial derivatives of the ideal observations, f_0, with respect to dynamic model parameters, $\bar{p}$, station location, $\bar{r}_s$, and timing bias, δt, are required in Equations (7-2). The partials are determined by transforming observation partials with respect to the local tangent state. For example the partial of f_0 with respect to dynamic model parameters, $\bar{p}$, is

$$\frac{\partial f_0}{\partial \bar{p}} = \frac{\partial f_0}{\partial \bar{r}_{1t}} \frac{\partial \bar{r}_{1t}}{\partial \bar{R}} \frac{\partial \bar{R}}{\partial \bar{p}} + \frac{\partial f_0}{\partial \dot{\bar{r}}_{1t}} \left(\frac{\partial \dot{\bar{r}}_{1t}}{\partial \bar{R}} \frac{\partial \bar{R}}{\partial \bar{p}} + \frac{\partial \dot{\bar{r}}_{1t}}{\partial \dot{\bar{R}}} \frac{\partial \dot{\bar{R}}}{\partial \bar{p}} \right) \tag{7-17}$$

The partials of $\bar{r}_{1t}$ and $\dot{\bar{r}}_{1t}$ with respect to $\bar{R}$ and $\dot{\bar{R}}$ are obtained from Equations (7-6), (7-7), (7-3), and (7-4) to be

$$\frac{\partial \bar{r}_{1t}}{\partial \bar{R}} = M_{1t} H G \tag{7-18}$$

$$\frac{\partial \dot{\bar{r}}_{1t}}{\partial \bar{R}} = M_{1t} \dot{H} G \tag{7-19}$$

$$\frac{\partial \dot{\bar{r}}_{1t}}{\partial \dot{\bar{R}}} = M_{1t} H G. \tag{7-20}$$

The partials of $\bar{R}$ and $\dot{\bar{R}}$ at time t with respect to $\bar{p}$, at time t_0 are obtained by numerical integration of the variational equations as discussed in Chapters 5 and 6. The vector $\bar{p}$ can optionally contain, as components, any of five representations of the satellite's position and velocity at time t_0.

The partials of f_0 with respect to $\bar{r}_{1t}$ and $\dot{\bar{r}}_{1t}$ are obtained by differentiating the ideal observation equations of Section 7.2.2. These are as follows:

- Range, ρ

$$\frac{\partial \rho}{\partial \bar{r}_{1t}} = \frac{\bar{r}_{1t}^T}{\rho} \tag{7-21a}$$

$$\frac{\partial \rho}{\partial \dot{\bar{r}}_{1t}} = 0 \tag{7-21b}$$

- Range-Rate, $\dot{\rho}$

$$\frac{\partial \dot{\rho}}{\partial \bar{r}_{1t}} = \frac{1}{\rho}\left[\dot{\bar{r}}_{1t}^{T} - \left(\frac{\dot{\rho}}{\rho}\right)\bar{r}_{1t}^{T}\right] \tag{7-22a}$$

$$\frac{\partial \dot{\rho}}{\partial \dot{\bar{r}}_{1t}} = \frac{\bar{r}_{1t}^{T}}{\rho} \tag{7-22b}$$

Utilizing the range difference formula of Equation (2-15), a linear combination of the range partials in Equation (7-21) is required.

- Azimuth Angle, A

$$\frac{\partial A}{\partial \bar{r}_{1t}} = \frac{1}{(x_{1t}^2 + y_{1t}^2)}\left[y_{1t},\ -x_{1t},\ 0\right] \tag{7-23a}$$

$$\frac{\partial A}{\partial \dot{\bar{r}}_{1t}} = 0 \tag{7-23b}$$

- Elevation Angle, E

$$\frac{\partial E}{\partial \bar{r}_{1t}} = \frac{1}{\rho^2}\left[\frac{-x_{1t}\,z_{1t}}{\sqrt{x_{1t}^2 + y_{1t}^2}},\ \frac{-y_{1t}\,z_{1t}}{\sqrt{x_{1t}^2 + y_{1t}^2}},\ \sqrt{x_{1t}^2 + y_{1t}^2}\right] \tag{7-24a}$$

$$\frac{\partial E}{\partial \dot{\bar{r}}_{1t}} = 0 \tag{7-24b}$$

- Gimbal Angle, X

$$\frac{\partial X}{\partial \bar{r}_{1t}} = \frac{1}{(x_{1t}^2 + y_{1t}^2)}\left[z_{1t},\ 0,\ -x_{1t}\right] \tag{7-25a}$$

$$\frac{\partial X}{\partial \dot{\bar{r}}_{1t}} = 0 \tag{7-25b}$$

- Gimbal Angle, Y

$$\frac{\partial Y}{\partial \bar{r}_{1t}} = \frac{1}{\rho^2}\left[\frac{-x_{1t}\, y_{1t}}{\sqrt{x_{1t}^2 + z_{1t}^2}},\ \sqrt{x_{1t}^2 + z_{1t}^2},\ \frac{-y_{1t}\, z_{1t}}{\sqrt{x_{1t}^2 + z_{1t}^2}}\right] \tag{7-26a}$$

$$\frac{\partial Y}{\partial \dot{\bar{r}}_{1t}} = 0 \tag{7-26b}$$

- Direction Cosine, ℓ

$$\frac{\partial \ell}{\partial \bar{r}_{1t}} = \frac{1}{\rho^3}\left[(y_{1t}^2 + z_{1t}^2),\ -x_{1t}\, y_{1t},\ -x_{1t}\, z_{1t}\right] \tag{7-27a}$$

$$\frac{\partial \ell}{\partial \dot{\bar{r}}_{1t}} = 0 \tag{7-27b}$$

- Direction Cosine, m

$$\frac{\partial m}{\partial \bar{r}_{1t}} = \frac{1}{\rho^3}\left[-x_{1t}\, y_{1t},\ (x_{1t}^2 + z_{1t}^2),\ -y_{1t}\, z_{1t}\right] \tag{7-28a}$$

$$\frac{\partial m}{\partial \dot{\bar{r}}_{1t}} = 0 \tag{7-28b}$$

The partial of the ideal observation, f_0, with respect to station location, r_s, in Equation (7-2) is

$$\frac{\partial f_0}{\partial \bar{r}_s} = \frac{\partial f_0}{\partial \bar{r}_{1t}}\,\frac{\partial \bar{r}_{1t}}{\partial \bar{r}_s} \tag{7-29}$$

where, from Equation (7-6)

$$\frac{\partial \bar{r}_{1t}}{\partial \bar{r}_S} = - M_{1t} \cdot \tag{7-30}$$

The partial of the ideal observation, f_0, with respect to the timing bias, δt, in Equation (7-2) is

$$\frac{\partial f_0}{\partial (\delta t)} = \dot{f}_0 = \frac{\partial f_0}{\partial \bar{r}_{1t}} \dot{\bar{r}}_{1t} + \frac{\partial f_0}{\partial \dot{\bar{r}}_{1t}} \ddot{\bar{r}}_{1t} \tag{7-31}$$

where $\ddot{\bar{r}}_{1t}$ is obtained by differentiating Equations (7-7) and (7-4) and combining to give

$$\dddot{\bar{r}}_{1t} = M_{1t} \ddot{H} (\alpha_g) G(t) \bar{R}(t) + 2 M_{1t} \dot{H} (\alpha_g) G(t) \dot{\bar{R}} + M_{1t} H (\alpha_g) G(t) \ddot{\bar{R}}. \tag{7-32}$$

7.3 ATMOSPHERIC EFFECTS

All satellite tracking observations from ground tracking stations are affected by the propagation of the electromagnetic radiations through the earth's atmosphere. The bending or refraction of the rays means that the measurement of the direction of the signal propagation at the ground does not correspond with the direction of the straight relative position vector between the spacecraft and tracking station. This ray bending also requires that the interpretation of the Doppler-shift measurement must be based upon the projection of the appropriate velocity along the local propagation path direction - not along the relative position vector. Since the propagation speed through the atmosphere is different from the vacuum speed, the interpretation of time-delay measurements must account for this effect.

In principle, these refraction effects may be characterized in terms of the variable local index of refraction, n, of the medium through which the signal is propagated. It is assumed that the atmosphere is spherically symmetric with respect to the center of the earth; therefore, n varies only with altitude (measured radially). The nature of this altitude dependence is discussed in the following two sections. The next three sections present the mathematical forms for characterizing the three basic refraction effects mentioned above (References 1, 2, 3).

7.3.1 Troposphere Model

The troposphere is the familiar gaseous atmosphere, extending from the earth's surface upward to a sensible limit of about 30 kilometers. For the microwave frequencies of interest in spacecraft tracking, the troposphere is said to be a nondispersive medium; that is, the index of refraction, n, is independent of the frequency of the signal transmission through it. Within this region, n is expressed as

$$n = 1 + N_T \tag{7-33}$$

where the tropospheric refractivity, N_T, depends only upon the thermodynamic properties of the air. Since temperature and pressure data are not readily available at altitude, surface data are used to compute the surface refractivity, N_S, and an exponential decay with altitude is assumed.

$$N_T = N_S \, e^{-h/H_T} \tag{7-34}$$

where

$H_T \sim$ the troposphere scale height.

The National Bureau of Standards Central Radio Propagation Laboratory (NBS CRPL) gives values of the scale height for different values of the surface refractivity. Reference 4 stresses the importance of using corresponding values of H_T and N_S. (Some formulations have fixed H_T at a standard value, allowing only N_S to vary.) It is assumed that GSFC will receive surface refractivity data from NBS CRPL for all tracking stations of interest. The time spacing of these points is assumed to be sufficiently short that polynomial interpolation will yield accurate values of H_T and N_S at any station at any time. The polynomial coefficients are determined in a data preprocessor program and then stored in a data base for use in the GTDS. Data updates occur every month and include measured data for the past month and predicted data for the next three months.

7.3.2 Ionosphere Model

Above the troposphere is an electromagnetic atmosphere, called the ionosphere, extending from about 80 kilometers to beyond 1000 kilometers. The

index of refraction, n, is less than one in this dispersive medium and it is expressed rigorously in terms of ionospheric refractivity, N_I. Note that for the sign convention chosen, the ionospheric refractivity $N_I > 0$ and

$$n^2 = 1 - 2 N_I. \tag{7-35}$$

Since the difference from unity is small, to first order in refractivity N_I, n can be written analogous to the tropospheric form as

$$n = 1 - N_I. \tag{7-36}$$

The refractivity depends upon the electron density, N_e, (in electrons/m^3) and the radio signal frequency, ν, (in Hz) according to

$$N_I = \frac{40.3\, N_e}{\nu^2}. \tag{7-37}$$

The electron density profile for the ionosphere varies from a maximum value N_{em} at altitude h_m, decaying to zero very rapidly below and very slowly above. The exact shape of the profile and the values of N_{em} and h_m are highly variable functions of geographical location, time of day, season, and sunspot activity. If sufficient ionospheric sounding data are measured at a given location and time, a reasonably accurate construction can be made of the electron density profile. Generally, however, the data are insufficient for such an accurate construction. The NBS CRPL makes ionosonde measurements at a series of stations around the world. From these data, interpolated to the time and geographic location of interest, the values of N_{em} and h_m may be estimated.

The quantities N_{em} and h_m define only one point on the electron density versus altitude profile. The other points are assumed to lie on a modified Chapman profile in the form (Reference 5)

$$N_e = N_{em}\, e^{(1-z-e^{-z})} \tag{7-38}$$

where

$$z = \frac{h - h_m}{H_I} \tag{7-39}$$

$h \sim$ altitude

$H_I \sim$ the ionosphere scale height estimated from the NBS CRPL data.

It is generally conceded that the modified Chapman profile in Equation (7-38) does not represent the best possible normalized profile. The fixed ratio of the total electron content above the maximum point to that below tends to be too large, on the average, compared with the observed diurnal variation. However, the theoretical foundation upon which Chapman based the derivation (Reference 6) and the susceptibility of the function to treatment of refraction effects in closed analytic form (Reference 1) argue for continuance of its use. If one adopts the empirical point of view that the constants N_{em}, h_m, and H_I are refraction model parameters subject to adjustment (in a given pass over a given station) for best fit to the data, then a much more flexible approach is possible to determination of refraction effects (Reference 1). Such an estimation procedure for the more sophisticated (four parameter) model given by the unmodified Chapman profile is

$$N_e = N_{em}\, e^{(1-z-\gamma e^{-z})}. \tag{7-40}$$

The numerical multiplicative parameter γ can be varied to match the ratio of the total electron content above and below the maximum point to the true diurnal variation. At VHF where ionospheric effects are so large and so uncertain, this type of approach appears to be very attractive.

The modified Chapman profile in Equation (7-38) is assumed to be valid. Substituting this profile into Equation (7-37) gives

$$N_I = \frac{40.3\, N_{em}}{\nu^2}\, e^{(1-z-e^{-z})} \tag{7-41}$$

as the altitude variation of the ionospheric refractivity. As in the case of the tropospheric data, it is assumed that GSFC will receive ionospheric data from

NBS CRPL for the tracking stations desired. The preprocessor converts these data to values of N_{em}, h_m, and H_I as functions of time. Polynomial coefficients for interpolating the data are determined and stored in the data base to provide first estimates in the GTDS processor. Again, the basic NBS CRPL data are updated each month and give a three-month prediction.

7.3.3 Propagation Time Delay

There are two speeds associated with electromagnetic signal propagation through a medium of index of refraction, n,

$$c_p = \text{phase speed} = \frac{c}{n} \tag{7-42}$$

$$c_g = \text{group speed} = \frac{c}{n + \nu \dfrac{dn}{d\nu}} \tag{7-43}$$

where

$c \sim$ vacuum speed of light.

The former, c_p, is the speed associated with a phenomenon sensed by a phase measurement. The latter, c_g, is the speed associated with a measurement of the transmission time of an energy pulse. In a nondispersive medium, such as the troposphere, $dn/d\nu = 0$, by definition, therefore, the phase and group speeds are the same. The ionosphere, however is dispersive and the two speeds are different. Differentiating Equations (7-35) and (7-37) and substituting into Equation (7-43) shows that to first order in N_I

$$c_g = n\,c \cong (1 - N_I)\,c \approx \frac{c}{1 + N_I} \tag{7-44}$$

if a group-speed measurement is made. In form, this is identical to the expression for the tropospheric propagation speed; therefore, the time associated with the transmission of a signal over a path of length, L, may be written

$$\Delta t = \int_0^L \frac{dS}{c_g} = \frac{1}{c} \int_0^L (1 + N)\,dS \tag{7-45}$$

where

$N \sim$ the appropriate (tropospheric or ionospheric) refractivity

$d s \sim$ the increment of length along the signal propagation path.

The first term in Equation (7-45) represents the vacuum transmission time and the second term the additional delay, Δt, caused by the atmosphere. The evaluation of Equation (7-45), by substituting for the refractivities from Equations (7-34) and (7-41) yields the total atmospheric additional time delay for a one-way **transmission** to be

$$\Delta t = \frac{\csc E}{c} [Q + U - (P + V) \cot^2 E] \tag{7-46}$$

where

$$Q = \frac{40.3 N_{em} e H_I}{\nu^2} e^{-e^{-z}} \tag{7-47}$$

$$P = \frac{40.3 N_{em} e H_I}{\nu^2 r_S} \left\{ h[e^{-e^{-z}} - 1] - H_I \left[S(z) - S\left(-\frac{h_m}{H_I}\right) \right] \right\} \tag{7-48}$$

$$U = H_T N_S \tag{7-49}$$

$$V = \frac{H_T^2 N_S}{r_S} \tag{7-50}$$

$E \sim$ the **elevation** angle of the relative position vector from tracking station to spacecraft

$h \sim$ the spacecraft altitude

$r_S \sim$ the tracking station radius from center of earth

$\nu \sim$ the frequency of signal transmission in (MHz)

$$S(z) = e^{-z} - \frac{e^{-2z}}{2 \cdot 2!} + \frac{e^{-3z}}{3 \cdot 3!} - \frac{e^{-4z}}{4 \cdot 4!} + \ldots . \qquad (7\text{-}51)$$

where

$$z = \frac{h - h_m}{H_I}.$$

7.3.4 Ray Angular Deflection

Bouguer's formula, the analogue to Snell's Law for a spherically stratified medium, gives

$$n\, r \sin i = \text{constant} \qquad (7\text{-}52)$$

along any ray through the medium. Here i is the local incidence angle between the ray and the radius vector of magnitude, r. Substituting $r_s + h$ for r in this formula and evaluating at two points on a ray yields a relation for the two incidences as functions of the altitudes and indices of refraction

$$\frac{\sin i_0}{\sin i} = \frac{n}{n_0} \left(\frac{r_s + h}{r_s + h_0} \right) \qquad (7\text{-}53)$$

If the initial point is taken at the tracking station, the apparent elevation angle of the ray is E_a (see Figure 2-3). The initial point yields

$$h_0 = 0 \qquad (7\text{-}54)$$

$$n_0 = 1 + N_s \qquad (7\text{-}55)$$

$$\sin i_0 = \cos E_a. \qquad (7\text{-}56)$$

Substituting equations (7-54) to (7-56) into (7-53) yields

$$\cos E_a = \frac{n\,(r_s + h)}{(1 + N_s)\, r_s} \sin i. \tag{7-57}$$

Knowing i (a priori) at the spacecraft position, then Equation (7-57) enables computation of the apparent elevation angle at the ground station. But i is not known and Equation (7-57) must be modified to reformulate the desired solution in terms of quantities which are known. Reference 1 presents the details involving an approximation to an integration along the ray. The final result is

$$\cos E_a = \frac{\cos E}{(1 + N_s)\,(1 + I)} \tag{7-58}$$

where

$$I = \frac{\cot E}{r_s\, \delta} \left[Q - U - (P - V)\,(2 + \cot^2 E)\right] \tag{7-59}$$

$$\delta = \cos^{-1}\left(\frac{r_s \cos E}{r_s + h}\right) - E. \tag{7-60}$$

7.3.5 Effect on Doppler Shift

The frequency, ν, of an electromagnetic signal is constant, regardless of the medium through which it is propagating. The phase propagation speed, c_p, and the wavelength, λ, change precisely in the same way to keep ν constant.

$$\nu = \frac{c_{P_0}}{\lambda_0} = \frac{c_p}{\lambda} = \text{constant}. \tag{7-61}$$

As a result of Equation (7-61), and since a Doppler measurement is a comparison of signal frequencies, it follows that the refractive aberration due to the presence of the atmosphere must be purely geometrical. Because the true propagation path is deflected from the straight relative position vector, the projection of the velocity vector, defining the relative range-rate, is different by the amount of this deflection. As long as the one-dimensional wave motion traverses the same propagation path (a geodesic), it makes no difference in the frequency whether the atmosphere is there or not.

Although the argument presented here is heuristic, the fundamental concepts may be used to construct a rigorous proof. Results excerpted from Reference 1 are applied to the two modes of data processing (metric and polynomial) described earlier. Since the measurement data for the metric mode are converted in the preprocessor to estimates of instantaneous range-rate, the refraction effect, computed in the GTDS processor, is also represented as an instantaneous range-rate correction.

$$\Delta \dot{\rho} = \frac{\dot{E}\, r_S\, (I - N_I) \cot E}{\left[\frac{r_S}{h}\left(\frac{r_S}{h} \sin^2 E + 2\right) + 1\right]^{1/2}} \tag{7-62}$$

The ionospheric refractivity N_I in this equation is obtained from Equation (7-41) at the spacecraft altitude h. The quantity, $\dot{E}$, represents the time rate of change of the elevation angle, E.

The computation of the Doppler refraction effect in the polynomial mode involves the uplink and downlink unit vectors $\bar{u}$ and $\bar{d}$. These vectors are computed from Equations (7-94) as functions of the station positions at times of signal transmission and signal reception, $\bar{r}_T\ (t_T)$ and $\bar{r}_S\ (t_S)$ respectively, and the spacecraftposition at time of signal reception, $\bar{r}_V\ (t_V)$. The paths $\bar{u}$ and $\bar{d}$ correspond to vacuum conditions and must be corrected for atmospheric effects by means of Equations (7-102) which require the correction vector $\Delta \bar{u}_S$, $\Delta \bar{d}_S$, $\Delta \bar{u}_V$ and $\Delta \bar{d}_V$. These correction vectors are computed from the following algorithm

$$\Delta \bar{\gamma} = (\bar{\alpha} \times \bar{\beta}) \times (A\bar{\alpha} - B\bar{\beta}) \tag{7-63}$$

which is used with the values of $\bar{\alpha}$, $\bar{\beta}$, A, and B as shown in the following table to determine $\Delta \bar{u}_T, \ldots, \Delta \bar{d}_S$.

The quantities in the table are defined as follows:

$$P_{u,d} = \frac{r_s \cos E_{u,d}}{r_s + h} \qquad (r_s = r_S \text{ or } r_T) \tag{7-64}$$

$\Delta\bar{\gamma}$	$\bar{\alpha}$	$\bar{\beta}$	A	B
$\Delta\bar{u}_T$	$\bar{u}$	$\dfrac{\bar{r}_T(t_T)}{r_T}$	$-\dfrac{N_S(t_T)+I_u}{2}$	$-A\csc E_u$
$\Delta\bar{d}_S$	$\bar{d}$	$\dfrac{\bar{r}_S(t_S)}{r_S}$	$-\dfrac{N_S(t_S)+I_d}{2}$	$-A\csc E_d$
$\Delta\bar{u}_V$	$\bar{u}$	$\dfrac{\bar{r}_V(t_V)}{r_V}$	$B\left\{\dfrac{1-P_u^2[1+N_I(t_V)-I_u]}{(1+P_u^2)^{1/2}}\right\}$	$\dfrac{1}{(\bar{\alpha}\times\bar{\beta})\cdot(\bar{\alpha}\times\bar{\beta})}$
$\Delta\bar{d}_V$	$\bar{d}$	$\dfrac{\bar{r}_V(t_V)}{r_V}$	$B\left\{\dfrac{1-P_d^2[1+N_I(t_V)-I_d]}{(1-P_d^2)^{1/2}}\right\}$	$\dfrac{1}{(\bar{\alpha}\times\bar{\beta})\cdot(\bar{\alpha}\times\bar{\beta})}$

$E_{u,d}$ ~ the uplink and downlink vacuum elevation angles

$I_{u,d}$ ~ the integral given by Equation (7-59), evaluated for uplink and downlink paths

$\bar{u}$ ~ the unit vector pointing up along vacuum uplink path

$$\bar{u} = \frac{\bar{r}_V(t_V) - \bar{r}_T(t_T)}{|\bar{r}_V - \bar{r}_T|} \tag{7-65}$$

$\bar{d}$ ~ the unit vector pointing down along the vacuum downlink path

$$\bar{d} = \frac{\bar{r}_S(t_S) - \bar{r}_V(t_V)}{|\bar{r}_S - \bar{r}_V|} . \tag{7-66}$$

7.4 OPTION A (METRIC) PROCESSING PROCEDURES

The processing procedures described in this section assume that the data have been preprocessed as described in Section 2.2.1. In particular, simplifying assumptions were made in the preprocessor to convert the measurement data into components of the instantaneous relative state vector, except for the Minitrack data and Doppler data in range-difference form. This greatly simplifies the data processing in the GTDS.

As noted earlier, the preprocessed data are stored in the permanent data base with time tags in UTC. When these data are retrieved from the permanent data base and put into a working file in the GTDS, certain one-time only computations are performed. One of these, common to all data types, is the conversion of the time tags from UTC to A1 according to the transformation given in Chapter 3. Another, also common to all data types, is the retrieval of tropospheric and ionospheric refraction data. In Sections 7.3.1 and 7.3.2, descriptions were given of the method for representing the time dependence of the parameters N_S, H_T, N_{em}, h_m, and H_I, for a given station, by polynomial interpolating coefficients. To minimize the amount of data to be stored in the GTDS working files, the polynomial coefficients are transferred, rather than interpolated parameter values for each data point. The number of coefficients is greater than the five parameters required per point; but the same coefficients can apply for a large number of points.

As described in Section 7.2, the spacecraft position and/or velocity at the observation time is transformed to the tracking station local tangent coordinate system. The instantaneous relative position and velocity, so obtained, is then transformed to the ideal (vacuum) observations.

Section 7.3 describes how the functions P, Q, U, and V are common to atmosphere corrections for all types of observations described. The functions P and Q are related to the ionosphere, and U and V are related to the troposphere. Their definitions are given in conjunction with Equation (7-46). Note that explicit calculation of E by Equation (7-14) is not required to compute P, Q, U, and V, and only sin E and cos E are required for the range correction. Elevation angle and range-rate data, however, do require E and two additional functions δ and I, defined in conjunction with Equation (7-58) in Section 7.3.4. All quantities, P, Q, U, V, δ and I, depend on the spacecraft altitude.

7.4.1 GRARR VHF Data

7.4.1.1 Gimbal Angles X, Y

From the instantaneous station relative position of the spacecraft at time $t + \delta t$, the GTDS computes the vacuum azimuth and elevation angles by means of Equations (7-13) and (7-14). The quantities P, Q, U, V, δ, and I are calculated. Equation (7-58) is then solved explicitly for the desired apparent elevation angle as follows

$$E_a = \cos^{-1}\left[\frac{\cos E}{(1 + N_S)(1 + I)}\right] \qquad 0 \le E_a \le \frac{\pi}{2} \tag{7-67}$$

Equation (7-67) can be simplified under the assumption that N_S and I are small compared with unity. Neglecting second- and higher-order terms in these quantities, Equation (7-67) becomes

$$E_a = \cos^{-1}\left[(1 - N_S - I)\cos E\right]. \tag{7-68}$$

The advantage of this form lies in the simple combination of the two contributions to the refraction correction into a single term $N_S + I$. This quantity may then be stored from one iteration to the next. In the event that the combined correction is small and does not change much with successive iterations, it is not necessary to recompute it each time. Updating of the correction could be done every n^{th} iteration, where n is specified.

The gimbal angles, X_c and Y_c are computed as functions of A and E_a as follows:

$$X_c = \tan^{-1}(\sin A \cot E_a) + b_X$$

and (7-69)

$$Y_c = \sin^{-1}(\cos A \cos E_a) + b_Y$$

where b_X and b_Y are constant biases.

7.4.1.2 Range

The range observation is modeled in the GTDS as

$$\rho_c = \rho + \Delta\rho + b_\rho \tag{7-70}$$

where

$$\Delta\rho = \csc E\,[Q + U - (P + V)\cot^2 E] \tag{7-71}$$

and b_ρ is the range bias which is station dependent.

The ideal range, ρ, is calculated from Equation (7-8) and the atmosphere effect $\Delta\rho$ from Equation (7-71) and Equations (7-46) through (7-51). This computed observation is compared with the preprocessed data given by Equation (2-9). Similar to the procedure suggested for the angle data, the additive correction term $\Delta\rho$ may be separately stored for use in subsequent iterations if desired.

7.4.1.3 Range-Rate

The range-rate computed observation, to be compared with data preprocessed according to Equation (2-13) is

$$\dot{\rho}_c = \dot{\rho} + \Delta\dot{\rho} + b_{\dot{\rho}} \tag{7-72}$$

where ρ is computed by Equation (7-9); $\Delta\dot{\rho}$, the separately stored atmospheric refraction effect, is given by Equation (7-62); and $b_{\dot{\rho}}$ is a station dependent range-rate bias. The elevation angle rate, $\dot{E}$, in Equation (7-62) is computed by differentiating the cofunction

$$E = \sin^{-1}\left(\frac{z_{1t}}{\rho}\right) \tag{7-73}$$

yielding

$$\dot{E} = \frac{\dot{z}_{1t} - \sin E\left(\frac{\dot{\bar{r}}_{1t}}{r_{1t}} \cdot \dot{\bar{r}}_{1t}\right)}{r_{1t}\cos E}. \tag{7-74}$$

If the data are preprocessed for greater accuracy, according to the range difference formula, Equation (2-14), then the computed observation is determined from the range-difference formula in Equation (2-15). This, in contradistinction with the other metric data procedures, requires iterative solution of the uplink and downlink light paths which terminate at the tracking station at the two times, t_s and $t_s + \Delta t_{RR}$.

7.4.2 C-Band Radar Data

The C-band range and angle data are modeled precisely the same as the corresponding data for the GRARR system. Therefore, Equations (7-12) through

(7-14), and (7-67), (7-68), and (7-70) are applicable, with the refraction functions computed with appropriate station atmospheric data and radar frequency.

7.4.3 Minitrack Data

The derivation of the equation for the Minitrack observation requires that we reconsider the fine phase data, a_F, after ambiguity resolution and after all corrections have been applied. Denote the azimuth and apparent elevation angles of the signal path at the station by A and E_a, respectively. The definitions are the same as those given by Equations (7-13), (7-14) and (7-67). The actual direction cosines of this signal path relative to the E-W and N-S baselines, respectively, are

$$\begin{aligned} \ell_a &= \cos E_a \sin A \\ m_a &= \cos E_a \cos A \end{aligned} \qquad (7\text{-}75)$$

Therefore, the Minitrack fine phase reading may be expressed as

$$\bar{a}_F = \left(\frac{B_F}{\lambda_S} \cos E_a\right) F \qquad (7\text{-}76)$$

where

$F = \begin{Bmatrix} \sin A \\ \cos A \end{Bmatrix}$, when a_F is the phase difference along the $\begin{Bmatrix} \text{E-W} \\ \text{N-S} \end{Bmatrix}$ baseline

$B_F \sim$ the baseline length in metric units

$\lambda_S \sim$ the wavelength (in meters) of the radio signal as received at the tracking station.

So long as the relative motion between the spacecraft and station remains uniform, the transmission frequency is constant along a propagation path. The relationship between the wavelength and the index of refraction is obtained by combining Equations (7-42) and (7-61)

$$\nu = \frac{c_p}{\lambda} = \frac{c}{n\lambda} \tag{7-77}$$

where c, as defined earlier, is the vacuum speed of light. Denoting the frequency apparent to the spacecraft by ν_v, the wavelength-index of refraction relationship is

$$\nu_v = \frac{c}{n_v \lambda_v} = \frac{c}{\lambda_{v_0}}. \tag{7-78}$$

Similarly, denoting the frequency as seen by the tracking station by ν_s, we have

$$\nu_s = \frac{c}{n_s \lambda_s}. \tag{7-79}$$

The two frequencies, ν_v and ν_s differ by virtue of the relative motion between spacecraft and tracking station. This effect will be considered later. Dividing Equation (7-78) by Equation (7-79), solving explicitly for λ_s and substituting into Equation (7-76) yields

$$\bar{a}_F = \left[\frac{B_F}{\lambda_{v_0}}\left(\frac{\nu_s}{\nu_v}\right)(1 + N_s)\cos E_a\right] F \tag{7-80}$$

where Equation (7-33) was used to replace the index n_s by the surface refractivity, N_s.

As discussed in Sections 2.1.3 and 2.2.3, the spacecraft transmitter frequency may not correspond with the nominal 136-MHz value. Thus

$$\lambda_{v_0} = \lambda_{136}\frac{136}{\nu_v} \qquad (\nu_v \text{ in MHz}) \tag{7-81}$$

which, together with Equation (7-58), transforms Equation (7-80) to

$$\bar{a}'_F = \frac{B_F}{\lambda_{136}} \left(\frac{\nu_V}{136}\right)\left(\frac{\nu_S}{\nu_V}\right)\left(\frac{\cos E}{1 + I}\right)F. \tag{7-82}$$

Denoting the direction cosines of the relative position vector by ℓ and m, we have

$$\begin{aligned} \ell &= \cos\ E\ \sin\ A \\ m &= \cos\ E\ \cos\ A \end{aligned} \tag{7-83}$$

and noting that $B_F/\lambda_{136} = N_F$, the baseline length expressed in nominal vacuum wavelengths (46 or 57), Equation (2-37) leads to

$$\begin{aligned} \ell' &= \frac{\bar{a}_{F_{E-W}}}{N_{F_{E-W}}}\left(\frac{136}{\nu_V}\right) = \left(\frac{\nu_S}{\nu_V}\right)\frac{\ell}{1 + I} \\ m' &= \frac{\bar{a}_{F_{N-S}}}{N_{F_{N-S}}}\left(\frac{136}{\nu_V}\right) = \left(\frac{\nu_S}{\nu_V}\right)\frac{m}{1 + I}. \end{aligned} \tag{7-84}$$

The pseudo direction cosines ℓ' and m' are precisely the output quantities defined in Equation (2-37) for the Minitrack data preprocessor. The comment made in Chapter 2 that these would be the correct direction cosines for the case of no relative motion and no atmosphere becomes obvious upon inspection of the right sides of Equation (7-84). No relative motion would give $\nu_S/\nu_V = 1$ and no atmosphere would give I = 0.

For the sake of compatibility with the procedures for processing the other types of metric data, the computation of ℓ and m should be done in the local tangent coordinate system. As noted in Section 2.2.1, the use of straight relative position vectors in this coordinate system assumes no motion of the tracking station and, hence, neglects the apparent curvature of the light path. The light-time correction, therefore, requires that the relative position vector, $\bar{r}_{1t}$, be computed at a time Δt_p earlier than the observation time tag, t_s. We have

$$\bar{r}_{1t} = \bar{r}_{1t}\ (t_s - \Delta\ t_p) \tag{7-85}$$

where

$$\Delta t_p = \frac{r_{1t}(t_s - \Delta t_p)}{c} . \tag{7-86}$$

An iteration procedure is required to solve Equations (7-85) and (7-86) rigorously. This can be circumvented, however, by representing the range magnitude in terms of a first-order variation in time

$$r_{1t}(t_S + \Delta t_p) = r_{1t}(t_S) - \dot{r}_{1t}(t_S)\,\Delta t_p . \tag{7-87}$$

Substituting this approximation into Equation (7-86) and solving explicitly for the propagation time gives

$$\Delta t_p = \frac{\frac{r_{1t}(t_S)}{c}}{1 + \frac{\dot{r}_{1t}(t_s)}{c}} = \frac{\frac{r_{1t}(t_S)}{c}}{1 + \frac{\bar{r}_{1t}(t_S)}{r_{1t}(t_S)} \cdot \frac{\dot{\bar{r}}_{1t}(t_S)}{c}} . \tag{7-88}$$

Therefore, the procedure requires the determination of the relative state at the desired observation time, t_S. Equation (7-88) gives the light time, correct to first order in $\dot{r}_{1t}/c$, and the equations of motion can then be solved for the relative state at the corrected time $t_S - \Delta t_p$. The direction cosines required for Equation (7-84) are then computed by

$$\ell = \frac{x_{1t}(t_S - \Delta t_p)}{r_{1t}(t_S - \Delta t_p)}$$

$$m = \frac{y_{1t}(t_S - \Delta t_p)}{r_{1t}(t_S - \Delta t_p)} . \tag{7-89}$$

The significance of the Doppler effect in calculating (ν_S/ν_V) in Equation (7-84) will now be considered. The special relativistic one-way Doppler-shifted frequency ratio is given by Equation (A-8) in Appendix A. Considering the station velocity to be zero and $\dot{\bar{r}}_{1t}$ to be the spacecraft's instantaneous relative velocity, Equation (A-8) becomes

$$\left(\frac{\nu_S}{\nu_V}\right) = \sqrt{1 - \frac{\dot{\bar{r}}_{1t} \cdot \dot{\bar{r}}_{1t}}{c^2}} \left[1 + \frac{\bar{r}_{1t}}{r_{1t}} \cdot \frac{\dot{\bar{r}}_{1t}}{c}\right] \approx 1 + \frac{\bar{r}_{1t}}{r_{1t}} \cdot \frac{\dot{\bar{r}}_{1t}}{c} - \frac{1}{2} \frac{\dot{\bar{r}}_{1t} \cdot \dot{\bar{r}}_{1t}}{c^2} \qquad (7\text{-}90)$$

where the term on the right includes only terms up to second order. Substituting Equations (7-89) and (7-90) into (7-84) and retaining only first-order terms in I and $\dot{\bar{r}}$ (the second-order term in $\dot{\bar{r}}_{1t}$ is assumed to be negligible) yields the calculated observation equation

$$\ell' = \frac{x_{1t}}{r_{1t}} \left(1 + \frac{\bar{r}_{1t}}{r_{1t}} \cdot \frac{\dot{\bar{r}}_{1t}}{c} - I\right) + b_\ell$$

$$m' = \frac{y_{1t}}{r_{1t}} \left(1 + \frac{\bar{r}_{1t}}{r_{1t}} \cdot \frac{\dot{\bar{r}}_{1t}}{c} - I\right) + b_m \qquad (7\text{-}91)$$

where b_ℓ and b_m are biases in the pseudo direction cosine observations. The second term in the parentheses is the first-order Doppler term.

7.5 OPTION B (POLYNOMIAL) PROCESSING CONCEPTS

The one-time conversion of the data time tags from UTC in the permanent data base to A1 in the working file is the same for the polynomial mode processor as for the metric data processor (see Section 7.4). The retrieval and storage of refraction correction data is likewise the same.

The metric data observation modeling is done in the local tangent coordinate system whereas the polynomial mode models the observables directly in the inertial coordinate system of the trajectory computation. There are two principal reasons for this:

1. The vacuum light paths may be assumed as straight lines in the inertial system with a higher degree of accuracy (see Section 2.2.1 and Figure 2-3).

2. Doppler effects in GRARR and Minitrack data may be modeled accurately in an inertial system only (see Section 2.2.1 or Reference 7).

The polynomial mode of data processing does not model observations at the precise times of the actual data measurements. Instead, the scalar quantity, corresponding to the same physical quantity actually measured, is computed at a sequence of conveniently chosen pseudo data times which span the actual data points. A polynomial in time is fitted to these pseudo points and the scalar measurements are then interpolated from this polynomial at the true measurement times.

The polynomial interpolation of the computed observation is the corollary of the smoothing and compacting procedures hitherto used in metric data preprocessing. Polynomials fit to the actual data, however, must be done regressively (i.e., least-squares) because of the random noise content in the data. Polynomials fit to the pseudo observation can be performed by classical deterministic interpolation techniques such as Newton's formula, Aitken's repeated process, etc., because of the lack of random noise in the pseudo data points. In GTDS, the Cowell numerical integration procedure provides a natural means for accomplishing the interpolation insofar as the state is concerned. The integrator stores polynomial coefficients for the spacecraft acceleration at the latest 11-time points. From the coefficients, interpolation formulas permit the accurate determination of the spacecraft state anywhere within the 11-point time arc.

For such an integrator mechanization, the polynomial mode of observation modeling may be implemented as follows. Assume that the first unprocessed observation in the working file has a time tag later than the latest integrator time point. The integrator is called to propagate the trajectory forward in time until this observation time is contained within the interval between the two earliest time points of the integrator span.

The integrator time span is divided into m - 1 equal parts and the spacecraft state is interpolated at the m points as defined. The value of m should be made as small as possible, consistent with the desired accuracy. Keeping the vehicle state fixed at each of these m points, the light path geometry appropriate to the type of observation is computed relative to the tracking station. This requires an iteration scheme since the tracking station location must be determined earlier and/or later in time to allow for the propagation time delay. A scheme similar to the one described in Section 7.4.3, Equation (7-88) is used to obtain a first estimate of the light time to start the iteration process.

Instead of rigorously modeling the atmospheric error correction terms due to propagation speed variations and ray path bending into the iterative procedure, only the basic observation in terms of straight line propagation at constant speed in a vacuum is included. The refraction effects are estimated separately after the converged iteration and provide additive corrections to the vacuum observations.

These pseudo observations and their associated refraction effects are fitted separately by polynomials in the computed ground receive times (not the spacecraft times at the m points). This is done for compatibility with the ground reception time tags of the actual data. The polynomial coefficients are stored temporarily to permit the interpolation of computed vacuum observations and the corresponding refraction effects at the desired actual data times. The interpolated refraction effects are added to the computed vacuum observations then stored separately with the actual observations in the working file. Since these refraction effects generally are quite insensitive to small variations in the orbit from one differential correction iteration to the next, the option is provided to retrieve previously computed values on subsequent iterations if desired.

After the foregoing procedure establishes the polynomial coefficients for the specific observation type over the integrator time span, the observation is computed by interpolation at the desired actual time and the next observation is read from the working file. If the time tag lies outside the integrator span, the orbit generator (integrator) is called. The entire procedure described above is repeated, advancing the trajectory, until the integrator time span contains the new observation time tag. However, if the next observation does lie within the integrator arc, there is no need to call the orbit generator. The observation type and station are ascertained and, if polynomial coefficients are available, the computed observation and its associated refraction effect are obtained by simple interpolation at the desired time. If the observation type or tracking station is different, new polynomial coefficients must be determined and placed in temporary storage. The computed observation is then interpolated as described previously.

The procedure described above is very inefficient in terms of the m pseudo observations required for the first actual data point. However, observation data of a given type generally are distributed in dense clusters over the tracking station locations. In this situation, a single integration time arc is expected to include not just one but a large number of actual observations. If this number is much larger than m, a significant computational advantage may be gained by calculating only m pseudo observations and then simply evaluating the fitted polynomial many times to retrieve the modeled scalar data at the desired times.

In the event it is known a priori that the data are sparse, an option will be provided to handle each observation separately. To implement this option exactly the same procedure described above is used but with only 3 or 4 pseudo observation points which straddle the observation time. The desired point is interpolated as before.

The following paragraphs describe the methods for modeling the various types of tracking observations and their associated refraction effects.

7.5.1 GRARR DATA

The geometry to be modeled for all GRARR data consists of the uplink and downlink propagation paths. Although only the downlink path is required for the angle data, the probability is very high that these data are closely followed and/or preceded by range and/or range-rate data. In addition, angle data generally are of such poor quality that they are used only in early orbit estimations. Once a good estimate is obtained, the angle data are generally discarded. Therefore, some slight inefficiency in angle data modeling is permissible – especially if the model, so obtained, is directly usable for the range and range-rate data.

If the spacecraft position at one of the m positions across the integrator span is denoted by $\bar{r}_V(t_V)$, the tracking station transmit and receive positions denoted by $\bar{r}_T(t_T)$ and $\bar{r}_S(t_S)$, respectively, then t_S and t_T are iteratively adjusted so that

$$\frac{|\bar{r}_V(t_V) - \bar{r}_S(t_S)|}{c} = t_S - t_V$$

$$\frac{|\bar{r}_T(t_T) - \bar{r}_V(t_V)|}{c} = t_V - t_T \qquad (7\text{-}92)$$

The inertial orientations of the earth at times t_T and t_S are given by the ephemeris. Knowledge of the geographic location of the tracking station on the earth permits the direct determinations of the positions $\bar{r}_T(t_T)$ and $\bar{r}_S(t_S)$, of the station, in the inertial coordinates at the two times. As noted earlier, the first estimates of t_T and t_S may be computed as

$$t_S = t_V + \Delta t_p$$

$$t_T = t_V - \Delta t_p \qquad (7\text{-}93)$$

where Δt_p is obtained from Equation (7-88), evaluated at the time t_V. The $\bar{r}$ and $\dot{\bar{r}}$ in that equation are the spacecraft state relative to the station.

Once the iteration procedure has converged (t_T and t_S values are such that Equations (7-92) are satisfied), the tracking station inertial states $\bar{r}_T(t_T)$, $\dot{\bar{r}}_T(t_T)$, $\bar{r}_S(t_S)$, and $\dot{\bar{r}}_S(t_S)$ are determined. The unit vectors i = east, j = north, and k = up, defining the station local tangent coordinate frame are transformed from the earth-fixed local tangent system to the inertial coordinate system at the two times t_T and t_S given by

$$\bar{i}_T,\ \bar{j}_T,\ \bar{k}_T \quad \text{and} \quad \bar{i}_S,\ \bar{j}_S,\ \bar{k}_S.$$

The uplink and downlink vacuum light-path directions are determined as

$$\bar{u} = \frac{\bar{r}_V(t_V) - \bar{r}_T(t_T)}{|\bar{r}_V(t_V) - \bar{r}_T(t_T)|}$$

$$\bar{d} = \frac{\bar{r}_S(t_S) - \bar{r}_V(t_V)}{|\bar{r}_S(t_S) - \bar{r}_V(t_V)|}. \tag{7-94}$$

The sines of the vacuum elevation angles of the two paths are

$$\sin E_u = \bar{k}_T \cdot \bar{u}$$

$$\sin E_d = -\bar{k}_S \cdot \bar{d} \tag{7-95}$$

and the angles are

$$E_u = \sin^{-1}(\bar{k}_T \cdot \bar{u}) \qquad 0 \le E_u \le \frac{\pi}{2}$$

$$E_d = \sin^{-1}(-\bar{k}_S \cdot \bar{d}) \qquad 0 \le E_d \le \frac{\pi}{2}. \tag{7-96}$$

The apparent elevation angle, E_a, for the downlink path is next computed by Equation (7-68) where the cos E_a utilized is obtained by means of Equation (7-95), that is

$$\cos E_d = [1 - \sin^2 E_d]^{1/2}$$
$$= [1 + (\bar{k}_S \cdot \bar{d}^2)]^{1/2} \qquad (7\text{-}97)$$

The spacecraft altitude above the geoid, used for calculating I in Equation (7-68), is determined at the turnaround time t_V (at the integrator point m). As noted in the discussion of Equation (7-68), the refraction effect $N_S + I$ is stored for possible use in future iterations.

The azimuth angle, A, is not corrected for refraction since the atmosphere is assumed to be spherically symmetric. Therefore,

$$A = \cos^{-1}\left(\frac{-\bar{j}_S \cdot \bar{d}}{\cos E_d}\right)$$
$$A = \sin^{-1}\left(\frac{-\bar{i}_S \cdot \bar{d}}{\cos E_d}\right) \qquad 0 \le A \le 2\pi. \qquad (7\text{-}98)$$

The time tag to be associated with A and E_a angle data is

$$t_A = t_S + \Delta t_d \qquad (7\text{-}99)$$

where Δt_d is computed by Equation (7-46) for the downlink leg.

The computed round-trip time-delay observation is given by

$$\Delta t_R = t_S - t_T + (\Delta t_u + \Delta t_d) \qquad (7\text{-}100)$$

where Δt_u and Δt_d are computed by Equation (7-46) for the uplink and downlink legs, respectively. The time tag, t_R, is the same as t_A for the angle data in Equation (7-99).

The angle and range data described above are determined for each of the m points across the integrator time arc. These data and the separate refraction corrections are fitted by polynomial functions of the computed observation time tags, (t_A and t_R). Computed observations may then be interpolated from these polynomials at desired times to compare with the actual data.

It is not possible to determine the computed Doppler-count observation data on the basis of the round-trip light path associated with a single pseudo point. Such a light path, however, does define the instantaneous Doppler frequency ratio (Reference 1, 7). The equation for the instantaneous frequency ratio is

$$\frac{\nu_S}{\nu_T} = \sqrt{\frac{1 - \frac{\dot{\bar{r}}_T \cdot \dot{\bar{r}}_T}{c^2}}{1 - \frac{\dot{\bar{r}}_S \cdot \dot{\bar{r}}_S}{c^2}}} \left[\frac{1 - \frac{\bar{u}_V \cdot \bar{r}_V}{c}}{1 - \frac{\bar{u}_T \cdot \bar{r}_T}{c}}\right] \left[\frac{1 - \frac{\bar{d}_S \cdot \bar{r}_S}{c}}{1 - \frac{\bar{d}_V \cdot \bar{r}_V}{c}}\right] \tag{7-101}$$

where

$$\begin{aligned} \bar{u}_V &= \bar{u} + \Delta \bar{u}_V \\ \bar{u}_T &= \bar{u} + \Delta \bar{u}_T \\ \bar{d}_S &= \bar{d} + \Delta \bar{d}_S \\ \bar{d}_V &= \bar{d} + \Delta \bar{d}_V \end{aligned} \tag{7-102}$$

The $\bar{u}$ and $\bar{d}$ terms, with and without subscripts, in the preceding equations, are the uplink and downlink unit vectors. The vacuum light path quantities $\bar{u}$ and $\bar{d}$ (unsubscripted) are computed by Equation (7-94). The Δ terms describe the atmospheric corrections to the straight-line vacuum paths and are computed by the algorithm given in Equation (7-63). Note that the vectors defined

in Equation (7-63) for the dummy variable $\overline{\beta}$ are all referred to the center of the earth (i.e., $\overline{\beta}$ is intended to be the local vertical unit vector at one of the three positions $\overline{r}_T(t_T)$, $\overline{r}_V(t_V)$, or $\overline{r}_S(t_S)$.

The accumulated Doppler count is

$$N_d = \nu_T (T - \Delta t_{RR}) \tag{7-103}$$

where

$$T = \int_{t_S}^{t_S + \Delta t_{RR}} \frac{\nu_S}{\nu_T} d\tau. \tag{7-104}$$

In this equation t_S is the actual time-tag and Δt_{RR} is the count time increment given by Equation (2-4). The procedure, therefore, is to fit the instantaneous quantities ν_S/ν_T (as computed by Equation (7-101) for each of the m points) with a polynomial in the ground receive time t_S. This time tag, t_S, is not corrected for the downlink propagation delays as were the angle and range time tags since the correction in Equation (7-46) is valid only for group speed measurements. The Doppler measurement, of course, involves a phase measurement. The correct delay expression could easily be obtained, but it is not necessary. The integral T is most sensitive to Δt_{RR}. Slight errors in t_S merely shift both limits the same. The integral is computed from the fitted polynomial. The form of Equation (7-104) is modified slightly to accommodate the desire to separate the refraction effect and the vacuum effect. Let

$$T = T_0 + \Delta T_R \tag{7-105}$$

where

$$T_0 = \int_{t_S}^{t_S + \Delta t_{RR}} \left(\frac{\nu_S}{\nu_T}\right)_{vac} d\tau$$

and (7-106)

$$\Delta T_R = \int_{t_S}^{t_S + \Delta t_{RR}} \left[\frac{\nu_S}{\nu_T} - \left(\frac{\nu_S}{\nu_T}\right)_{vac}\right] d\tau.$$

In these expressions, (ν_S/ν_T) is computed by setting the Δ terms to zero in Equation (7-102) and then evaluating Equation (7-101). Again, the separate terms are individually fitted and interpolated to obtain the total integral T. The refraction effect, ΔT_R, is stored with the data, as indicated earlier, for possible use in future iterations.

Note that the polynomials may be formally integrated and the integrals computed by evaluating the analytic forms at the upper and lower limits and differencing. In this respect, the procedure is akin to the range difference formula.

7.5.2 C-Band

The observation modeling and the equations for processing the data within the GTDS are precisely the same for the C-Band radar data as for the GRARR angle and range data, described in Section 7.5.1.

7.5.3 Minitrack

The Minitrack interferometer observation involves only the downlink transmission from the spacecraft to the receiver at the tracking station. Accordingly, the geometry is modeled as this one-way propagation. The iteration procedure for solving the tracking station position, $\bar{r}_S\ (t_S)$, corresponding to the spacecraft, $\bar{r}_V\ (t_V)$, at one of the m points on the integrator time span, is similar to that described in Section 7.5.1 for the GRARR modeling. The difference is that only the downlink leg is required for the Minitrack observation modeling. Therefore, the applicable equations are Equations (7-92a), (7-93a), (7-94b), (7-95b), and (7-97).

Equations (7-84) for modeling Minitrack observations were derived rigorously in Section 7.4.3. Since the interest there was for the metric mode of data processing the equations finally used to compute observations (Equation (7-91)) represented certain simplifications of the rigorous forms of Equations (7-84).

The special relativistic equation for the one-way Doppler-shifted frequency ratio is (References 1, 7).

$$\frac{\nu_S}{\nu_V} = \sqrt{\frac{1 - \dfrac{\dot{\bar{r}}_V \cdot \dot{\bar{r}}_V}{c^2}}{1 - \dfrac{\dot{\bar{r}}_S \cdot \dot{\bar{r}}_S}{c^2}}} \left[\frac{1 - \dfrac{\bar{d}_S \cdot \dot{\bar{r}}_S}{c}}{1 - \dfrac{\bar{d}_V \cdot \dot{\bar{r}}_V}{c}} \right] \tag{7-107}$$

where $\bar{d}_S$ and $\bar{d}_V$ are unit vectors (see Equation (7-102)) along the actual propagation paths at the station and the vehicle, respectivel. Thus $\bar{d}_S$ and $\bar{d}_V$ include effects due to refraction.

For $\dot{\bar{r}}_V$ = 8000 meter/second, the second-order term involving the radical in Equation (7-107) contributes an angle error, $\Delta\xi$, in the arc cosine of ℓ' or m' in Equation (7-84) of

$$\cos(\xi + \Delta\xi) = \sqrt{1 - \left(\frac{8000}{3 \times 10^8}\right)^2} \cos\xi = (1 - .35 \times 10^{-9}) \cos\xi$$

For $\xi = 1°$

$$\Delta\xi = -7.2 \times 10^{-5} = 0''.004$$

hence the radical may be safely reduced to unity.

The equations that are used for the polynomial mode, therefore, are modified as follows (see Equation (7-84)).

$$\begin{aligned} \ell' &= M\,\ell \\ m' &= M\,m \end{aligned} \tag{7-108}$$

where

$$M = \left[\frac{1 - \dfrac{\bar{d}_S \cdot \dot{\bar{r}}_S}{c}}{1 - \dfrac{\bar{d}_V \cdot \dot{\bar{r}}_V}{c}} \right] \tag{7-109}$$

M includes the combined effects due to Doppler shift and refraction. Similar to the procedure adopted for the radar data, M is expressed as a deviation from unity

$$M = 1 - \Delta M \tag{7-110}$$

where

$$\Delta M = 1 - \left[\frac{1 - \frac{\bar{d}_S \cdot \dot{\bar{r}}_S}{c}}{1 - \frac{\bar{d}_V \cdot \dot{\bar{r}}_V}{c}}\right]\left(\frac{1}{1 + I}\right). \tag{7-111}$$

As before, ΔM, ℓ' and m' are computed at each of the m integrator span points. These data are then interpolated at the actual data times. The interpolated values of ΔM are stored with the actual data points so that the Doppler shift and refraction computations may be avoided on subsequent iterations if desired.

The ℓ and m values of Equations (7-108) are the direction cosines of the straight relative position vector from the tracking station to the spacecraft. They are computed simply as

$$\ell = -\bar{i}_S \cdot \bar{d}$$

$$m = -\bar{j}_S \cdot \bar{d}. \tag{7-112}$$

The unit vector $\bar{d}$ is given by Equation (7-94b) and i_S, j_S are the east- and north-local tangent unit vectors (at time t_S) transformed to the inertial frame.

7.6 ESTIMATION MODEL

The deviations between the actual observation and the predicted observation is modeled as a first-order Taylor series expansion around the predicted observation. This expansion relates deviations in the observation residuals to deviations in dynamic parameters, station location, observation biases, time

bias and establishes the required set of linear regression equations. The estimation model for any observable may then be written as

$$O_0 - O_c = \frac{\partial O_c}{\partial \bar{q}} \Delta \bar{q} + n \qquad (7\text{-}113)$$

where

$O_0 \sim$ the actual observation with time tag, t

$O_c \sim$ the predicted observation based on a previous estimate of the parameter vector, $\bar{q}$

$\Delta \bar{q} \sim$ the correction to the parameter vector, $\bar{q}$

$n \sim$ the observation noise.

The parameter vector, $\bar{q}$, may consist of dynamic parameters, $\bar{p}$, (those parameters involved in the equations of motion); station locations, $\bar{r}_s$; observation biases, b; and observation time biases, δt. The total parameter vector may then be written as

$$\bar{q} = \begin{bmatrix} \bar{p} \\ \bar{r}_s \\ b \\ \delta t \end{bmatrix}. \qquad (7\text{-}114)$$

The modeled observation can be written functionally as

$$O_c = f(\bar{q}, t) = f(\bar{p}, \bar{r}_s, b, \delta t, t) \qquad (7\text{-}115)$$

Substituting the appropriate partial derivatives of Equation (7-115) into Equation (7-113) yields

$$O_0 - O_c = \left(\frac{\partial O_c}{\partial \bar{p}}\right) \Delta \bar{p} + \left(\frac{\partial O_c}{\partial \bar{r}_s}\right) \Delta \bar{r}_s + \left(\frac{\partial O_c}{\partial b}\right) \Delta b + \left(\frac{\partial O_c}{\partial (\delta t)}\right) \Delta (\delta t) + n \qquad (7\text{-}116)$$

which may be written in a more compact form as

$$O_0 - O_c = \left[\frac{\partial O_c}{\partial \bar{p}} \;\middle|\; \frac{\partial O_c}{\partial \bar{r}_s} \;\middle|\; \frac{\partial O_c}{\partial b} \;\middle|\; \frac{\partial O_c}{\partial (\delta t)}\right] \begin{bmatrix} \Delta \bar{p} \\ \Delta \bar{r}_s \\ \Delta b \\ \Delta (\delta t) \end{bmatrix} + n \qquad (7\text{-}117)$$

or

$$O_0 - O_c = F \Delta \bar{q} + n. \qquad (7\text{-}118)$$

Equation (7-118) defines the linear regression equations that are solved by the iterative weighted least-squares method described in Chapter 8. The formulation, as shown in Equation (7-118), describes m equations (for m observations) in p unknowns (the number of $\bar{q}$ parameters). The matrix F, in Equation (7-118) is of dimension (m × p). Chapter 8 derives the required solution to the normal equations in terms of F and the weighting matrix W under the assumption that W is a diagonal matrix, that is, the observations are uncorrelated. Under this assumption, the terms in the normal equations requiring F can be developed on an observation-by-observation basis thus yielding the solution of the normal equations but without explicitly forming the full (m × p) F matrix. This is a standard method for all existing least-squares orbit determination programs and is discussed in more detail in Chapter 8.

7.7 REFERENCES

1. Computer Sciences Corporation, Modeling of Atmospheric Refraction Effects Upon Spacecraft Tracking Observations from Earth, D. H. Novak, January 1971.

2. Goddard Space Flight Center, X-541-69-322, Description of the Goddard Range-Range Rate Data Processing Program for the CDC-160A, E. R. Watkins and D. H. Rose, August 1969.

3. Goddard Space Flight Center, X-571-69-149, Data Formats of the Goddard Range and Range Rate System and the Application Technological Satellite Range and Range Rate System, D. J. Zillig, April 1969.

4. Goddard Space Flight Center, X-514-70-55, GEOS Satellite Tracking Corrections for Refraction in the Troposphere, J. H. Berbert and H. C. Parker, February 1970.

5. Goddard Space Flight Center, NAS 5-9782, Final Report on Ionospheric Correction to Tracking Parameters, J. J. Freeman, 3 November 1965.

6. National Bureau of Standards, Monograph 80, Ionospheric Radio Propagation, K. Davies, 1 April 1965.

7. Computer Sciences Corporation, Mathematical Modeling of Radar Tracking Observations of Spacecraft, D. H. Novak, January 1971.

CHAPTER 8

ESTIMATION

The basic orbit estimation problem, as outlined in this chapter, involves solving for values of a set of parameters from an observational model so as to minimize, in the sense of weighted least-squares, the differences between a computed and an observed trajectory. The observation model is described in Chapter 7. The model parameters include the trajectory of the vehicle (and thus the initial conditions and differential equation parameters), the locations of the observing stations, and the bias errors in their instruments or their clocks (that may vary as a function of the pass over a station). In practice, one determines values for only a selected subset of the model parameters.

Since the observations made by a tracking system are imperfect, no trajectory fits these observations exactly. Therefore, at best only an estimate of the actual trajectory may be obtained from the data. As indicated above, GTDS uses a weighted least-squares estimation process. This estimator is derived in detail in Section 8.2. For a theoretical discussion of least squares estimation, see Appendix B. Supplemental material is also available in References 1 through 5.

8.1 DESCRIPTION OF PROBLEM

Let a set of m observations, denoted by an m-dimensional vector $\bar{y}$, be given. These observations are assumed to be equal to a known-vector function $\bar{f}$ of a set of p parameters, denoted by a p-dimensional vector $\bar{x}$ plus additive random noise, denoted by a vector $\bar{n}$

$$\bar{y} = \bar{f}(\bar{x}) + \bar{n}. \tag{8-1}$$

The above equation is called a nonlinear regression equation. The trajectory determination problem is to estimate $\bar{x}$, given $\bar{y}$, the functional form of $\bar{f}$, and the statistical properties of $\bar{n}$.

The estimation process attempts to estimate a value for $\bar{x}$ that minimizes the sum of the squares of weighted observation residuals, $[\bar{y} - \bar{f}(\bar{x})]$, between

the actual observations and the observations computed using the mathematical model. More precisely

$$Q(\bar{x}) = [\bar{y} - \bar{f}(\bar{x})]^T W [\bar{y} - \bar{f}(\bar{x})] \tag{8-2}$$

is minimized, where W is the m × m weighting matrix. This scalar quantity is called the loss function. An a priori estimate of the state, $\bar{x}_0$, is assumed to be available for use in the minimization. The deviation of $\bar{x}_0$ from the true value of the state is assumed to have zero mean and covariance $P_{\Delta x_0}$ in order to make subsequent statistical evaluation more amenable to interpretation.

A necessary condition for the loss function to be minimum with respect to $\bar{x}$ is that $\partial Q/\partial \bar{x} = 0$. Therefore, the value of $\bar{x}$ which minimizes Q is a root of the equation

$$\frac{\partial Q}{\partial \bar{x}} = -2 [\bar{y} - \bar{f}(\bar{x})]^T W \left(\frac{\partial \bar{f}}{\partial \bar{x}}\right) = 0. \tag{8-3}$$

The method of solving this nonlinear minimization is to linearize Equation (8-3) and then apply a standard Newton-Raphson procedure to iteratively solve the nonlinear problem. Expanding $\bar{f}(\bar{x})$ in a truncated Taylor series about the a priori estimate $\bar{x}_0$ yields

$$\bar{f}(\bar{x}) = \bar{f}(\bar{x}_0) + F \overline{\Delta x} \tag{8-4}$$

where

$$\overline{\Delta x} = \bar{x} - \bar{x}_0 \tag{8-5}$$

and

$$F = \left(\frac{\partial \bar{f}}{\partial \bar{x}}\right)_{(\bar{x} = \bar{x}_0)} \cdot \left\{ \begin{array}{l} \text{the } m \times p \text{ matrix of} \\ \text{partial derivatives of} \\ f(\bar{x}) \text{ with respect to } \bar{x} \\ \text{evaluated at } \bar{x} = \bar{x}_0 \end{array} \right\} \tag{8-6}$$

The linearized observation vector becomes

$$\overline{\Delta y} = F \overline{\Delta x} + \bar{n} \tag{8-7}$$

where

$$\overline{\Delta y} = \bar{y} - \bar{f}(\bar{x}_0). \tag{8-8}$$

Substituting Equations (8-4) and (8-7) into (8-3), the linearized partial of the loss function in Equation (8-3) becomes

$$-2(\overline{\Delta y} - F \overline{\Delta x})^T W F = 0 \tag{8-9}$$

which can immediately be solved for $\overline{\Delta x}$ yielding the classic equation for the best estimate $\widehat{\Delta x}$

$$\widehat{\Delta x} = (F^T W F)^{-1} F^T W \overline{\Delta y}. \tag{8-10}$$

The value of $\hat{x}$, the estimate derived from the linearized system is, therefore,

$$\hat{x} = \bar{x}_0 + \widehat{\Delta x}. \tag{8-11}$$

The symmetric matric $(F^T W F)$ is called the normal matrix.

As a result of the linearization performed in Equation (8-4), the correction $\widehat{\Delta x}$ must be small so as not to violate linearity. This means that the a priori estimate $\bar{x}_0$ must be reasonably close to the true extremal solution of Equation (8-2). If such is not the case the process is iteratively repeated in a standard Newton-Raphson fashion, each time using the last best estimate $\hat{x}$ as a reference for the linearization. The iterations continue until the differential correction vector $\widehat{\Delta x}$ is truly small (i.e., approaching zero), which is tantamount to the original nonlinear loss function Q(x) being minimum.

The inverse of the $p \times p$ normal matrix, $(F^T W F)$, is the covariance matrix of the error in the weighted least-squares estimate $\hat{x}$ after convergence

is achieved and when the following statistical assumptions of the measurement process are satisfied:

(a) The observation noise is unbiased, i.e., $\mathcal{E}\{\bar{n}\} = 0$.

(b) The errors in the observation vector components are uncorrelated and the covariance of the observation noise vector is known and its inverse is the weighting matrix W. Let σ_1^2 be the variance of the measurement noise component n_1, which corresponds to measurement y_1; σ_2^2 the variance of component n_2, which corresponds to y_2; and so on. The weighting matrix is

$$W = \begin{bmatrix} \sigma_1^{-2} & & & \\ & \sigma_2^{-2} & & 0 \\ & & \ddots & \\ 0 & & & \sigma_m^{-2} \end{bmatrix} \qquad (8\text{-}12)$$

Equating the inverse of W to the covariance matrix of measurement errors implies that multicomponent observations at a given time (e.g., range, azimuth, elevation) are not spatially correlated and that measurements at different times are not time-correlated.

(c) The mathematical models of the trajectory and observations characterize exactly the physics governing the observation process. All parameters such as biases, tracking station locations and physical constants that are not being estimated are known exactly.

The above criteria can never be met precisely in real spacecraft applications. As a result, the covariance matrix, $(F^T W F)^{-1}$, must be realistically interpreted with regard to the specific application. In orbit estimation applications using radar tracking data, the covariance (off-diagonal) elements of the measurement error are rarely available. In fact, for sensors that measure multicomponent vectors, the differing circuitry involved in the independent components frequently yields different time corrections for each component. This results in a measurement vector having components at different times. As a result, the GTDS considers the observations to be uncorrelated scalar measurements so that the weighting matrix W is always diagonal and contains only the variances as shown in Equation (8-12).

The variance for each observation is formed from the relationship

$$\sigma_k^2 = k_1 \tilde{\sigma}_k^2 + k_2 \bar{\sigma}_k^2 \qquad (8\text{-}13)$$

where

$\tilde{\sigma}_k$ ~ the a priori standard deviation of the observation noise

$\bar{\sigma}_k$ ~ the standard deviation of the data reduction curve fit obtained during preprocessing of the observation data. The curve fit is assumed to be polynomial in form

k_1 ~ a specified gain constant applied to $\tilde{\sigma}_k$

k_2 ~ a specified gain constant applied to $\bar{\sigma}_k$

Typical a priori weighting schemes for observations processed in the GTDS are presented in Appendix D.

Many current estimation programs, including GTDS, receive the observation data from independent preprocessing programs. The preprocessing programs smooth and compact the data by fitting low order polynomials to short spans of data in a regression manner. The actual measurements, within the span, are then replaced by a single value interpolated from the polynomial. In this manner, a few, more widely spaced, data points replace the large number of measurements input to the preprocessing program. Also, the deviations of the actual data from the smoothing polynomial are used to determine the standard deviation, $\bar{\sigma}_k$, of the compacted measurements. Caution should be taken in interpreting estimated results that are obtained by using such data for the following reasons: (1) The polynomial smoothing can easily introduce bias error and/or correlation into the data. This is especially true if multiple data points are interpolated from the same polynomial or if data spans for the smoothing polynomial overlap. (2) The standard deviations thus obtained merely reflect agreement or disagreement between the fitted polynomial and the original data. This generally is a good approximation for the random noise content in the data. However, it ignores completely the uncorrected systematic errors in the data which may not be accounted for in the estimation program.

Current plans are to provide the GTDS with two optional modes of operation the metric mode and the polynomial mode. In the metric mode, the program accepts smoothed and compacted data from an independent preprocessor as described above. In the polynomial mode, data in nearly raw condition are input

to GTDS having calibrations corrections only. The program then processes either all or selective subsets of data and estimates the systematic error corrections along with other solve-for variables without disturbing the data noise. In both modes, consideration will be given to adjusting $\bar{\sigma}_k$ in Equation (8-13) based on actual observation residuals during the estimation process.

There is still another, more subtle, qualification for identifying $(F^T WF)^{-1}$ with the covariance matrix of uncertainty. In nonlinear regression problem, such as trajectory estimation, the true covariance matrix is equal to $(F^T WF)^{-1}$ plus terms involving higher order partial derivatives of the computed observations with respect to the variables solved for. These higher order terms were neglected during linearization. So long as large deviations are not obtained, the linearity assumption is reasonably satisfied.

In the following section the specific estimator algorithm implemented in the GTDS and its associated covariance matrix are derived and discussed, and details concerning the application of the estimation process are described. Much of the material is from References 4 and 5.

8.2 ESTIMATOR ALGORITHM

To facilitate the derivation of an iterative weighted least-squares solution, the various quantities that are iteration dependent will be subscripted with an i to denote this dependence. Thus $\overline{\Delta x}$, in Equation (8-5), is written $\overline{\Delta x}_i = \bar{x} - \hat{x}_i$ where $\hat{x}_i$ is the best estimate of $\bar{x}$, the extended state, obtained from the ith iteration. At commencement of the process (0th iteration), $\hat{x}_0 = \bar{x}_0$ is the a priori value of these solve-for variables. We seek to determine $\hat{x}_{i+1}$ from $\hat{x}_i$ so as to minimize the loss function.

The initial assumption that the measurements vector, $\bar{y}$, can be related to the state and model parameters at epoch time, t_o, is given as

$$\bar{y} = \bar{f}(\bar{x}, \bar{z}) + \bar{n} \tag{8-14}$$

where two classes of variables are included. The p-dimensional vector $\bar{x}$, designated solve-for vector, contains as components the state and model parameters whose values are known with limited certainty and are to be estimated. The q-dimensional vector, $\bar{z}$, designated consider vector, contains as components all model parameters whose values are known with limited certainty but are not to

be estimated. Nevertheless, the uncertainty of $\bar{z}$ is to be considered. A priori values of $\bar{x}$ and $\bar{z}$ are specified to be $\bar{x}_0$ and $\bar{z}_0$ with respective covariance matrices $P_{\Delta x_0}$ and $P_{\Delta z_0}$, i.e.,

$$\mathcal{E}\{\bar{x}_0\} = \bar{x}, \qquad \text{cov}\{\bar{x}_0 - \bar{x}\} = P_{\Delta x_0} \tag{8-15}$$

$$\mathcal{E}\{\bar{z}_0\} = \bar{z}, \qquad \text{cov}\{\bar{z}_0 - \bar{z}\} = P_{\Delta z_0}. \tag{8-16}$$

On the ith iteration the loss function is defined to be

$$Q(\bar{x}) = [\bar{y} - \bar{f}(\bar{x}, \bar{z}_0)]^T W [\bar{y} - \bar{f}(\bar{x}, \bar{z}_0)] + (\bar{x} - \bar{x}_0)^T P_{\Delta x_0}^{-1} (\bar{x} - \bar{x}_0) \tag{8-17}$$

Note that the second term on the right has been added to the loss function to constrain the best estimate to the a priori specified $\bar{x}_0$, the degree of constraint being dependent upon the uncertainty $P_{\Delta x_0}$. This term accounts for the fact that $\bar{x}_0$ is known to be accurate to a confidence level given by $P_{\Delta x_0}$. Therefore, any solution is constrained to satisfy the a priori realization, $\bar{x}_0$, to within the limits of its uncertainty.

To obtain the weighted least-squares solution that minimizes $Q(\bar{x})$ in Equation (8-17), we proceed as in Section 8.1. First, $\partial Q/\partial \bar{x}$ is linearized; then a Newton-Raphson procedure is iteratively applied to solve the nonlinear minimization problem. For convenience, we will commence by considering the ith iterate, $\hat{x}_i$, available, and linearize the nonlinear regression equation as follows.

$$\bar{f}(\bar{x}, \bar{z}) = \bar{f}(\hat{x}_i, \bar{z}_0) + F_i \overline{\Delta x_i} + E_i \overline{\Delta z} \tag{8-18}$$

where

$$\overline{\Delta x_i} = \bar{x} - \hat{x}_i \tag{8-19}$$

$$\overline{\Delta z_i} = \bar{z} - \bar{z}_0 \tag{8-20}$$

and

$$F_i = \left(\frac{\partial \overline{f}}{\partial \overline{x}} \right)_{(\overline{x},\ \overline{z} = \hat{x}_i,\ \overline{z}_0)} \tag{8-21a}$$

$$E_i = \left(\frac{\partial \overline{f}}{\partial \overline{z}} \right)_{(\overline{x},\ \overline{z} = \hat{x}_i,\ \overline{z}_0)} \tag{8-21b}$$

Note that since the consider variables, $\overline{z}$, are not being estimated, their values remain equal to $\overline{z}_0$.

Substituting terms with non-zero mean from Equation (8-18) into Equation (8-17) yields the linearized loss function

$$\begin{aligned} Q'(\overline{\Delta x_i}) = {} & [\overline{\Delta y_i} - F_i\, \overline{\Delta x_i}]^T\, W\, [\overline{\Delta y_i} - F_i\, \overline{\Delta x_i}] \\ & + (\overline{\Delta x_i} - \Delta \tilde{x}_i)^T\, P_{\Delta x_0}^{-1}\, (\overline{\Delta x_i} - \tilde{\Delta x}_i) \end{aligned} \tag{8-22}$$

where the measurement residuals are

$$\overline{\Delta y_i} = \overline{y} - \overline{f}\,(\hat{x}_i,\ \overline{z}_0) \tag{8-23}$$

and the deviation of the a priori from the ith iterative estimate is

$$\tilde{\Delta x}_i = \overline{x}_0 - \hat{x}_i. \tag{8-24}$$

The value of $\overline{\Delta x_i}$ that minimizes Q', denoted by $\hat{\Delta x}_{i+1}$, is therefore

$$\hat{\Delta x}_{i+1} = \left(F_i^T\, W\, F_i + P_{\Delta x_0}^{-1} \right)^{-1} \left[F_i^T\, W\, \overline{\Delta y_i} + P_{\Delta x_0}^{-1}\, \tilde{\Delta x}_i \right] \tag{8-25}$$

and the best estimate of the solve-for variables is

$$\hat{x}_{i+1} = \bar{x}_0 + \sum_{k=1}^{i+1} \hat{\Delta x}_k = \hat{x}_i + \hat{\Delta x}_{i+1}. \tag{8-26}$$

This estimation process is iteratively repeated until convergence criteria (discussed in Section 8.8.3) are satisfied.

Equation (8-25) is the estimator algorithm used in GTDS. It requires the inversion of a p-dimensional matrix, the same dimension as the vector of solve-for variables. Insofar as the estimator algorithm is concerned, it makes no difference whether consider variables are included. Equation (8-25) depends only on the values $\bar{z}_0$ but not on the uncertainty $P_{\Delta z_0}$. This might be expected since the uncertainty resulting from the inclusion of consider variables solely affects the second order statistics or covariances (i.e., ensemble properties). The last term on the right in Equation (8-25) can only be included subsequent to the initial iteration since on the initial iteration, $\tilde{\Delta x} = 0$.

The estimator algorithm in Equation (8-25) differs slightly from the classical weighted least-squares algorithm in Equation (8-10). This difference results from the addition of the second term on the right in the loss function, Equation (8-17).

8.3 MEAN AND COVARIANCE OF ESTIMATE

The best estimate, $\hat{x}$, which results from convergence of the estimator algorithm will next be examined to determine its statistical properties. Two quantities are of concern – the expected (mean) value and the convariance of the estimate. The expected value of the deviation, $\hat{\Delta x}$, yields the amount of bias in the estimate, and the covariance the amount of dispersion or uncertainty. Obviously, zero bias and minimum dispersion are the desirable qualities sought.

In the following discussion, it is assumed that the iterations have converged and the unsubscripted variables, $\bar{x}$, $\Delta\bar{x}$, $\Delta\bar{y}$, etc., correspond to the converged solution and perturbations about it.

The expected value and covariance of the measurement noise vector, $\bar{n}$, are assumed to be

$$\mathcal{E}\{\bar{n}\} = 0 \tag{8-27a}$$

$$\text{cov}\{\bar{n}\} = W^{-1} \tag{8-27b}$$

and the linearized vector of observation residuals can be written as follows

$$\overline{\Delta y} = F\,\overline{\Delta x} + E\,\overline{\Delta z} + \bar{n}. \tag{8-28}$$

Therefore the expected value of $\overline{\Delta y_i}$ is

$$\mathcal{E}\{\overline{\Delta y}\} = F\,\overline{\Delta x} \tag{8-29}$$

since $\mathcal{E}\{\bar{n}\} = \mathcal{E}\{\overline{\Delta z}\} = 0$. The covariance of $\overline{\Delta y}$ is

$$\begin{aligned}
\operatorname{cov}\{\overline{\Delta y}\} &= \mathcal{E}\{[\overline{\Delta y} - \mathcal{E}(\overline{\Delta y})]\,[\overline{\Delta y} - \mathcal{E}(\overline{\Delta y})]^T\} \\
&= E\,\mathcal{E}\{\overline{\Delta z}\,\overline{\Delta z}^T\}\,E^T - E\,\mathcal{E}\{\overline{\Delta z}\,\bar{n}^T\} - \mathcal{E}\{\bar{N}\overline{\Delta z}^T\}\,E^T + \mathcal{E}\{\bar{n}\,\bar{n}^T\} \qquad (8\text{-}30) \\
&= E\,P_{\Delta z_0}\,E^T + W^{-1}
\end{aligned}$$

where the correlation between the consider variable errors and the measurement noise is assumed zero, i.e.,

$$\mathcal{E}\{\overline{\Delta z}\,\bar{n}^T\} = 0. \tag{8-31}$$

The mean of the best estimate $\hat{x}_{i+1}$ is

$$\begin{aligned}
\mathcal{E}\{\hat{x} - \bar{x}\} &= \mathcal{E}\{\widehat{\Delta x} - \overline{\Delta x_i}\} \\
&= \left(F^T W F + P^{-1}_{\Delta x_0}\right)^{-1}\left[F\,W\,\mathcal{E}\{\overline{\Delta y}\} + P^{-1}_{\Delta x_0}\,\mathcal{E}\{\Delta \tilde{x}\} - \left(F^T W F\right.\right. \qquad (8\text{-}32) \\
&\quad \left.\left. + P^{-1}_{\Delta x_0}\right)\,\mathcal{E}\{\overline{\Delta x}\}\right] \\
&= \left(F^T W F + P^{-1}_{\Delta x_0}\right)^{-1} P^{-1}_{\Delta x_0}\,\mathcal{E}\{\bar{x}_0 - \bar{x}\}.
\end{aligned}$$

But $\bar{x}_0$ was defined to have an expected value equal to $\bar{x}$, (see Equation (8-15)). Therefore

$$\mathcal{E}\{\hat{x} - \bar{x}\} = 0 \quad \text{and} \quad \mathcal{E}\{\hat{x}\} = \bar{x}. \tag{8-33}$$

Equation (8-33) shows that the best estimate is unbiased. The covariance of the error in the estimate is

$$\begin{aligned} P_{\Delta x} &= \mathcal{E}\{[\hat{x} - \bar{x}]\,[\hat{x} - \bar{x}]^T\} = \mathcal{E}\{[\widehat{\Delta x} - \overline{\Delta x}]\,[\widehat{\Delta x} - \overline{\Delta x}]^T\} \\ &= \psi \Big\{ F^T W E P_{\Delta z_0} E^T W F + F^T W F + P^{-1}_{\Delta x_0} \\ &+ F^T W \Big[E\,\mathcal{E}\{\overline{\Delta z}\,(\overline{\Delta x} - \widetilde{\Delta x})^T\}\, P^{-1}_{\Delta x_0} + E\,\mathcal{E}\{\overline{\Delta z}\,\bar{n}^T\}\, W F \Big] \\ &+ \Big[P^{-1}_{\Delta x_0}\,\mathcal{E}\{(\overline{\Delta x} - \widetilde{\Delta x})\,\overline{\Delta z}^T\}\, E^T + F^T W\,\mathcal{E}\{\bar{n}\,\overline{\Delta z}^T\}\, E \Big] W F \\ &+ P^{-1}_{\Delta x_0}\,\mathcal{E}\{(\overline{\Delta x} - \widetilde{\Delta x})\,\bar{n}^T\}\, W F + F^T W\,\mathcal{E}\{\bar{n}\,(\overline{\Delta x} - \widetilde{\Delta x})^T\}\, P_{\Delta x_0} \Big\} \psi^T \end{aligned} \tag{8-34}$$

where

$$\psi = \left(F^T W F + P^{-1}_{\Delta x_0} \right)^{-1}. \tag{8-35}$$

To simplify Equation (8-34) the following definitions are made

$$\begin{aligned} C_{\Delta x_0 \Delta z} &= \mathcal{E}\{(\overline{\Delta x} - \widetilde{\Delta x})\,\overline{\Delta z}^T\} = \mathcal{E}\{(\bar{x} - \bar{x}_0)\,(\bar{z} - \bar{z}_0)^T\} \\ C^T_{\Delta x_0 \Delta z} &= \mathcal{E}\{\overline{\Delta z}\,(\overline{\Delta x} - \widetilde{\Delta x})^T\} = \mathcal{E}\{(\bar{z} - \bar{z}_0)\,(\bar{x} - \bar{x}_0)^T\} \end{aligned} \tag{8-36}$$

$$\begin{aligned} C_{\Delta zn} &= \mathcal{E}\{\overline{\Delta z}\,\bar{n}^T\} = \mathcal{E}\{(\bar{z} - \bar{z}_0)\,\bar{n}^T\} = 0 \\ C^T_{\Delta zn} &= \mathcal{E}\{\bar{n}\,\overline{\Delta z}^T\} = \mathcal{E}\{\bar{n}\,(\bar{z} - \bar{z}_0)^T\} = 0 \end{aligned} \tag{8-37}$$

$$C_{\Delta x_0 n} = \mathcal{E}\{(\overline{\Delta x} - \tilde{\Delta x})\,\bar{n}^T\} = \mathcal{E}\{(\bar{x} - \bar{x}_0)\,\bar{n}^T\} = 0$$

$$C^T_{\Delta x_0 n} = \mathcal{E}\{\bar{n}\,(\overline{\Delta x} - \tilde{\Delta x})^T\} = \mathcal{E}\{\bar{n}\,(\bar{x} - \bar{x}_0)^T\} = 0 \tag{8-38}$$

Therefore Equation (8-34) becomes

$$P_{\Delta x} = \psi\{F^T W E P_{\Delta z_0} E^T W F + \psi^{-1} + F^T W E C^T_{\Delta x_0 \Delta z} P^{-1}_{\Delta x_0} + P^{-1}_{\Delta x_0} C_{\Delta x_0 \Delta z} E^T W F\}\,\psi^T. \tag{8-39}$$

In Equation (8-37) and (8-38) it is assumed that no statistical correlation exists between the measurement noise and the error in the solve-for or consider variables. The correlation between errors in the a priori solve-for and consider variables, $C_{\Delta x_0 \Delta z}$, is neglected in GTDS primarily because a priori values of this correlation matrix are usually unavailable. The terms are maintained in Equation (8-39) for completeness and for possible use in error analysis application discussed later. In the event that no consider variables are included, Equation (8-39) reduces to

$$P_{\Delta x} = \psi = (F^T W F + P^{-1}_{\Delta x_0})^{-1} \tag{8-40}$$

which is the gain matrix in the estimator algorithm, Equation (8-25).

It was stated previously that a desirable quality of an estimate is small dispersions. It is evident from Equation (8-40) that the covariance matrix of error in the estimate, $P_{\Delta x}$, is directly proportional to the measurement uncertainty, W^{-1}, and the a priori covariance matrix of the solve-for variable uncertainty, $P_{\Delta x_0}$. Equation (8-39) shows that $P_{\Delta x}$ is also directly proportional to the covariance matrix of uncertainty in the consider variables, $P_{\Delta z_0}$. Therefore, minimizing the measurement noise, as well as the a priori uncertainty in the solve-for and consider variables will result in reducing the dispersion or uncertainty in the estimated variables.

The correlation between errors in the solve-for and consider variables, which results from the processing, is

C.5

$$C_{\Delta_x \Delta_z} = \mathcal{E}\{(\hat{x} - \bar{x})(\bar{z} - \bar{z}_0)^T\}$$

$$= \psi\left\{P^{-1}_{\Delta_{x_0}} C_{\Delta_{x_0}\Delta_z} + F^T W E P_{\Delta_{z_0}}\right\}. \tag{8-41}$$

Note that even if the a priori correlation, $C_{\Delta_{z_0}\Delta_z}$, is assumed zero, a correlation between errors in the solve-for and consider variables will result because of their dependency in the processing model.

8.4 ORDERING OF VARIABLES AND NORMAL MATRIX FORMATION

Throughout Sections 8.2 and 8.3, we have ignored the components of the solve-for and consider vectors, $\bar{x}$ and $\bar{z}$, and how the components and their error covariances P_{Δ_x} and P_{Δ_z} are associated with a specific time or epoch. Furthermore, it has been assumed in Equation (8-14) that the calculated measurements at various times ($t_1, t_2, \ldots, t_m$) can be related to the solve-for and consider variables at epoch time, t_0. In Equation (8-18) it is assumed that time varying matrices, F_i and E_i, can be calculated which linearly relate the calculated measurements to variables at epoch time. In the following section, we will focus attention upon the solve-for and consider vector components, the manner in which the time dependency is accomplished, and properties of the normal matrix which are utilized in its formation.

8.4.1 Observation Partials and Normal Matrices

The general estimation (solve-for) vector, $\bar{x}$, in the regression equation, Equation (8-14), and estimator equation, Equation (8-25), contains variables from $\bar{q}$ in Equation (7-114), i.e.,

$$\bar{x} \in \bar{q} = \begin{bmatrix} \bar{p} \\ \bar{r}_s \\ b \\ \delta t \end{bmatrix} = \{\text{solve-for vector}\} \tag{8-42}$$

where

$\bar{p}$ ~ the dynamic parameters consisting of the vehicle's state components at epoch, and model parameters in the acceleration model, Equation (4-1). These parameters include gravity constants, drag parameter, solar radiation constant, thrust, and attitude parameters.

$\bar{r}_s$ ~ tracking station locations in earth-fixed coordinates

$\bar{b}$ ~ measurement biases

δt ~ measurement timing bias.

The specified components of the solve-for vector are ordered as follows:

- the six (or less) position and velocity components, $\bar{R}_0$ and $\dot{\bar{R}}_0$ or equivalent elements
- drag parameter, ρ_1
- solar radiation parameter, $k = P_s A/m_0$
- gravitational potential constant μ, μ_k, C_n^m, and S_n^m
- thrust acceleration parameters, $a_0, \ldots, a_4, \alpha_0, \ldots \alpha_3$ and $\delta_0, \ldots, \delta_3$
- attitude control parameters, $a_x, a_y, a_z, b_x, \ldots, c_z$
- tracking station locations, $\bar{r}_s$
- observation biases, b and δt.

Either of the four optional characterizations of the epoch position and velocity, described in Section 1.6 can be solved-for. The mean of 1950.0 Cartesian coordinates $\bar{R}_0$ and $\dot{\bar{R}}_0$ are used below for the purpose of describing the method.

Each row of the F(t) matrix in equation (8-21) contains partials of the computed observation with respect to $\bar{R}_0$ and $\dot{\bar{R}}_0$ and the other specified components of $\bar{p}$, $\bar{r}_s$, b, and δt. The dynamic variables, $\bar{p}$, must be related to epoch time through the state transition matrix, $\Phi(t_i, t_0)$, as discussed in Chapters 5 and 6. Partials with respect to $\bar{r}_s$, b, and δt are not dependent upon an epoch and can be obtained by differentiating the observation equation explicitly.

The nonlinear observation equation is written in Equation (7-1) as follows

$$O_c = f_0 \left[\bar{r}_{1t}\,(t + \delta t,\ \bar{p},\ \bar{r}_s),\ \dot{\bar{r}}_{1t}\,(t + \delta t,\ \bar{p},\ \bar{r}_s)\right] + b + RF_\gamma \qquad (8\text{-}43)$$

where

$\bar{r}_{1t}$, $\dot{\bar{r}}_{1t}$ ~ vehicle position and velocity vectors expressed in local tangent coordinates with respect to a tracking station located at $\bar{r}_s$

RF_c ~ systematic error correction to observation due to ionospheric refraction, light time, etc.

The partials of an observation, O_c, at time T_j, with respect to the solve-for variables $\bar{x}$ are

$$\bar{a}_j = \frac{\partial O_c}{\partial \bar{x}} = \left[\frac{\partial f_0(T_j)}{\partial \bar{R}(T_j)} \quad \frac{\partial f_0(T_j)}{\partial \dot{\bar{R}}(T_j)} \quad \frac{\partial f_0(T_j)}{\partial \bar{r}_s} \quad \frac{\partial f_0(T_j)}{\partial b} \quad \frac{\partial f_0(T_j)}{\partial \delta t}\right] \begin{bmatrix} \dfrac{\partial \bar{R}(T_j)}{\partial \bar{p}(t_0)} \\ \dfrac{\partial \dot{\bar{R}}(T_j)}{\partial \bar{p}(t_0)} \\ 1 \\ 1 \\ 1 \end{bmatrix} \qquad (8\text{-}44)$$

The first matrix on the right is explicitly determined from the observation equations in Section 7. The second matrix on the right must be obtained by integrating the variational equations as described in Chapter 6. Equation (8-44) constitutes a single row, $\bar{a}$, of the F matrix.

On each iteration, the m observations are sequentially processed to form the normal matrix, $F^T W F$. Since the weighting matrix, W, is diagonal, the recursive relation for accumulating the normal matrix is

$$F^T W F = \sum_{j=1}^{m} \frac{\bar{a}_j^T \bar{a}_j}{\sigma_j^2} \qquad (8\text{-}45)$$

where

$$\bar{a}_j = \frac{\partial f\,[\hat{x}_i\,(t_j),\ z_0]}{\partial \bar{x}} = \{j^{th} \text{ row of F matrix given by Equation (8-44)}\}$$

and σ_j, is the standard deviation of the j^{th} observation.

By forming F^TWF row-by-row instead of manipulating the full (m × p) F matrix, a saving in storage and computation time is realized. Since the matrix F^TWF is symmetric, elements below the main diagonal need not be computed nor stored.

The general consider vector, $\bar{z}$, in the regression equation, Equation (8-14), can have as components any model parameters in $\bar{p}$, $\bar{r}_s$, b, or δt.

Each row of the E(t) matrix in Equation (8-21) contains partials of the computed observations with respect to the specified components of $\bar{z}$. The partials with respect to the dynamic variables $\bar{p}$ specified in $\bar{z}$ can be calculated simultaneously with the dynamic partisl in F(t) as described in Chapter 6. However, the partials in E(t) need only be computed on the final converged iteration since the estimator equation, Equation (8-25), is not dependent upon E(t).

In GTDS, the components of the vectors $\bar{x}$ and $\bar{z}$ are merged, on the final iteration to an expanded state vector, $\bar{u}$. The elements of $\bar{u}$ are ordered as described above. The observation partials are then calculated with respect to $\bar{u}$ and a (p+q) × (p+q) expanded state normal matrix $\tilde{F}^TW\tilde{F}$ is sequentially accumulated as described above. When all m observations have been processed, selected elements of $\tilde{F}^TW\tilde{F}$ are extracted to form F^TWF, E^TWE, and E^TWF, which are required to computed the covariance and correlation matrices in Equations (8-39) through (8-41). It should be noted that only elements on and above the main diagonal of $\tilde{F}^TW\tilde{F}$ need be calculated and stored.

8.5 COVARIANCE MATRIX TRANSFORMATIONS

The converged estimate, $\hat{x}$, covariance matrix, P_{Δ_x}, and correlation matrix $C_{\Delta_x\Delta_z}$, resulting from the differential correction process correspond to epoch time t_0. Since GTDS can optionally estimate the state in any of five subsets, the first six components of $\hat{x}$ can correspond to Cartesian coordinates in mean-of-1950.0 or true-of-epoch axes, classical Keplerian orbital elements, spherical coordinates or DODS variables. For discussion purposes denote the first six components of $\hat{x}$ by $\bar{s}$ to denote state. The vector $\bar{s}$ can optionally be

$$\bar{s} = \begin{bmatrix} X \\ Y \\ Z \\ \dot{X} \\ \dot{Y} \\ \dot{Z} \end{bmatrix}_{\substack{\text{Mean-of-} \\ 1950.0}} = \begin{bmatrix} x \\ y \\ z \\ \dot{x} \\ \dot{y} \\ \dot{z} \end{bmatrix}_{\substack{\text{True-of-} \\ \text{Epoch}}} = \begin{bmatrix} a \\ e \\ i \\ \Omega \\ \omega \\ M \end{bmatrix}_{\substack{\text{Keplerian} \\ \text{Elements}}} = \begin{bmatrix} r \\ \alpha \\ \delta \\ V \\ A \\ \beta \end{bmatrix}_{\substack{\text{Spherical} \\ \text{Elements}}} = \begin{bmatrix} x_1 \\ x_2 \\ x_3 \\ x_4 \\ x_5 \\ x_6 \end{bmatrix}_{\substack{\text{DODS} \\ \text{Variables}}}$$

depending on the variable set used in the differential correction process. The upper left 6×6 submatrix of P_{Δ_x}, denoted P_{Δ_s}, also corresponds to the variables used in the differential correction process.

GTDS transforms the estimated state, $\bar{s}$, and its covariance matrix, P_{Δ_s}, to any of the other variable sets shown above. Note that the constant solve-for parameters and consider parameters in $\hat{x}$ and $\bar{z}$ of the original differential correction problem are not coordinate dependent. Only the state (position and velocity) depends upon the coordinate system utilized. Therefore only the subset $\bar{s}$ of $\hat{x}$ and submatrix P_{Δ_s} of P_{Δ_x} need be concerned in the coordinate transformation.

Denoting the set to which $\bar{s}$ and P_{Δ_s} are being transformed by $\bar{s}'$ and $P_{\Delta_s'}$, the nonlinear transformation can be written as

$$\bar{s}'(t_0) = h[\bar{s}(t_0)]. \tag{8-46}$$

Transformations of this type between Cartesian and spherical coordinates are presented in Section 3.3.3, and between Cartesian and Keplerian elements in Section 3.3.7.

To transform the covariance matrix, P_{Δ_s}, Equation (8-46) is linearized yielding

$$\overline{\Delta s}'(t_0) = H(t_0)\,\overline{\Delta s}(t_0) \tag{8-47a}$$

where

$$H(t_0) = \left(\frac{\partial \bar{s}'}{\partial \bar{s}}\right)_{t=t_0} \tag{8-47b}$$

These partial derivatives between Cartesian and spherical coordinates and Cartesian and Keplerian elements are presented in Sections 3.3.3 and 3.3.7 respectively. The covariance matrix, P_{Δ_s}, is defined to be

$$P_{\Delta_s}(t_0) = \mathcal{E}\{[\hat{\Delta s}(t_0) - \overline{\Delta s}(t_0)]\ [\hat{\Delta s}(t_0) - \overline{\Delta s}(t_0)]^T\} \tag{8-48}$$

where $\hat{\Delta s}$ and $\overline{\Delta s}$ correspond to the first six components of $\hat{\Delta x}$ and $\overline{\Delta x}$, defined previously. The covariance matrix of transformed variables, $P_{\Delta_s'}$, is defined to be

$$P_{\Delta_s'}(t_0) = \mathcal{E}\{[\hat{\Delta s}'(t_0) - \overline{\Delta s}'(t_0)]\ [\hat{\Delta s}'(t_0) - \overline{\Delta s}'(t_0)]^T\}. \tag{8-49}$$

Substituting Equation (8-47a) into Equation (8-49) yields

$$P_{\Delta_s'}(t_0) = H(t_0)\, P_{\Delta_s}(t_0)\, H^T(t_0). \tag{8-50}$$

A second type of transformation occasionally encountered concerns the timewise propagation of the estimate, $\hat{x}$, and covariance matrix, P_{Δ_x}. The estimate $\hat{x}(t_0)$ is transformed timewise by merely integrating the equations of motion from initial conditions $\hat{x}(t_0)$ to other times of interest. The best estimate of all model parameters is used in this integration.

The timewise propagation of the covariance matrix of state and model parameters is slightly more complicated. Note, first of all, that the propagation is separate from the differential correction process and that model parameters other than those estimated or considered in the differential correction process can be treated as uncertain in the propagation process. Denote the best estimate of the uncertain state and model parameters at epoch time t_0 by $\hat{u}(t_0)$ and their covariance matrix by $P_{\Delta_u}(t_0)$. If the variables resulted from a differential correction process, then

$$\hat{u} = \begin{bmatrix} \hat{x} \\ \\ \bar{z}_0 \end{bmatrix} \quad \text{and} \quad P_{\Delta_u} = \left[\begin{array}{c|c} P_{\Delta_x} & C_{\Delta_x \Delta_z} \\ \hline C^T_{\Delta_x \Delta_z} & P_{\Delta_{z_0}} \end{array}\right]$$

Consider $\hat{u}$ and P_{Δ_u} to be composed of state components $\bar{s}$ and uncertain model parameters $\bar{u}^*$. Perturbations about $\bar{u}(t)$ are related as follows:

$$\overline{\Delta u}(t) = \phi(t, t_0)\, \overline{\Delta u}(t_0) \tag{8-51a}$$

where the transition matrix ϕ is

$$\phi(t, t_0) = \left[\begin{array}{c|c} \Phi(t, t_0) & \theta(t, t_0) \\ \hline 0 & I \end{array}\right] \tag{8-51b}$$

with

$$\Phi(t, t_0) = \left(\frac{\partial \bar{s}(t)}{\partial \bar{s}(t_0)}\right) \quad \text{and} \quad \theta(t, t_0) = \left(\frac{\partial s(t)}{\partial u^*}\right) \tag{8-51c}$$

By definition, the covariance matrix of $\hat{u}$ at time t is

$$P_{\Delta_u}(t) = \mathcal{E}\{[\widehat{\Delta u}(t) - \overline{\Delta u}(t)]\, [\widehat{\Delta u}(t) - \overline{\Delta u}(t)]^T\}. \tag{8-52}$$

Substituting Equation (8-51a) into Equation (8-52) yields

$$P_{\Delta_u}(t) = \phi(t, t_0)\, P_{\Delta_u}(t_0)\, \phi^T(t, t_0). \tag{8-53}$$

The covariance matrix of state (upper left 6 × 6 submatrix of P_{Δ_u}) is obtained by partitioning ϕ and P_{Δ_u} into their $\bar{s}$ and $\bar{u}^*$ subparts as follows:

$$\begin{aligned} P_{\Delta_s}(t) = {} & \Phi(t, t_0)\, P_{\Delta_s}(t_0)\, \Phi^T(t, t_0) + \theta(t, t_0)\, C^T_{\Delta_s \Delta_{u^*}}\, \Phi^T(t, t_0) \\ & + \Phi(t, t_0)\, C_{\Delta_s \Delta_{u^*}}\, \theta^T(t, t_0) + \theta(t, t_0)\, P_{\Delta_{u^*}}\, \theta^T(t, t_0) \end{aligned} \tag{8-54a}$$

If no uncertain model parameters are included in the propagation, Equation (8-54a) reduces to

$$P_{\Delta_s}(t) = \Phi(t, t_0)\, P_{\Delta_{s(t_0)}}\, \Phi^T(t, t_0). \tag{8-54b}$$

8.6 COVARIANCE MATRIX INTERPRETATION

In the previous sections, equations have been presented for calculating the mean, $\hat{x}$, and the covariance matrix, P_{Δ_x}, of the errors in the estimated state and model parameters. There is little difficulty in recognizing the value of the mean, or estimated value; but interpretation of the covariance and correlation matrix in terms of the variables uncertainty is not quite as clear. Yet the covariance matrix yields a great deal of information on the statistical character of the variables. Some of these characteristics are described below.

8.6.1 Augmented Vector and Covariance

The estimation process yields the mean and covariance of errors, $\hat{x}$ and P_{Δ_x}, respectively, of the solve-for variables, and the matrix relating errors in solve-for and consider variables $C_{\Delta_x \Delta_z}$. The mean and covariance, z_0 and $P_{\Delta_{z_0}}$, respectively, of the consider variables are known a priori. As a aid in understanding the role of each of the matrices, consider the augmented or expanded state vector, $\bar{u}$, defined to be $(\bar{x}, \bar{z})^T$. The best estimate (or expected value) of u is $(\hat{x}, \bar{z}_0)^T$. The covariance matrix of errors of $\bar{u}$ is P_{Δ_u} which can be partitional into the following components

$$P_{\Delta_u} = \left| \begin{array}{c|c} P_{\Delta_x} & C_{\Delta_x \Delta_z} \\ \hline C_{\Delta_z \Delta_x} & P_{\Delta_{z_0}} \end{array} \right|$$

P_{Δ_u} is a positive definite symmetric matrix, therefore

$$C_{\Delta_z \Delta_x} = C^T_{\Delta_x \Delta_z}.$$

The submatrix $P_{\Delta_{z_0}}$ remains constant throughout the processing, since the consider variable uncertainty cannot be improved through estimation.

The following sections present a geometric heuristic interpretation of the covariance matrices P_{Δ_u}, P_{Δ_x}, and/or $P_{\Delta_{z_0}}$ in terms of hyperdimensional volumes of constant probability in the $(p+\bar{q})$, $\bar{p}$, and/or q-dimensional Euclidean space of the vector components.

8.6.2 Hyperellipse Probabilities

In the following discussion, the random vector $\bar{x}$ with uncertainty $P_{\Delta x}$ is considered. The discussion is equally applicable to the random variables $\bar{u}$ and $\bar{z}$ above.

Assuming the random vector, $\bar{x}(t)$, is normally distributed it can be completely described by its mean and covariance. The assumption that $\bar{x}(t)$ is normally distributed is partially justified as a result of an analogue of the Central Limit Theorem which states: "If a large number of random variables are combined in a reasonably complicated fashion to form a single multivariate random variable, then this random variable will have a nearly normal distribution."

For the following discussion, we will assume that the random vector of errors, $\overline{\Delta x}$, about the mean, $\hat{x}$, is composed of six components. It is normally distributed with zero mean and covariance $P_{\Delta x}$. Its probability density function can be written

$$p_X(\overline{\Delta x}) = \frac{1}{(2\pi)^3 |P_{\Delta x}|^{1/2}} \exp\left[-\frac{1}{2} \Delta \bar{x}^T P_{\Delta x}^{-1} \Delta \bar{x}\right] \tag{8-55}$$

If $P_{\Delta x}$ is a diagonal matrix, then $\bar{x}$ has components that are statistically independent (uncorrelated), and $p_X(\Delta \bar{x})$ can then be factored into a product of six univariate functions of $x_1, x_2, \ldots, x_6$, respectively (the one-dimensional marginal probability density functions of the six components of the state). This constitutes a sufficient condition for independence of the marginal random variables $x_1, \ldots, x_6$.

By virtue of its definition, $P_{\Delta x}$ is a non-negative definite matrix so that it has non-negative eigenvalues. Hence a similarity transformation

$$\overline{\Delta y} = S\,\overline{\Delta x} \tag{8-56}$$

is always possible to diagonalize $P_{\Delta x}$. That is, the hypersurface of constant likelihood (constant value of probability density) in six-dimensional space is a hyperellipsoid, and by a rotation of axes, it is possible to use the principal axes of the hyperellipsoid as coordinate axes (i.e., to transform to another random variable space having uncorrelated or independent components). Note that Δy in Equation (8-56) represents space coordinates and is unrelated to the observations.

We are frequently interested in the probability that $x_1, x_2, \ldots, x_6$ lie within the hyperellipsoid

$$\overline{\Delta x}^T P_{\Delta x}^{-1} \overline{\Delta x} = \ell^2 \tag{8-57}$$

where ℓ is constant. By transforming to principal axes, this expression becomes

$$\frac{\Delta y_1^2}{\sigma_1^2} + \frac{\Delta y_2^2}{\sigma_2^2} + \cdots + \frac{\Delta y_6^2}{\sigma_6^2} = \ell^2 \tag{8-58}$$

where $\sigma_1, \sigma_2, \ldots, \sigma_6$ are the eigenvalues of $P_{\Delta x}$. The transformation matrix from $\Delta \overline{x}$ to $\Delta \overline{y}$ space is accomplished by the matrix of eigenvectors S. By a second transformation, $\Delta z_i = \Delta y_i / \sigma_i$, the expression in Equation (8-58) becomes the equation for a hypersphere in six dimensions

$$\Delta z_1^2 + \Delta z_2^2 + \cdots + \Delta z_6^2 = \ell^2. \tag{8-59}$$

The probability of finding $\overline{\Delta z}$ inside this hypersphere is

$$\int\int\cdots\int_{\text{volume}} \frac{1}{(2\pi)^3} \exp\left\{-\frac{1}{2}(\Delta z_1^2 + \cdots + \Delta z_6^2)\right\} d\,\Delta z_1\, d\,\Delta z_2 \cdots d\Delta z_6 \tag{8-60}$$

where the integration is carried over the volume of the hypersphere of radius Δr, where

$$\Delta r^2 = \Delta z_1^2 + \Delta z_2^2 + \cdots + \Delta z_6^2. \tag{8-61}$$

Thus the probability of finding $\Delta x_1, \Delta x_2, \ldots, \Delta x_6$ inside the hyperellipsoid $\overline{\Delta x}^T P_{\Delta x}^{-1} \overline{\Delta x} = \ell^2$ is

$$Pr = \frac{1}{(2\pi)^3} \int_0^{\ell} e^{-1/2 \Delta r^2} f(\Delta r)\, d\Delta r \tag{8-62}$$

where $f(\Delta r)$ is the spherically symmetric differential volume element.

In six-dimensional space, Equation (8-62) is

$$Pr = \frac{1}{(2\pi)^3} \int_0^{\ell} e^{-1/2 \Delta r^2} (\pi^3 \Delta r^5)\, d\Delta r = \left[1 - \frac{1}{2} e^{-1/2 \ell^2} \left(\frac{\ell^4}{4} + \ell^2 + 2\right)\right]. \tag{8-63}$$

For $\ell = 1$, 2, and 3, the probability is 0.014, 0.332, and 0.826, respectively. Also of interest are hyperellipsoids of other dimensions. Considering an m-dimensional random vector where m = 1 through 7, the probabilities corresponding to ℓ = 1 through 4 (often called one-, two-, three-, and four-sigma probabilities) are as shown in Table 8-1.

Table 8-1
Hyperellipse Probabilities

m \ ℓ	1	2	3	4
1	0.683	0.955	0.997	1.00
2	0.394	0.865	0.989	1.00
3	0.200	0.739	0.971	0.999
4	0.090	0.594	0.939	0.997
5	0.037	0.450	0.891	0.993
6	0.014	0.323	0.826	0.986
7	0.005	0.220	0.747	0.975

The problem of evaluating the hyperellipsoid, however, remains very difficult since it cannot be visualized. The equation for the ellipsoid can be transformed to its principal axes by means of the eigenvector transformation. The resulting diagonal matrix of eigenvalues yields the maximum excursions of the state variables. But these excursions are in the transformed (prinicipal) axes and therefore are maximum excursions for combinations of $\Delta x_1, \Delta x_2, \ldots, \Delta x_6$ and still difficult to visualize.

8.6.3 Hyperrectangle Probabilities

Another means of interpreting the confidence regions of state variable uncertainty is by means of hyperrectangles instead of hyperellipses. Consider a two-dimensional case where $P_{\Delta x}$ is the covariance matrix

$$P_{\Delta x} = \begin{bmatrix} \sigma^2_{\Delta x_1} & \sigma_{\Delta x_1 \Delta x_2} \\ \sigma_{\Delta x_1 \Delta x_2} & \sigma^2_{\Delta x_2} \end{bmatrix} \tag{8-64}$$

The quadratic form $\overline{\Delta x}^T P^{-1}_{\Delta x} \overline{\Delta x} = \ell^2$ is

$$\sigma^2_{\Delta x_2} \Delta x_1^2 - 2\, \sigma_{\Delta x_1 \Delta x_2} \Delta x_1 \Delta x_2 + \sigma^2_{\Delta x_1} \Delta x_2^2 = \ell^2 \, |P_{\Delta x}| . \tag{8-65}$$

This quadratic equation represents an ellipse typical of that in Figure 8.1.

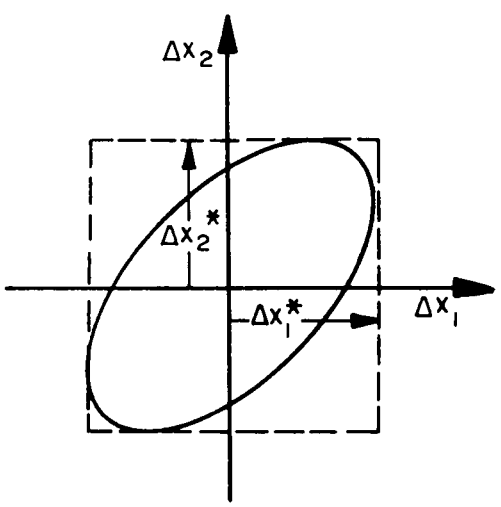

Figure 8-1. Error Ellipse and Rectangle

The width, Δx_1^*, and height, Δx_2^*, of the rectangle enclosing the ellipse are determined from Equation (8-65) for the condition that $d\Delta x_2 / d\Delta x_1 = 0$ and $d\Delta x_1 / d\Delta x_2 = 0$, respectively, yielding

$$\Delta x_2^* = \ell\, \sigma_{\Delta x_2}$$
$$\Delta x_1^* = \ell\, \sigma_{\Delta x_1}. \qquad (8\text{-}66)$$

Thus the probability that Δx_1 lies within the region $-3\,\sigma_{\Delta x_1} \leq \Delta x_1 \leq 3\,\sigma_{\Delta x_1}$ is 0.997, Δx_2 falling wherever it may. The probability that Δx_2 lies within the region $-3\,\sigma_{\Delta x_2} \leq \Delta x_2 \leq 3\,\sigma_{\Delta x_2}$ is also 0.997, Δx_1 falling wherever it may. The probability the Δx_1 and Δx_2 simultaneously lie with the respective regions $-3\,\sigma_{\Delta x_1} \leq \Delta x_1 \leq 3\,\sigma_{\Delta x_1}$ and $-3\,\sigma_{\Delta x_2} \leq \Delta x_2 \leq 3\,\sigma_{\Delta x_2}$ is therefore $(0.997)^2$ or 0.994. The probability that Δx_1 and Δx_2 lie within the 3σ ellipse is 0.989, slightly less than that for the rectangle as a result of the lesser area.

Extending this interpretation to six dimensions, the probability that Δx_1, $\Delta x_2, \ldots, \Delta x_6$ simultaneously lie within their 3σ hyperrectangles is $(0.997)^6$ or 0.982. The probability that they lie within the six-dimensional hyperellipsoid is 0.826, significantly lower because of the smaller volume. The hyperrectangle probabilities corresponding to ℓ = 1, 2, 3, and 4 and from m = 1 through 7 are presented in Table 8-2.

Table 8-2
Hyperrectangle Probabilities

m \ ℓ	1	2	3	4
1	0.683	0.955	0.997	1.00
2	0.466	0.912	0.994	1.00
3	0.319	0.872	0.991	1.00
4	0.218	0.832	0.988	1.00
5	0.149	0.794	0.985	1.00
6	0.102	0.759	0.982	1.00
7	0.069	0.724	0.979	1.00

The hyperrectangle probabilities are much easier to analyze since the various sides of the hyperrectangles are multiples of the square root of the variances. However, it is important to maintain awareness of the fact that the boundary of the hyperrectangle merely encloses a volume of space and in no way can be regarded as a boundary of constant probability as is the case with hyperellipses.

The hyperrectangle probabilities are particularly convenient during program checkout. By processing simulated data having Gaussian random error with zero mean and known variances, the residuals of the estimated vector can be compared with the calculated standard deviations. The distribution of residuals should satisfy the 1, 2, 3, and 4 sigma probabilities in Table 8-2.

8.6.4 Correlation Coefficient

It has been shown that the off-diagonal covariance elements of a covariance matrix determine the deviation between the random vector components coordinate axes and the principal axes of the hyperellipse of constant probability. When the covariance elements are zero, the principal axes are aligned with the coordinate axes and the components are independent of each other. Furthermore, the normal density function, Equation (8-55), can then be factored into a product of n univariate functions of $\Delta x_1, \Delta x_2, \ldots, \Delta x_n$.

Another measure of the dependence of two random vectors, $\Delta\bar{x}$ and $\Delta\bar{z}$, having a (p × q) correlation matrix

$$C_{\Delta x \Delta z} = \begin{bmatrix} \operatorname{cov}(\Delta x_1, \Delta z_1) & \operatorname{cov}(\Delta x_1, \Delta z_2) \cdots \operatorname{cov}(\Delta x_1, \Delta z_q) \\ \operatorname{cov}(\Delta x_2, \Delta z_1) & \\ \vdots & \\ \operatorname{cov}(\Delta x_p, \Delta z_1) & \operatorname{cov}(\Delta x_p, \Delta z_2) \cdots \operatorname{cov}(\Delta x_p, \Delta z_q) \end{bmatrix} \tag{8-67}$$

is the correlation coefficient, defined to be

$$\rho_{ij} = \rho(\Delta x_i, \Delta z_j) = \frac{\operatorname{cov}(\Delta x_i, \Delta z_j)}{\sqrt{\operatorname{var}(\Delta x_i)\operatorname{var}(\Delta z_j)}} \tag{8-68}$$

The variance elements are the squares of the standard deviations for Δx_i and Δz_j, respectively, and lie along the main diagonal of $P_{\Delta x}$ and $P_{\Delta z}$, respectively. The correlation coefficient satisfies the following conditions.

- $\rho = 0$ if and only if Δx_i and Δz_j (and therefore x_i and z_j) are uncorrelated
- $|\rho| \leq 1$
- $\rho = \pm 1$, if and only if

$$\left\{\frac{\Delta x_i}{\sigma_{\Delta x_i}}\right\} = \pm \left\{\frac{\Delta z_j}{\sigma_{\Delta z_j}}\right\} \tag{8-69}$$

where

$\sigma_{\Delta x_i}$, $\sigma_{\Delta z_j}$ ~ the standard deviations of the errors x_i and z_j, respectively.

8.7 ERROR ANALYSIS APPLICATION

The weighted least-squares estimator algorithm and associated covariance and correlation matrices, derived in Sections 8.2 and 8.3, are summarized below.

Estimator

$$\Delta\hat{x}_{i+1} = \left[F_i^T W F_i + P_{\Delta x_0}^{-1}\right]^{-1} \left(F_i^T W \Delta \bar{y}_i + P_{\Delta x_0}^{-1} \Delta \bar{x}_i\right) \tag{8-70}$$

Covariance of Estimate

$$\begin{aligned} P_{\Delta x} = \psi \Big[& F^T W E P_{\Delta z_0} E^T W F + F^T W E C_{\Delta x_0 \Delta z} P_{\Delta x_0}^{-1} \\ & + P_{\Delta x_0}^{-1} C_{\Delta x_0 \Delta z} E^T W F + F^T W F + P_{\Delta x_0}^{-1} \Big] \psi^T \end{aligned} \tag{8-71}$$

Correlation of Estimate and Consider Variables

$$C_{\Delta x \Delta z} = \psi \left[P_{\Delta x_0}^{-1} C_{\Delta x_0 \Delta z} + F^T W E P_{\Delta z_0}\right] \tag{8-72}$$

where

$$\psi = [F^T W F + P^{-1}_{\Delta x_0}]^{-1} \quad \text{(8-73a)}$$

$$P_{\Delta x_0} = \mathcal{E}\{(\bar{x}_0 - \bar{x})(\bar{x}_0 - \bar{x})^T\} \quad \text{(8-73b)}$$

$$P_{\Delta x} = \mathcal{E}\{(\hat{x} - \bar{x})(\hat{x} - \bar{x})^T\} \quad \text{(8-73c)}$$

$$P_{\Delta z_0} = \mathcal{E}\{(\bar{z}_0 - \bar{z})(\bar{z}_0 - \bar{z})^T\} \quad \text{(8-73d)}$$

$$C_{\Delta x_0 \Delta z} = \mathcal{E}\{(\bar{x}_0 - \bar{x})(\bar{z}_0 - \bar{z})^T\} \quad \text{(8-73e)}$$

$$C_{\Delta x \Delta z} = \mathcal{E}\{(\hat{x} - \bar{x})(\bar{z}_0 - \bar{z})^T\} \quad \text{(8-73f)}$$

($\hat{x}$ is the converged $\hat{x}_i$).

One observes in Equations (8-70) through (8-72) that only the estimator requires measurement data. The equations for the covariance and correlation matrices require only the statistics, W, of the observations which are usually known for specific classes of trackers and sensors. Therefore, if one assumes that the a priori reference trajectory, $\bar{x}_0$, is the best estimate, the estimator equation can be omitted and the covariance and correlation matrix can be determined for specific mission sensors and observation profiles. It must also be assumed that the mathematical models in the program accurately characterize the physical situation. Since actual measurements are not required, the manner of operation can be performed during preflight studies to determine:

- the effect of measurement data errors (random and systematic), measurement time spans, and sampling rates on the accuracy of the estimated state and model parameters
- the effect of the trajectory dynamics and the trajectory/sensor relative geometry on the accuracy of the estimated state and model parameters
- the relative effects of different types of measurements on the accuracy of the estimated state and model parameters.

Such problems are referred to as Error Analysis problems, since they are solely concerned with the influence that errors in problem variables have on the accuracy of the estimate. This type of analysis can strongly influence the design and enhancement of spacecraft missions as well as establish requirements for observation sensor accuracies, sampling rates, tracking times, and sensor locations.

The method for solving Equations (8-71) and (8-72) in GTDS is nearly identical to that for estimating applications. An a priori estimate of the solve-for and consider variables, $\bar{x}_0$ and $\bar{z}_0$, respectively, along with their covariance matrices, $P_{\Delta x_0}$ and $P_{\Delta z_0}$, is specified. The measurement schedule and measurement uncertainty, W, is also specified a priori. The program then proceeds to integrate the nonlinear differential equations of motion and their corresponding variational equations to the measurement times and compute the measurement partials. The rows of the matrices F and E in Equations (8-71) and (8-72) are accumulated as the measurement statistics are processed. Ultimately the covariance and correlation matrices $P_{\Delta x}$ and $C_{\Delta x \Delta z}$ are calculated at the epoch time. The covariance and correlation matrices are then propagated to specified times $T_1, T_2, \ldots, T_S$ by means of Equations (8-51 and (8-54). Since the estimation equation is not being solved, iterating is unnecessary.

It would appear that since an estimate is not actually being determined, it should make little difference whether model parameters are associated with the solve-for vector, $\bar{x}$, or the consider vector, $\bar{z}$. A subtle difference does exist. Components of the consider vector, $\bar{z}$, are maintained at their a priori specified values throughout the processing, and therefore have no possibility for improvement through estimation. As, a result, their covariances are never improved compared to that initially specified, i.e., $P_{\Delta z_0}$ in Equations (8-71) and (8-69). The solve-for variables, $\bar{x}$, have their values continually improved through the estimation process, and this is reflected through the usually reduced variance elements in $P_{\Delta x}$. Because of the coupling, the uncertainty of the state components is affected differently if the same model parameter is associated with $\bar{x}$ than if it is associated with $\bar{z}$.

8.8 ESTIMATION RELATED TECHNIQUES

Specific techniques involved in the estimation process concern matrix inversion, editing of residuals, iteration control, residual statistics, and hypothesis tests.

8.8.1 Matrix Inversion

The normal matrix is inverted by recursively inverting smaller matrices and by the use of the Schur identity. The symmetrical properties of the normal matrix are utilized during the inversion process. The Schur identity method is developed by assuming the matrix to be inverted is of the form

$$[M] = \left[\begin{array}{c|c} [M_{11}] & [M_{12}] \\ \hline [M_{21}] & [M_{22}] \end{array}\right] \tag{8-74}$$

with the inverse given by

$$[M]^{-1} = \left[\begin{array}{c|c} [H_{11}] & [H_{12}] \\ \hline [H_{21}] & [H_{22}] \end{array}\right]. \tag{8-75}$$

Since

$$[M]\,[M]^{-1} = \left(\begin{array}{c|c} [I] & [0] \\ \hline [0] & [I] \end{array}\right) \tag{8-76}$$

then we must have

$$\begin{aligned} [M_{11}]\,[H_{11}] + [M_{12}]\,[H_{21}] &= [I] \\ [M_{21}]\,[H_{11}] + [M_{22}]\,[H_{21}] &= [0] \end{aligned} \tag{8-77}$$

Eliminating $[H_{21}]$ from Equation (8-77) and solving for $[H_{11}]$ gives

$$[M_{11}]\,[H_{11}] + [M_{12}]\,[M_{22}]^{-1}\,[M_{21}]\,[H_{11}] = [I] \tag{8-78}$$

or

$$[H_{11}] = [M_{11}]^{-1} - [M_{11}]^{-1}\,[M_{12}]\,[M_{22}]^{-1}\,([M_{21}]\,[H_{11}]). \tag{8-79}$$

Premultiplying Equation (8-78) by $[M_{21}]\,[M_{11}]^{-1}$ gives

$$[M_{21}]\,[H_{11}] + [M_{21}]\,[M_{11}]^{-1}\,[M_{12}]\,[M_{22}]^{-1}\,[M_{21}]\,[H_{11}] = [M_{21}]\,[M_{11}]^{-1} \tag{8-80}$$

or

$$[M_{21}]\,[H_{11}] = \left[[I] + [M_{21}]\,[M_{11}]^{-1}\,[M_{12}]\,[M_{22}]^{-1}\right]^{-1}\,[M_{21}]\,[M_{11}]^{-1} \tag{8-81}$$

Substituting Equation (8-81) into Equation (8-79) gives

$$\begin{aligned}[H_{11}] = [M_{11}]^{-1} - [M_{11}]^{-1}\,[M_{12}]\,[M_{22}]^{-1}\,\Big[[I] \\ + [M_{21}]\,[M_{11}]^{-1}\,[M_{12}]\,[M_{22}]^{-1}\Big]^{-1}\,[M_{21}]\,[M_{11}]^{-1}.\end{aligned} \tag{8-82}$$

The matrices $[H_{22}]$, $[H_{12}]$, and $[H_{21}]$ may be derived in a similar manner. The results are

$$\begin{aligned}[H_{22}] &= -\left[[M_{21}]\,[M_{11}]^{-1}\,[M_{12}] + [M_{22}]\right]^{-1} \\ [H_{12}] &= -[M_{11}]^{-1}\,[M_{12}]\,[H_{22}] \\ [H_{21}] &= [M_{22}]^{-1}\,[M_{21}]\,[H_{11}].\end{aligned} \tag{8-83}$$

Assume that the inverse of $[M_{11}]$ is known and that $[M_{22}]$ is in all cases a (1 x 1) matrix. The matrix inversions required in Equations (8-82) and (8-83) are simply the reciprocal of the element of the respective matrices. The inversion begins by setting $[M_{11}]$ as

$$[M_{11}]^{-1} = \frac{1}{m_{11}} \tag{8-84}$$

and

$$[M_{22}]^{-1} = -\frac{1}{m_{22}}. \tag{8-85}$$

Equations (8-82) and (8-83) are then employed to determine the inverse of

$$\begin{bmatrix} m_{11} & m_{12} \\ m_{21} & m_{22} \end{bmatrix} \tag{8-86}$$

The result is called $[M_{11}]$ and the diagonal element following (in this case m_{33}) is used to form a new $[M_{22}]$. The process is continued along the diagonal until the required matrix is inverted. GTDS takes full advantage of the symmetry of the normal matrix by computing and storing only the upper triangle of the matrix. The inversion process is then designed to invert a matrix in upper triangular form and store the result in the same manner.

8.8.2 Editing of Observation Residuals

The observation residual, as computed by GTDS, is defined as the actual observation minus the computed observation that is based on the trajectory specified by the current state vector solution. Deletion of an observation from the differential correction computation may be accomplished by one or more of the following tests that are made on each iteration for each observation:

- By number. After examination of a previous run's residual print, the user may elect to delete some residuals by sequence number.
- By time. The observation falls outside a specified time span.
- By type. The observation type is among those to be rejected.
- By station. The identifier of the station making the observation is among those to be rejected.
- By nth observation. Only every nth observation of this type is to be processed.
- By deviation. From the orbit established by the previous iteration, e.g. "3σ" editing
- By geometry. When the elevation angle of the line of sight from the tracking station is below a specified minimum value.

If a residual is deleted by any test, then the row of the augmented matrix F (matrix of partial derivatives of the observations with respect to the estimated parameters) corresponding to the observation is not computed. Appendix C presented a more detailed treatment of residual analysis.

8.8.3 Iteration Control

Conditions that may cause termination of the differential correction process are as follows:

- Convergence of solution
- Maximum number of consecutive divergent iterations reached
- Maximum number of iterations reached.

The convergence criteria in GTDS are based on iterative reduction of the square root of the mean square of the observation residuals. This quantity, denoted by RMS, is calculated as follows on the ith iteration

$$RMS = \left\{ \frac{1}{m} \left(\overline{\Delta y_i}^T W \overline{\Delta y_i} + \tilde{\Delta x}_i P_{x_0}^{-1} \tilde{\Delta x}_i \right) \right\}^{1/2} \tag{8-87}$$

where $\overline{\Delta y_i}$ and $\tilde{\Delta x}_i$ are defined in Equations (8-23) and (8-24), and m is the number of observations. If the value of RMS decreases during two consecutive iterations, the solution is converging. After a prespecified number of consecutive divergent iterations, the problem is terminated. After testing for convergence or divergence, a predicted RMS is calculated for the next iteration as follows

$$RMSP = \left\{ \frac{1}{m} \left(\overline{\Delta y_i} - F_i \hat{\Delta x}_{i+1} \right)^T W \left(\overline{\Delta y_i} - F_i \hat{\Delta x}_{i+1} \right) + \left(\hat{\Delta x}_{i+1} - \tilde{\Delta x}_i \right)^T P_{\Delta x_0}^{-1} \left(\hat{\Delta x}_{i+1} - \tilde{\Delta x}_i \right) \right\}^{1/2} \tag{8-88}$$

where $\hat{\Delta x}_{i+1}$, $\tilde{\Delta x}_i$, and F_i are defined in Equations (8-25), (8-24), and (8-21) respectively. Note that the second term on the right is exactly correct for the (i+1)th iteration. The first term on the right linearly corrects the measurement residuals to account for the differential correction, $\hat{\Delta x}_{i+1}$. If the

regression equation, Equation (8-14), were linear, the predicted RMSP would be exactly correct. The iterations are considered converged and the problem terminated when the following criterion is met

$$\left| \frac{\text{RMSB} - \text{RMSP}}{\text{RMSB}} \right| < \epsilon \tag{8-89}$$

where

RMSB $\sim$ the smallest RMS achieved compared to all previous iteration

$\epsilon \sim$ the improvement ratio criterion specified by input.

8.8.4 Iteration Statistics

Upon completion of each iteration, a summary of the observation residual statistics is calculated and printed. The statistical quantities that comprise the summary are computed for residual groups, which contain data from specific tracking stations, and data types. The following abbreviations are used in the statistical relations

$\overline{\Delta y_j} \sim$ the j^{th} residual $y_j - f[\hat{x}_i(t_j), \overline{z}_0]$

$n_s \sim$ the total number of residuals for a station and data type (group).

- Root Mean Square Error

  The total weighted RMS, the predicted total RMSP, and the RMS for each station and data type are calculated from Equations (8-87) and (8-88). It is desirable that RMS be small, preferably zero.

- Group Mean

  The mean value of each residual group is a measure of bias in the observation and is calculated as follows

$$\overline{m} = \frac{1}{n_s} \sum_{j=1}^{n_s} \Delta y_j . \tag{8-90}$$

It is desirable that $\bar{m}$, for each group, be zero to be consistent with the assumption in Equation (8-27) that the measurement noise have zero mean.

- Sum of Squares About Mean

The sum of the squares of the residuals about the mean of each residual group is

$$S = \sum_{j=1}^{n_s} (\Delta y_j - \bar{m})^2. \tag{8-91}$$

- Sample Standard Deviation

The sample standard deviation of each residual group is a measure of the dispersion of the observation data and is calculated as follows

$$\sigma = \left(\frac{1}{n_s} \sum_{j=1}^{n_s} (\Delta y_j - \bar{m})^2 \right)^{1/2} = \left(\frac{S}{n_s} \right)^{1/2}. \tag{8-92}$$

The standard deviation should be consistent with the values used in the a priori weighting matrix W.

- Confidence Interval for Group Mean

If the observation residual group population is normally distributed with zero mean, then the variable

$$t = \frac{\bar{m}}{\sqrt{S^2/n_s}} \tag{8-93}$$

has a t-distribution (student's) with $(n_s - 1)$ degrees of freedom. Hence from tables of the t-distribution one can construct confidence intervals for the mean. As n_s gets large, the t-distribution approaches the normal distribution.

- Observation Residual Groups

  On each iteration the following data is printed for each residual group:

  - number of observations, n_s
  - number of rejected and accepted observations
  - histograms of observations by true anomaly.

8.9 COMPUTATIONAL SEQUENCE

The following section describes conceptually how the estimator and covariance equations are solved in GTDS. Figure 8-2, the computational flow schematic, will aid in the discussion. The figure is divided into functional blocks and the following discussion is similarly organized. It should be noted that the logic shown in Figure 8-2 bears no resemblence to the specific source logic in GTDS but is merely presented to characterize the concepts.

8.9.1 A Priori Input

To commence the process all necessary input data is specified at (A). This includes the estimated and considered variables and their covariances, as well as measurement time spans, and times at which the best estimates of the state and covariances are to be propagated. The state is input optionally in any of several convenient coordinate systems. It is transformed to the basic coordinate system used in GTDS (i.e., mean equinox and equator of 1950.0 or true equinox and equator of a given epoch) for subsequent processing. These transformations, are described in Chapter 3.

8.9.2 Data Management

The observation data is next prepared for processing at (B) and (C). This encompasses relocating the data, within the specified measurement span, from the original input device (cards, single or multiple tapes, disk, or keyboard) to a working file convenient for subsequent retrieval during processing. During this relocation function, the data sequence can optionally be edited considering the type of observation, the source of the data, the tracking station, and time span between adjacent points. The data on the working file are chronologically numbered, and the number of the data point which bounds the initial epoch time, t_0, from below is recorded. The data management function also includes the

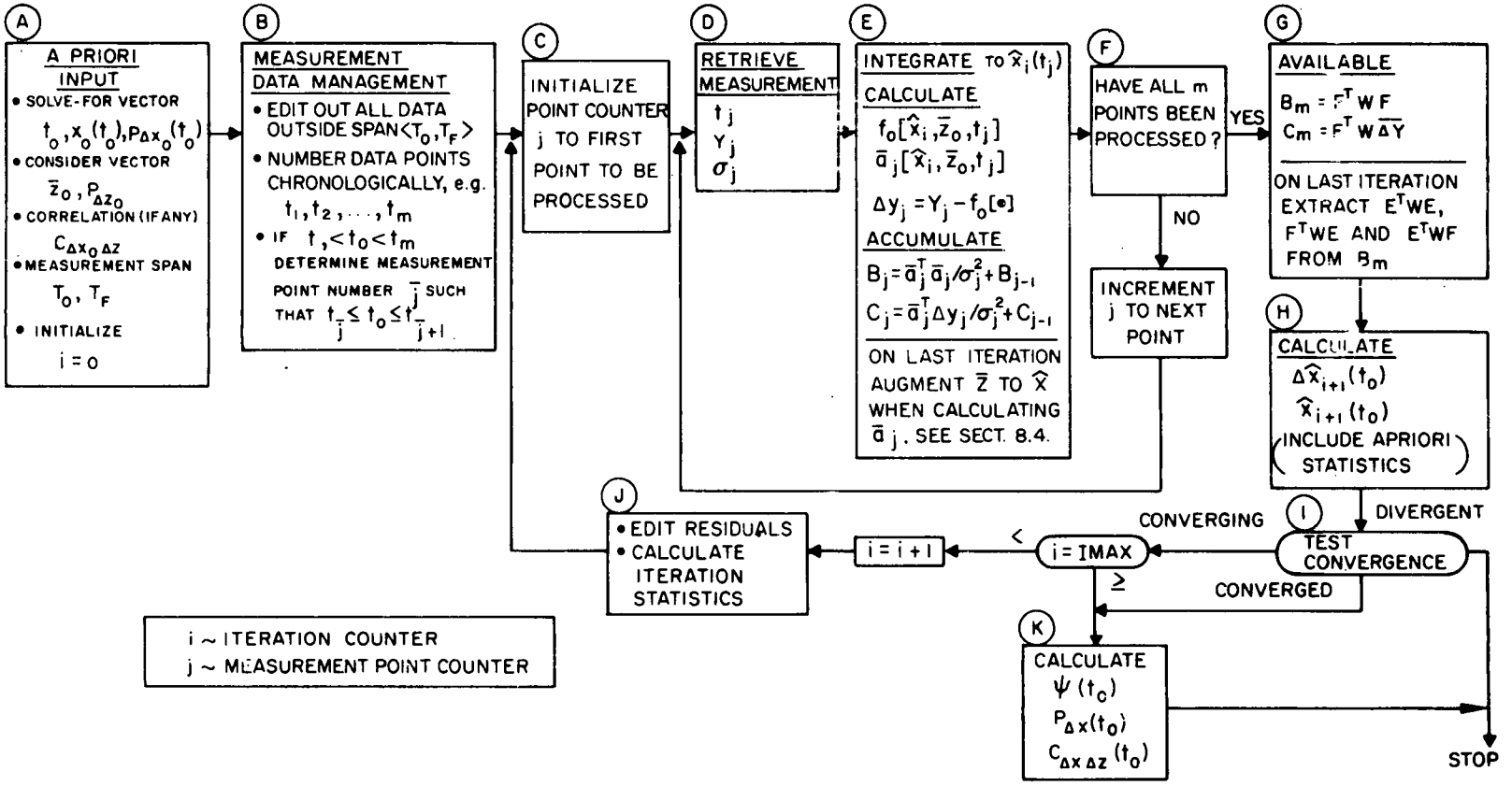

Figure 8-2. Computational Sequence

determination of whether the initial epoch time is less than the first data time, between the first and last data time, or larger than the last data time. For the first case the data are processed sequentially from the first point at t_1 to the last point at t_m. For the second case the processing commences backwards in time from the initial epoch to the first data point. It then switches back to the initial epoch and proceeds forward in time to the last data point. In the third case the data are processed backwards in time from the last (chronological) data point to the first.

8.9.3 Processing Loop

The processing loop commences by retrieving the first data point to be processed from the working file (D). The nonlinear equation of motion (see Chapter 4) and associated variational equations (see Chapter 5) are numerically integrated (see Chapter 6) to the data time (E). The best estimate of the measurement and its related residual, Δy_j, are calculated (see Chapter 7) along with the single row, $\bar{a}_j$, of the F matrix corresponding to the measurement. To minimize core storage, the matrix products $F^T W\overline{\Delta y}$ and $F^T WF$ are accumulated as each row of F is calculated, as described in Section 8.4. It is apparent from Equation (8-25) that only these matrix products are required for determining the estimate. All symmetric matrices (e.g., $F^T WF$) are stored in upper triangular form. On the last iteration, the matrix products $F^T WF$, $E^T WE$, $F^T WE$, and $E^T WF$ are accumulated for subsequent use in computing the covariance and correlation matrices. At (F),, tests are performed to determine if all m data points have been processed. If not, the measurement point counter, j, as incremented or decremented depending on whether the data is being processed forward or backward in time. The logic then returns to the beginning of the processing loop to retrieve the next point to be processed.

8.9.4 Estimation Computation

When all m data points have been processed, the complete matrix products $F^T W$ and $F^T WF$ are available at (G) as well as the measurement residual vector Δy. On the last iteration, $F^T WE$, $E^T WF$, and $E^T WE$ are also available. The best estimate of the perturbations, $\hat{\Delta x}_{i+1}$, and variables, $\hat{x}_{i+1}$, are then calculated via Equations (8-25) and (8-26) at (H).

8.9.5 Iteration Loop

After determining an estimate at (H), the iteration is complete and convergence tests are performed at (I). The convergence criteria are described

in Section 8.8.3. If the iterations are converging, the iteration counter, i, is tested against the maximum number of iterations allowable. If the maximum has not been reached, the iteration counter is incremented and logic proceeds through (J) to commence the next iteration at (C). At (J), the measurement residual vector can be used to edit the data as discussed in Section 8.8.2, as well as to determine iteration statistics as discussed in Section 8.8.4. If the convergence test at (I) determines that divergence is occurring, the problem can be terminated. If the iteration have converged, or the maximum number of iterations has been reached, then the covariance and correlation matrices at epoch t_0 are calculated at (K). Finally, the state vector, the covariance matrix, and the correlation matrix can be transformed to other space and time sets as described in Section 8.5.

8.10 REFERENCE

1. Schmidt, S. F., The Application of State Space Methods to Navigation Problems, Advances in Control Systems, Volume 3, Academic Press, 1966 (C. T. Leondes, editor).

2. Deutsch, R., Estimation Theory, Prentice-Hall, 1965

3. Doob, J. L., Stochastic Processes, John Wiley and Sons, New York, 1963

4. Goddard Space Flight Center, 70-FMT-792A, Houston Operations Predictor/ Estimator (HOPE) Engineering Manual, T. H. de Salima, June 1970

5. Air Force Systems Command, TR-669(9990)-3, TRACE Orbit Determination Program, Version D, C. C. Tonies, et al, September 1966

APPENDIX A

DEVELOPMENT OF RANGE-RATE FORMULAE

This appendix presents the salient aspects in the development of formulas which relate the tracker to spacecraft range-rate to the Doppler shift in a transmitted signal. A more complete development is presented in Reference 1. For a definition of mathematical symbols refer to Sections 2.1.1 which describes the GRARR VHF System.

Consider the rigorous general relativistic expression for the one-way Doppler-shifted frequency ratio from a transmitter T to receiver R

$$\frac{\nu_R}{\nu_T} = \frac{a_T}{a_R}\left[\frac{1 - F_R\,\bar{n}_R \cdot \dot{\bar{r}}_R}{1 - F_T\,\bar{n}_T \cdot \dot{\bar{r}}_T}\right] \tag{A-1}$$

where

$$a = \sqrt{g_{00} + \frac{2}{c}\sum_{i=1}^{3} g_{0i}\,\dot{x}^i + \frac{1}{c^2}\sum_{i,j=1}^{3} g_{ij}\,\dot{x}^i\,\dot{x}^j} \tag{A-2}$$

$$F = \frac{1}{c\,g_{00}}\left[\sqrt{\sum_{i,j=1}^{3}(g_{01}\,g_{0j} - g_{00}\,g_{ij})\frac{dx^i}{dS}\,\frac{dx^j}{dS}} - \sum_{i=1}^{3} g_{0i}\,\frac{dx^i}{dS}\right] \tag{A-3}$$

and

$\bar{n}$ ~ the unit vector along propagation path

T, R ~ the subscripts indicating that the designated quantities are evaluated at the transmitter and receiver, respectively

$\dot{\bar{r}}_T$, $\dot{\bar{r}}_R$ ~ the velocities of the transmitter and receiver defined with respect to the coordinate time t

g_{ij} ~ the elements of the metric matrix, defining the nature of the space-time frame

x^i ~ the components of the space coordinates

S ~ the arc length along the propagation path.

Thus the derivatives, dx^i/dS, are merely the direction cosines of the progapation path and hence the components of the unit vector $\bar{n}$.

The metric coefficients in the case of special relativity are

$$\left.\begin{aligned} g_{00} &= 1 \\ g_{ii} &= -1 \\ g_{ij} &= 0,\ i \neq j \end{aligned}\right\} \quad i,\ j = 1,\ 2,\ 3. \tag{A-4}$$

Hence

$$a = \sqrt{1 - \frac{\dot{\bar{r}} \cdot \dot{\bar{r}}}{c^2}} \tag{A-5}$$

and

$$F = \frac{1}{c} \tag{A-6}$$

and the propagation path, the straight relative position vector from $\bar{r}_T$ to $\bar{r}_R$, is given by

$$\bar{n}_T = \bar{n}_R = \bar{n} = \frac{\bar{r}_R - \bar{r}_T}{|\bar{r}_R - \bar{r}_T|}. \tag{A-7}$$

Under these conditions, Equation (A-1) reduces to

$$\frac{\nu_R}{\nu_T} = \sqrt{\frac{1 - \frac{\dot{\bar{r}}_T \cdot \dot{\bar{r}}_T}{c^2}}{1 - \frac{\dot{\bar{r}}_R \cdot \dot{\bar{r}}_R}{c^2}}} \left[\frac{1 - \frac{\bar{n} \cdot \dot{\bar{r}}_R}{c}}{1 - \frac{\bar{n} \cdot \dot{\bar{r}}_T}{c}} \right] \tag{A-8}$$

the special relativistic formula.

By neglecting atmospheric refraction and denoting

$\bar{r}_T \sim$ the station position in transmission time, t_T

$\bar{r}_V \sim$ the vehicle position at turnaround time, t_v

$\bar{r}_S \sim$ the station position at reception time t_S

the two-way frequency ratio is

$$\frac{\nu_S}{\nu_T} = \frac{\nu_V}{\nu_T} \cdot \frac{\nu_S}{\nu_V}$$

$$= \sqrt{\frac{1 - \frac{\dot{\bar{r}}_T \cdot \dot{\bar{r}}_T}{c^2}}{1 - \frac{\dot{\bar{r}}_V \cdot \dot{\bar{r}}_V}{c^2}}} \left[\frac{1 - \bar{u} \cdot \frac{\dot{\bar{r}}_V}{c}}{1 - \bar{u} \cdot \frac{\dot{\bar{r}}_T}{c}} \right] \sqrt{\frac{1 - \frac{\dot{\bar{r}}_V \cdot \dot{\bar{r}}_V}{c^2}}{1 - \frac{\dot{\bar{r}}_S \cdot \dot{\bar{r}}_S}{c^2}}} \left[\frac{1 - \bar{d} \cdot \frac{\dot{\bar{r}}_S}{c}}{1 - \bar{d} \cdot \frac{\dot{\bar{r}}_V}{c}} \right] \tag{A-9}$$

$$= \sqrt{\frac{1 - \frac{\dot{\bar{r}}_T \cdot \dot{\bar{r}}_T}{c^2}}{1 - \frac{\dot{\bar{r}}_S \cdot \dot{\bar{r}}_S}{c^2}}} \left[\frac{1 - \bar{u} \cdot \frac{\dot{\bar{r}}_V}{c}}{1 - \bar{u} \cdot \frac{\dot{\bar{r}}_T}{c}} \right] \left[\frac{1 - \bar{d} \cdot \frac{\dot{\bar{r}}_S}{c}}{1 - \bar{d} \cdot \frac{\dot{\bar{r}}_V}{c}} \right]$$

In this Equation,

$\bar{u} \triangleq \dfrac{\bar{r}_V - \bar{r}_T}{|\bar{r}_V - \bar{r}_T|}$ = the unit vector up along uplink path

$$\bar{d} \triangleq \frac{\bar{r}_S - \bar{r}_V}{|\bar{r}_S - \bar{r}_V|} = \text{the unit vector down along downlink path.}$$

The derivatives indicated in Equations (A-1), (A-8), and (A-9) are taken with respect to coordinate time. The frequency ratio on the left of Equation (A-9) may be related to the measurement data. The two-way Doppler-shifted frequency at any instant at the ground receive station is

$$\nu_d = \nu_S - \nu_T = \nu_T \left(\frac{\nu_S}{\nu_T} - 1 \right). \tag{A-10}$$

The Doppler count may be approximated as

$$N - \nu_b \, \Delta t_{RR} = \int_{t_S}^{t_S + \Delta t_{RR}} \nu_d \, d\tau = \nu_T \int_{t_S}^{t_S + \Delta t_{RR}} \left(\frac{\nu_S}{\nu_T} - 1 \right) d\tau. \tag{A-11}$$

The representation is approximate in the sense that the counter accumulates whole numbers, whereas the integral gives a continuously variable whole number plus fraction. For large count, N, this error becomes negligible.

The cycle count, N, and the bais frequency, ν_b, are fixed; the observation consists of the two quantities Δt_{RR} and t_S (see Section 2.2.1, Equation (2-3) and (2-4)). The integration time argument on the right side of Equation (A-11) is understood to correspond with the clock time or proper time at the ground receive station.

To evaluate the integral, Equation (A-9) is substituted into Equation (A-11). This relates the measured quantities to the station-to-vehicle geometry. The degree of analytical rigor in the representation is dependent upon the simplifying assumptions, if any, which must be made in the evaluation. Derivations are presented for two different representations. Both require that the expressions in Equation (A-9), which are rigorous within the limitations of special relativity, be simplified to the case where the intertial speed of the tracking station remains constant, i.e.

$$\dot{\bar{r}}_T \cdot \dot{\bar{r}}_T = \dot{\bar{r}}_S \cdot \dot{\bar{r}}_S. \tag{A-12}$$

This condition is satisfied when spacecraft orbits can be computed with sufficient accuracy in an earth-centered coordinate system. In such an inertial frame, the tracking station speed is determined by the nearly constant rotation rate of the earth.

With this simplification, the derivation of the most rigorous solution proceeds from the following reduced form of Equation (A-9)

$$\frac{\nu_S}{\nu_T} = \left[\frac{1 - \bar{u} \cdot \frac{\dot{\bar{r}}_V}{c}}{1 - \bar{u} \cdot \frac{\dot{\bar{r}}_T}{c}}\right] \left[\frac{1 - \bar{d} \cdot \frac{\dot{\bar{r}}_S}{c}}{1 - \bar{d} \cdot \frac{\dot{\bar{r}}_V}{c}}\right]. \tag{A-13}$$

The geometry of the uplink and downlink ranges are related to the light times according to

$$\rho_u \triangleq |\bar{r}_V - \bar{r}_T| = c\,(t_V - t_T) \tag{A-14}$$

and

$$\rho_d \triangleq |\bar{r}_S - \bar{r}_V| = c\,(t_S - t_V). \tag{A-15}$$

The derivatives of these ranges with respect to coordinate time changes at the receiver are

$$\frac{d\,\rho_u}{d\,t_S} = \bar{u} \cdot \left(\dot{\bar{r}}_V \frac{dt_V}{dt_S} - \dot{\bar{r}}_T \frac{dt_T}{dt_S}\right) = c\left(\frac{dt_V}{dt_S} - \frac{dt_T}{dt_S}\right) \tag{A-16}$$

$$\frac{d\,\rho_d}{d\,t_S} = \bar{d} \cdot \left(\dot{\bar{r}}_S - \dot{\bar{r}}_V \frac{dt_V}{dt_S}\right) = c\left(1 - \frac{dt_V}{dt_S}\right). \tag{A-17}$$

Explicit solution for the coordinate time derivatives gives

$$\left.\begin{aligned} \frac{d\,t_V}{d\,t_S} &= \frac{1 - \bar{d}\cdot\frac{\dot{\bar{r}}_S}{c}}{1 - \bar{d}\cdot\frac{\dot{\bar{r}}_V}{c}} = 1 - \frac{1}{c}\,\frac{d\,\rho_d}{d\,t_S} \\ \frac{d\,t_T}{d\,t_S} &= \frac{1 - \bar{u}\cdot\frac{\bar{r}_V}{c}}{1 - \bar{u}\cdot\frac{\dot{\bar{r}}_T}{c}}\left(\frac{d\,t_V}{d\,t_S}\right) = 1 - \frac{1}{c}\left(\frac{d\,\rho_d}{d\,t_S} + \frac{d\,\rho_u}{d\,t_S}\right). \end{aligned}\right\} \qquad \text{(A-18)}$$

Equations (A-18) show that a coordinate time increment of given length at the receive station corresponds to increments of different lengths at the spacecraft and the transmitter, considering the arrivals of photons tagged at t_T and $t_T + dt_T$ to mark the interval.

Substituting the second of Equations (A-18) into Equation (A-13) and this result into Equation (A-11) yields

$$N - \nu_b\,\Delta\,t_{RR} = -\frac{\nu_T}{c}\int_{t_S}^{t_S + \Delta t_{RR}}\left(\frac{d\,\rho_d}{d\,t_S} + \frac{d\,\rho_u}{d\,t_S}\right) d\,\tau. \qquad \text{(A-19)}$$

At the receiving station, the relationship between coordinate and proper time is

$$d\,\tau_S = \sqrt{1 - \frac{\dot{\bar{r}}_S\cdot\dot{\bar{r}}_S}{c^2}}\;d\,t_S. \qquad \text{(A-20)}$$

Therefore

$$\frac{d\,\rho}{d\,t_S} = \frac{d\,\rho}{d\,\tau_S}\sqrt{1 - \frac{\dot{\bar{r}}_S\cdot\dot{\bar{r}}_S}{c^2}} \qquad \text{(A-21)}$$

and, recalling that we have assumed $\dot{\bar{r}}_S \cdot \dot{\bar{r}}_S$ = constant, Equation (A-19) becomes

$$N - \nu_b \Delta t_{RR} = -\frac{\nu_T}{c}\sqrt{1 - \frac{\dot{\bar{r}}_S \cdot \dot{\bar{r}}_S}{c^2}} \left\{ \int_{\rho_u(t_S)}^{\rho_u(t_S + \Delta t_{RR})} d\rho_u + \int_{\rho_d(t_S)}^{\rho_d(t_s + \Delta t_{RR})} d\rho_d \right\} \tag{A-22}$$

$$= -\frac{\nu_T}{c}\sqrt{1 - \frac{\dot{\bar{r}}_S \cdot \dot{\bar{r}}_S}{c^2}}\, \Delta\rho$$

where

$$\Delta\rho \triangleq (\rho_u + \rho_d)_{t_S + \Delta t_{RR}} - (\rho_u + \rho_d)_{t_S} \tag{A-23}$$

Equation (A-22) is the rigorous form of the range-difference Doppler equation. The only restrictive assumptions made in its derivation were

- Special relativity
- Constant tracking station inertial speed.

Since $|\dot{\bar{r}}_S|$ is bounded by 500 meters/second, the contribution of the radical

$$\frac{\dot{\bar{r}}_S \cdot \dot{\bar{r}}_S}{2c^2} < \frac{1}{2}\left(\frac{500}{3 \times 10^8}\right)^2 = 1.4 \times 10^{-12}$$

is insignificant compared with the instrumentation precision. If it is neglected, the more familiar form of the range-difference formula results. The data preprocessor calculation for this case is obtained by solving Equation (A-22) explicitly for the observed value (designated by the subscript 0)

$$\Delta\rho_0 = \frac{c}{\nu_T}(\nu_b \Delta t_{RR} - N). \tag{A-24}$$

The observation components to be passed to the processor in the GTDS are $\Delta\rho_0$, Δt_{RR}, and t_S.

The second method for representing the Doppler observable involves going back to Equation (A-9) and assuming that the tracking station motion is uniform in inertial space. Thus

$$\dot{\bar{r}}_S = \dot{\bar{r}}_T = \text{constant (inertially)} \tag{A-25}$$

and the coordinate system may be considered to be fixed at the tracking station and moving with it (so that $\dot{\bar{r}}_S = \dot{\bar{r}}_T = 0$). In this case, $\bar{u} = -\bar{d}$ and Equation (A-9) becomes

$$\frac{\nu_S}{\nu_T} = \frac{1 - \bar{u} \cdot \frac{\dot{\bar{r}}_V}{c}}{1 + \bar{u} \cdot \frac{\dot{\bar{r}}_V}{c}} . \tag{A-26}$$

Since the tracking station is motionless in this coordinate frame, the unit vector $\bar{u}$ may be defined in terms of the instantaneous relative position vector

$$\bar{u} = \frac{\bar{r}_V (t_V) - \bar{r}_S (t_V)}{|\bar{r}_V (t_V) - \bar{r}_S (t_V)|} \tag{A-27}$$

at the vehicle turnaround time t_V. The instantaneous relative range at this time is

$$\rho = |\bar{r}_V (t_V) - \bar{r}_S (t_V)| \tag{A-28}$$

and the rate of change with coordinate time is

$$\dot{\rho} = \bar{u} \cdot \dot{\bar{r}}_V . \tag{A-29}$$

If this is substituted into Equation (A-26) and that result is substituted into Equation (A-11), the following is obtained

$$N - \nu_b \Delta t_{RR} = - 2 \nu_T \int_{t_S}^{t_S + \Delta t_{RR}} \frac{\dot{\rho}}{c + \dot{\rho}} \, d\tau . \tag{A-30}$$

Applying the Theorem of the Mean gives

$$N - \nu_b \Delta t_{RR} = -2 \nu_T \left(\frac{\dot{\rho}}{c + \dot{\rho}} \right)_{avg} \Delta t_{RR}. \tag{A-31}$$

Writing $\dot{\rho}_{avg}$ for the value of range-rate which produces the correct average value in this equation and solving explicitly for $\dot{\rho}_{avg}$ gives

$$\dot{\rho}_{avg} = \frac{c \left(\nu_b - \frac{N}{\Delta t_{RR}} \right)}{2 \nu_T - \left(\nu_b - \frac{N}{\Delta t_{RR}} \right)}. \tag{A-32}$$

This equation is the form in current use in the preprocessing of Doppler data (Reference 2, 3, 4, 5, and 6).

This metric observation is time-tagged at the midpoint of the vehicle turnaround-time increment, Δt_V, corresponding to the receiving station count interval Δt_{RR}. The relationship between Δt_V and Δt_{RR} can be obtained from the first of Equations (A-18), by the approximation

$$\dot{\rho}_{avg} = \frac{d \rho_d}{d t_S} \tag{A-33}$$

and by substituting Equation (A-32) for $\dot{\rho}_{avg}$

$$\frac{d t_V}{d t_S} = \frac{\nu_T - \left(\nu_b - \frac{N}{\Delta t_{RR}} \right)}{\nu_T - \frac{1}{2} \left(\nu_b - \frac{N}{\Delta t_{RR}} \right)} = \frac{\Delta t_V}{\Delta t_{RR}}. \tag{A-34}$$

The time tag, therefore, is approximately equal to

$$\begin{aligned} t_{RR} &= t_S - \Delta t_R + \frac{\Delta t_V}{2} \\ &= t_S - \Delta t_R + \left[\frac{\nu_T - \nu_b + \frac{N}{\Delta t_{RR}}}{2 \nu_T - \nu_b + \frac{N}{\Delta t_{RR}}} \right] \Delta t_{RR} \end{aligned} \tag{A-35}$$

where

$t_S \sim$ data sample time, given by Equation (2-3)

$\Delta t_R \sim$ one-way light time (Equation (2-9)) for the range sample corresponding to this range-rate sample.

$\nu_T \sim$ transmitter reference or carrier frequency

$b \sim$ bias frequency

$N \sim$ fixed Doppler-plus-bias cycle count

$\Delta t_{RR} \sim$ Doppler-plus-bias count-time increment, given by Equation (2-6).

It is important to emphasize the nature of the average value given by Equation (A-32). Although it is usually interpreted as the average value of the range-rate over the counting interval, the derivation of Equation (A-32) clearly demonstrates that it defines a value of $\dot{\rho}$ which gives the correct average value (in the sense of the Theorem of the Mean) of the quantity

$$\frac{\dot{\rho}}{c + \dot{\rho}} \approx \frac{\dot{\rho}}{c} - \left(\frac{\dot{\rho}}{c}\right)^2. \tag{A-36}$$

For a range-rate of 10^4 meters/second, a value which may be exceeded at a trans-lunar or interplanetary trajectory insertion, the second order term above is approximately

$$\left(\frac{10^4}{3 \times 10^8}\right)^2 \approx 1.1 \times 10^{-9}.$$

This corresponds to a difference of about 0.3 meter/second between the range-rate given by Equation (A-32) and the integrand which this value averages. This does not mean that the range-rate value computed by this equation is in error by 0.3 meter/second in this instance. It merely means that the value obtained corresponds to that required to average a quantity different from itself by 0.3 meter/second. Clearly, in the hypothetical case where the range-rate is constant over the count interval, there would be no difference between the quantity computed by Equation (A-32) and the correct average range-rate (a constant). However, when the range-rate is variable over the count interval, as is actually the case, the value produced by Equation (A-32) differs from the averaged range-rate.

A true assessment of the error must be calculated by updating the analysis of Reference 7. In that source, the error was estimated between the true instantaneous range-rate at the midpoint of the vehicle turnaround interval, Δt_v, and the mean value of the range-rate integrated over the same interval and divided by Δt_v. This type of analysis was aimed at determination of the error committed by arbitrarily time-tagging the mean value at the midpoint of the 0.5 meter/second. Since the discrepancy between the mean value and the midpoint value depend upon the function being integrated, the analysis of Reference 7 should be updated by evaluating this difference for the function

$$\frac{\dot{\rho}}{c + \dot{\rho}}$$

with the same orbital geometry used before.

REFERENCES

1. Computer Sciences Corporation, Mathematical Modeling of Radar Tracking Observations of Spacecraft, D. H. Novak, January 1971.

2. Goddard Space Flight Center, X-551-69-137, A Review of Goddard Range and Range Rate System Measurements and Data Processing Techniques, T. J. Grenchik and F. H. Putney, April 1969.

3. Goddard Space Flight Center, X-551-69-3, The Conversion of Fundamental Tracking Data to Metric Form, P. E. Schmid, January 1969.

4. Goddard Space Flight Center, X-541-69-322, Description of the Goddard Range-Range Rate Data Processing Program for the CDC-160A, E. R. Watkins and D. H. Rose, August 1969.

5. Goddard Space Flight Center, X-571-69-149, Data Formats of the Goddard Range and Range Rate System and the Application Technological Satellite Range and Range Rate System, D. J. Zillig, April 1969.

6. Goddard Space Flight Center, X-551-70-212, The Conversion of Goddard Range and Range Rate TrackingData to Metric Units, J. F. Cook, June 1970.

7. Goddard Space Flight Center, X-513-65-100, The Range Rate Error Due to The Averaging Techniques of Doppler Measurements, B. Kruger, 5 March 1965.

APPENDIX B

THEORETICAL DISCUSSION OF LEAST-SQUARES ESTIMATION

The theory of least-squares estimation may be viewed in two different though complementary ways. From one view, it is a numerical procedure for operating on observational data to arrive at an estimate of a parameter. This aspect of least-squares estimation has its own difficulties, mainly the convergence of iterative procedures and the numerical problems involved in the inversion of large matrices. But these difficulties though frequently intractible are comprehensible to individuals interested in the application of least-squares estimation to orbit determination.

From the other view of least-squares estimation, the numerical procedure, or algorithm, used to obtain the least-squares estimate of a parameter defines a random variable whose probability structure must be defined in some way. It is this probabilistic or statistical aspect of the theory which causes confusion in applications. In order to avoid this confusion, it is necessary to understand the assumptions invoked in the derivation of the statistics associated with the least squares estimator. In what follows, the usual formulas are derived for the statistics of the least-squares estimator. But it is necessary to clarify the nature of the various assumptions utilized in the derivations. The best way to clarify these points is to present the theory of least-squares estimation in a context more general than that supplied by the orbit determination problem. This is the approach used within this Appendix. The specific application of the theory to the orbit determination problem is discussed in Chapter 8.

B.1 DERIVATION OF THE LEAST-SQUARES ESTIMATOR AND ITS ASSOCIATED COVARIANCE MATRIX

Let $\tilde{x}$ be a real-valued vector representing a physical state. Let $\tilde{y}$ be another real-valued vector representing a state which in some way is directly observable. Furthermore, supposed that $\tilde{y}$ is functionally related to $\tilde{x}$ by means of a known vector function, $\bar{f}$, thus $\tilde{y} = \bar{f}(\tilde{x})$. Although $\tilde{y}$ is directly observable, assume that the observation process is inherently imperfect and that the imperfection cannot be conveniently modeled in a deterministic way. As such, the imperfection in the observation is modeled as a random vector $\bar{n}$ whose dimension is the same as that of $\tilde{y}$. The random vector $\bar{n}$ is frequently

referred to as the noise on the observation of $\tilde{y}$, and the observation process is said to yield a valuation of the random vector $\tilde{y} + \bar{n}$ ("true" plus "noise"). The only assumption on the probabilistic structure of $\bar{n}$ is that the covarinace matrix P_n of $\bar{n}$ is known. It is also assumed that a valuation of another random vector, $\bar{U}$, is available, whose dimension is the same as that of $\tilde{x}$, whose expectation is equal to $\tilde{x}$, and whose covariance $P_{\Delta_{x_0}}$ is known. The random vector $\bar{U}$ is then by definition and unbiased estimator of $\tilde{x}$. In this appendix, a valuation of $\bar{U}$ is called an a-priori estimate of $\tilde{x}$. The problem to be solved may now be formulated. Given one valuation of the random vector $\tilde{y} + \bar{n}$, which is designated by the symbol $\bar{y}$, and one valuation of the random vector $\bar{U}$, which is designated by the symbol $\bar{x}_0$, a best estimate of x is sought.

It is necessary to clarify in what "best" sense $\tilde{x}$ is to be estimated. The approach taken is to define a so-called loss function Q, with the argument of Q a variable vector $\bar{x}$ whose dimension is the same as that of $\tilde{x}$. The loss function is a measure of how well the observations $\bar{y}$ and the a-priori estimate $\bar{x}_0$ fit our mathematical model if the variable $\bar{x}$ is assumed to be $\tilde{x}$. The value of $\bar{x}$ which minimizes Q is then, according to our criteria, the estimate of $\tilde{x}$ which best fits the data. The loss function is the weighted sum of the squares of the differences between the actual observations, $\bar{y}$ and $\bar{f}(\bar{x})$, and the weighted sum of the squares of the differences between $\bar{x}$ and the a-priori estimate. Using matrix formalism, the loss function Q may be defined as

$$Q(\bar{x}) = (\bar{f}(\bar{x}) - \bar{y})^T W (\bar{f}(\bar{x}) - \bar{y}) + (\bar{x} - \bar{x}_0)^T Z (\bar{x} - \bar{x}_0) \qquad \text{(B-1)}$$

where $[\bar{f}(x) - y]$ and $(\bar{x} - \bar{x}_0)$ are column vectors, and W and Z are positive definite matrices with the same dimensions as $\bar{y}$ and $\bar{x}$, respectively.

Thus, it can be seen that Q is a scalar-valued vector function. The weighting matrices, W and Z, permit ranking between various components of $\bar{y}$ and $\bar{x}_0$ in terms of the impact desired on the loss function and thus our best estimate of $\tilde{x}$. The natural procedure is to weight the various components in inverse proportion to their variances. If we define $W = P_n^{-1}$ and $Z = P_{\Delta_{x_0}}^{-1}$, the final form of the loss function is defined as

$$Q(\bar{x}) = (\bar{f}(\bar{x}) - \bar{y})^T P_n^{-1} (\bar{f}(\bar{x}) - \bar{y}) + (\bar{x} - \bar{x}_0)^T P_{\Delta_{x_0}}^{-1} (\bar{x} - \bar{x}_0) \qquad \text{(B-2)}$$

The least-squares estimate $\hat{x}$ of $\tilde{x}$ is defined as that value of $\bar{x}$ which minimizes the loss function of Equation (B-2). The question of the existence of this estimator is avoided except to say that in almost all practical applications it does exist.

A necessary condition for a value of $\bar{x}$ to be a minimum of Equation (B-2) is that it be a root of the first variation of the right side of Equation (B-2). Thus, the problem of finding the least squares estimate $\hat{x}$ of $\tilde{x}$ reduces to the problem of locating the proper root of the matrix equation

$$0 = F^T(\bar{x})\, P_n^{-1}\, (\bar{f}(\bar{x}) - \bar{y}) + P_{\Delta x_0}^{-1}\, (\bar{x} - \bar{x}_0) \tag{B-3}$$

where $F(\bar{x}) = d\bar{f}(\bar{x})/d\bar{x}$ (i.e., the $(i, j)^{th}$ element of $F(\bar{x})$ is the partial derivative of the i^{th} component of $\bar{f}(\bar{x})$ with respect to the j^{th} component of $\bar{x}$). If the state $\tilde{x}$ has p components, then Equation (B-3) represents a set of p generally nonlinear equations in p unknowns. A standard Newton-Raphson iterative procedure will suffice in most cases to solve this system numerically. To employ the method, one defines $\bar{x}_i = \bar{x}_0$ and linearizes the right side of Equation (B-3) about $\bar{x}_i$ and obtains the following estimate of $\hat{x}$

$$\hat{x} = \bar{x}_i - (F^T(\bar{x}_i)\, P_n^{-1}\, F(\bar{x}_i) + P_{\Delta x_0}^{-1})^{-1} \tag{B-4}$$

$$[F^T(\bar{x}_i)\, P_n^{-1}\, (\bar{f}(\bar{x}_i) - \bar{y}) + P_{\Delta x_0}^{-1}\, (\bar{x}_i - \bar{x}_0)]\,.$$

The value obtained on the left side of Equation (B-4) is then redefined as $\bar{x}_i$ and is again used to generate a new estimate of $\hat{x}$. If $\bar{x}_0$ is in a sufficiently close proximity to the minimum of Equation (B-2), this iterative procedure rapidly converges to the desired value. A criteria for convergence may be obtained by terminating the iterative procedure when the loss function of Equation (B-2) ceases to change by more than a certain percentage. For example, letting $\hat{x}_n$ be the n^{th} estimate of $\hat{x}$ obtained by the iterative procedure of Equation (B-4) and ϵ a number between zero and one, the iterative procedure can be terminated at the first value of n for which

$$0 < \left| \frac{Q(\hat{x}_{n-1}) - Q(\hat{x}_n)}{Q(\hat{x}_n)} \right| < \epsilon. \tag{B-5}$$

This criteria also terminates the procedure if divergence occurs. In this eventually, a new starting value should be located and the process begun again.

In evaluating the quality of the least-squares estimate $\hat{x}$ of $\tilde{x}$, two factors are usually considered. The first is the extent to which the estimator is biased. Viewing $\hat{x}$ now as a random variable, the bias is defined as

$$B = \mathcal{E}\ [\hat{x} - \tilde{x}]\ . \tag{B-6}$$

If B = 0, the least-squares estimator has the property of being unbiased, a very desirable quality in estimators. The other factor to be considered is the dispersion D of the estimator $\hat{x}$ about $\tilde{x}$. D is a square matrix defined as

$$D = \mathcal{E}\ [(\hat{x} - \tilde{x})\ (\hat{x} - \tilde{x})^T]\ . \tag{B-7}$$

Neither the bias nor the dispersion of the least-squares estimator may be readily calculated without the imposition of certain assumptions. First, assume that the expected value of the noise $\bar{n}$ is zero. This is an assumption of unbiasedness concerning the measurement of the observable state $\tilde{y}$. Second, assume that $\bar{f}$ can be represented by a linear expansion of itself about $\tilde{x}$, i.e.,

$$\bar{f}\ (\bar{x}) \approx \bar{f}\ (\tilde{x}) + F\ (\tilde{x})\ (\bar{x} - \tilde{x}). \tag{B-8}$$

If the root $\hat{x}$ of Equation (B-3) is sufficiently close to $\tilde{x}$ to permit the use of Equation (B-8), then Equation (B-3) may be written as

$$\begin{aligned} &F^T\ (\tilde{x})\ P_n^{-1}\ \bar{f}\ (\tilde{x}) + F^T\ (\tilde{x})\ P_n^{-1}\ F\ (\tilde{x})\ (\hat{x} - \tilde{x}) \\ &\qquad - F^T\ (\tilde{x})\ P_n^{-1}\ \bar{y} + P_{\Delta x_0}^{-1}\ (\hat{x} - \bar{x}_0) = 0 \end{aligned} \tag{B-9}$$

and solving Equation (B-9) for $\hat{x}$ yields

$$\hat{x} = (F^T(\tilde{x})\, P_n^{-1}\, F(\tilde{x}) + P_{\Delta x_0}^{-1})^{-1}\, F^T(\tilde{x})\, P_n^{-1}\, \bar{y} + (F^T(\tilde{x})\, P_n^{-1}\, F(\tilde{x}) + P_{\Delta x_0}^{-1})^{-1} P_{\Delta x_0}^{-1}\, \bar{x}_0$$

$$-(F^T(\tilde{x})\, P_n^{-1}\, F(\tilde{x}) + P_{\Delta x_0}^{-1})^{-1}\, F^T(\tilde{x})\, P_n^{-1}\, (\bar{f}(\tilde{x}) - F(\tilde{x})\, \tilde{x}). \qquad \text{(B-10)}$$

By reinterpretating symbols $\hat{x}$, $\bar{y}$, and $\bar{x}_0$ to mean random variables rather than valuations of random variables, Equation (B-10) becomes a relationship between random variables and the expectations of both sides can be equated

$$\begin{aligned} \mathcal{E}(\hat{x}) &= (F^T(\tilde{x})\, P_n^{-1}\, F(\tilde{x}) + P_{\Delta x_0}^{-1})^{-1}\, F^T(\tilde{x})\, P_n^{-1}\, \mathcal{E}(\bar{y}) \\ &+ (F^T(\tilde{x})\, P_n^{-1}\, F(\tilde{x}) + P_{\Delta x_0}^{-1})^{-1} P_{\Delta x_0}^{-1}\, \mathcal{E}(\bar{x}_0) \\ &- (F^T(\tilde{x})\, P_n^{-1}\, F(\tilde{x}) + P_{\Delta x_0}^{-1})^{-1}\, F^T(\tilde{x})\, P_n^{-1}\, (\bar{f}(\tilde{x}) - F(\tilde{x})\, \tilde{x}). \end{aligned} \qquad \text{(B-11)}$$

Since $= \mathcal{E}[\bar{f}(\tilde{x}) + \bar{n}] = \bar{f} = \bar{f}(\tilde{x}) + \mathcal{E}(\bar{n}) = \bar{f}(\tilde{x})$ and $\mathcal{E}(\bar{x}_0) = \tilde{x}$, we may write

$$\begin{aligned} \mathcal{E}(\hat{x}) &= (F^T(\tilde{x})\, P_n^{-1}\, F(\tilde{x}) + P_{\Delta x_0}^{-1})^{-1}\, F^T(\tilde{x})\, P_n^{-1}\, \bar{f}(\tilde{x}) \\ &+ (F^T(\tilde{x})\, P_n^{-1}\, F(\tilde{x}) + P_{\Delta x_0}^{-1})^{-1} P_{\Delta x_0}^{-1}\, \tilde{x} \\ &- (F^T(\tilde{x})\, P_n^{-1}\, F(\tilde{x}) + P_{\Delta x_0}^{-1})^{-1}\, F^T(\tilde{x})\, P_n^{-1}\, (\bar{f}(\tilde{x}) - F(\tilde{x})\, \tilde{x}) \\ &= (F^T(\tilde{x})\, P_n^{-1}\, F(\tilde{x}) + P_{\Delta x_0}^{-1})^{-1}\, (F^T(\tilde{x})\, P_n^{-1}\, F(\tilde{x}) + P_{\Delta x_0}^{-1})\, \tilde{x} \\ &= \tilde{x}. \end{aligned} \qquad \text{(B-12)}$$

Hence under the previously mentioned assumptions, the least-squares estimator is unbiased.

In the case of an unbiased estimator, the dispersion D of Equation (B-7) is the same as the covariance of the estimator. So the covariance of $\hat{x}$ is a measure of its dispersion. The further assumption is made that the random variables $\bar{y}$ and $\bar{x}_0$ are independent, i.e., assume that the a-priori information are obtained by a process which is in no way related to the observation process. Also notice that the covariance matrices of both $\bar{y}$ and $\bar{x}_0$ are

$$\begin{aligned} \operatorname{cov}(\bar{y}) &= \operatorname{cov}(\bar{n} + \bar{f}(\tilde{x})) = \operatorname{cov}(\bar{n}) = P_n \\ \operatorname{cov}(\bar{x}_0) &= P_{\Delta x_0}. \end{aligned} \tag{B-13}$$

Then by employing the following matrix substitutions

$$\begin{aligned} \phi_1 &= (F^T(\tilde{x}) P_n^{-1} F(\tilde{x}) + P_{\Delta x_0}^{-1})^{-1} F^T(\tilde{x}) P_n^{-1} \\ \phi_2 &= (F^T(\tilde{x}) P_n^{-1} F(\tilde{x}) + P_{\Delta x_0}^{-1})^{-1} P_{\Delta x_0}^{-1} \\ \phi_3 &= (F^T(\tilde{x}) P_n^{-1} F(\tilde{x}) + P_{\Delta x_0}^{-1})^{-1} (F^T(\tilde{x}) P_n^{-1} \bar{f}(\tilde{x}) - F(\tilde{x}) \tilde{x}). \end{aligned} \tag{B-14}$$

Equation (B-10) may be written as

$$\hat{x} = \phi_1 \bar{y} + \phi_2 \bar{x}_0 - \phi_3 \tag{B-15}$$

and since $\bar{x}_0$ and $\bar{y}$ are assumed independent

$$\operatorname{cov}(\hat{x}) = \phi_1 P_n \phi_1^T + \phi_2 P_{\Delta x_0} \phi_2^T. \tag{B-16}$$

Eliminating ϕ_1 and ϕ_2 from Equation (B-16) by means of the substitution of Equation (B-14) yields

$$\text{cov}\,(\hat{x}) = (F^T(\tilde{x})\,P_n^{-1}\,F(\tilde{x}) + P_{\Delta x_0}^{-1})^{-1}\,F^T(\tilde{x})\,P_n^{-1}\,F(\tilde{x})\,(F^T(\tilde{x})\,P_n^{-1}\,F(\tilde{x}) + P_{\Delta x_0}^{-1})^{-1}$$

$$+ (F^T(\tilde{x})\,P_n^{-1}\,F(\tilde{x}) + P_{\Delta x_0}^{-1})^{-1}\,P_{\Delta x_0}^{-1}\,(F^T(\tilde{x})\,P_n^{-1}\,F(\tilde{x}) + P_{\Delta x_0}^{-1})^{-1}$$

$$= (F^T(\tilde{x})\,P_n^{-1}\,F(\tilde{x}) + P_{\Delta x_0}^{-1})^{-1}\,(F^T(\tilde{x})\,P_n^{-1}\,F(\tilde{x}) + P_{\Delta x_0}^{-1})$$

$$(F^T(\tilde{x})\,P_n^{-1}\,F(\tilde{x}) + P_{\Delta x_0}^{-1})^{-1}$$

and therefore

$$\text{cov}\,(\hat{x}) = (F^T(\tilde{x})\,P_n^{-1}\,F(\tilde{x}) + P_{\Delta x_0}^{-1})^{-1} \tag{B-17}$$

The true state $\tilde{x}$ is never known. But according to the linearity assumption of Equation (B-8), $F(\tilde{x}) = F(\hat{x})$, where $\hat{x}$ now represents a valuation of the least-squares estimator obtained by the iterative procedure of Equation (B-4). Thus by Equation (B-17)

$$\text{cov}\,(\hat{x}) = (F^T(\hat{x})\,P_n^{-1}\,F(\hat{x}) + P_{\Delta x_0}^{-1})^{-1}. \tag{B-18}$$

B.2 ERROR ANALYSIS OF THE LEAST-SQUARES ESTIMATOR

The replacement of a parameter by a statistical estimate of the parameter involves an error. In the case of the least-squares estimate, a state, $\tilde{x}$, is replaced with its least-squares estimate, $\hat{x}$. It is frequently important to place statistical bounds on the size of this error. This forms regions about $\tilde{x}$, not necessarily spherical, in which, for example, 95% or 99% of the distribution of the least-squares estimator is to be found. The ability to form such critical regions often permits probabilities to be placed on the success of projects which involve least-squares estimates.

In some cases, these critical regions are easy to obtain. If it is assumed the observations are unbiased, the linearity assumption of Equation (B-5) is valid,

and the a-priori information is independent of the noise on the observations; then, Equations (B-12) and (B-18) provide the mean and covariance of the least-squares estimator. In general, the mean and covariance of a random variable do not serve to specify the distribution of the random variable. But if the above mentioned assumptions are true, then Equation (B-4) gives $\hat{x}$ as a linear function of $\bar{y}$ and $\bar{x}_0$. If the further assumption is made that $\bar{y}$ and $\bar{x}_0$ as random variables are distributed in a multivariate normal fashion, then $\hat{x}$ as a linear function of multivariate normal random variables is also a multivariate normal random variable.

In this case, its mean and covariance, as given by Equations (B-12) and (B-18), specify the distribution of $\hat{x}$. According to Equation (B-12) $\mathcal{E}(\hat{x}) = \tilde{x}$. It is therefore, not difficult to construct critical regions about $\tilde{x}$. The first step in the procedure is to obtain the covariance matrix, P_{Δ_x}, of $\hat{x}$ given by Equation (B-18). If P_{Δ_x} is nondiagonal, then the elements of $\hat{x}$, as randum variables, are correlated. This correlation introduces difficulties in constructing critical regions. The difficulty is corrected by multiplying $\hat{x}$ by an orthogonal matrix S to obtain a new random variable $\bar{z} = S\hat{x}$. The covariance matrix P_{Δ_z} of $\bar{z}$ is given by

$$P_{\Delta_z} = S\, P_{\Delta_x}\, S^T \tag{B-19}$$

It is possible to choose S so that P_{Δ_z} is a diagonal matrix. There are many computer programs which provide the matrix S which diagonalizes a positive definite matrix, P_{Δ_x}, and which also provides the values along the resultant diagonal matrix. These are called the eigenvalues of P_{Δ_x}. Since $\bar{z}$ is an uncorrelated, random variable, it is easy to construct p-dimensional rectangular critical regions for $\bar{z}$. Suppose a confidence level of q, where $0 < q < 1$, is desired. The goal then is to construct a critical region A in a p-dimensional space such that the probability density function of $\bar{z}$ when integrated over A equals q. Corresponding to any confidence level q, there exists a critical value α_q such that the probability density function of the standard normal random variable when integrated between $-\alpha_q$ and α_q provides a value of q. The value α_q for any q may be found in any table of critical values of the standard normal random variable. Let $\sigma^2_{\Delta_{zi}}$ be the i^{th} diagonal element of the diagonal matrix P_{Δ_z} and let $R = q^{1/p}$ where q is the confidence level for which we wish to construct a critical region. Then the hyperrectangle defined as the set of p-tuples $(x_1, x_2, \ldots x_p)$ such that for all $0 < i \leq p$

$$-\alpha_R \sqrt{\sigma_{\Delta_{zi}}} \leq x_i \leq \alpha_R \sqrt{\sigma_{\Delta_{zi}}} \tag{B-20}$$

is the critical region for $\bar{z}$ corresponding to q. The inverse image of A, under the transformation defined by the matrix S, is another hyperrectangle A' and the probability of the random variable $\hat{x} - \tilde{x}$ having a valuation in A' is q.

The above outlined procedure for constructing critical regions of the least-squares estimator is easy to implement but does not always lead to correct answers. The reason is that the assumptions on which the procedure rests are not always satisfied. The assumption that the measurement process is unbiased implies that all significant systematic errors have been eliminated in the observations. If significant errors occur in the measurement process and if these errors introduce a significant bias in the observations, then no estimation procedure is likely to yield accurate results. Hence, nothing appears to be lost in the assumption of unbiased measurements. The assumption of normality also has more to recommend it than just mathematical convenience. The justification for modeling the random component of the observations, $\bar{n}$, and the random variable, $\bar{U}$, as multivariate normal rests on the vague meta-statistical analogue to the central limit theorem. This analogue may be stated as follows: "If a large number of random variables are combined in a reasonably complicated fashion to form a single multivariate random variable, then this random variable will have a nearly normal distribution." The assumptions of this meta-statistical principle are frequently satisfied when observations are made in nature. Thus, the assumption, that $\bar{n}$ and $\bar{U}$ are normally distributed has at least some support. Also, the assumption that $\bar{n}$ and $\bar{U}$ are independent is usually satisfied in the application of least-squares estimation. The linearity implied by Equation (B-8) is more difficult to justify. From a probabilistic point of view, an assumption is made that a significant portion of the distribution of $\hat{x}$ is in a region of $\tilde{x}$ in which the linear expansion of $\bar{f}$ given in Equation (B-8) is valid. The validity of this assumption is related both to the statistical spread of $\hat{x}$ and to the degree of nonlinearity of $\bar{f}$ around the point $\tilde{x}$. Consequently, it is very difficult to decide beforehand when the assumption will be satisfied. An application of Equations (B-12) and (B-18) is not permissible in answering these questions since this would involve a circularity. This linearity assumption is the weak point in the simple error analysis procedure outlined above.

B.3 THE AUGMENTED STATE VECTOR AND THE CONSIDER OPTION

In the least-squares estimation procedure, consideration is given to a state $\tilde{x}$, which is to be estimated, and another state $\tilde{y}$ called the observation state, which is observed directly. It is also assumed that a deterministic vector function, $\bar{f}$, exists such that $\tilde{y} = \bar{f}(\tilde{x})$. The function $\bar{f}$ may be given in closed form or as a computational algorithm, but in physical applications the representation of $\bar{f}$ generally contains physical parameters such as the speed of light, the radius of

the earth, or perhaps just the reading of a voltage on a voltmeter. No physical parameter is known perfectly and it may happen that the functional relationship between $\tilde{x}$ and $\tilde{y}$ contains parameters with which are associated significant uncertainties. Since no provision exsits for modeling uncertainty or randomness in the function, $\bar{f}$, there appears to be no way for permitting these uncertainties to have an impact on our estimation procedure. Yet, these uncertainties should have a negative impact on the quality of the least-squares estimator in the way that they should cause a widening of the distribution of the estimator. Thus, to ignore the uncertainties in these parameters would give a falsely optimistic picture of the quality of the least-squares estimator. There are two options at our disposal for removing this false optimism. As usual, both have their advantages and disadvantages.

The first option involves an augmentation of the estimated state vector. This solution to the problem is straightforward, easy to understand, and mathematically rigorous. But at times, it offers numerical difficulties which are quite serious. In essence, it involves a redefinition of the function $\bar{f}$ so that the parameters in $\bar{f}$ with which are associates significant uncertainties are treated as arguments of $\bar{f}$ rather than parameters. They become part of the state vector $\tilde{x}$. The least-squares estimation technique may then proceed in the usual fashion with the state $\tilde{x}$ augmented to include these certain parameters. An improved estimate of these parameters is obtained in the process, and the covariance matrix of Equation (B-18) reflects the impact of the uncertainties of the parameters on the least-squares estimate of elements of the unaugmented state $\tilde{x}$.

To be more precise, suppose that $\tilde{x}_1$ is a state of dimension p and is to be estimated in the least-squares fashion from a set of observations $\bar{y}$. Assume that $\tilde{y} = \bar{f}(\tilde{x}_1)$, where $\tilde{y}$ is the true observation state and $\bar{f}$ is a vector function containing a set of q parameters. Also assume that there exists a random variable $\bar{U}_1$ of dimension p such that $\mathcal{E}(\bar{U}_1) = \tilde{x}_1$ and cov $(\bar{U}_1) = P_1$, where P_1 is a given covariance matrix. Let $\bar{x}_{10}$ be a valuation of $\bar{U}_1$ and let P_1 be the covariance of the random component of the observation vector. We postulate that the measurement process is unbiased and that the linearity condition of Equation (B-8) is valid. The least-squares estimate $\hat{x}_1$ of $\tilde{x}_1$ is by definition a root of the equation

$$0 = F_1^T(\bar{x}_1) P_n^{-1} (\bar{f}(\bar{x}_1) - \bar{y}) + P_1^{-1} (\bar{x}_1 - \bar{x}_{10}) \qquad \text{(B-21)}$$

and the covariance of this estimate is

$$\text{cov}(\hat{x}_1) = (F_1^T(\hat{x}_1) P_n^{-1} F_1(\hat{x}_1) + P_1^{-1})^{-1} \qquad \text{(B-22)}$$

where $F_1(\bar{x}) = d\bar{f}(\bar{x})/d\bar{x}$. The dimension of $F_1(\bar{x})$ is p by m, where m is the dimension of the observation state. If the q parameters used in the definition of $\bar{f}$ have significant uncertainties associated with their evaluation, then the above covariance matrix gives a falsely optimistic picture of the statistical spread of the least-squares estimate of $\tilde{x}$. To correct this, define a new state vector of dimension n = p + q as

$$\tilde{x} = \begin{bmatrix} \tilde{x}_1 \\ \tilde{x}_2 \end{bmatrix} \tag{B-23}$$

where the components of $\tilde{x}_2$ are the true valued of the q parameters used in $\bar{f}$. $\bar{f}$ is redefined at this point so that these parameters are viewed as arguments of $\bar{f}$ rather than as constants. The argument of $\bar{f}$ is then a n-dimensional vector rather than a p-dimensional vector. With this new definition of $\bar{f}$, we have $\tilde{y} = \bar{f}(\tilde{x})$. The goal now is to obtain a least-squares estimate of the augmented state vector $\tilde{x}$. To do this assume the existence of a random variable $\bar{U}$ of dimension n, such that $\mathcal{E}(\bar{U}) = \tilde{x}$ and cov $(\bar{U}) = P_{\Delta x_0}$, where P is a known covariance matrix. Let $\bar{x}_0$ be a valuation of $\bar{U}$. The assumption that there exists a valuation of $\bar{U}$ implies that we have the means to obtain an unbiased estimate of the parameters $\tilde{x}_2$ as well as $\tilde{x}_1$. It is also assumed that we possess not only the variances of our estimated of the q parameters but a full set of covariances between the parameters set estimates and the a-priori estimates of $\tilde{x}_1$. The least-squares estimate of $\hat{x}$ and $\tilde{x}$ may be obtained as the root of

$$0 = F^T(\bar{x}) P_n^{-1} (\bar{f}(\bar{x}) - \bar{y}) + P_{\Delta x_0}^{-1} (\bar{x} - \bar{x}_0) \tag{B-24}$$

where the F matrix is dimensioned c × m. The last q rows of F are the partial derivatives of $\bar{f}$ with respect to the q parameters now considered as arguments of $\bar{f}$. The covariance matrix of $\hat{x}$ is given by

$$\text{cov}(\hat{x}) = (F^T(\hat{x}) P_n^{-1} F(\hat{x}) + P_{\Delta x_0}^{-1})^{-1} \tag{B-25}$$

The p × q matrix, obtained by deleting the last q rows and columns from cov $(\hat{x})$, represents the covariance matrix of the marginal distribution of the least-squares estimate of $\hat{x}_1$. A covariance matrix so-obtained accurately reflects the negative effect of the uncertainties of the q parameters on the quality of the least-squares estimate of $\tilde{x}_1$. As a byproduct of this process, the last q components of $\hat{x}$ are obtained as a least-squares estimate of the parameters $\tilde{x}_2$.

In some cases, this is not a byproduct at all but the main reason for augmenting the state vector $\tilde{x}$.

If the only interest is in obtaining an accurate representation of the covariance of the least-squares estimate of $\tilde{x}_1$, then the augmented state vector approach has an obvious disadvantage; namely work is expended in obtaining information in which there is no interest. For instance, a least squares estimate of each of the q added parameters is obtained though it may not be required. This complicates the iterative process implied by Equation (B-4) for it forces a $n \times n$ matrix to be inverted in each step of the iterative process instead of only a $p \times p$ matrix. This increase in the dimension of the matrix, which must be inverted, may cause prohibitive numerical difficulties. Also, only a certain portion of the covariance matrix of the least-squares estimate of the augmented state $\tilde{x}$ is of interest. The rest is discarded. This suggests that augmenting the state vector $\bar{x}_1$ may, in some cases, be an inefficient procedure.

There is a way of considering the impact of uncertainties of the $\tilde{x}_2$ parameters on the distribution of the least-squares estimate $\hat{x}_1$ without solving for these parameters in a least-squares sense and without increasing the dimension of the matrix which must be inverted. The strategy is to utilize a linearity assumption in order to explicitly represent the least-squares estimate, $\hat{x}_1$, as a function of the a-priori estimate, $\bar{x}_{20}$, of the unsolved parameters $\tilde{x}_2$. Then viewing this least-squares estimate, $\hat{x}_1$, as a random variable permits the uncertainty in the a-priori estimate of $\tilde{x}_2$ to have its proper impact on the covariance matrix of $\hat{x}_1$.

Again, let P_1 be the covariance matrix of the a-priori estimate $\bar{x}_{10}$ of $\tilde{x}_1$ and let P_2 be the covariance matrix of the a-priori estimated $\bar{x}_{20}$ of the considered parameters $\tilde{x}_2$. The observation vector y is a function of both $\tilde{x}_1$ and $\tilde{x}_2$. Thus, we write $\bar{y} = \bar{f}(\tilde{x}_1, \tilde{x}_2) + \bar{n}$ where, as usual, $\bar{n}$ is the noise inherent in the observation process. It is necessary to impose a linearity assumption. Assume that

$$\bar{f}(\bar{x}_1, \bar{x}_2) = \bar{f}(\tilde{x}_1, \tilde{x}_2) + F_1(\bar{x}_1 - \tilde{x}_1) + F_2(\bar{x}_2 - \tilde{x}_2) \qquad \text{(B-26)}$$

where

F_1 represents a matrix of partial derivatives of the elements of the observations state with respect to the solved-for parameters $\tilde{x}_1$.

F_2 represents a matrix of partial derivatives of the elements of the observation state with respect to the considered parameters $\tilde{x}_2$. The weighted least squares estimate $\hat{x}_1$ of $\tilde{x}_1$ is defined as that value of $\bar{x}_1$ which minimizes the loss function

$$Q(\bar{x}_1) = (\bar{f}(\bar{x}_1, \bar{x}_{20}) - \bar{y})^T P_n^{-1} (\bar{f}(\bar{x}_1, \bar{x}_{20}) - \bar{y}) + (\bar{x}_1 - \bar{x}_{10})^T P_1^{-1} (\bar{x}_1 - \bar{x}_{10}). \quad \text{(B-27)}$$

By obtaining the first variation of Equation (B-27), setting it equal to zero, and imposing linearity condition in Equation (B-26), the least-squares estimate $\hat{x}_1$ of $\tilde{x}_1$ is obtained

$$\begin{aligned} \hat{x}_1 = {} & (F_1^T P_n^{-1} F_1 + P_1^{-1})^{-1} F_1^T P_n^{-1} \bar{y} + (F_1^T P_n^{-1} F_1 + P_1^{-1})^{-1} P_1^{-1} \bar{x}_{10} \\ & + (F_1^T P_n^{-1} F_1 + P_1^{-1})^{-1} F_1^T P_n^{-1} F_2 (\bar{x}_{20} - \tilde{x}_2) \\ & - (F_1^T P_n^{-1} F_1 + P_1^{-1}) F_1^T P_n^{-1} (\bar{f}(\tilde{x}_1, \tilde{x}_2) - F_1 \tilde{x}_1). \end{aligned} \quad \text{(B-28)}$$

By reinterpreting symbols $\hat{x}_1$, $\bar{y}$, $\bar{x}_{10}$, and $\bar{x}_{20}$ as random variables rather than valuations of random variables, Equation (B-28) becomes a relationship among random variables; and the covariance of $\hat{x}_1$ may be obtained from knowledge of the covariances of $\bar{y}$, $\bar{x}_{10}$, and $\bar{x}_{20}$. In this way, the uncertainty in the a-priori estimate $\bar{x}_{20}$ of $\tilde{x}_2$ is acknowledged and permitted to have its proper influence on the covariance of $\hat{x}_1$. We introduce the following symbols

$$\begin{aligned} \phi_1 &= (F_1^T P_n^{-1} F_1 + P_1^{-1})^{-1} F_1^T P_n^{-1} \\ \phi_2 &= (F_1^T P_n^{-1} F_1 + P_1^{-1})^{-1} P_1^{-1} \\ \phi_3 &= (F_1^T P_n^{-1} F_1 + P_1^{-1})^{-1} F_1^T P_n^{-1} F_2 \\ \phi_4 &= -(F_1^T P_n^{-1} F_1 + P_1^{-1})^{-1} F_1^T P_n^{-1} (\bar{f}(\tilde{x}_1, \tilde{x}_2) - F_1 \tilde{x}_1). \end{aligned} \quad \text{(B-29)}$$

Equation (B-28) may now be written

$$\hat{x}_1 = \phi_1 \bar{y} + \phi_2 \bar{x}_{10} + \phi_3 (\bar{x}_{20} - \tilde{x}_2) + \phi_4. \tag{B-30}$$

Now, assume that the random variables $\bar{y}$, $\bar{x}_{10}$, and $\bar{x}_{20}$ are mutually independent, then the covariance of $\hat{x}_1$ may be obtained as

$$\text{cov}(\hat{x}_1) = \phi_1 \text{ cov}(\bar{y})\, \phi_1^T + \phi_2 \text{ cov}(\bar{x}_{10}) \phi_2^T + \phi_3 \text{ cov}(\bar{x}_{20}) \phi_3^T. \tag{B-31}$$

Since cov $(\bar{y}) = P_n$, cov $(\bar{x}_{10}) = P_1$, and cov $(\bar{x}_{20}) = P_2$, eliminate ϕ_1, ϕ_2, and ϕ_3 from Equation (B-31) to obtain

$$\text{cov}(\hat{x}_1) = (F_1^T P_n^{-1} F_1 + P_1^{-1})^{-1} \left[I + F_1^T P_n^{-1} F_2 P_2 F_2^T P_n^{-1} F_1 (F_1^T P_n^{-1} F_1 + P_1^{-1})^{-1} \right]. \tag{B-32}$$

If the certainties in the consider parameters were ignored ($P_2 = 0$), then Equation (B-18) would yield the covariance of $\hat{x}_1$ as

$$\text{cov}(\hat{x}_1) = (F_1^T P_n^{-1} F_1 + P_1^{-1})^{-1} = \phi \tag{B-33}$$

where the minus sign used as an upper right hand superscript implies the ignoring of uncertainties in the considered parameters. Let the symbol ϕ^+ represent the covariance of $\hat{x}_1$ with the uncertainties properly considered. Then, Equation (B-32) may be written (see Equation 8-39)

$$\phi^+ = \phi^- \left[I + F_1^T P_n^{-1} F_2 P_2 F_2^T P_n^{-1} F_1 \phi^- \right]. \tag{B-34}$$

Equation (B-34) represents a convenient formula for correcting the covariance of a least-squares estimate in order to properly reflect uncertainties in parameters which have not been solved.

B.4 RECURSIVE ESTIMATION

By using the weighted least-squares estimation procedure, we assume the possession of a m-dimensional observational vector $\bar{y}$ which is thought of as the sum of the true observation state $\tilde{\bar{y}}$ and zero mean noise $\bar{n}$ whose covariance is P_n. A known functional relationship $\bar{f}$ is assumed to exist between $\tilde{\bar{y}}$ and the state to be estimated, symbolized by $\tilde{\bar{x}}$. From this information and an unbiased estimate $\bar{x}_0$ of $\tilde{\bar{x}}$ and an a-priori covariance matrix $P_{\Delta x_0}$, a weighted least-squares estimate of $\tilde{\bar{x}}$ is obtained. Next, a useful variation of this procedure is discussed. Suppose the observation vector, $\bar{y}$, is expressed

$$\bar{y} = \begin{bmatrix} \bar{y}_1 \\ \bar{y}_2 \\ \cdot \\ \cdot \\ \cdot \\ \bar{y}_k \end{bmatrix} \tag{B-35}$$

where the vector $\bar{y}_i$ represents a set of observations of dimension n_i which are stochastically independent of observations represented by $\bar{y}_j$ of dimension n_j where $i \neq j$. An intuitively appealing approach now presents itself. We could process only the first stochastically independent set of observations $\bar{y}_1$ by the weighted least-squares process. The covariance matrix, P_{n1}, of $\bar{y}_1$ is obtained by deleting all but the first n_1 rows and columns of P_n. The functional relationship between $\tilde{\bar{y}}_1$ and $\tilde{\bar{x}}$ is readily obtained from the functional relationship $\bar{f}$ between $\tilde{\bar{y}}$ and $\tilde{\bar{x}}$ and is called $\bar{f}_1$. By imposing a linearity assumption on $\bar{f}_1$, similar to that of Equation (B-8), the weighted least-squares estimate $\hat{\bar{x}}_1$ of $\tilde{\bar{x}}$, obtained by processing the $\tilde{\bar{y}}_1$ measurements, may be written as

$$\hat{\bar{x}}_1 = \bar{x}_0 - (F_1^T(\bar{x}_0)\, P_{n1}^{-1}\, F_1(\bar{x}_0) + P_{\Delta x_0}^{-1})^{-1} (F_1^T(\bar{x}_0)\, P_{n1}^{-1} (\bar{f}_1(\bar{x}_0) - \bar{y}_1)) \tag{B-36}$$

where

$$F_1(\bar{x}) = d[\bar{f}_1(\bar{x})]/d\bar{x}.$$

The covariance matrix ϕ_1 of $\hat{\bar{x}}_1$, as a statistical estimate, may be written as

$$\phi_1 = (F_1^T(\hat{x}_0)\, P_{n1}^{-1}\, F_1(\hat{x}_1) + P_{\Delta x_0}^{-1})^{-1}. \tag{B-37}$$

The next step is to process the $\bar{y}_2$ measurements using the estimate $\hat{x}_1$ as an a-priori estimate and ϕ_1 as the a-priori statistics. This process is clearly recursive and may be repeated k times until all the observations in the observation vector $\bar{y}$ of Equation (B-35) are utilized. The measurement statistics P_{ni} used in the i^{th} recursion of this process is obtained by retaining only those rows and columns of P_n which contain the statistics of the y measurements. The functional relationship between $\tilde{y}_i$, the actual or true values of the $\bar{y}_i$ measurements, and $\tilde{x}$ is symbolized by $\bar{f}_i$. Thus, $\tilde{y}_i = \bar{f}_i(\tilde{x})$. The initial values of the recursion are given by the a-priori information. Let

$$\begin{aligned} \hat{x}_0 &= \bar{x}_0 \\ \phi_0 &= P_{\Delta x_0} \end{aligned} \tag{B-38}$$

An examination of Equation (B-36) and (B-37) provides the inductive steps of the recursion relation as

$$\hat{x}_{N+1} = \hat{x}_N - \phi_{N+1}\,(F_{N+1}^T(\hat{x}_N)\, P_{n_{N+1}}^{-1}\,(\bar{f}_{N+1}(\hat{x}_N) - \bar{y}_{N+1})) \tag{B-39}$$

where

$$F_{N+1}(\bar{x}) = d\,[\bar{f}_{N+1}(\bar{x})]/d\,\bar{x} \tag{B-40}$$

and

$$\phi_{N+1}^{-1} = F_{N+1}^T(\hat{x}_N)\, P_{n_{N+1}}^{-1}\, F_{N+1}(\hat{x}_N) + \phi_N^{-1}. \tag{B-41}$$

If for all i, $\bar{y}_i$ has dimension 1, then our recursive procedure represents a pointwise or sequential estimator, and no inversion of matrices is involved in the recursion relation of Equation (B-39). Unfortunately, the recursion relation of Equation (B-41), as it is now written, involved the inverting of a matrix whose dimension is the same as that of $\tilde{x}$. Since this is sometimes quite large, a numerical difficulty is presented. It is possible, however, to construct a recursive procedure which avoids this difficulty. Since $P_{n_{N+1}}$ is assumed to be positive definite, we may introduce a matrix $\beta_{N+1}(\bar{x})$ defined as

$$\beta^T_{N+1}(\bar{x}) = F^T_{N+1}(\bar{x})\, P^{-1/2}_{n_{N+1}} \tag{B-42}$$

Equation (B-41) may be written

$$\phi^{-1}_{N+1} = \beta^T_{N+1}(\hat{x}_N)\, \beta_{N+1}(\hat{x}_N) + \phi^{-1}_N. \tag{B-43}$$

By multiplying Equation (B-43) on the left by ϕ_{N+1} and on the right by ϕ_N, we obtain

$$\phi_N = \phi_{N+1} + \phi_{N+1}\, \beta^T_{N+1}(\hat{x}_N)\, \beta_{N+1}(\hat{x}_N)\, \phi_N. \tag{B-44}$$

With the aid of several matrix manipulations, Equation (B-44) can be solved for ϕ_{N+1} to obtain

$$\phi_{N+1} = \phi_N \left[I - \beta^T_{N+1}(\hat{x}_N) \left[\beta_{N+1}(\hat{x}_N)\, \phi_N\, \beta^T_{N+1}(\hat{x}_N) + I\right]^{-1} \beta_{N+1}(\hat{x}_N)\, \phi_N\right] \tag{B-45}$$

The matrix in the brackets of Equation (B-45) which must be inverted is of the same dimension as $\bar{y}_{N+1}$. If the estimation proceeds pointwise, then no matrix inversion is involved. In this case, Equation (B-45) may be written in a more convenient form. Let q_{N+1} be the variance of the noise on the N + 1 scalar observation $\bar{y}_{N+1}$ which is being processed at the $(N+1)^{st}$ step of the recursion procedure. Then, Equation (B-45) may be written

$$\phi_{N+1} = \phi_N \left(I - F^T_{N+1}(\hat{x}_N)\, q^{-1}_{N+1} \left[q^{-1}_{N+1} F_{N+1}(\hat{x}_N)\, \phi_N\, F^T_{N+1}(\hat{x}_N) + 1\right]^{-1} F_{N+1}(\hat{x}_N)\, \phi_N\right). \tag{B-46}$$

The following is a summation of the above results. Assume that the observation vector $\bar{y}$ may be written as

$$\bar{y} = \begin{bmatrix} \bar{y}_1 \\ \bar{y}_2 \\ \vdots \\ \bar{y}_k \end{bmatrix} \tag{B-47}$$

where

$y_i \sim$ a column vector of dimension n_i

and the noise on $\bar{y}_i$ is stocastically independent of the noise on $\bar{y}_j$, $j \neq i$. A recursive procedure is defined for estimating a state $\tilde{x}$. Write $\tilde{y} = \bar{f}(\tilde{x})$ where

$$\bar{f}(\tilde{x}) = \begin{bmatrix} \bar{f}_1(\tilde{x}) \\ \cdot \\ \cdot \\ \cdot \\ \bar{f}_k(\tilde{x}) \end{bmatrix} \tag{B-48}$$

The symbol $\bar{f}_i(\tilde{x})$ represents the true value of the observation vector $\bar{y}_i$ and $F_i(\bar{x}) = d\bar{f}_i(\bar{x})/d\bar{x}$.

The covariance matrix P_n of the random component of Y may be written as

$$P_n = \begin{bmatrix} P_{n1} & & & & \\ & P_{n2} & & & \\ & & \cdot & & \\ & & & \cdot & \\ & & & & P_{nk} \end{bmatrix} \tag{B-49}$$

where P_{ni} is an n_i-dimensional covariance matrix of the noise on the $\bar{y}_i$ observations. Given an unbiased estimate of $\bar{x}_0$ of $\tilde{x}$ with covariance $P_{\Delta x_0}$, the following set of recursion relationships define a procedure for processing this information in order to obtain the recursive form of the weighted least squares estimator of $\tilde{x}$.

$$\hat{x}_0 = \bar{x}_0 \tag{B-50a}$$

$$\phi_0 = P_{\Delta x_0} \tag{B-50b}$$

$$\beta_N^T(\bar{x}) = F_N^T(\bar{x})\, P_{n_N}^{1/2}, \qquad N \le k \tag{B-50c}$$

$$\phi_{N+1} = \phi_N \left[I - \beta_{N+1}^T(\hat{x}_N)\left[\beta_{N+1}\phi_N\beta_{N+1}^T(\hat{x}_N) + 1\right]^{-1}\beta_{N+1}(\hat{x}_N)\phi_N\right], \quad N \le k \tag{B-50d}$$

$$\hat{x}_{N+1} = \hat{x}_N - \phi_{N+1}\left(F_{N+1}^T(\hat{x}_N) P_{n_{N+1}}^{-1}\left(\bar{f}_{N+1}(\hat{x}_N) - \bar{y}_{N+1}\right)\right), \quad N \le k. \tag{B-50e}$$

If the estimation is pointwise, Equation (B-50d) may be written in the following form, with q_n representing the variance of the noise on the n^{th} observation

$$\phi_{N+1} = \phi_N\left(I - F_{N+1}^T(\hat{x}_N)\, q_{N+1}^{-1}\left[q_{N+1}^{-1} F_{N+1}(\hat{x}_N)\phi_N F_{N+1}^T(\hat{x}_N) + 1\right]^{-1} F_{N+1}(\hat{x}_N)\phi_N\right),$$

$$N \le k$$

The above defined recursive procedure coincides with the standard weighted least-squares estimator when the function $\bar{f}$, which relates the true state $\tilde{x}$ to the observations $\bar{y}$, is linear, or when the process is applied iteratively for nonlinear problems.

APPENDIX C

ANALYZING RESIDUALS OF AN ORBIT DETERMINATION PROCESS

The residuals of an orbit determination process are defined as the vector

$$\bar{R} = \bar{y} - \bar{f}(\hat{x}) \tag{C-1}$$

where

$\bar{y} \sim$ the measurement of the observation state, generally tracking data

$\bar{f} \sim$ a function relating the estimated state, x, to the observation state

$\hat{x} \sim$ the weighted least-squares best estimate of $\bar{x}$.

In the mathematical model for the weighted least-squares process it is assumed that the vector $\bar{y}$ is the sum of the true state $\tilde{y}$ and a realization of a random variable $\bar{n}$ thought to be the noise on the observations. Further assumptions are frequently made concerning the multivariate random variable $\bar{n}$. For instance, the imposition of certain numerical procedures in the weighted least-squares process depends on the assumption that the covariance matrix of the noise $\bar{n}$ is diagonal. The vector of residuals obtained by Equation (C-1) is not a realization of $\bar{n}$; but, loosely speaking, it is close enough to a realization of $\bar{n}$ to obtain inferences concerning the statistical structure of $\bar{n}$ from the statistical and sequential properties of $\bar{R}$.

In what follows, various statistical tests are discussed. These tests may be performed on a realization of a multivariate random variable permitting inferences concerning the random variable in question to be hypothesized. Algorithms for these tests are presented with the rigorous justification left to the references.

A random sequence of numbers is a sequence in which the particular values of the elements are not a function of their position in the sequence. A less precise definition of a random sequence of numbers is a sequence in which nothing deterministic is taking place. However, if statistical tests are to be developed on a rigorous basis, a considerably more precise definition of a random sequence must be given. To develop such a definition, assume that the i^{th} element of a given sequence is a valuation of a random variable, which is associated with a

C 6

probability density function $p_i(\bar{x})$. For present purposes, a sequence is assumed to be random if the valuations performed to form the sequence are independent; and furthermore, if for any valuations i and j, $p_i(\bar{x}) = p_j(\bar{x})$. This definition also implies that the multivariate random variable, of which the sequence is a realization, has a diagonal covariance matrix.

It should be clear that if this definition is satisfied, then no particular order in which the values of a random sequence present themselves is any more likely to have occurred than any other order. This notion that each permutation of a random sequence has the same probability of occurring is the basis of all the statistical tests for randomness which follow.

C.1 RUNS TESTS

Several tests for randomness in sequences are based on the concept of runs and on the probability density function which follows. Consider two sets A and B containing N_a and N_b elements, respectively. Let the elements of the sets form a sequence of $N_a + N_b$ points. Each maximal contiguous subsequence of elements of like kind in this sequence is called a run. The two types of runs must alternate. For example, letting the symbol "a" represent a number from a set A and the symbol "b" represent a number from a set B, the sequence

aababbaababb

contains eight runs. If it is assumed that each permutation of the $N_a + N_b$ elements is equally likely to occur, then the probability density function of the number of runs in the sequence u, in terms of binomial coefficients, is given by

$$p(u) = \frac{2\binom{N_a - 1}{\frac{u}{2} - 1}\binom{N_b - 1}{\frac{u}{2} - 1} N_a ! \, N_b !}{N !} \qquad \text{(C-2)}$$

for u an even integer; and

$$p(u) = \frac{\left[\binom{N_a - 1}{\frac{u-1}{2} - 1}\binom{N_b - 1}{\frac{u+1}{2} - 1} + \binom{N_a - 1}{\frac{u+1}{2} - 1}\binom{N_b - 1}{\frac{u-1}{2} - 1}\right] N_a ! \, N_b !}{N !} \qquad \text{(C-3)}$$

for u an odd integer. A detailed derivation of this probability density function is provided in Reference 1. Extensive tables for summed values of this function for various values of N_a and N_b along with several examples of their use are given in Reference 2.

An application of the concept of runs and of the probability density function (see Equations (C-2) and (C-3)), is provided in the so-called median test. The procedure is as follows: given a sequence to be tested for randomness, determine the median of the sequence. A run of length L is a sequence of values of length L such that either all the values are above the median or all the values are below the median. If the null hypothesis is to be that the sequence is random, each permutation of its elements is as likely to occur as another. Hence, the number of runs of the type just described is a random variable whose probability density function is given by Equations (C-2) and (C-3). Thus, to any given confidence level, the tables provided in Reference 2 can be used to test the hypothesis that the sequence is random. For instance, suppose a sequence of length 100 is the sequence in question. The numbers N_a and N_b of Equations (C-2) and (C-3) are defined, respectively, as the number of elements above and below the median; thus, by definition, $N_a = N_b = 50$. If a confidence coefficient of .95 is chosen, then the tables of Reference 2 reveal that with a probability of .95, the number of runs accurring should be between 41 and 62. If the number of runs is not between 41 and 62, then with a confidence coefficient of .95, the hypothesis that the sequence is random can be rejected.

It should be clear that if a sequence tends to be periodic with a relatively long period, several long runs would be introduced and since the sequence is finite, this condition would tend to produce fewer runs than would be expected in a random sequence. Conversely, if a sequence has a deterministic component with a very short periodicity, too many runs would be expected. Thus, the median test should be useful in detecting periodicities of long or short duration. This discussion leaves open the question of what, insofar as the median test is concerned, constitutes a periodicity of a long or short duration. In other words, is it true that random sequences exhibit a sort of periodicity of their own? In a sense, the answer appears to be yes. If one divides the expected value of the probability density function in Equations (C-2) and (C-3) by the length of the runs of this type in the ordered set of $N_a + N_b$ elements, the result is invariably approximately 1/2. Thus, a periodic sequence of period four points exhibits approximately the same number of runs as a random sequence of the same length. In this crude sense, a random sequence may be said to have a natural period of around four points. Hence, the median test should not be expected to be sensitive to periodicities of this length.

C.2 A TWO-SAMPLE TEST

The concept of runs and the probability density function, (see Equations (C-2) and (C-3)), are useful in constructing statistical tests of a nonsequential nature. Consider the problem of determining when two different sets of numbers are sets of values of the same random variable. A test may be constructed in this manner. Suppose there are N_a elements in sample A and N_b elements in sample B. Arrange the total of $N_a + N_b$ elements in descending order of magnitude. If it is assumed as a null hypothesis that each set consists of values of the same random variable, the $N_a + N_b$ elements constitute a set of values from this random variable; hence, all permutations of the elements should be equally likely to have occurred when ordered in descending magnitude. Thus, if a run of length L is defined as L elements in a row all from the same set, either A or B, then the probability density function is given by Equations (C-2) and (C-3). The tables in Reference 2 may be used to test the null hypothesis in the same way as with the runs test. An example of this sort of test is given in Reference 3. The two-sample tests are useful in testing residuals of an orbit determination process when it is suspected that the residuals reflect discontinuities in the noise on the basic observations. It should be mentioned that it is possible to derive the probability density function for the longest run of any particular sort in a sequence and base a test for randomness of this statistic. This possibility is discussed in Reference 4.

C.3 WILCOXON'S TEST

Another method for testing the hypothesis that two sets of numbers are values of the same random variable is the Wilcoxon test. It differs from the two-sample test, mentioned in the preceding paragraph, in that it in no way relies on the concept of runs or on the probability density function in Equations (C-2) and (C-3). Consider two sets of data A and B of N_a and N_b points, resepectively. Arrange the $N_a + N_b$ points in descending order of magnitude. Let I_a be the set of all integers i, such that an element from A occupies the i^{th} position in this sequence. If set A and set B consist of values from the same random variable, each set of N_a places occupied by the elements from A in the sequence is as likely to occur as any other set of N_a places. By making this assumption, a probability density function for the statistic

$$S = \sum_{i \in I_a} i \qquad \text{(C-4)}$$

may be derived. The derivation of the probability density function of the random variable defined by Equation (C-4) along with tables of its summed values are provided in Reference 4. Examples of the use of those tables to test the hypotesis that two sets of numbers are values of the same random variable may be found in Reference 3.

C.4 SERIAL CORRELATION

If a sequence of numbers is random, no particular correlation would be expected to exist between a value in the sequence and the value, for example, K places in front of it. That is, if X_i is defined to be the value in the i^{th} position in the sequence and Y_i to be X_{i+k}, the correlation between X_i and Y_i should not be significant. Based on this notion, a nonparametric method of testing sequences for randomness can be devised if it is assumed that all permutations of the sequence are equally probable. Assume that a sequence of length N is to be tested for randomness. Let $Y_i = X_{i+k}$ for i = 1, 2, . . ., N-K and $Y_{n-k+i} = X_i$ for i = 1, 2, . . . K.

The so-called circular form of the serial correlation statistic is defined as

$$R_K = \sum_{i=1}^{N} X_i Y_i \qquad \text{(C-5)}$$

where

K = the "lag number" associated with the serial correlation statistic.

If it is assumed that the values on the sequence constitute a set of independent values of a random variable with low-order moments, then it can be shown that the random variable, R, of Equation (C-5) possesses an approximately normal probability density function for N sufficiently large. The details may be found in Reference 5. In order to test the sequence for randomness, it suffices to know the mean and variance of R as a normal random variable. The necessary values are

$$U_r = \frac{S_1^2 - S_2}{N - 1} \qquad \text{(C-6)}$$

and

$$\sigma_r = \frac{S_2^2 - S_4}{N - 1} + \frac{S_1^4 - 4 S_1^2 S_2 + 4 S_1 S_3 + S_2^2 - 2 S_4}{(N - 1)(N - 2)} \qquad \text{(C-7)}$$

where

$$S_j = \sum_{i=1}^{N} (X_i)^j. \qquad \text{(C-8)}$$

The serial correlation statistic with lag number K is useful in constructing tests to detect periodicities of approximately K data points. Since it is suspected that the runs test is not sensitive to periodicities of four data points, the serial correlation test may be used in conjunction with the runs test with the lag number set at four. This procedure effectively corrects the previously mentioned deficiency in the runs test. Otherwise, the lag is simply set at the periodicity which one suspects might occur. An example of the application of the serial correlation test is given in Reference 1.

C.5 THE PERIODOGRAM

A common method of detecting hidden periodicities in a sequence is the method of periodogram analysis. Assume that the values of a sequence can be written in the following manner

$$X_T = \sum_{r=1}^{K} (a_r \cos \lambda_r T + B_r \sin \lambda_r T) + \epsilon_T \qquad \text{(C-9)}$$

where

ϵ_T ~ a value of random variable with a unspecified probability density function.

To detect the periods $2\pi/\lambda_r$ that are hidden by the random disturbances ϵ_T the following statistic proves useful

$$I_N(\lambda) = \frac{1}{4\pi} [A^2(\lambda) + B^2(\lambda)] \qquad \text{(C-10)}$$

where

$$A(\lambda) = \sqrt{\frac{2}{N}} \sum_{T=1}^{N} X_T \cos \lambda T \tag{C-11}$$

$$B(\lambda) = \sqrt{\frac{2}{N}} \sum_{T=1}^{N} X_T \sin \lambda T. \tag{C-12}$$

I_N is defined as the periodogram of the sequence where N is the number of points in the sequence. The maxima of $I_N(\lambda)$ correspond to $\lambda = \lambda_r$, r = 1, 2, . . . K. Hence, the peaks of the periodogram correspond to hidden periodicities of the sequence. The difficulty with the technique is that there is no rigorous way of deciding when the height of a peak is significant without making assumptions about the random variable which produced the values of ϵ_T. If it is assumed that the random variable in question is normal, then a rigorous test for the significance of the height of the maximum peak can be based on the statistic

$$g = \frac{(S_r)_{max}}{\sum_{i=1}^{N} S_i} \tag{C-13}$$

where, for i = 1, 2, . . . N

$$S_i = \frac{2}{N} \left[\left(\sum_{J=1}^{N} X_j \cos \frac{2\pi i J}{N} \right)^2 + \left(\sum_{J=1}^{N} X_J \sin \frac{2\pi i J}{N} \right) \right] \tag{C-14}$$

The distribution function for the statistic g of Equation (C-13) is derived in Reference 6. The functional form is

$$(g \leq X) = \frac{N(1-X)^{N-1}}{1!} - \frac{N(N-1)(1-2X)^{N-2}}{2!} + \cdots$$

$$\cdots + \frac{N(N-1)\cdots(N-K+1)(1-KX)^{N-K}}{K!} \qquad \text{(C-15)}$$

where

$K \sim$ the largest integer such that $K < 1/X$.

The distribution function in Equation (C-15) can be used to test for periodicities in the data in a rigorous fashion provided that it is assumed that the data consists of a periodic signal or signals to which have been added noise generated by a normal random variable. As such this test when used rigorously is not as general as the tests mentioned previously.

C.6 RECOMMENDATIONS FOR STATISTICAL TESTING OF RESIDUALS

When a program is developed to test orbit residuals for randomness, it is important to decide what type of nonrandomness the program is expected to detect. The most important dichotomy on nonrandom sequences seems to be the one which differentiates between periodic and nonperiodic nonrandomness. Experience indicates that the runs test, the serial correlation test, and the periodogram are effective in detecting periodic nonrandomness and the two-sample test and the serial correlation test with lag number one are effective in detecting nonperiodic nonrandomness. The tests used in the detection of nonrandomness should be chosen before the data to be tested is seen. Any other procedure can ruin the statistical rigor of the test and seriously bias the outcome.

The runs test is found to be an efficient tool in detecting periodicities of period 10 points or more. It is a flexible test in the sense that one need not have a hint of the length of the period of the nonrandom disturbance in order to apply the test effectively. The penalty for this flexibility is a lack of precision. If it is known that a certain set of residuals has failed the runs test, one might suspect the presence of a nonrandom periodic disturbance.

The runs test, however, gives no indication of the period of the disturbance. The case with the serial correlation test is precisely the opposite. It is not effective unless one has a suspicion of the period of the nonrandom periodicity which may be present. But the serial correlation test has the power to confirm almost positively any such suspicion.

The periodogram test has both the flexibility of the runs test and the precision of the serial correlation test. The hypothesis it tests is not simply that a given sequence is random, but that a sequence is random and that its elements are values of a normal random variable. Thus, it cannot be applied rigorously to the large number of situations that the other tests can.

Of the two types of nonrandomness discussed above, nonperiodic nonrandomness is more difficult to detect and classify. One might suspect that the runs test would be useful in detecting nonperiodic disturbances, but limited experience has not shown this to be the case. Futhermore, the two-sample test is designed to test the same statistical hypothesis as the Wilcoxon test, namely, that two samples are sets of independent values of the same random variable. Therefore, there is no rigorous reason for using one test in preference to the other. But, again, experience indicates that the two-sample test is somewhat more effective in detecting nonrandomness. The serial correlation test with lag number one has been found effective in detecting gradual drifts in the mean of the sequence. Drifts in the variance are more difficult to detect. In fact, it appears that unless the drift in variance is drastic, there is no test completely adequate in discovering it.

REFERENCES

1. Hoel, P. G. Introduction to Mathematical Statistics. New York: John Wiley & Sons, Incorporated, 1954.

2. Swed, Frieda S., and Eisenhart, C.; "Tables for Testing Randomness of Grouping in a Sequence of Alternatives," Annals of Mathematical Statistics, 1964, Volume 14, pp. 66-87.

3. Johnson, N. L., and F. C. Leone, Statistics and Experimental Design in Engineering and the Physical Sciences, Volume I. New York: John Wiley & Sons, Incorporated, 1964.

4. Mosteller, F., "Note on an Application of Runs to Quality Control Charts," Annals of Mathematical Statistics, 1941, Volume 12, pp. 228-232.

5. Wald, A. and J. Wolfowtiz, "An Exact Test for Randomness in the Non-Parametric Case Based on Serial Correlation," Annals of Mathematical Statistics, 1943, Volume 14, pp. 378-388.

6. Fisher, R. A., "Tests of Significance in Harmonic Analysis," Proc. Roy Society, London, 1929, Volume 125, pp. 54-59.

APPENDIX D

OBSERVATION WEIGHTING

Tables D-1 and D-2 define typical a-priori standard deviations and dynamic weighting factors for several observation types that are processed in the GTDS. The dynamic weighting factors are used in the following manner: let σ^2 be the a-priori variance for a given observation type and ρ_F be the dynamic weighting factor, then the data weight for an observation is formed as

$$w = \rho_F / \sigma^2 \tag{D-1}$$

or for those observations where a dynamic weighting factor is not specified

$$w = 1/\sigma^2. \tag{D-2}$$

Table D-1
Typical A-Priori Data Standard Deviations

Observation Type	A-Priori Standard Deviation
Range (VHF)	300 meters
Range-Rate (VHF)	10 centimeters/second
X_{30} Orientation angle (VHF)	50 seconds of arc
Y_{30} Orientation angle (VHF)	50 seconds of arc
Minitrack direction cosine ℓ	0.3 mils
Minitrack direction cosine M	0.3 mils
Range (S-Band)	25 meters
Range-Rate (S-Band)	10 centimeters/second
Azimuth (S-Band)	50 seconds of arc
Elevation (S-Band)	50 seconds of arc

Table D-2
Dynamic Weighting Factors

Observation Type	Dynamic Weighting Factor*
Minitrack direction cosine ℓ	$\sqrt{1 - \ell^2}$
Minitrack direction cosine m	$\sqrt{1 - m^2}$
Range	C_1 sin (Elevation) + C_2
Range-Rate	C_1 sin (Elevation) + C_2
Elevation	C_1 sin (Elevation) + C_2
Azimuth	C_3 cos (Elevation) + C_4

* C_1, C_2, C_3, C_4 are user-supplied constants.

APPENDIX E

GLOSSARY OF MATHEMATICAL SYMBOLS

A – Azimuth angle in Sections 2.2.2, 3.2.3, and 7.2.2.

– Reference satellite area for aerodynamic drag in Sections 4.3 and 5.3.

– Satellite area exposed to direct solar radiation in Section 4.4 and 5.4.

A, a_{ij} – Precession transformation in Section 3.3.1.

A, B, C, D – Matrices of time varying coefficients in variational differential equations in Sections 5.0, 6.3, and 6.4.

– Coefficients of polynomial fitted to Minitrack rectified ambiguity data in Section 2.2.3.

$A.1$ – Atomic time in Section 3.5.

A_2, B_2, C_2 – Principal moments of inertia of the moon in Section 4.2.

a – Semimajor axis of satellite orbit in Section 3.2.6.

– Magnitude of spacecraft thrust acceleration in Section 4.6.

a_x, a_y, a_z – Constant coefficients of the polynomial characterizing the attitude control system acceleration in Sections 4.5 and 5.5.

$a_F, \bar{a}_F, \bar{a}'_F$ – Minitrack fine baseline fractional phase difference in Sections 2.2.3 and 7.4.3.

$\bar{a}_j$ – Represents the j^{th} row of matrix of measurements partials, F, in Section 8.4.

a_m – Smoothed midframe value of Minitrack fine baseline data in Section 2.2.3.

a_p – Planet radius (usually equatorial radius) in Sections 3.6.1 and 4.2

a_T, a_R – Parameter used in general relativistic expression and defined in Appendix A.

a_0, a_1 . . . a_4 – Coefficients of the polynomial characterizing the spacecraft thrust acceleration versus time in Sections 4.6 and 5.6.

a_1, a_2 . . . a_5 – Minitrack fine phase difference readings in Sections 2.2.3 and 2.3.3.

B, C, D, A – See A, B, C, D above

B_C, B_F, B_M – Minitrack course, fine and medium baseline lengths in Section 7.4.3.

B_1 – Greenwich siderial time transformation in Section 3.3.1.3.

B_2 – Polar motion transformation in Section 3.3.1.4.

B_2, C_2, A_2 – See A_2, B_2, C_2 above.

b – Measurement bias in Section 7.1.

b, b_0 – Relative phase change on each Minitrack baseline without and with $\beta = 0$ in Section 2.3.3.

$\bar{b}$, b_x, b_y, b_z – Coefficients of the linear term of the polynomial characterizing the attitude control system acceleration in Sections 4.5 and 5.5.

b' – Oblate planet radius at apofocal and perifocal subvehicle points in Section 3.6.2.

b_{Ai} – Rectified Minitrack fine baseline ambiguity differences in Section 2.2.3.

C – Transformation matrix from true of epoch coordinates to local plane coordinates in Section 3.3.3.

C, D, A, B – See A, B, C, D above.

C_A – Abbreviation for C_M and C_C in Section 2.2.3.

C_F, C_M, C_C – Quadratic polynomial fitted to rectified fine, medium and coarse Minitrack ambiguity data, $\bar{b}_{Ai}$, in Section 2.2.3.

C_D, C_{D0} – Aerodynamic drag coefficient with and without systematic error corrections in Sections 4.3.4 and 5.3.

C_n^m – Gravitational harmonic coefficients in Sections 3.6, 4.2 and 5.2.

C_{ab} – Correlation coefficients in Section 8.3.

$C_{\Delta x_0 \Delta z}$ – Correlation between errors in $\bar{x}_0$ and $\bar{z}_0$.

$C_{\Delta x \Delta z}$ – Correlation between errors in $\bar{x}$ and $\bar{z}_0$.

$C_{\Delta x_0 n}$ – Correlation between errors in $\bar{x}_0$ and $\bar{n}$.

$C_{\Delta z n}$ – Correlation between errors in $\bar{z}$ and $\bar{n}$.

C_0, C_1 – Count of the number of cycles of the GRARR Doppler reference frequency, ν_{R2} and the range reference frequency, ν_{R1}, in Chapters 2 and 7.

C_2, A_2, B_2 – See A_2, B_2, C_2 above.

c, c_0 – Vacuum speed of light in Chapters 2, 4, 7 and Appendix A.

c_i – Rectified Minitrack fine baseline ambiguity differences in Section 2.3.3.

$\bar{c}$, c_x, c_y, c_z – Coefficients of the quadratic term of the polynomial characterizing the attitude control system acceleration in Sections 4.5 and 5.5.

c_g, c_p – The group speed and phase speed of propagation of an electromagnetic signal in Section 7.3.3.

D – Parameter used in solving Barker's equation for parabolic motion in Section 3.3.7.

– Parameter used to determine if the spacecraft is within the cylindrical shadow of a celestial body in Section 4.4.

D(t) – Time varying coefficients of the linear first order system of variational equations in Section 6.5.

D, A, B, C – See A, B, C, D above.

D_n – Quantity used to solve Kepler's equation for elliptical motion in Section 3.3.7.

d – Number of days past $0^h\ 0^m\ 0^s$ January 1, 1950 ET in Section 3.3.2.

$\bar{d}$ – Unit vector pointing down along the vacuum downlink path from the vehicle to the tracking station in Section 7.3.5 and Appendix A.

E – Transformation matrix from true of epoch coordinate system to the orbit plane system in Section 3.3.4.

– Elevation angle in Chapter 7.

– Orbital eccentric anomaly in Section 3.3.7.

– Matrix of partial derivatives of the nonlinear measurement equations, f(x, z) with respect to consider variables, z, in section 8.2.

E_a – Observed elevation angles in Sections 2.2.1 and 7.3.4.

e – Orbital eccentricity in Sections 3.2.6 and 3.3.7.

– Eccentricity of the planet's figure in Section 3.3.5.

F – Hyperbolic anomaly in Section 3.3.7.

– Abbreviation for forces in Chapter 4.

– Abbreviation for Sin A or Cos A in Section 7.4.3.

– Matrix of partial derivatives of observations with respect to solve – for variables in Sections 7.6 and Chapter 8.

F_T, F_R – Parameter used in general relativistic expression and defined in Appendix A.

$F_{10.7}$ – 10.7 cm solar flux in Section 4.3.

f – Planet's flattening coefficient in Sections 3.3.5 and 3.6.2, 4.3.5 and 5.3.

– True anomaly in Section 3.3.7.

– Used in Chapter 6 to denote a general time varying function.

f, f_0 – Nonlinear measurement equations in Sections 7.1 and 8.1.

G – Transformation matrix from mean equinox and equator of 1950.0 to true of epoch in Section 3.3.1. This transformation accounts for precession and nutation of the earth's spin axis.

– Universal gravitational constant in Section 4.1.

g, g' – Mean anomaly of the moon and sun in Section 3.3.2 and 3.5.1.

g(t) – Inner product of position and velocity vectors in Section 3.6.5.

g_{ij} – Elements of the metric matrix defining the nature of the space-time frame in Appendix A.

H – Transformation matrix from true equinox and equator of epoch coordinate system to body fixed coordinates in Sections 3.3.1.3, 3.3.1.4 and 3.3.1.5.

– Parameter used for solving for two-body hyperbolic motion in Section 3.3.7.3.

– Atmospheric scale height in Section 4.3.5.

– Matrix used for expressing the Cowell corrector formula in matrix form in Section 6.3.

H_I – Ionospheric scale height in expression for refractivity in Section 7.3.2.

H_T – Tropospheric scale height in expression for refractivity in Section 7.3.1

h – Altitude measured as the perpendicular distance from the surface of the ellipsoidal planet model to the point being measured. See Section 3.2.2, 3.3.5, and 4.3.

– Numerical integration stepsize in Chapter 7.

$\bar{h}, h_x, h_y, h_z$ – Orbital angular momentum vector and Cartesian components in Section 3.3.7.

h_a, h_p – Apofocal and perifocal altitude in Section 3.3.7.3.

$h_1, \ldots, h_8$ – Coefficients of time polynomials in Section 3.5.2.

I – Moment of inertia about moon-spacecraft line in Section 4.2, Equation (4-29).

– Identity matrix.

– Abbreviation used in ray angular deflection formula in Section 7.3.4, Equation (7-59).

I_{S_n}, II_{S_n} – Sums for Adams-Cowell formulas in Section 6.1.

I_{P_n}, II_{P_n}

I_M – Inclination of the mean lunar equator to the ecliptic in Section 3.3.2.

i – Orbital inclination defined in Sections 3.2.6 and 3.3.7.3.

– Incidence angle of electromagnetic ray and a radius vector of constant magnitude in Section 7.3.4.

i_s – Inclination of the moon's equatorial plane to the earth's equatorial plane in Section 3.3.2.

JD – Julian day number.

K – GRARR frame sample number in Section 2.2.1.2.

k – Universal gravitational constant in Section 4.2.

– Solar pressure model parameter in Section 5.4.

k_1, k_2 – Gain constants used to compute measurement variances in Section 8.1, Equation (8-13).

L_s – Mean longitude of the sun in Section 3.3.2.

– Luminosity of the sun in Section 4.4.

ℓ – Direction cosine of the angle between the station-vehicle vector and the local tangent east pointing axis. This angle is measured by the Minitrack system and described in Sections 2.1.3 and 7.2.2.

– Integer number which scales the hyperellipse of constant (normal) probability in terms of the standard deviations. See Section 8.6.2.

M – Orbital mean anomaly in Sections 3.2.6 and 3.3.7.

– Abbreviation for the Doppler frequency shift effect on Minitrack direction cosines in Section 7.5.3.

M, m_{ij} – Transformation matrix from selenocentric to selenographic coordinates in Section 3.3.2.

M, M_{ij}, m_{ij} – Abbreviation used in describing the matrix inversion procedure in Section 8.8.1.

M_{lt} – Transformation matrix from body-fixed coordinates, centered at a tracking station, to local tangent coordinates at the station in Section 3.3.6.

m_r – Mass of r^{th} attracting gravitational body in Sections 4.1 and 5.1.

m_0 – Mass of spacecraft in Chapters 4 and 5.

m – Group mean in Section 8.8.4.

N – Number of cycles of the Doppler-plus-bias signal counted over the Doppler counting cycle. See Section 2.1.1 as well as Chapters 2, 7 and Appendix A.

– The distance along the normal vector from the intersection of the normal and the ellipsoid to the z_b axis. See Figure 3-13 and Section 3.3.5.

– The tropospheric or ionospheric refractivity in Section 7.3.3.

N, n_{ij} – Transformation matrix from mean of epoch to true of epoch coordinates in Section 3.3.1.

N_d – The integral of the Doppler signal frequency over the Doppler counting cycle interval in Section 2.3.1.2 and 7.5.1.

N_e , N_{em} – Electron density and maximum electron density in Section 7.3.2.

N_F – The Minitrack fine baseline lengths in terms of vacuum wavelengths of the nominal 136.0 MHz frequency signal in Section 2.2.3.

N_I, N_T – Ionospheric and tropospheric refractivity in Section 7.3.2.

N_S – Surface refractivity in Section 7.3.2.

n – Orbital mean motion in Section 3.3.7.2.

– Adjustable parameter exponent on the cosine variation between Harris-Priester's maximum and minimum density profiles in Sections 4.3.5 and 5.3.

– Variable local index of refraction in Section 7.3.

– Measurement noise in Section 7.6 and Chapter 8.

$\bar{n}$ – Unit vector along signal propagation path in Appendix A-1.

n_s – Total number of residuals for a tracking station and data type in Section 8.8.4.

O_c, O_0 – The computed and actual observations in Sections 7.1 and 7.6.

P – Orbital period in Section 3.3.7.3.

– Perturbative accelerations additional to the primary body's inverse square gravity in Section 6.2.

– Abbreviation used in the equation for atmospheric time delay of a one-way transmission in Section 7.3.3.

P, P_{ij} – Transformation matrix from orbital rectangular coordinates to true of epoch coordinates in Section 3.3.7.

P_A, P_T – Adopted and true pole of earth in Section 3.3.1.4.

P_A, P_K, P_N – Anomalistic period, Keplerian period and nodal period in Section 3.6.4.

P_n^m – Legendre functions in Sections 4.2 and 5.2.

P_s – The force on a perfectly absorbing surface due to solar radiation pressure at one astronomical unit in Sections 4.4 and 5.4.

P_u, P_d – Abbreviations in the atmospheric corrections for the range-rate calculation. See Section 7.3.5.

$P_{\Delta a}$ – Covariance matrices in Chapter 8.

$P_{\Delta x_0}$ – Covariance matrix of apriori solve-for variable errors.

$P_{\Delta x}$ – Covariance matrix of estimated solve-for variable errors.

$P_{\Delta z}$ – Covariance matrix of consider variable errors.

p – Semi-latus rectum of orbit in Section 3.3.7.

– Dimension of the solve-for vector in Chapter 8.

$\bar{p}$ – Vector of dynamic parameters in the acceleration model which can be estimated. See Sections 5.0, 6.4 and 8.4.

$\bar{p}^*$ – The remaining components of $\bar{p}$ after excluding satellite position and velocity variables. See Section 5.0.

p_x – Normal probability density function in Section 8.6.2.

Q – Abbreviation used in the equation for atmospheric time delay of a one-way transmission in Section 7.3.3.

– Least square loss function defined in Sections 8.1 and 8.2.

Q, q_{ij} – Transformation matrix from spacecraft body axes to true of epoch coordinates in Sections 4.5 and 5.5.

q – Parameter used to solve Kepler's equation for parabolic motion in Section 3.3.7.

– The total parameter vector of all candidate solve-for variables in Sections 7.6 and 8.4.

– Dimension of the consider vector in Chapter 8.

$\bar{R}$ – Position vector in mean equator and equinox of 1950.0 coordinates.

R_e, R_p – Equatorial and polar radius of earth or reference body in Section 3.3.5.

RF_c – Observation correction due to refraction and light time in Section 7.1.

RMS – Actual root mean square error in Section 8.8.3.

RMSP – Predicted root mean square error in Section 8.8.3.

RMSB – The smallest RMS over all prior iterations

R_s – Position vector of the sun in the inertial mean of 1950.0 coordinate system in Section 4.4 and 5.4

R_{sun} – One astronomical unit used in Sections 4.4 and 5.4.

R_u – Right ascension of a point representing a fictious mean sun on the mean equator of epoch and measured from the mean equinox of epoch. See Section 3.4.3.

R_{vs} – Distance from the spacecraft to the sun in Section 4.4.

R_x, R_y, R_z – Individual precession and nutation transformations in Sections 3.3.

$\bar{r}$ – Position vector in true of epoch coordinates in Section 3.2.1.

r_a – Magnitude of the apofocal radius vector in Section 3.3.7.

$\bar{r}_b$, $\bar{r}_b$ – Position vector expressed in body-fixed and pseudo body-fixed coordinates in Sections 3.2.2 and 3.3.1.3 and 3.3.1.4.

$\bar{r}_E$ – Position vector in Cartesian coordinates referred to the mean equinox and equator of epoch in Sections 3.2.1 and 3.3.1.

$\bar{r}_{lt}$ – Position vector referred to the local tangent coordinate system in Sections 3.2.4 and 3.3.6.

$\bar{r}_{op}$ – Position vector referred to the orbit plane coordinate system. See Sections 3.2.5 and 3.3.4.

$\bar{r}_p$ – Position vector referred to the orbital rectangular coordinate system with x_p-axis direct at perifocus. See Section 3.3.7.

r_p – Magnitude of the perifocus radius vector in Section 3.3.7.3.

$\bar{r}_R$, $\bar{r}_T$ – Position vectors of the receiver and transmitter in inertial Cartesian coordinates in Appendix A.

$\bar{r}_S$ – Body-fixed coordinates of the tracking station in Sections 3.3.6 and 7.2.1.

$\bar{r}_S$, $\bar{r}_T$, $\bar{r}_V$ – Position vectors of the tracking station at signal reception and signal transmission, and position vector of the vehicle. All are referred to inertial Cartesian coordinates in Sections 7.3.5, 7.5.1 and Appendix A.

r_s – Geocentric radius and body axis components of a point on the surface of the ellipsoidal planet. See Section 3.3.5.

S – Mean solar flux constant at one astronomical unit in Section 4.4.

– Orbital period in regularized time system. See Section 6.9.

– Arc length along the signal propagation path in Section 7.3.3 and Appendix A.

– Series involved in atmospheric signal propagation time delay. See Section 7.3.3.

– Eigenvector transformation from basic coordinate frame to principal axes in Section 8.6.2.

– Sum of squares of residuals about the mean in each residual group. See Section 8.8.4.

– Heating due to extreme ultraviolet and corpuscular heat source used as a parameter in the Harris-Priester atmosphere model in Section 4.3.4.

S_c – The projection of the spacecraft position vector into the plane normal to the sun vector in the shadow model of Section 4.4.

S_n^m – Gravitational harmonic coefficients in Sections 4.2 and 5.2.

SV – Universal time correction due to seasonal variations in the rotation of the earth. See Section 3.4.6.

T – Ephemeris time in Julian centuries (36525 Julian days) elapsed since 1950.0 epoch (JD 243 3282.5). See Section 3.3.1.1.

– The integral of the instantaneous Doppler frequency ratio over the count time interval. See Section 7.5.1.

T_{ac1} , T_{ac2} – Epoch times at which the attitude control acceleration polynomials are turned on and turned off. See Section 4.5.

T_b – Rocket motor's effective burn time in Section 4.6.

T_E – The time in Julian centuries (36525 Julian days) elapsed since 1900 Jan 0^d 12^h (ET = JD 2415020.0). See Sections 3.3.1.2 and 3.5.1.

T_0 – The vacuum part of T, the integral of the instantaneous Doppler frequency over the count time interval. See Section 7.5.1.

T_o, T_f – The effective initiation and termination times of the spacecraft motor burn. See Sections 4.6 and 5.6.

T_u – Number of Julian centuries (36525 Julian days) elapsed from 1900 Jan 0^d 0^h (JD = 2415020.0) to the UT1 time of epoch. See Sections 3.3.1.3 and 3.4.3.

T_1, T_2, T_3 – Integration error bounds. See Section 6.8.

t – Coordinate time measured in A1 seconds from epoch. The independent variable of the equations of motion.

– The z_b-axis intercept of the vector normal to the surface of the ellipsoidal planet model. See Figure 3-13 and Section 3.3.5.3.

– Variable defined in Section 8.8.4 for testing residuals to determine the confidence interval for the group mean.

t_A – Time tag for gimbal angle data in Section 2.2.1.1.

t_{DR} – The time increment between consecutive samples of GRARR range and range-rate data. See Section 2.2.1.2.

t_F – Time commencing the frame time interval for the GRARR and Minitrack systems. See Sections 2.1.1, 2.2.1 and 2.2.3.

t_m – The corrected midframe time of the Minitrack system. See Section 2.2.3.

t_o – Epoch time in Section 4.3.

t_R – The time tag of the C-Band range data. See Section 2.2.2.

t_{RM} – The time of the return signal of the GRARR system. See Section 2.2.1.2.

t_{RR} – The time tag of the metric range-rate measurement. It approximates the midpoint of the vehicle turnaround time increment corresponding to the receiving station count interval. See Section 2.2.1.3.

t_S – The sample time of the tracker range and range-rate data. See Section 2.2.1.2 for GRARR and 2.2.2.2 for C-Band systems.

– The time at which the station receives the return signal in Chapter 7 and Appendix A.

t_T – Signal transmission time at the station in Chapter 7 and Appendix A.

t_V – The vehicle turnaround time in Chapter 7 and Appendix A.

$\bar{U}$ – Unit vector directed at the satellite and referred to the geocentric inertial Cartesian coordinate system. See Section 3.3.4.

U – Abbreviation used in atmospheric time delay Equation in Section 7.3.3.

$\bar{U}_B, U_{B_x}, U_{B_y}, U_{B_z}$ – Unit vector directed toward the apex of the diurnal bulge expressed in inertial geocentric coordinates. See Section 4.3.5.

$\bar{U}_N$ – Unit vector normal to orbital plane in the direction of the angular momentum vector. See Section 3.3.3.2.

U_S – Unit vector directed at the sun from a shadowing body and expressed in inertial Cartesian components. See Section 4.4.

$\bar{U}_T$ – Unit vector directed along thrust axis and referred to geocentric inertial Cartesian coordinate system. See Section 4.6.

UT – Universal time. See Section 3.4.3.

UTC – Universal time coordinated. See Section 3.4.7.

UT0 – Uncorrected universal time. See Section 3.4.4.

UT1 – UT0 corrected for polar motion. See Section 3.4.5.

UT2 – UT1 corrected for periodic seasonal variations. See Section 3.4.6.

$\bar{U}_{Z_{1p}}$ – Unit vector in the local plane z_{1p} -axis direction and referred to geocentric inertial Cartesian system. See Section 3.3.3.2.

$\bar{U}_\alpha$, $\bar{U}_\delta$ – Partial derivatives of $\bar{U}_T$ with respect to the right ascension, α, and declination, δ. See Section 5.6.

$u(\zeta)$ – Function used in Sections 4.5 and 5.5 defined as follows

$$u(\zeta) = 0 \text{ if } \zeta < 0$$

$$u(\zeta) = 1 \text{ if } \zeta \geq 0$$

$\bar{u}$ – Unit vector pointing along the vacuum uplink signal propagation path from the station to the vehicle. See Section 7.3.5.

– Expanded state vector containing as components the merged vectors $\bar{x}$ and $\bar{z}$. See Section 8.4.

$\bar{V}$ – Spacecraft's velocity vector magnitude.

– Abbreviation used in atmospheric time delay equation in Section 7.3.3.

$\bar{V}$ – Unit vector normal to the geocentric position vector and lying in the orbital plane. See Section 3.3.4.

V_n – Abbreviation used in Section 6.3 for describing the Cowell integrator for linear systems.

W – Unit vector directed normal to the orbit plane in the direction of the angular momentum vector. See Section 3.3.4.

– Weight matrix in the least squares loss function in Chapter 8.

X, Y – Gimbal angles for the GRARR system. See Section 2.1.1 for description.

X, Y, Z – Inertial Cartesian components of spacecraft position in the mean of 1950.0 coordinate system. See Section 3.2.1.

X_n – Abbreviation used in Section 6.3 for describing the Cowell integrator for linear systems.

$\bar{x}$ – General vector function of time used in Section 6.1 for describing the Adams-Cowell ordinate second sum integrator technique.

$\bar{x}$, $\hat{x}_i$, $\bar{x}_i$ $\bar{x}_0$ – Epoch values of the solve-for or expanded state vector of p-dimension in Chapter 8. The vector $\hat{x}_i$ is the best estimate of $\bar{x}$ obtained on the i^{th} iteration. The vector $\bar{x}_{i-1}$ is the reference solution on the i^{th} iteration. The vector $\bar{x}_0$ is the a priori specified reference state.

x, y, z – Inertial Cartesian components of spacecraft position in the true of epoch coordinate system. See Section 3.2.1.

x_b, y_b, z_b – Components of spacecraft position in body-centered rotating coordinates of the principal gravitating body. See Section 3.2.2.

– Also used to denote the spacecraft's roll, pitch and yaw axes in Section 4.5.

x_E, y_E, z_E – Inertial components of spacecraft position in the mean of epoch coordinate system. See Section 3.2.1.

x^i – Components of the space coordinates in Appendix A.

x_{1p}, y_{1p}, z_{1p} – Components of spacecraft position in geocentric local plane coordinates (up, east, north). See Section 3.2.3.

x_{1t}, y_{1t}, z_{1t} – Components of spacecraft position in topocentric local tangent coordinates (east, north, up). See Section 3.2.4.

x_{op}, y_{op}, z_{op} – Components of spacecraft position in geocentric orbit plane coordinates. See Section 3.2.5.

x_p, y_p – Cartesian components of polar motion. See Figure 3-10 and Section 3.3.1.4.

x_p, y_p, z_p – Cartesian components of spacecraft position in orbital coordinates i.e., x_p directed at perigee, z_p in direction of angular momentum. See Section 3.3.7.1.

x_s, y_s, z_s – Coordinates of a point s on the surface of ellipsoidal planet expressed in body-centered rotating coordinates. See Section 3.3.5.

Y – See X, Y, Z above.

Y – See X, Y above.

Y – Dependent variable vector in the second order linear differential system of variational equations in Sections 5.0 and 6.4.

$\bar{y}$ – The m-dimensional vector of measurement data in Chapter 8.

y – See x, y, z above.

y_b – See x_b, y_b, z_b above.

y_E – See x_E, y_E, z_E above.

y_{1p} – See x_{1p}, y_{1p}, z_{1p} above.

y_{1t} – See x_{1t}, y_{1t}, z_{1t} above.

y_{0p} – See x_{0p}, y_{0p}, z_{0p} above.

y_p – See x_p, y_b above.

y_p – See x_p, y_p, z_p above.

y_s – See x_s, y_s, z_s above.

Z – See X, Y, Z on preceding page.

Z_A – Correction to the Minitrack's medium and coarse baseline ambiguity data to account for errors in baseline orientations, errors in locations of centers of antennas, inequalities in lengths of cables to counters, etc. See Section 2.2.3.

Z_F – Correction to the Minitrack's fine baseline smoothed phase difference data to account for baseline orientation errors, errors in locations of centers of antennas, inequalities in lengths of cables to counters, etc. See Section 2.2.3.

z – Non-dimensional altitude used in the Chapman profile for electron density in Sections 7.3.2 and 7.3.3.

$\bar{z}$ – **The** q-dimensional consider vector containing as components all model parameters whose values are known with limited certainty but are not to be estimated. See Chapter 8.

z – See x, y, z above.

z_b – See x_b, y_b, z_b above.

z_E – See x_E, y_E, z_E above.

z_{1p} – See x_{1p}, y_{1p}, z_{1p} above.

z_{1t} – See x_{1t}, y_{1t}, z_{1t} above.

z_{0p} – See x_{0p}, y_{0p}, z_{0p} above.

z_p – See x_p, y_p, z_p above.

z_s – See x_s, y_s, z_s above.

α – Right ascension of the spacecraft relative to the true of date system. See Section 3.2.1.

α_g – **Var**iously called true Greenwich sidereal time, Greenwich hour angle of the true equinox of epoch, or right ascension of Greenwich. See Section 3.3.1.3.

α_{GM} – Mean Greenwich sidereal time. Measured in the mean equator and equinox of date system. See Section 3.3.1.3.

α_i, β_i – Coefficients of the Adams-Cowell predictor formulas (ordinate form) in Chapter 6.

α_i^*, β_i^* – Coefficients of the Adams-Cowell corrector formulas (ordinate form) in Chapter 6.

α_s – Right ascension of the sun in Section 4.3.5.

α_T – Right ascension of the spacecrafts thrust axis in Section 4.6.

$\alpha_0, \cdots, \alpha_4$ – Coefficients of polynomial characterizing the thrust axis right ascension in Section 4.6.

β – Correction to the integrated Minitrack phase rates to account for unknown initial conditions in Section 2.3.3.

– Flight path angle measured from the geocentric position vector to the velocity vector. See Section 3.2.3.

$\overline{\beta}$ – Abbreviation used in the Doppler refraction correction algorithm in Section 7.3.5.

Γ'_M – Mean longitude of the moon's perigee in Section 3.3.2.

$\overline{\Gamma}_n$ – Vector containing powers of the thrust burning time in Section 5.6.

Γ_S – Mean longitude of the sun's perigee in Section 3.3.2.

γ – Parameter equal to 1 plus the reflectivity coefficient in Section 4.4 and 5.4.

γ'_i, γ''_i – Coefficients in the Adams-Cowell formulas in Section 6.1.

Δ – Auxiliary angle used in determining the transformation from true of date selenocentric to selenographic coordinates in Section 3.3.2.

Δf_{cesium} – The correction to the frequency f_{cesium} = 9, 192, 631, 770 cycles of cesium per ephemeris second in Section 3.5.1.

ΔH – The correction to mean right ascension to account for nutation in Section 3.3.1.3.

ΔL_A – The measured difference in Minitrack medium and coarse baseline cable lengths from the two antennas to the counter. See Section 2.2.3.

ΔM – Deviation from unity of the Doppler frequency shift effect on Minitrack direction cosines. See Section 7.5.3.

Δr – Radius of the error hypersphere in Section 8.6.2.

ΔT_{1958} – The difference ET-UT2 on 1 January 1958, 0^h, 0^m 0^s UT2 minus the periodic terms in the ET to A.1 transformation in Section 3.5.1.

Δt_A – Time correction on medium and coarse baseline Minitrack data which accounts for signal delay between arrival at the antenna to arrival at the counter and for the multiplexing sequence. See Section 2.2.3.

Δt_F – The time increment between Minitrack frames. See Section 2.2.3.

Δt_{FF} – Time delay on Minitrack fine baseline data due to the 10 Hz filter delay. See Section 2.2.3.

Δt_p – One-way light time correction on Minitrack data time tag. See Section 7.4.3.

Δt_R – One-way light time correction on radar signals. See Sections 2.2.1 and 2.2.2.

Δt_{RB} – Timing bias on C-Band data due to equipment signal paths and delays. This bias is determined by on-site calibration. See Section 2.1.2.

Δt_{RD} – The GRARR system range measurement delay which accounts for the combined effects of signal propagation delay between the antenna and counter and the counter delay itself. This delay is determined by on-site calibration. See Section 2.2.1.2.

Δt_{RR} – Doppler count time increment. See Section 2.2.1.2.

Δt_{RT} – Two-way light time of radar signal. See Section 2.3.2.

Δt_3 – Correction to the time corresponding to the smoothed midframe Minitrack data to account for the finite time required by the counter to measure a changing sequal. See Section 2.2.3.

$\overline{\Delta} x_i$ – Perturbation in the solve-for vector about the i^{th} iterated estimate $\hat{x}_i$. See Section 8.2.

$\Delta \hat{x}_i$ – Best estimate of $\overline{\Delta}x$ in a weighted least squares sense. See Section 8.2.

$\Delta \tilde{x}_i$ – Deviation of the a priori and the i^{th} iterated estimate of $\bar{x}$. See Section 8.2.

$\overline{\Delta} y_i$ – Vector of deviation between the actual measurements and the i^{th} iterated estimate of the measurements. (Note $\overline{\Delta}y = \overline{\Delta}y_0$). See Section 8.1 and 8.2.

$\overline{\Delta z}$ – Perturbations of the consider vector, $\bar{z}$, about its a priori value. See Section 8.2.

Δz_i – Components of transformed state vector which constitute the coordinates of a hypersphere. See Section 8.6.2.

$\Delta \lambda$ – Difference between the adopted and true longitude in Section 3.3.1.4.

ΔP – The uplink plus downlink range difference. See Section 2.2.1.3 and Appendix A.

$\Delta \tau$ – Spacecraft transponder time delay in Section 2.2.1.

$\Delta \phi$ – Difference between the adopted and true latitude in Section 3.3.1.4.

δ – Declination angle. See Section 3.2.1.

– Latitude angle. See Section 3.2.2.

– Abbreviation used in atmospheric refraction correction of the elevation angle in Section 7.3.4.

$\delta_1, \ldots, \delta_4$ – First differences of Minitrack fine baseline phase difference points. See Section 2.2.3.

$\delta_0, \ldots, \delta_4$ – Coefficients of polynomial characterizing the thrust axis declination in Section 4.6.

δ_s – Declination of the sun in Section 4.3.5.

δ_T – Declination of the spacecraft's thrust axis relative to the true equinox and equator of epoch. See Section 4.6.

δt – Timing bias in observation data. See Section 7.1.

$\delta\epsilon$ – Difference between the true and mean obliquity. See Section 3.3.1.2.

$\delta\psi$ – Nutation angles in Section 3.3.1.2.

ϵ – Improvement ratio criterion specified for least squares iteration convergence. See Section 8.8.3.

$\bar{\epsilon}, \tilde{\epsilon}$ – Mean and true obliquity. See Section 3.3.1.2.

ϵ_n – Local error of the numerical integration in Section 6.8.

ϵ_1, ϵ_2 – Parameters used in Section 3.6.6 to determine altitude extremes. ϵ_1 corresponds to the ratio of the planet's polar and equatorial radii; ϵ_2 corresponds to square of the eccentricity of the ellipsoidal planet.

$\mathcal{E}$ ( ) – Denotes the expected value.

ζ_0 – Precession Angle in Section 3.3.1.1.

η – Surface reflectivity coefficient in Section 4.4.

θ – Transition matrix between perturbations in solve-for variable and perturbations in consider variables in Section 8.5.

θ_p – Precession angle in Section 3.3.1.1.

λ – Longitude measured last from the prime meridian.

$\overline{\lambda}$ – Lag angle between the sun line and the apex of the diurnal bulge. See Section 4.3.

λ_A – Adopted longitude in Section 3.3.1.4.

λ_g – Geomagnetic longitude in Section 3.6.1.

λ_M – Geocentric mean longitude of the moon in Section 3.3.2.

λ_0 – Geographic longitude of the north magnetic pole in Section 3.6.1.

λ_s – Wavelength of signal received at Minitrack station in Section 7.4.3.

λ_T – Instantaneous longitude with polar motion neglected.

λ_V – Wavelength of signal apparent at the spacecraft in Section 7.4.7.

μ – Gravitational parameter of the reference body, i.e. the product of the universal gravitational parameter times the mass of the body.

ν – Eclipse factor in Section 4.4 and 5.4.

– Radio signal frequency in Chapters 2 and 7.

ν_b – Bias frequency on Doppler signal. See Section 2.1.1.

ν_d – Doppler signal frequency. See Section 2.1.1.

ν_{du} – Deviation of the uplink signal received by spacecraft from the nominal carrier frequency. See Section 2.2.1.2.

ν_L – Low frequency ranging tone in Section 2.1.1.

ν_R – Received signal frequency in Section 2.1.1 and Appendix A.

ν_{R1}, ν_{R2} – Reference frequency for the GRARR range and range-rate measurements. See Section 2.1.1.

ν_s – Frequency of received signal at tracking station in Chapter 7 and Appendix A.

ν_T – Frequency of signal transmitted at the tracking station. See Section 2.1.1.

ν_V – Frequency of uplink signal apparent at the vehicle. See Section 2.1.1.

ξ_p – Precession angle in Section 3.3.1.

ρ – One-way range which is the distance from the tracking station to the spacecraft in Chapter 2 and 7.

– Planet's mass density in Section 4.2.

– Atmospheric density in Sections 4.3 and 5.3.

ρ_a – Range ambiguity number. See Section 2.2.1.2.

ρ_u, ρ_d – One-way range distance corresponding to the uplink and downlink signal path. See Section 2.2.1.3 and Appendix A.

ρ_{ij} – Correlation coefficient. See Section 8.6.4.

ρ_M – Physical libration in the inclination of the mean lunar equator in Section 3.3.2.

ρ_1, ρ_2, ρ_3 – Systematic error coefficients in the atmospheric density model. See Section 4.3.5.

σ – Sample standard deviation in Section 8.8.4.

σ_k – The standard deviation of the k^{th} observation in Chapter 8.

$\tilde{\sigma}_k$ – A priori standard deviation of the noise on the k^{th} observation. See Section 8.1.

$\bar{\sigma}_k$ – The standard deviation of the data reduction curve fit obtained during preprocessing of the k^{th} observation. See Section 8.1.

σ_M – Hayn's physical libration in the mean ascending node of the lunar orbit. See Section 3.3.2.

τ – Time measured from effective ignition of the thruster. See Section 4.6 and 5.6.

– The independent variable for the transform time regularized system. See Section 6.9.

τ_M – Hayn's physical libration in longitudes. See Section 3.3.2.

– Fundamental matrix solution of linear system of first order of differential equations in Section 6.5.

$\phi(T_i, t_0)$ – State transition matrix relating state perturbations at time t_0 to state perturbations at time T_i. See Section 8.5.

ϕ – Euler angle in roll used to orient the spacecraft's body-fixed axes to the inertial Cartesian true of epoch system in Section 4.5 and 5.5.

ϕ, ϕ' – Geodetic and geocentric latitude angles. See Section 3.2.2.

ϕ_A, ϕ_T – Latitude corresponding to the adopted pole and the true pole. See Section 3.3.1.4.

ϕ_g, ϕ_0 – Geomagnetic latitude and latitude of the north magnetic pole in Section 3.6.1.

ψ – Gravitational potential in Section 4.2.

– Angle between the satellite position vector and the apex of the diurnal bulge. See Section 4.3.1 and 4.3.5.

– Abbreviation for the covariance matrix of the estimated state in the absence of consider variables in Section 8.3.

Ω – Right ascension of the orbital ascending node. See Section 3.2.6.

Ω' – Right ascension of the ascending node of the lunar orbit. See Section 3.3.2.

Ω_M – Longitude of the mean ascending node of the lunar orbit. See Section 3.3.2.

Ω_ω – Skew matrix containing as elements components of the earth's rotation vector. See Section 5.3.

ω – Argument of perigee of satellite orbit. See Section 3.2.6.

$\overline{\omega}$ – Angular rotation vector of earth expressed in mean of 1950.0 coordinates. See Section 4.3.

ω_M – The moon's argument of perigee. See Section 3.3.2.

Subscripts

$( )_A$ – refers to adopted pole.

$( )_a$ – apofocus

$( )_{avg}$ – average

$( )_b$ – body

$( )_c$ – coarse baseline (Minitrack)

$( )_d$ – Doppler or downlink

$( )_D$ – drag

$( )_E$ – mean of epoch

$( )_{E-W}$ – east-west

$( )_e$ – equatorial

$( )_F$ – frame or fine baseline (Minitrack)

$( )_g$ – geomagnetic

$( )_{lp}$ – local plane

$( )_{lt}$ – local tangent

$( )_M$ – medium baseline (Minitrack) or maximum

$( )_m$ – midframe or minimum

$( )_{NS}$ – non-spherical

$( )_{N-S}$ – north-south

$( )_{op}$ – orbit plane

$( )_p$ – polar or perifocus

$( )_{PM}$ – point mass

$( )_R$ – range or receiver

$( )_{RR}$ – range rate

$( )_{REL}$ – relative

$( )_S$ – station

$( )_s$ – sun

$( )_{SR}$ – solar radiation

$( )_T$ – thrust or transmitter

$( )_{TAC}$ – attitude control system

$( )_u$ – uplink

Superscripts

$( )^{c}$ – corrector

$( )^{d}$ – day

$( )^{h}$ – hour

$( )^{m}$ – minute

$( )^{p}$ – predictor

$( )^{s}$ – second

$( )^{T}$ – transpose

Operational Symbols

$[\cdot]$ – fractional part, Section 2.2.3.

$\{\cdot\}$ – minimum phase difference, Section 2.2.3.

∇ – gradient or difference operator

$() \times ()$ – cross product

$()\cdot()$ – dot product

E – shifting operator, Section 6.1

D – differential operator, Section 6.1

I – identity operator

$(\hat{})$ – best estimate

$(\bar{})$ – vector

$\mathcal{E}( )$ – expected value

Cov ( ) – covariance

Var ( ) – variance